Specific Absorption Rate Perturbations in the Eyes and Head by Metallic Spectacles at Personal Radio Communication Frequencies

William Whittow

Thesis submitted to the University of Sheffield for the degree of Doctor of Philosophy in the Faculty of Engineering

Department of Electronic and Electrical Engineering
University of Sheffield
Mappin Street, Sheffield S1 3JD, UK

August 2004

SUMMARY

The research in this thesis involves the absorption in the human head of microwaves in the frequency range 0.5 to 3GHz with the excitation positioned in front of the face. It is hypothesised that metallic spectacles can significantly affect the absorption in the head.

The effects of metallic spectacles have been primarily investigated using computer modelling. The finite-difference time-domain (FDTD) is the most common computational tool used in bioelectromagnetics. For this research an independent, specially written FDTD code has been used. The accuracy of the code was carefully validated against controls. Two anatomically accurate heads were implemented into the FDTD code.

Different shapes and sizes of metallic spectacles were modelled. The materials that the spectacles were made of were also investigated. Realistic and geometric spectacles were considered. Vertically and horizontally polarised plane waves as well as vertically and horizontally orientated dipoles are used as sources. A genetic algorithm (GA) was employed as a search technique to optimise the spectacles for the specific absorption rates (SAR) in the eyes and the head.

Measurements were also made of a phantom with metallic spectacles. Results showed good agreement with the FDTD code. Results confirmed the hypothesis that metallic spectacles can significantly affect the SAR in the head and particularly in the eyes.

ACKNOWLEDGEMENTS

I would like to express my sincere and foremost gratitude to my supervisor, Dr. Rob. Edwards, for his guidance, enthusiasm and valuable discussions throughout this work. I would also like to extend my sincere appreciation to Patrick McEvoy and Dr. Jon Rigglesford for invaluable assistance with measurements. I am also grateful to Dr. Greg Cook for his wisdom and his ideas about the overall project.

Informative and constructive discussions with my colleagues are of great help to me and are very much appreciated.

Last but not least, I would like to thank my parents, my brother, my sister and friends for their continuous support, encouragement and for attempting to be interested in technical details of the project.

PUBLICATIONS, PRESENTATIONS AND CITATIONS

1. Whittow, W.G. and R.M. Edwards, *A study of changes to specific absorption rates in the human eye close to perfectly conducting spectacles within the radio frequency range 1.5 to 3.0GHz.* IEEE Trans. Antennas and Propagation, Accepted for publication for February 2005.
2. Whittow, W.G. and R.M. Edwards, *Application of a genetic algorithm for identification of maxima in specific absorption rates in the human eye close to perfectly conducting spectacles.* IEE Proceedings Science, Measurement & Technology, Accepted subject to revisions.
3. Whittow, W.G., R.M. Edwards, and G. Cook, G. *A study of changes to specific absorption rates in the human eye close to perfectly conducting spectacles within the radio frequency range 1.5 to 3.0GHz. Twelfth International Conference on Antennas & Propagation,*. 2003. Exeter, UK. p. 300
4. Whittow, W.G. and R.M. Edwards. *Implications for SAR when using a symmetric phantom exposed to RF radiation using the FDTD method. Technical Seminar on Antenna Measurements and SAR (AMS 2004).* 2004. Loughborough, UK. p. 67-70
5. Whittow, W.G., Edwards R. M. *Changes in specific absorption rates in the human eye due to perfectly conducting spectacles illuminated by radio waves of frequencies within the range 1.5 to 3.0GHz. Institute of Physics. RF Interactions with Humans: Mechanisms, Exposure and Medical Applications.* 2003. London, UK.
6. Citation: Chalmers, M., *A fresh look at hand-held communication devices.* PhysicsWorld, 2003. **16**(5): p. 20-21.

ACRONYMS

ABC	Absorbing boundary conditions
CAD	Computer aided design
CT	Computerized x-ray tomography
dB	Decibels
E	Electric
EM	Electromagnetic
EMF	Electromagnetic fields
FCC	Federal Communications Commission
FDTD	Finite-difference time-domain
GA	Genetic algorithm
GMT	Generalised multipole technique
H	Magnetic
HP	Horizontally polarised
ICNIRP	International Commission Non-Ionizing Radiation Protection
ICRP	International Commission on Radiological Protection
MMP	Multiple multipole
MRI	Magnetic resonance imaging
PDA	Personal digital assistant
PDE	Partial differential equations
PEC	Perfect electrical conductor
PMC	Perfect magnetic conductor
PML	Perfectly matched layer
RAM	Radar absorbing material
RF	Radiofrequency
SAM	Standard anthropomorphic model
SAR	Specific absorption rate
TFSF	Total field / scattered field
VP	Vertically polarised

LIST OF NOTATIONS

B	Magnetic flux density (W/m²)
c	Speed of light (m/s)
C	Specific heat capacity (J/Kg·K)
D	Electric flux density (D/m²)
d	Distance inside PML layer (Yee cells)
E	Electric field intensity (V/m)
E_0	Amplitude of electric field
E_{inc}	Incident electric field (V/m)
E_{scat}	Scattered electric field (V/m)
E_{tot}	Total electric field (V/m)
E_z	Electric field component in z direction (V/m)
E_{zx}	PML split field component in z direction (V/m)
f	Frequency (Hz)
g	Ratio of conductivity from one cell to next in PML region
H	Magnetic field intensity (A/m)
Hz	Magnetic field component in z direction (A/m)
i	Position of Yee cell in x direction
$i_0, i_1, j_0, j_1, k_0, k_1$	Edge of total field region
j	Position of Yee cell in y direction
J_e	Electric current (A/m²)
J_m	Magnetic current (V/m²)
k	Position of Yee cell in z direction
L	Grid point in PML region
m	Number of chromosomes copied for elitism
M	Number of Yee cells in problem space
n	Time step number
N	Thickness of PML (Yee cells)
nt	Total number of time steps in FDTD simulation

P	Percentage error on whole grid (%)
R	Reflection factor of PML region
SAR	Specific absorption rate (W/Kg)
SAR_{10g}	SAR averaged over 10g of tissue (W/Kg)
SAR_{1g}	SAR averaged over 1g of tissue (W/Kg)
W	Radian frequency ($w=2\pi f$) (Rad/s)
Δt	Time increment (s)
ΔT	Temperature increase (K)
Δt_e	Duration of the exposure (s)
Δx	Size of Yee cell in x direction (m)
ε_r	Relative permittivity
λ	Wavelength (m)
ρ'	Magnetic resistivity (Ω/m)
σ	Conductivity (S/m)
ε	Electric permittivity (F/m)
μ	Magnetic permeability (H/m)
ρ	Density (Kg/m^3)
σ_x	x component of conductivity in PML region (S/m)
ρ'_x	x component of magnetic resistivity in PML region (Ω/m)

CONTENTS

Chapter 1

INTRODUCTION

1.1 Previous research into radiofrequency interactions with humans

The possible effect of mobile phones on human health has been topical over the last several years. The Stewart Report [1] highlighted some of the scientific research that has been carried out in this area. It stated that the mobile phone market has increased very rapidly over recent years, and estimated that market penetration in the UK could be 75% by 2005. The report concluded that the rapid advance of the technology and its popularity had not allowed sufficient time to adequately research the health effects of mobile phones and that more science is needed. It is likely, that as technology improves, mobile phones will be used for many more functions and, therefore, for longer periods every day [2], compounding any possible health effects. New technologies such as photo, video and text messaging will mean the phone is positioned in front of the head as opposed to at the side [3]. The long-term effects of using a mobile phone will probably not be known for decades and it is vital to give biological researchers accurate information about the amplitude and location of the radiofrequency (RF) absorption from mobile phones.

The presence of a human disturbs the radiation patterns of a mobile phone and affects its performance [4-7]. The other reason to investigate this area is from the point of view of the amount of energy absorbed by the human body, with values varying from 10% to 50% depending on different phones, distances etc. [6-8]. Obviously the two different

areas are very closely linked and lower absorption within humans will require less power to be transmitted from the mobile phone antenna to communicate with base stations.

Mobile phones have been linked to many different health concerns [1], with both thermal and athermal effects. There are various publications which review the research into biological effects from RF [1, 9, 10] but, as yet, there is no evidence that mobile phones are harmful to human health. There is criticism of electromagnetic field (EMF) research that results can not be reproduced, even within the same laboratory [9]. There is also the criticism that much of the research has been carried out using frequencies and power densities that differ from real popular [1]. Van Leeuwen [11] predicted a maximum temperature increase in the brain of 0.11°C which suggests that there is not enough power in mobile devices for there to be thermal effects, as the temperature increase is small compared to the temperature increase in the head during normal activities such as exercise [8, 12]. It is also hypothesised that local heating in the ear is due to the lack of convection that is possible from the hand covering the ear [13]. Research also shows that, in normal conditions the temperature rise in the eye is not great enough for there to be a risk of cataract formation [14-17], although athermal effects in the eye and in the head could be important [1, 8].

This absorption of energy must comply with international safety limits. The standard dosimetric parameter is the specific absorption rate (SAR) which is the power absorbed by a unit mass of tissue (W/Kg). There are two internationally recognised standards; the International Commission on Non-Ionizing Radiation Protection (ICNIRP) [18], in effect in Europe and Japan, which defines a limit of 2W/Kg averaged over 10g for 6 minutes and the Federal Communications Commission (FCC) [19], in America, which

sets a slightly stricter limit of 1.6W/Kg over 1g for 30 seconds. The averaging procedure is a source of some ambiguity as to whether it should be a cubic shape or an irregular shape and whether air can be included [20, 21].

There are two popular methods [22] that have been used to investigate the electromagnetic fields radiated from handheld RF devices in this application. These are: 1) measurements with anatomically shaped phantoms (both thermal and electromagnetic measurements) and 2) a computational modelling method. Both these techniques have advantages and disadvantages [22]. The thermal phantom method investigates the change in temperature of a phantom by means of a temperature probe [23, 24], however these effects are less than 1°C [11] and are small compared to the inaccuracies of the system [25]. Temperature measurements are time consuming as thermal equilibrium must be achieved prior to each measurement [26]. Using specially made devices with increased output power makes it hard to investigate realistic devices [24]. The electromagnetic phantom method involves filling a 'human-shaped' shell with a dielectric fluid with similar electrical properties to the body and using an electric field probe to measure the field strengths throughout the phantom [6, 25, 27, 28]. The use of phantoms is generally limited to simple buildable exterior shapes and a homogeneous liquid, representing the body, thus the detail of the internal structure is limited and includes no cavities or dielectric boundaries [29]. Yu, for example, used a frequency specific fluid with electrical properties of the average of white and grey matter of the brain [30]. Good agreement has been found [6, 22, 27] when comparing measurements with computer modelling of simple geometric phantoms.

1.2 Hypothesis

It was predicted that adding metallic spectacles to a head could affect the SAR when a mobile device is used in front of the face. Both increases and decreases in SAR are expected. The effects are thought to be most significant around the eye region. It is hypothesised that different shapes and sizes of spectacles will produce different effects.

1.3 Advantages of FDTD

Finite-difference time-domain (FDTD) is a computer modelling technique that simulates electromagnetic fields propagating in a problem space. FDTD is now the most widely used computer modelling tool for problems involving RF absorption in biological bodies [31-35]. Such simulations are clearly advantageous as it is unethical to use human cadavers to study the effects of RF interaction with the human body, and using phantoms as outlined in Section 1.1 makes modelling the complexity of the human anatomy very difficult. Method of moments (MOM), and the generalised multipole technique (GMT) are two techniques which are used to model antennas but are suited to largely homogeneous structures [9] and, therefore, are not ideal methods to handle the complexity and inhomogenity of the human body. The finite-element method allows more complex shapes, however, its implementation is not straightforward [9].

The advantages of FDTD over other computer simulation tools are that it is an intuitive method, which can deal with heterogeneous materials that have complex shapes. The advances in computer memory and processing power have allowed ordinary computers to be able to solve FDTD problems.

There are of course disadvantages to FDTD compared to other modelling techniques. It requires large amounts of memory and must perform millions of calculations [31]. Martens states that the memory required is proportional to the number of grid points M and the computational time is proportional to $M^{\frac{4}{3}}$ [8]. A common theme to FDTD is the need to reduce the computational time and memory requirements. This can be done either by using the fact that many problems are symmetrical and therefore only a half or even a quarter of the grid needs to be considered, or by truncating the body in one direction and assuming that most of the energy is lost close to the surface [17, 31]. The problem of limited computer resources is compounded at higher frequencies, as more Yee cells are needed to sample the fields accurately [32].

Other disadvantages include the difficulty in quantifying errors and the use of non-perfect absorbing boundary conditions, that inevitably result in errors in the field strengths [33]. Gandhi [36] stated that the accuracy of FDTD has been shown to be within 5-10% of analytical or experimental values when using simple dipoles near spheres. Yu [30] modelled ten telephones with FDTD and produced results within 25% of experimental values. The FDTD method itself is based on three approximations [37], which produce small inaccuracies.

There are also stair-casing errors arising from constructing continuous curved surfaces out of a series of finite cubes [14]. The effects of building the eye from 1mm and 2mm cubic Yee cells are shown in Figure 1.1. The stair-casing approximation becomes more accurate as the cell size decreases. In the limit of infinitesimal Yee cells the model is continuous and the object is more accurately represented, albeit with severe increases to computational costs.

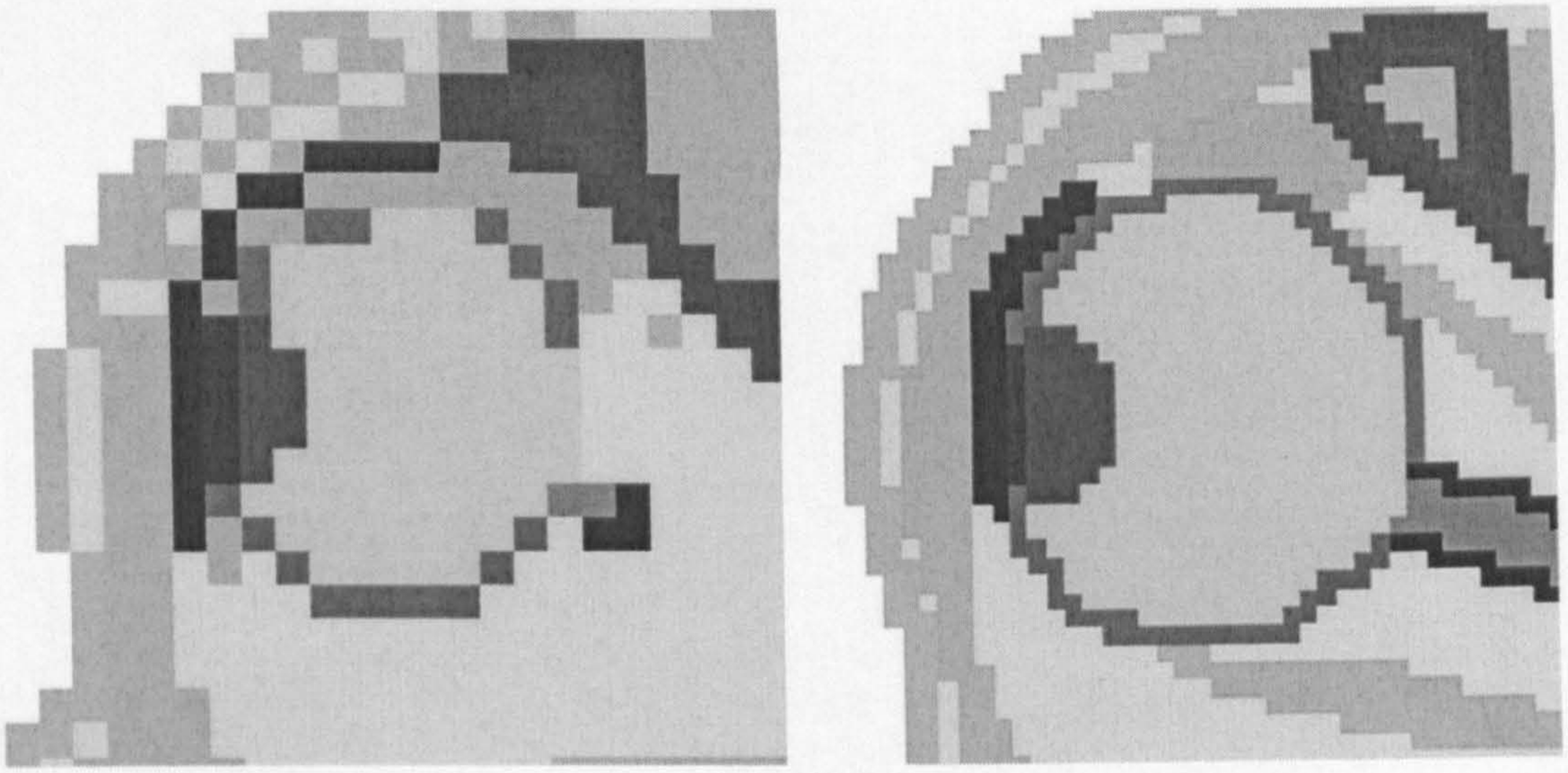

Figure 1.1. The eye composed of Yee cells, at 2mm (left) and 1mm (right) resolutions.

Errors exist in the accuracy of the FDTD method in modelling both the source and the phantom. Problems with modelling the source include; antenna distance to the head which varies from user to user [13], the geometry of the internal components of the phone [29], the position of the hand relative to the antenna [38], Tinniswood [32] mentioned problems modelling the thin dielectric coating and suggested that the phones were not metalised enough and electromagnetic (EM) waves could penetrate into the box and cause resonance with the circuit boards and other internal components. Nikita [33] commented on the difficulty in accurately building a source out of Yee cells and stated that the position of the source compared to the head was very important. Schiaviani [27] reported errors associated with the alignment of the phone and the head. There are also problems with modelling the head accurately in Yee cells [27, 33, 35] and the flexibility of the shape of the ear also causes uncertainties for mobile phones [39]. Errors due to discrepancies in the values of dielectric constants assigned to

the body have been documented [33, 35, 40, 41]. Gandhi [36] reported that conductivity and relative permittivity could be up to 100% higher in young children and showed that peak SAR averaged over 1g and 10g could be increased by 68% at 1900MHz due to the higher conductivity.

1.4 Realistic and geometric phantoms

There have been many published papers in the last few years using FDTD to investigate the amount of energy absorbed by biological matter especially from mobile phones. These absorption models include simple homogenous shapes such as cubes and spheres [24, 42], realistically shaped but homogeneous heads [28] and realistic heterogeneous heads with up to 37 different tissues [43]. In this thesis, a realistic head is defined as one that contains more detail than a simple geometric shape to replicate the concave shape of the head, thereby including the nose, ears and eye sockets. It is found that a homogenous head overestimates the SAR compared to a heterogeneous head [28, 44]. A simple shape such as a sphere gives a reasonable order of magnitude answer but is not very accurate [28, 43, 45]. The whole human body has been modelled and excited with a plane wave [40, 43], however many papers [36, 46, 47] use the assumption that the wavelength of excitation is small compared to the human body and therefore the head can be considered on its own. Dimbylow [48] showed this assumption was valid to within 1% above 600MHz. At 500MHz the absence of the body begins to become relevant. There has also been work, calculating the temperature rise in a body, that incorporates blood flow into the model [11].

Dimbylow [46] excited a heterogeneous phantom with a dipole and a simple box model of a mobile phone with a monopole antenna. Both vertical and horizontal orientations of phone were compared to a simple dipole antenna. He considered that a dipole provides a conservative estimate compared to a box-monopole phone model and that a dipole can be used advantageously as it reduces the run time required. The phone has been modelled using a monopole on different sizes of metallic box [38, 39, 44]. Lazzi [49] also modelled a helical antenna on top of a metal box. Tinniswood [32] modelled a more accurate phone by using CAD files and found that this extra level of detail in the phone model had little effect. Gandhi [36] concluded that a plastic-covered metal box provides a good approximation (±10%) of a real phone. Lazzi [29] tilted the head whilst the phone was kept in a vertical orientation. This produced a more realistic exposure geometry without inducing stair-casing errors modelling the source.

The hand holding the phone has also been modelled. Watanabe [38] found that the hand had little effect as long as it did not shield the antenna. Okoniewski [45] and Dimbylow [46] found that the presence of the hand decreased the SAR in the head at 900MHz, and Dimbylow [46] found the hand increased the SAR in the head at 1800MHz as the hand reflected energy back into the head. The hand in these examples was modelled as a simple block model and lacks realism. Kuster [50] measured the SAR in a phantom head with a real phone held by an actual hand. Negligible effects of the hand were found at both 900 and 1800MHz and he concluded that the hand should not be included in the computer model to produce realistic results. However, Anderson [51] also made measurements with a real hand holding a real phone and found that the hand increased the SAR in the head from 4 to 17%. The effect of the hand depended on the phone used.

1.5 Exposure from the front of the head

This section will briefly review studies exciting the head from the front, concentrating on the effects in the eyes. Taflove looked at the effect of a plane wave illuminating the eye using FDTD in 1975 [14], and observed hot spots forming in the centre of the eyes due to the resonance. However this model included little surrounding tissue so is not directly analogous to a real head. Moneda [52] used analytical techniques to position two spherical eyes inside a layered spherical head. Although this model is simplified compared to a real head, it showed that the absorption becomes more superficial and the total power absorbed in the head decreases as the frequency increases. Moneda [52] found a resonance in the eyes at 2.4GHz and showed the eyes absorb more energy when the excitation is from the front.

Dimbylow [53] excited the whole head with a plane wave in the frequency range 0.6 – 3.0GHz using a cell size of 3.2mm. The eyes were found to be areas with high levels of absorption compared to other areas of the head and exhibited signs of resonance when the size of the eye was approximately equal to 0.4 times the incident wavelength. Dimbylow also noted that there was a higher average SAR in a scaled down infant's eye compared to that of an adult, highlighting the differences for children exposed to electromagnetic waves.

Hirata has done various research concerning the eye, showing that resonance is caused by the geometric shape of the eye [54]. He noted that hot spots were formed in the eye between 900MHz and 3GHz. He concluded that the temperature increase was related to the average SAR and not the maximum SAR. However, the temperature increase in the eye of 0.3°C is within normal biological variations [15]. Closed eyelids were found to

reduce the average SAR by 15% at 5GHz. This is important as the digital head models can have closed eyelids. Increasing the size of the eye caused the resonance frequency to decrease. In a recent paper, the angle of incidence was varied [55]. As expected, moving the incoming plane wave to left or right relative to the nose increases the average SAR in the near eye and decreases it in the far eye. The average SAR in the eyes is generally reduced if the angle of incidence is above or below the horizontal.

Bernardi [16] exposed the eye, set in a truncated head model, to a plane wave from the front of the head but at a higher frequency range of 6 to 30GHz. He noted that, as the frequency increased, the maximum SAR increased but the average SAR in the eye fell. This is because, as frequency increases, the relative permittivity of human tissues decreases [17] causing better matching between the air and the eye. As the conductivity of the eye increases with frequency, the power will penetrate less deeply into the body and thus more energy is absorbed towards the front of the head [17]. This effect is augmented by the penetration depth decreasing with increasing wavelength [56].

The head has also been irradiated from in front of the eye using realistic mobile phone models [8, 13, 46] situated close to the eye in a walkie-talkie position, as shown in Figure 1.2. Dimbylow [46] modelled a monopole on a box to represent a phone positioned in front and also at the side of a realistic heterogeneous head. The highest SAR was found when the phone was positioned in front of the eye. Wainwright [13] used the finite element method with the Pennes 'bioheat equation' mechanism to investigate temperature increases in the head when excited with a transceiver held in front of the eye. The Pennes bioheat equation uses knowledge of the blood flow in the head to calculate the heat that is transported away by the blood flowing around the body. The maximum temperature increase in the brain was found to be 0.1°C.

Wainwright also considered the implications of the averaging volume used by the safety standards [13]. He noted that the heating of a long thin strip is likely to have lesser thermal consequences than heating a cubic or spherical shape as thermal clearance by conduction is more rapid due to the increased surface area.

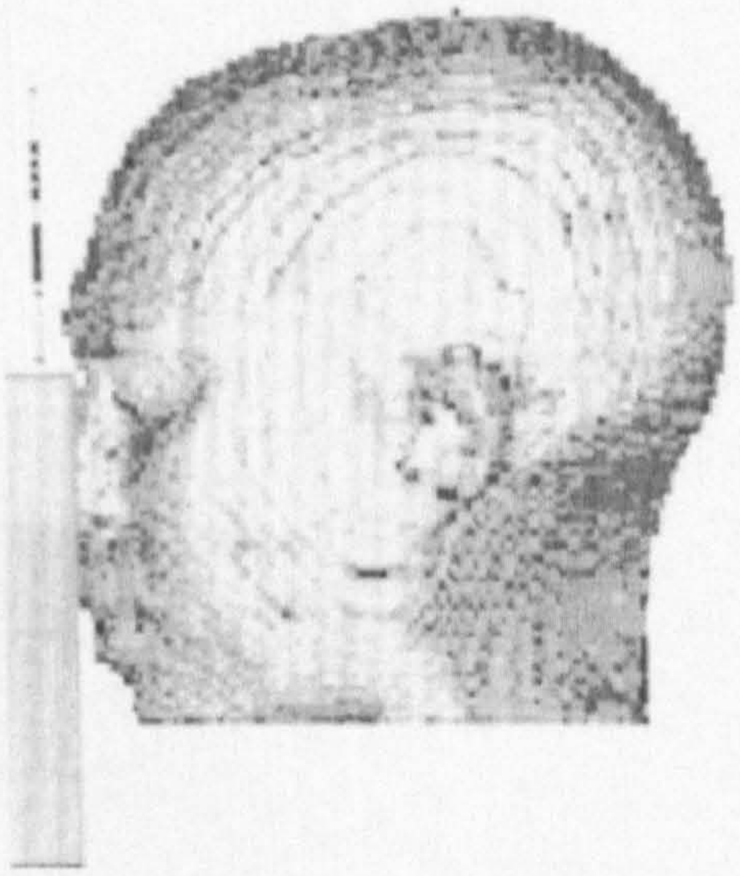

Figure 1.2. A head irradiated by a phone model in a 'walkie-talkie' position [46].

1.6 Sensitivity of the eyes

In 1998 Canada's federal health department proposed that the government adopt a separate, stricter limit for RF exposure of the eyes from cellular phones and walkie-talkies [57]. In 1999 a Royal Society of Canada panel concluded that eye research was a priority [57]. The eyes are considered to be particularly sensitive organs [16] due to their proximity to the surface, with no protective layer of skin. The eyes are particularly at risk to thermal damage as there is little blood flow to take heat away from the area [16] and, as there is negligible heat loss between the eyes and the surrounding tissues [14], the lens is also susceptible to cataract formation if there is a temperature rise of

3°C [17]. Lin [3] reviewed the possibility of cataract formation and showed that the temperature increases were too small to cause cataracts under normal conditions. Hirata [54] has done some work on this area and found that, at 1.9GHz, an incident power density of 22mW/cm² was enough to cause the 3°C temperature increase needed for cataract formation. This is larger than the maximum permissible exposure of 5mW/cm² [58, 59] by a factor of 4.4. This is a concern as this research will show that metallic spectacles can significantly increase the power absorbed by the eye. Dimbylow [46] also stresses the vulnerability of the eyes as they have a tendency to accumulate damage and cellular debris. The Stewart Report [1] noted that the fibres that make up the lens have only a limited capacity for self-repair. The eye is therefore at risk from both thermal and athermal effects.

The Stewart Report [1] includes a brief summary of experimental studies into RF effects on the eye and Elder produced a more detailed analysis [60]. They reported that pulsed RF fields at 2.45GHz, at moderate SAR levels, produced harmful effects in primates including lesions in the corneal endothelium and increased vascular leakage from the blood vessels of the iris. The threshold for these effects was dramatically reduced when the primates were pre-treated with ophthalmic drug timolol maleate. However, Elder [60] stated that these results had not been replicated and reported that they could be caused by other procedures or by repetitive use of drugs and anaesthetics.

In a small epidemiology study, Stang [61] found that users of walkie-talkies were over three times more likely to develop uveal melanoma, the most common type of eye cancer, and users of mobile phones were four times more likely. Holly [62] found a two-fold increase in uveal melanoma among subjects with occupational exposure to microwaves and radar units. However these were small studies with crude assessment

methodologies, and a cautious approach is advised in response to their findings [63]. Elder [60] was also sceptical about these results, referring to a study in Denmark where no increase in the incidence of eye cancer was found, despite the widespread use of mobile phones. In general, epidemiology studies have produced mixed results, showing a lack of repeatability and the Stewart Report [1] concluded that there was no evidence to link mobile phones to cancer. The Stewart Report [1] concluded that the eyes are at risk, especially from pulsed high powered sources. Other reasons for concentrating on the eyes are that they are the parts of the body with the highest SAR [53, 64]. And more power is absorbed in the eyes when irradiated from the front, as opposed to the side [52]. The frequency range used in this paper includes the resonance hot spot frequency range for the eyes considered to be above 1.5GHz [14] and less than 3GHz [14, 15, 52, 64]. It is also hypothesised that metallic spectacles can increase the SAR in the eye region, hence the eyes are considered to be especially at risk.

1.7 Research concerning the eyes

As previously mentioned, the eyes are considered to be vulnerable when the excitation is from the front; hence much of the research about eyes and microwave exposure has been covered in Section 1.5. At 30GHz, Bernardi [65] showed the absorption of energy was very superficial and that the modelling of the eyelids was very important. Simplified models of the head and eye excited by microwaves have also been briefly reported [64, 66, 67]. Heat transfer in human and rabbit eyes has also been mathematically modelled [68, 69]. Guy [70] showed that the threshold for cataract formation in rabbit eyes, which are anatomically similar to human eyes, is 3°C.

Berjano [71] used the finite element method to study cornea heating with RF currents used in medical applications. Lazzi [72] and DeMarco [73] used a 2-D FDTD model to investigate the induced SAR and temperature increase by an implanted retinal stimulator – a microchip designed to help a patient with limited vision. Temperature increases of up to 0.6°C in the midvitreous of the human eye have been found.

1.8 Metallic objects near humans

Tinniswood [32] considered the problem of wires and circuit boards becoming resonate structures inside a phone. It is therefore expected that other metal objects could also be resonant. A metallic object can be modelled in FDTD by setting a Yee cell to have very high conductivity or by setting the tangential electric field components to zero [33].

Burkhardt [9] reviewed the area of RF and human interaction and stressed the need to reduce the uncertainty that was associated with phantoms and modelling the head, including effects of jewellery and optical glasses. Meier has done some research into the area of metallic accessories [74] and this has been summarised by Kuster [50]: increased SAR values due to currents in the metallic objects were found if the source was positioned some distance from the head. Cooper [75] modelled a metal wall near a simple spherical head, discovering that it could increase the SAR averaged over 10g of tissue by 60%. He also noted that a dipole could couple to a metal wall, reducing its radiation resistance, therefore making the antenna radiate less efficiently. This results in the phone increasing its power to compensate. Bernardi [76] modelled a wall near a realistic heterogeneous head, finding that the power absorbed in the head could be increased by 86%. A vertical wall, parallel to a dipole antenna was found to increase the

SAR everywhere in the head. A horizontal wall increased the SAR in the eye, averaged over 1g, by four times. Glass walls (with conductivity $\sigma = 0$ and relative permittivity $\varepsilon_r = 4$) appeared to have little effect. Martinez-Burdalo [77] placed a metallic wall near a simple spherical head containing a spherical eye and noted increases in the SAR in the eye of up to 50%. Cooper [78] considered metal implantations inside the head, which resonated when the wavelength was roughly twice the size of the implantation. The effect was at its greatest when the metal implantation was parallel to the dipole. Increases in local SAR of up to 38 times were observed.

1.9 Metallic spectacles

Spectacles have received limited attention in the literature and the attention given to them is brief. This concludes to novelty in this thesis. Bernardi [16] investigated adding a glass lens in front of the eye in a 2-D FDTD model, and found that the lens could act as an adapter, increasing the power absorbed in the eye by up to 31%.

Troulis [79] used the FDTD method to briefly examine thin metallic spectacles with no lens on a heterogeneous phantom with a resolution of 5mm. The excitation used was a monopole on a metallic box positioned at the side of the head. The paper showed that metallic spectacles can re-distribute the energy produced by the cell phone's antenna, causing the efficiency to drop and the peak SAR to increase. Griffin [80] performed measurements with a phantom and metallic spectacles and showed that spectacles can increase or decrease the level of radiation near the eyes by up to 20dB due to shielding, enhancement and depolarisation effects. Anderson [51] also performed measurements

with a phantom wearing metallic spectacles. With phones operating at 835MHz next to the ear, the SAR in the eye closest to the phone was found to increase by up to 29%.

Wang [81] modelled a monopole on a metallic box positioned by the ear of a human head wearing spectacles at 1.5GHz using the FDTD method. Metallic spectacles were added by using Yee cells with the conductivity of titanium. The average SAR in the eye increased by up to 2.7 times. The electric fields were shown to be small in between the frames but enhanced just above the frames. Wang postulated that these enhancements in the SAR in the head were due to the current on the spectacles.

1.10 Genetic algorithms with electromagnetics

Chapter 5 of this thesis gives details of results of searches for the maximum and minimum effects of adding metallic spectacles to the digital head. The optimization technique used is a genetic algorithm (GA). As the name suggests, the genetic algorithm is a mathematical search tool which is based on Darwin's theory of evolution. In the natural world, animals are filtered by survival of the fittest. The animals which have the best capacity to survive, breed with each other and their favourable genes are passed onto the next generation. Random mutations also occur in nature to keep the population from converging and to remain diverse. This allows the species to cope with changes to the environment.

The last decade has seen the GA become a popular search tool in electromagnetics.

Haupt [82] and Johnson [83] have reviewed the use of GAs in this area. Many problems

have benefited by being optimised by a GA, including wire antennas, array design, FSS design, image reconstruction, microwave absorber design and patch antennas [83].

GAs are popular because they are robust stochastic search methods which are applicable to electromagnetic problems [83]. Random searches are slow [82]. Gradient methods converge quickly but require the calculation of gradients and knowledge is needed to guess the starting position, otherwise this search can get stuck in local minima [82]. GAs are global optimisers and therefore converge towards a global maximum regardless of the initial guess. GAs also have the advantage that they can handle both discrete and continuous parameters [83]. The convergence may be slower than with gradient methods but in electromagnetic-design problems, convergence rate is often not as important as getting to a solution [83].

1.11 Novel contributions

The research in this thesis concerns exciting a heterogeneous head with metallic spectacles from the front. This geometry has received limited attention in scientific journals; therefore the results without metallic spectacles, presented in this thesis, are valuable in consolidating previous research and in covering new areas. Horizontal and vertical polarisations of source are both investigated and can be compared. Two different anatomical heads are investigated allowing a direct comparison that has not previously been made with this geometry. The eyelids of the two different numerical heads have been opened, and the effects of this have been investigated over the frequency range of 0.5 to 5GHz. Previously the effects of opening eyelids has only been reported at the specific frequency of 5GHz [15] and 30GHz [65].

The major novelty of this research is the addition of metallic spectacles with the excitation positioned in front of the head. As mentioned in Section 1.9, a few journals have briefly considered the addition of spectacles but with the excitation predominantly at the side of the head. This work reports a novel geometry and thus is fundamentally different from the previous research concerning spectacles.

The research in this thesis covers many new aspects of the effects of spectacles that have not previously been considered even with the different excitation geometry. Different materials of the lens and the frames have been investigated. Previous research into spectacles has only considered one pair of spectacles. The results in this thesis will include many different shapes and sizes of both geometric and realistically shaped spectacles. The shape and size of the spectacles are found to be very important in determining their effects. Different positions of the spectacles have also been investigated. The effects of spectacles are compared on two different heads. Previous research has considered the effects of spectacles at one specific frequency, the research considered in this thesis will cover the range of 0.5 to 3.0GHz, therefore including many novel frequencies. Additionally, different sources with different polarisations are used.

A genetic algorithm (GA) will be employed to find the range of SAR that different spectacles can produce in the eye and in the head. The application of a GA to a bioelectromagnetics problem has not been previously reported in the literature and is therefore a novel application of a GA. The GA finds spectacles that both increase and decrease the SAR in the eye. This is interesting both in terms of finding the maximum effect of spectacles and investigating possible reductions in absorption.

This thesis also includes results of measurements with metallic spectacles. SAR measurements with the source positioned in front of a phantom head wearing spectacles, is a novel application. Computation and measurement results of the effects of spectacles are compared for the first time. An additional measurement setup has been made that allows the effects of spectacles to be measured thoughout the head. This is novel, as previously only the fields at a single point in the eye have been investigated.

1.12 An overview of this thesis

As stated earlier FDTD is the most popular computational tool used to investigate RF interaction with biological bodies and is the tool used in this thesis. Thus, Chapter 2 will give a brief summary of the theory and practicalities of the FDTD method. This chapter is needed as it provides the theoretical basis and explains how the electromagnetic waves propagate through the problem space and how the SAR is calculated.

Chapter 2 outlines the theory of FDTD which then needs to be applied accurately to more complicated structures. Chapter 3 will explain the application of the FDTD code to a detailed model of the human head. This chapter is important as it demonstrates how the work can be replicated. Chapter 3 provides details of the three anatomical heads considered and justifies the assumptions used in the model. These assumptions together with the head model will be validated against published results to show that all aspects of the code are accurate. As this thesis concentrates on the eyes, a specific validation of the SAR in the eyes is included. This extensive range of validations provides confidence in the FDTD model. Chapters 2 and 3 together explain the theory of the FDTD method and show that it has been applied to modelling the human head giving good results.

These two chapters provide the basis for allowing the code to be applied to novel applications.

The hypothesis of this thesis is that metallic spectacles worn close to the human face can increase the SAR in the head. To test this theory, metallic spectacles need to be added to the model of the head. The fourth chapter will explain in detail how the spectacles have been modelled. Results will show that the hypothesis is correct and that both geometric and realistically shaped spectacles can significantly affect the SAR in the head. Particular attention is given to the eyes, demonstrating that metallic spectacles can both increase and decrease the SAR in the eye.

Chapter 4 shows the effects of arbitrarily chosen spectacles. However further analysis is needed to investigate the entire range of spectacles that are possible. Chapter 5 will use a GA to search for maximal effects of spectacles on the SAR in the eye. Both minimum and maximum SAR in the eye will be considered. There will be a brief statistical analysis with a number of random spectacles. Different polarisations of plane wave and dipoles orientated in different directions will be considered. Two different numerical heads are compared to indicate the effects of the same spectacles on different people.

Chapter 3 includes results of validations of the FDTD code. However, the novel area of metallic spectacles can not be validated with previous works and thus the results need to be validated with an alternative method. Chapter 6 shows details of measurements of the effect of metallic spectacles positioned on a phantom filled with brain-simulating fluid. Different spectacles and different orientations of excitation are investigated, producing the same effects as found with the FDTD code. Thus the FDTD code and the measurements validate each other in this novel area of research.

A final chapter, Chapter 7, is included to summarise and conclude the research considered in this thesis.

1.13 References

1. Stewart, W., *Mobile Phones and health.* 2000, IEGMP.
2. Rahmat-Samii, Y., *Guest editorial, Special issue on wireless communications.* IEEE Trans. Antennas and Propagation, 1998. **46**(6): p. 745-747.
3. Lin, J., *Cataracts and cell-phone radiation.* IEEE Antennas and Propagation Magazine, 2003. **45**(1): p. 171-174.
4. Green, B.M. and M.A. Jensen, *Diversity performance of dual-antenna handsets near operator tissue.* IEEE Trans. Antennas and Propagation, 2000. **48**(7): p. 1017-1024.
5. Jensen, M.A. and Y. Rahmat-Samii, *Performance Analysis of antennas for hand-held transceivers using FDTD.* IEEE Trans. Antennas and Propagation, 1994. **42**(8): p. 1106-1113.
6. Lazzi, G., S.S. Pattnaik, C.M. Furse, and O.P. Gandhi, *Comparison of FDTD computed and measured radiation patterns of commercial mobile telephones in presence of the human head.* IEEE Transactions on Antennas and Propagation, 1998. **46**(6): p. 943-944.
7. Toftgard, J., S.N. Hornsleth, and J.B. Anderson, *Effects on portable antennas of the presence of a person.* IEEE Trans. Antennas and Propagation, 1993. **41**(6): p. 739-746.
8. Martens, L., J. Demoerloose, D. Dezutter, J. Depoorter, and C. Dewagter, *Calculation of the electromagnetic-fields induced in the head of an operator of a cordless telephone.* Radio Science, 1995. **30**(1): p. 283-290.
9. Stone, R.W., *The review of radio science 1996-1999*, ed. R.W. Stone. 1999, Oxford.
10. Moulder, J.E., L.S. Erdreich, R.S. Malyapa, J. Meritt, W.F. Pickard, and Vijayalaxim., *Cell phones and cancer: What is the evidence for a connection?* Radiation Research, 1999. **151**: p. 513-531.
11. Van Leeuwen, G.M.J., J.J.W. Lagendijk, B.J.A. Van Leersum, A.P.M. Zwamborn, S.N. Hornsleth, and A.N.T.J. Kotte, *Calculation of change in brain temperatures due to exposure to a mobile phone.* Physics in Medicine and Biology, 1999. **44**(10): p. 2367-2379.
12. Hirata, A. and T. Shiozawa, *Correlation of maximum temperature increase and peak SAR in the human head due to handset antennas.* IEEE Trans. Microwave Theory Techniques, 2003. **51**(7): p. 1834-1840.

13. Wainwright, P., *Thermal effects of radiation from cellular telephones.* Physics in Medicine and Biology, 2000. **45**: p. 2363-2372.

14. Taflove, A. and M.E. Brodwin, *Computation of the electromagnetic fields and induced temperatures within a model of the microwave-irradiated human eye.* IEEE Trans. Microwave Theory Technology, 1975. **23**(11): p. 888-896.

15. Hirata, A., S. Matsuyama, and T. Shiozawa, *Temperature rises in the human eye exposed to EM waves in the frequency range 0.6-6 GHz.* IEEE Transactions on Electromagnetic Compatibility, 2000. **42**(4): p. 386-393.

16. Bernardi, P., M. Cavagnaro, S. Pisa, and E. Piuzzi, *SAR distribution and temperature increase in an anatomical model of the human eye exposed to the field radiated by the user antenna in a wireless LAN.* IEEE Transactions on Microwave Theory and Techniques, 1998. **46**(12): p. 2074-2082.

17. Hirata, A., G. Ushio, and T. Shiozawa, *Calculation of temperature rises in the human eye exposed to EM waves in the ISM frequency bands.* IEICE Transactions on Communications, 2000. **E83B**(3): p. 541-548.

18. ICNIRP, *Health issues related to the use of hand-held radiotelephones and base transmitters.* Health Phys, 1996. **70**: p. 587-593.

19. ANSI/IEEE, *IEEE standard for safety levels with respect to human exposure to radio frequency fields 3kHz to 300GHz.* Standard C95.1-1992, 1992.

20. Stevens, N. and L. Martens, *Comparison of averaging procedures for SAR distributions at 900 and 1800 MHz.* IEEE Transactions on Microwave Theory and Techniques, 2000. **48**(11): p. 2180-2184.

21. Caputa, K., M. Okoniewski, and M.A. Stuchly, *An algorithm for computations of the power deposition in human tissue.* IEEE Antennas and Propagation Magazine, 1999. **41**(4): p. 102-107.

22. Bahr, A., S. Pan, T. Beck, R. Kastle, T. Schmid, and N. Kuster, *A comparison between numerical and experimental near-field evaluation of a DCS mobile telephone.* Radio Science, 1998. **33**(6): p. 1553-1563.

23. Lin, J., *Specific absorption rates (SARs) induced in head tissues by microwave radiation from cell phones.* IEEE Antennas and Propagation Magazine, 2000. **42**(5): p. 138-140.

24. Okano, Y., K. Ito, I. Ida, and M. Takahashi, *The SAR evaluation method by a combination of thermographic experiments and biological tissue-equivalent phantoms.* IEEE Transactions on Microwave Theory and Techniques, 2000. **48**(11): p. 2094-2103.

25. Balzano, Q., O. Garay, and T.J. Manning, *Electromagnetic energy exposure of simulated users of portable cellular telephones.* IEEE Trans. Vehicular Technology, 1995. **44**(3): p. 390-403.

26. Pokovic, K., T. Schmid, and N. Kuster, *Millimeter-resolution E-field probe for isotropic measurement in lossy media between 100MHz and 20GHz.* IEEE Trans. Instrumentation and Measurements, 2000. **49**(4): p. 873-877.

27. Schiavoni, A., P. Bertotto, G. Richiardi, and P. Bielli, *SAR generated by commercial cellular phones - Phone modeling, head modeling, and*

measurements. IEEE Transactions on Microwave Theory and Techniques, 2000. **48**(11): p. 2064-2071.

28. Hombach, V., K. Meier, M. Burkhardt, E. Kuhn, and N. Kuster, *The dependance of EM energy absorption upon human head modelling at 900 MHz.* IEEE Trans. Microwave Theory Technology, 1996. **44**(10): p. 1865-1873.

29. Lazzi, G., *Realistically tilted and truncated anatomically based models of the human head for dosimetry of mobile telephones.* IEEE Trans. Electromagnetic Compatability, 1997. **39**(1): p. 55-60.

30. Yu, Q.S., O.P. Gandhi, M. Aronsson, and D. Wu, *An automated SAR measurement system for compliance testing of personal wireless devices.* IEEE Transactions on Electromagnetic Compatibility, 1999. **41**(3): p. 234-245.

31. Lazzi, G., O.P. Gandhi, and D.M. Sullivan, *Use of PML absorbing layers for the truncation of the head model in cellular telephone simulations.* IEEE Transactions on Microwave Theory and Techniques, 2000. **48**(11): p. 2033-2039.

32. Tinniswood, A.D., C.M. Furse, and O.P. Gandhi, *Computations of SAR distributions for two anatomically based models of the human head using CAD files of commercial telephones and the parallelized FDTD code.* IEEE Transactions on Antennas and Propagation, 1998. **46**(6): p. 829-833.

33. Nikita, K.S., M. Cavagnaro, P. Bernardi, N.K. Uzunoglu, S. Pisa, E. Piuzzi, J.N. Sahalos, G.I. Krikelas, J.A. Vaul, P.S. Excell, G. Cerri, S. Chiarandini, R. De Leo, and P. Russo, *A study of uncertainties in modeling antenna performance and power absorption in the head of a cellular phone user.* IEEE Transactions on Microwave Theory and Techniques, 2000. **48**(12): p. 2676-2685.

34. Furse, C.M., J.Y. Chen, and O.P. Gandhi, *The use of the frequency-dependent finite-difference time-domain method for induced current and SAR calculations for a heterogeneous model of the human-body.* IEEE Transactions on Electromagnetic Compatibility, 1994. **36**(2): p. 128-133.

35. Sullivan, D.M., *A frequency-deendant FDTD method for biological applications.* IEEE Trans. Microwave Theory Technology, 1992. **40**(3): p. 532-539.

36. Gandhi, O. and G. Kang, *Some present problems and a proposed experimental phantom for SAR compliance testing of cellular telephones at 835 and 1900 MHz.* Physics in Medicine and Biology, 2002. **47**: p. 1501-1518.

37. Taflove, A., *Computational electrodynamics. The finite-difference time-domain method.* 1995: Artech House, Inc.

38. Watanabe, S., M. Taki, T. Nojima, and O. Fujiwara, *Characteristics of the SAR distributions in a head exposed to electromagnetic fields radiated by a hand-held portable radio.* IEEE Transactions on Microwave Theory and Techniques, 1996. **44**(10): p. 1874-1883.

39. Burkhardt, M. and N. Kuster, *Appropriate modeling of the ear for compliance testing of handheld MTE with SAR safety limits at 900/1800 MHz.* IEEE Trans. Microwave Theory Technology, 2000. **48**(11): p. 1927-1934.

40. Mason, P.A., W.D. Hurt, T.J. Walters, J.A. D'Andrea, P. Gajsek, K.L. Ryan, D.A. Nelson, K.I. Smith, and J.M. Ziriax, *Effects of frequency, permittivity and voxel size on predicted specific absorption rate values in biological tissue during electromagnetic-field exposure.* IEEE Trans. Microwave Theory Technology, 2000. **48**(11): p. 2050-2058.

41. Hurt, W.D., J.M. Ziriax, and P.A. Mason, *Variability in EMF permittivity values: Implications for SAR calculations.* IEEE Trans. Biomedical Engineering, 2000. **47**(3): p. 396-401.

42. Riu, P.J. and K.R. Foster, *Heating of tissue by near-field exposure to a dipole: A model analysis.* IEEE Transactions on Biomedical Engineering, 1999. **46**(8): p. 911-917.

43. Dimbylow, P.J., *FDTD calculations of the whole-body averaged SAR in an anatomically realistic voxel model of the human body from 1 MHz to 1 GHz.* Physics in Medicine and Biology, 1997. **42**(3): p. 479-490.

44. Gandhi, O., G. Lazzi, and C.M. Furse, *Electromagnetic absorption in the human head and neck for mobile telephones at 835 and 1900MHz.* IEEE Trans. Microwave Theory Technology, 1996. **44**(10): p. 1884-1897.

45. Okoniewski, M. and M.A. Stuchly, *A study of the handset antenna and human body interaction.* IEEE Transactions on Microwave Theory and Techniques, 1996. **44**(10): p. 1855-1864.

46. Dimbylow, P.J. and S.M. Mann, *SAR calculations in an anatomically realistic model of the head for mobile communication transceivers at 900-MHz and 1.8-GHz.* Physics in Medicine and Biology, 1994. **39**(10): p. 1537-1553.

47. Tinniswood, A., G. Lazzi, and O.P. Gandhi, *The use of the expanding-grid FDTD method for simulation of CAD-derived personal wireless telephones.* Microwave and Optical Technology Letters, 1999. **22**(1): p. 24-29.

48. Dimbylow, P.J., *Finite difference calculations of current densities in a homogenous model of a man exposed to extremely low frequencies.* Bioelectromagnetics, 1987. **8**: p. 355-377.

49. Lazzi, G. and O.P. Gandhi, *On modeling and personal dosimetry of cellular telephone helical antennas with the FDTD code.* IEEE Transactions on Antennas and Propagation, 1998. **46**(4): p. 525-530.

50. Kuster, N., R. Kastle, and T. Schmid, *Dosimetric evalution of handheld mobile communications equipment with known precision.* IEICE Transactions on Communications, 1997. **E80-B**(5): p. 645-652.

51. Anderson, V. and K.H. Joyner, *Specific absorption rate levels measured in a phantom head exposed to radiofrequency transmissions from analog hand-held mobile phones.* Bioelectromagnetics, 1995. **16**(1): p. 60-69.

52. Moneda, A.P., M.P. Ionnidou, and D.P. Chrissoulidis, *Analytical study of radiowave absorption by the brain and the eyes in an eccentric spheres model of the human head.* 11th International Conference on Antennas and Propagation, 2001: p. 774-778.

53. Dimbylow, P.J. and O.P. Gandhi, *Finite-difference time-domain calculations of SAR in a realistic heterogeneous model of the head for plane-wave exposure from 600MHz to 3GHz.* Physics in Medicine and Biology, 1991. **36**(8): p. 1075-1089.

54. Hirata, A., G. Ushio, and T. Shiozawa, *Formation of hot spots in the human eye for plane wave exposure.* Microwave Conference, 1999 Asia Pacific, 1999. **2**: p. 477-480.

55. Hirata, A., H. Watanabe, and T. Shiozawa, *SAR and temperature increase in the human eye induced by obliquely incident plane waves.* IEEE Trans. Electromagnetic Compatibility, 2002. **44**(4): p. 592-594.

56. Kraus, J.D., *Electromagnetics*. 4th ed. 1981.

57. Slesin, L., *German study: More eye cancer among mobile phone users.* Microwave News, 2001. **January/February**: p. 9.

58. ICNIRP, *Guidelines for limiting exposure to time-varying electric, magnetic and electromagnetic fields (up to 300GHz).* Health Phys, 1998. **74**: p. p. 494-522.

59. FCC, F.C.C. *Effects of radiofrequency radiation. ET Docket No.93-62*. 1996. Washington, DC.

60. Elder, J., A., *Occular effects of radiofrequency energy.* Bioelectromagnetics, 2003. **Supplement 6**: p. S148-S161.

61. Stang, A., G. Anastassiou, and W. Ahrens, *The possible role of radiofrequency radiation in the development of uveal melanoma.* Epidemiology, 2001. **12**(1): p. 7-12.

62. Holly, E.A., D.A. Aston, and D.K. Ahn, *Intraocular melanoma linked to occupations and chemical exposures.* Epidemiology, 1996. **7**: p. 55-61.

63. Inskip, P.D., *Frequent radiation exposures and frequency-dependent effects: The eyes have it.* Epidemiology, 2001. **12**(1): p. 1-4.

64. Hui, H., *Characteristics of the SAR distribution in homogeneous phantoms exposed to electromagnetic field radiated hand-held portable telephones.* Antennas, Propagation and EM Theory, 2000. Proceedings. ISAPE 2000. 5th International Symposium on , 2000, 2000: p. 664-667.

65. Bernardi, P., M. Cavagnaro, and S. Pisa, *Assessment of the potential risk for humans exposed to milimetre-wave wireless LANs: the power absorbed in the eye.* Wireless Networks, 1997. **3**: p. 511-517.

66. Mokhtech, K.E., G.Y. Delisle, and A.G. Roberge. *SAR mapping within the human eye due to portable transceivers. Electromagnetic Compatibility, 1994. Symposium Record. Compatibility in the Loop. IEEE International Symposium, 22-26 Aug. 1994*. 1994. Chicago, USA. p. 26-30

67. Loskovska, S. *EMF effects in human eye exposed to high frequency electromagnetic fields. Antennas and Propagation Society International Symposium, 2001. IEEE*. 2001. Boston, MA , USA. p. 84-87

68. Scott, J.A., *A finite element model of heat transport in the human eye.* Physics in Medicine and Biology, 1988. **33**(2): p. 227-241.

69. Lagendijk, J.J.W., *A mathematical model to calculate temperature distributions in human and rabbit eyes during hyperthermic treatment.* Physics in Medicine and Biology, 1982. **27**(11): p. 1301-1311.

70. Guy, A.W., J.C. Lin, and O.P. Kramar, *Effect of 2450MHz radiation on the rabbit eye.* IEEE Trans. Microwave Theory Techniques, 1975. **23**: p. 492-498.

71. Berjano, E.J., J. Saiz, and J.M. Ferrero, *Radio-frequency heating of the cornea: Theoretical model and in vitro experiments.* IEEE Trans. Biomedical Engineering, 2002. **49**(3): p. 196-205.

72. Lazzi, G., S.C. Demarco, W. Liu, J.D. Weiland, and M.S. Humayun, *Computed SAR and thermal elevation in a 0.25mm 2-D model of the human eye and head in response to an implanted retinal stimulator -Part II: Results.* IEEE Trans. Antennas and Propagation, 2003. **51**(9): p. 2286-2295.

73. Demarco, S.C., G. Lazzi, W. Liu, J.D. Weiland, and M.S. Humayun, *Computed SAR and thermal elevation in a 0.25mm 2-D model of the human eye and head in response to an implanted retinal stimulator -Part I: Models and methods.* IEEE Trans. Antennas and Propagation, 2003. **51**(9): p. 2274-2285.

74. Meier, K., *Scientific bases for dosimetric assesments in compliance tests.*, in *PhD Thesis, Diss. ETH Nr.11722*. 1996: Zurich.

75. Cooper, J. and V. Hombach, *The specific absorption rate in a spherical head model from a dipole with metallic walls nearby.* IEEE Transactions on Electromagnetic Compatibility, 1998. **40**(4): p. 377-382.

76. Bernardi, P., M. Cavagnaro, and S. Pisa, *Evaluation of the SAR distribution in the human head for cellular phones used in a partially closed environment.* IEEE Transactions on Electromagnetic Compatibility, 1996. **38**(3): p. 357-366.

77. Martinez-Burdalo, M., L. Nonidez, A. Martin, and R. Villar, *FDTD analysis of the maximum SAR when operating a mobile phone near a human eye and a wall.* Microwave and Optical Technology Letters, 2001. **28**(2): p. 83-85.

78. Cooper, J. and V. Hombach, *Increase in specific absorption rate in humans from implantations.* Electronic Letters, 1996. **32**(24): p. 2217-2219.

79. Troulis, S.E., W.G. Scanlon, and N.E. Evans. *Effect of 'hands-free' leads and spectacles on SAR for a 1.8 GHz cellular handset. 1st Joint IEI / IEE Symposium on Telecommunications Systems Research.* 2001. Dublin. p. 1675-1684

80. Griffin, D.W., *A microwave antenna method of measuring the effect of metal-framed spectacles on microwaves near the eye.* Antennas and Propagation Society International Symposium, 1983. **21**: p. 253-256.

81. Wang, J., T. Joukou, and O. Fujiwara, *Localized specific absorption rate in the human head in metal-framed spectacles for 1.5GHz Hand-held mobile telephones.* Trans IEE of Japan, 1998. **118-A**(11): p. 1234-1240.

82. Haupt, R.L., *An introduction to genetic algorithms for electromagnetics.* IEEE Antennas and Propagation Magazine, 1995. **37**(2): p. 7-15.

83. Johnson, J.M. and Y. Rahmat-Samii, *Genetic algorithms in engineering electromagnetics.* IEEE Antennas and Propagation Magazine, 1997. **39**(4): p. 7-25.

Chapter 2

THE FDTD METHOD

2.1 Introduction

This chapter covers some of the basics of the FDTD method. The derivation of the FDTD equations from Maxwell's equations is shown. This allows an electromagnetic wave to travel throughout the grid. Both dipole and plane wave excitations are considered. Details are included about the modelling of dielectric materials and the calculation of SAR. Also covered is a method of terminating the grid with absorbing boundary conditions so the system can be modelled in free space.

2.2 History and applications of FDTD

The FDTD technique has found many areas of use, modelling such varied electromagnetic problems as microchips and the radar cross-section of fighter aircraft [1]. The origin of FDTD is widely credited to Yee's paper [2] in 1966 implementing interleaved electric and magnetic field components in a Cartesian grid and derived their equations from Maxwell's curl equations. However, Yee himself was unaware of the potential worth of this discovery and the technique was ignored until Taflove discovered it in an old journal. In 1975 Taflove published a paper [3] with details of the numerical stability criteria and implemented it into a 3-D grid. In 1980 Taflove coined the term FDTD [4]. However problems remained with the method that restricted its popularity.

Computers were not advanced enough to be able to handle the amount of calculations needed and there existed no way of terminating the problem space without causing reflections from the outgoing waves. This was important as it meant an object could not be modelled in free space. In 1981 this problem was solved by Mur [5] who invented Mur's second order absorbing boundary conditions (ABCs). This new development and ever-improving computers increased the popularity of FDTD. In 1990 Maloney [6] and Katz [7] introduced the modelling of simple antennas. In 1994 Berenger [8] presented a new absorbing boundary condition which was an order of 40dB better than Mur's ABC [1]. This allowed problems in open space to be modelled with greater accuracy as the unphysical errors from the boundary reflections were reduced.

2.3 Maxwell's equations

There are four equations that can be used to describe the behaviour of electromagnetic fields in a source-free region of space. Collectively these have become known as Maxwell's equations, shown in differential form in (2-1) to (2-4):

From Faraday's law $$\frac{\partial \vec{B}}{\partial t} = -\nabla \times \vec{E} - \vec{J}_m \qquad (2\text{-}1)$$

From Ampere's law $$\frac{\partial \vec{D}}{\partial t} = \nabla \times \vec{H} - \vec{J}_e \qquad (2\text{-}2)$$

Gauss's Law for E-field $$\nabla . \vec{D} = 0 \qquad (2\text{-}3)$$

Gauss's Law for H-field $$\nabla . \vec{B} = 0 \qquad (2\text{-}4)$$

where H is the magnetic field intensity (A/m); E is the electric field intensity (V/m); B is the magnetic flux density (W/m²); D is the electric flux density (D/m²); J_m is the magnetic current (V/m²); J_e is the electric current (A/m²). Assuming the materials are linear, isotropic and non dispersive, the relationships in (2-5) and (2-6) apply:

$$\vec{B} = \mu\vec{H} \tag{2-5}$$

$$\vec{D} = \varepsilon\vec{E} \tag{2-6}$$

where μ is the magnetic permeability (H/m); ε is the electric permittivity (F/m) and using a loss mechanism to allow energy to be converted into heat, magnetic and electrical currents can be included, see (2-7) and (2-8):

$$\vec{J}_m = \rho'\vec{H} \tag{2-7}$$

$$\vec{J}_e = \sigma\vec{E} \tag{2-8}$$

where σ is the conductivity (S/m) and ρ' is the magnetic resistivity (Ω/m). For lossless materials $\rho' = \sigma = 0$.

Substituting (2-5) to (2-8) into (2-1) and (2-2) and rearranging produces six partial differential equations (PDEs) for each Cartesian field components. The equation for E_z is shown in (2-9). The other five equations are listed in Appendix A.

$$\frac{\partial E_z}{\partial t} = \frac{1}{\varepsilon}\left(\frac{\partial H_y}{\partial x} - \frac{\partial H_x}{\partial y} - \sigma E_z\right) \tag{2-9}$$

2.4 The Yee algorithm

Two texts on FDTD are [1, 9]. Yee [2] split the electric and magnetic field into their three Cartesian components forming a discretised 3-D space lattice. This is shown in the Yee cell in Figure 2.1, which forms the structure of FDTD.

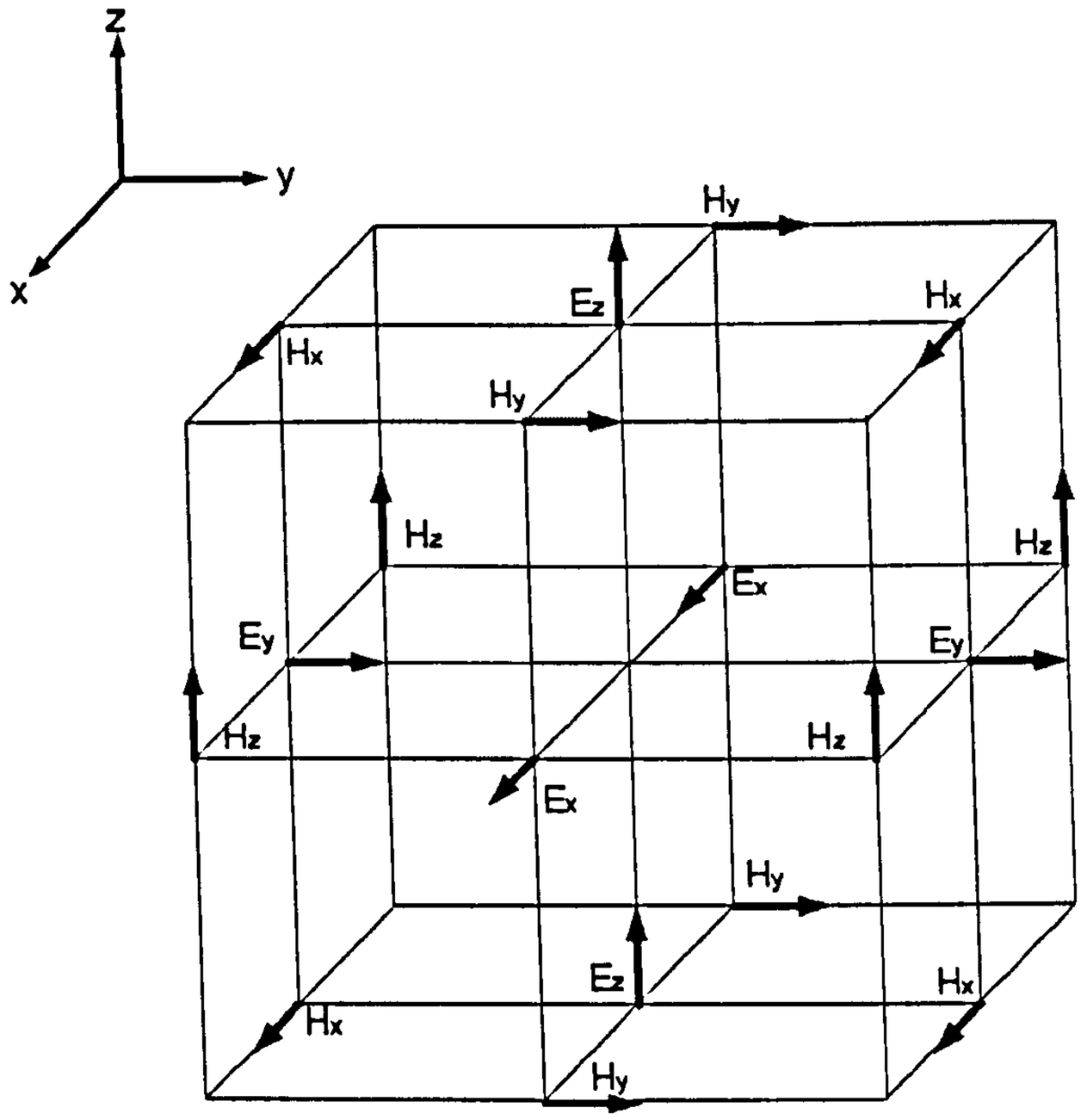

Figure 2.1. The Yee cell.

Many of these Yee cells then tessellate together to fill the entire problem space. The problem space is defined as being the region inside the ABCs. The size of the Yee cell, $\Delta x \times \Delta y \times \Delta z$ is small relative to the object of interest, for example Tinniswood [10] uses about a million of these Yee cells to model the human head. It should be noted that each electric field component is surrounded by four magnetic field

components. Likewise, four circulating electric field components surround each magnetic field component. This idea is crucial to FDTD as it means the electric and magnetic fields can be calculated using separate equations yet still interact with each other. The new field component is related to its old value at a previous time step and to the four circulating components. The electric and magnetic fields are calculated at alternate half time step intervals and are said to leapfrog each other in time. This process is continued until the variations in the field components are due entirely to the oscillating excitation and thus stability has been achieved. The whole FDTD process can be more clearly seen in the flowchart in Figure 2.2.

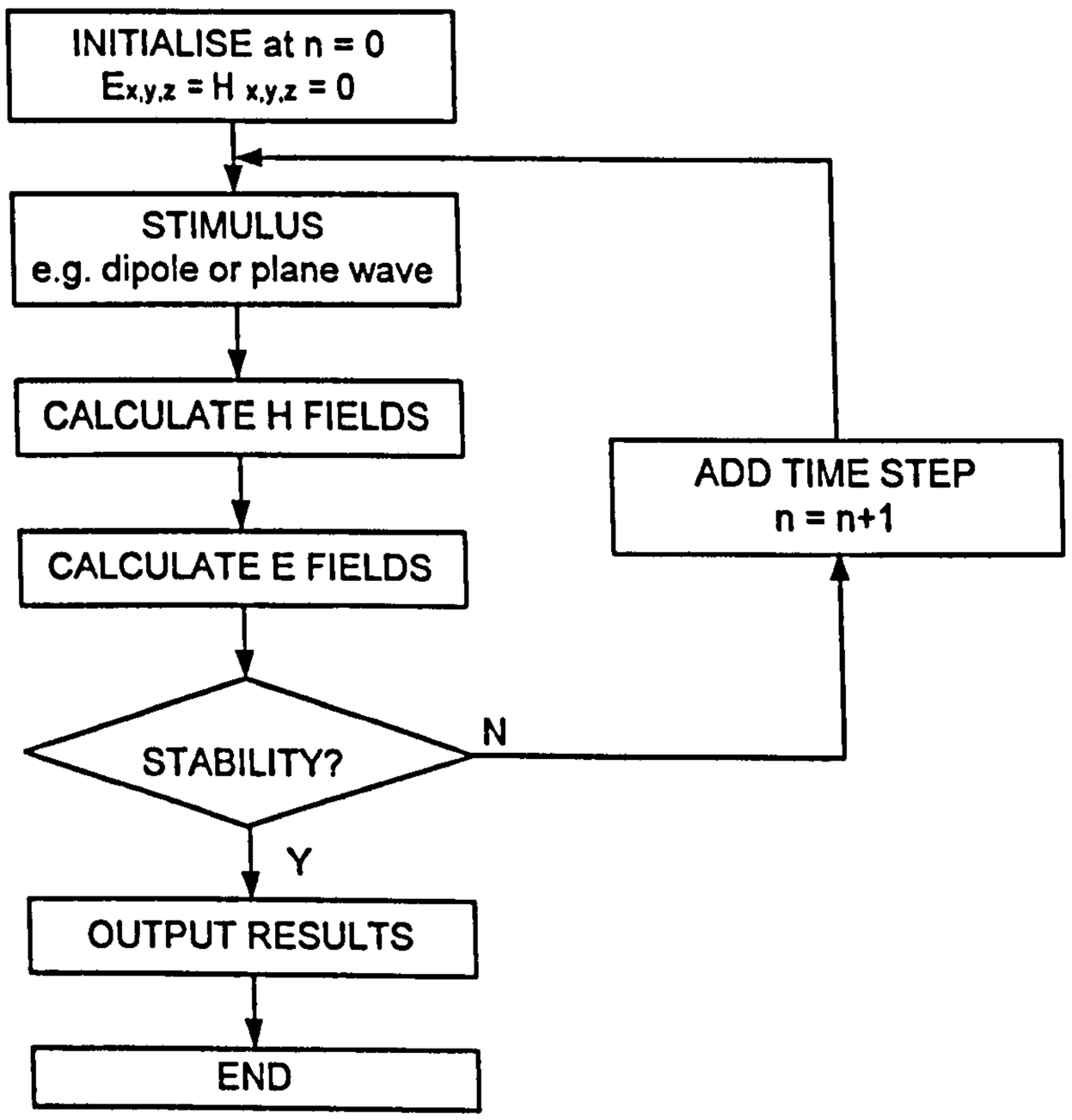

Figure 2.2. The Flowchart of FDTD iteration.

The six PDE expressions of (2-9) are still in their differential form and are not readily accessible. This is rectified by replacing both the space and time derivatives with finite differences. These two approximations are the basis of the FDTD

technique and allow Maxwell's equations to become discrete in space and time. The Finite difference expressions for space and time are listed in (2-10) and (2-11). These two equations represent the partial differentials in time and space of an arbitrary function u. They are second order accurate, and the accuracy of the approximation increases as the space and time increments decrease.

$$\frac{\partial u}{\partial x}(i,j,k,n) \cong \frac{u^{n}_{i+1/2,j,k} - u^{n}_{i-1/2,j,k}}{\Delta x} \tag{2-10}$$

$$\frac{\partial u}{\partial t}(i,j,k,n) \cong \frac{u^{n+1/2}_{i,j,k} - u^{n-1/2}_{i,j,k}}{\Delta t} \tag{2-11}$$

The notation that Yee introduced uses (i, j, k) as the position of the field component in the grid, where i, j and k are integer multiples of the size of an individual Yee cell, Δx, Δy and Δz respectively. The n subscript refers to the time step at which the field is to be calculated. The total time elapsed at time step n, is the multiple of the number of time steps, n and the size of the time step Δt.

Substituting the finite difference expressions, (2-10) and (2-11), into the six partial differential equations, (2-9), results in the formation of six new equations. (2-12) is the equation for E_z; the other five have a similar structure and are listed in Appendix B.

$$\frac{E_z\big|^{n+1}_{i,j,k} - E_z\big|^{n}_{i,j,k}}{\Delta t} = \frac{1}{\varepsilon_{i,j,k}}\left(\frac{H_y\big|^{n+1/2}_{i+1/2,j,k} - H_y\big|^{n-1/2}_{i-1/2,j,k}}{\Delta x} - \frac{H_x\big|^{n+1/2}_{i,j+1/2,k} - H_x\big|^{n+1/2}_{i,j-1,2,k}}{\Delta y} - \sigma_{i,j,k} E_z\big|^{n+1/2}_{i,j,k}\right) \tag{2-12}$$

Notice that the electric fields are calculated at integer time steps and magnetic fields at quadrature time steps. Examining the last term on the right hand side of (2-12), the

value of E_z is required at time step $n+1/2$. However, the electric fields are never known at half integer time steps due to the leapfrogging in time. This problem can be resolved by using another approximation. The field value at the unknown time step can be estimated by taking the average of the two field values, half a time step either side of the field value at the unknown time step as in (2-13).

$$E_z\Big|_{i,j,k}^{n+1/2} \equiv \frac{E_z\Big|_{i,j,k}^{n} + E_z\Big|_{i,j,k}^{n+1}}{2} \tag{2-13}$$

Use of the approximation (2-13) completes the derivation of the six FDTD equations. The E_z equation is shown in (2-14) and the other five are shown in Appendix C.

$$E_z\Big|_{i,j,k}^{n+1} = \left(\frac{1-\frac{\sigma_{i,j,k}\Delta t}{2\varepsilon_{i,j,k}}}{1+\frac{\sigma_{i,j,k}\Delta t}{2\varepsilon_{i,j,k}}}\right) E_z\Big|_{i,j,k}^{n} + \left(\frac{\frac{\Delta t}{\varepsilon_{i,j,k}}}{1+\frac{\sigma_{i,j,k}\Delta t}{2\varepsilon_{i,j,k}}}\right)\left(\frac{H_y\Big|_{i+1/2,j,k}^{n+1/2} - H_y\Big|_{i-1/2,j,k}^{n+1/2}}{\Delta x} - \frac{H_x\Big|_{i,j+1/2,k}^{n+1/2} - H_x\Big|_{i,j-1/2,k}^{n+1/2}}{\Delta y}\right) \tag{2-14}$$

The equation set (2-14) is known as the FDTD equations. The six field components are calculated using this set of six equations, throughout the problem space. Equation (2-14) shows that the field component is related to its previous value and the four surrounding components. The equation becomes much simpler in free space where the conductivity, σ, is zero and the relative permittivity, ε_r is one. The work in this thesis assumes that the materials are non-magnetic and therefore the coefficients in the H field equations can always be simplified.

2.5 Sampling and stability criteria

From the Nyquist theorem sampling must take place every $\lambda/2$ for the fields to be adequately sampled. Sampling in FDTD maps to the size of the Yee cell. As the FDTD method is based on approximations and is not exact, the space must be sampled more frequently than the Nyquist limit [9]. Reasonable results have been achieved with Δ as small as $\lambda/4$ [1] however it is usual to use at least ten cells per wavelength. In a dielectric material, $\varepsilon_r > 1$, the wave is compressed as the speed of light in a material is related to its permittivity and its permeability, see (2-15).

$$c = \sqrt{\frac{1}{\mu\varepsilon}} \tag{2-15}$$

Therefore, using $\lambda = c/f$, the wavelength will be reduced by a factor of $\sqrt{\varepsilon_r}$. In a material such as the human body, where $\varepsilon_r \approx 64$, the size of each side of the Yee cell should be of the order of 1/80 of the free space wavelength.

As FDTD works on the principle of nearest neighbour interaction, it is important for numerical stability that the wave does not propagate more than one Yee cell in each time period. This enforces a relationship between the size of the cell and the time step duration and is known as the Courant condition [1], see (2-16). In the case of the cubic Yee cell, where $\Delta x = \Delta y = \Delta z = \Delta$, this conditions simplifies to (2-17) using algebraic manipulation.

$$\Delta t \leq \frac{1}{c\sqrt{\frac{1}{(\Delta x)^2} + \frac{1}{(\Delta y)^2} + \frac{1}{(\Delta z)^2}}} \tag{2-16}$$

$$\Delta t \leq \frac{\Delta}{c\sqrt{3}} \tag{2-17}$$

In this research a cubic Yee cell is always used. Often the time step $\Delta t = \Delta/2c$ is chosen which means the EM wave propagates one Yee cell in free space every two time steps. This is the time step used in this research.

2.6 Incident wave source conditions

The previous sections in this chapter have outlined the Yee cell structure of the FDTD method and have derived the equations that relate the field values. Another important point, the excitation mechanism, is considered here. Initially, all field values are set to zero. By introducing a non-zero value to one field location and by applying the FDTD equation set (2-14) to all points in the grid, an electromagnetic wave will propagate throughout the grid from the incident point. The incident wave needs to accurately model the physics of an electromagnetic source. It is advantageous to make the source as compact as possible to reduce the computational requirements.

2.6.1 Half-wave dipole excitation

A commonly used source is a sinusoidal hard source dipole. A hard source is a field value that oscillates with a time dependence and is independent of anything else in the grid. A z directed electric field hard source, with a maximum amplitude of E_0, can be applied at position i, j, k using (2-18). This is a continuous sinusoidal source and (2-18) replaces the FDTD equation (2-14) at the source position.

$$E_z\,|^n_{i,j,k} = E_0 \sin(w\Delta t) \tag{2-18}$$

A metallic dipole can be modelled by forcing a line of electric field components to zero either side of the source position, as shown in Figure 2.3. This can be achieved by setting a line of E_z components to zero in the z direction for all time steps. This produces a z directed PEC dipole with zero tangential electric fields. A commonly used source is a half-wave dipole; this is produced in FDTD by setting the appropriate number of electric field components to zero. Both the source and the metallic dipole are hard sources and do not allow reflections to travel through the source position. Such reflections are termed retroreflections. These retroreflections are very small in a 3-D grid, because they intercept negligible fractions of the total energy in the grid and Taflove assumed that they can be ignored [1].

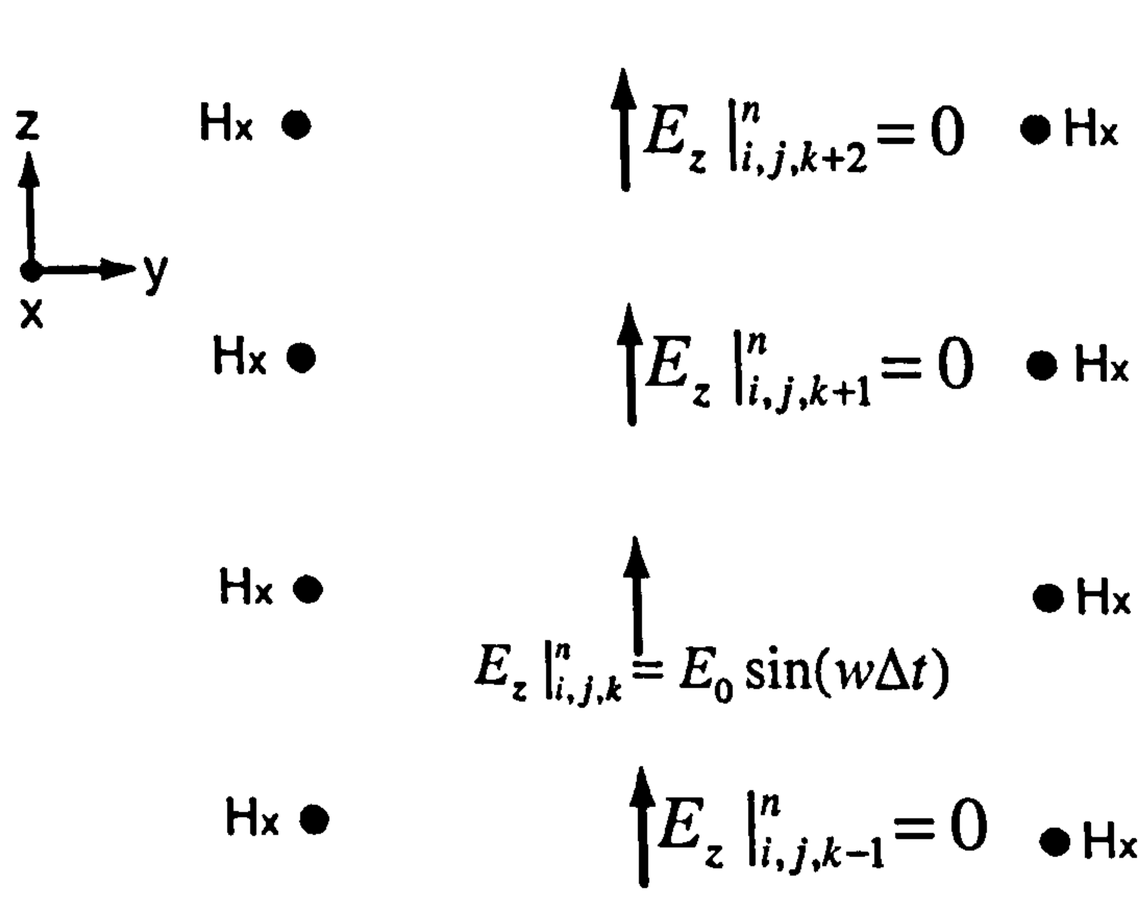

Figure 2.3. Setting the electric fields to zero either side of the source position to model a dipole excitation.

2.7 Representing the properties of materials in FDTD

As mentioned in Chapter 1, an advantage of FDTD is that it can handle complex heterogeneous shapes. Different properties can be assigned to each Yee cell such as permittivity, conductivity, permeability and magnetic resistivity. The Yee cell properties change the coefficients in the FDTD equation set (2-14). In this way, the properties of complex forms, for example the human head, can be mapped to the gridded Yee cells. Magnetic materials can also be modelled. However, in this work all materials will be assumed to be non-magnetic.

The FDTD method is a discontinuous method where each Yee cell has a finite size. The electric fields may be calculated at the interface of different materials and therefore the interfaces need to be assigned different electrical properties from the surrounding cells. In Figure 2.4 an E_z component is at the interface of four different materials.

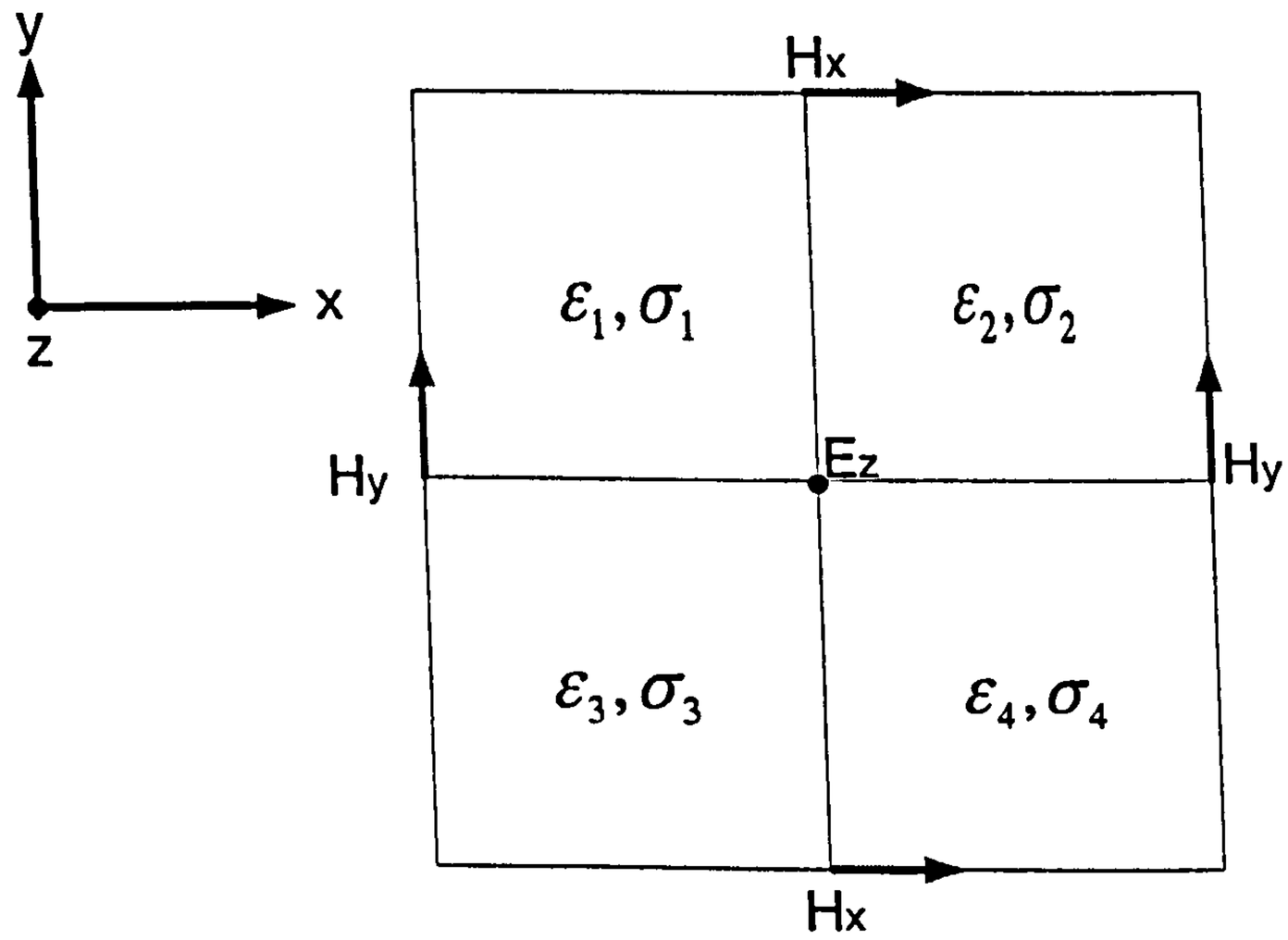

Figure 2.4. A 2-D cross section showing the interface of four different materials surrounding an *Ez* field component.

A smooth transition between cells is achieved by averaging the conductivity and permittivity by the values of materials in the four surrounding cells [11, 12]. The effective conductivity and relative permittivity at the *Ez* grid position in Figure 2.4 can be calculated using (2-19) and (2-20). These new values are then used to evaluate the coefficients in the FDTD equation set (2-14). Note that the effective properties will be different for all three Cartesian coordinates.

$$\sigma_{eff} = \frac{1}{4}(\sigma_1 + \sigma_2 + \sigma_3 + \sigma_4) \tag{2-19}$$

$$\varepsilon_{eff} = \frac{1}{4}(\varepsilon_1 + \varepsilon_2 + \varepsilon_3 + \varepsilon_4) \tag{2-20}$$

2.8 Algorithm for computations of EM absorption

Specific absorption rate (SAR), the standard criteria to measure the amount of electromagnetic energy absorbed in the body, is the power absorbed per unit mass. The SAR can be calculated by using the electric field strengths or the rate of temperature increase as shown in (2-21). This relation to the temperature increase is important as many biological effects are caused by the tissues being heated.

$$SAR = \frac{\sigma |E|^2}{\rho} = C\frac{\Delta T}{\Delta t_e} \quad \text{(W/Kg)} \tag{2-21}$$

Where $|E|^2$ is the root mean square of the electric field components, ρ is the density of the material (Kg/m^3) and σ is the conductivity (S/m). C is the specific heat (J/Kg·K), ΔT is the temperature increase (K) and Δt_e is the duration of the exposure (seconds). The

SAR is calculated with the twelve-field approach as used by Caputa [13]. This means that the SAR is calculated at a point at the centre of a cell bordered by twelve electric field components, hence each Ex, Ey and Ez component will be the average of four values. This is more accurate than just using three components in the same cell [13].

To compare results with the safety standards, SAR values need to be averaged over 1g and 10g. The SAR_{1g} and the SAR_{10g} are calculated, according to Caputa [13], using only head tissues - no air is included in the averaging cube. The exclusion of air in the averaging volume produces a lower SAR than including air or using irregular coherent volumes [14]. Wainwright [15] concluded that the averaging volume should be cubic, as thermal clearance by conduction is less rapid in a cubic volume. As only half the head has been considered the maximum SAR_{1g} and SAR_{10g} in the head have been calculated, assuming that the head is symmetric.

2.9 Absorbing boundary conditions - perfectly matched layer (PML)

Complications arise at the edge of the grid as at that point, there are no surrounding field components. One solution to this is to set either the electric fields or the magnetic fields to zero and effectively enclose the problem space within either a perfect electrical conductor or a perfect magnetic conductor. However, surrounding the space with either a PEC or PMC may cause reflections to re-enter the problem space and disturb the results. The size of the disturbance will be inversely related to the size of the grid. This is because the amplitude of the reflection decreases inversely with the distance squared. Therefore, to model an object in free space, a very large grid needs to be used, wasting

valuable computational time and memory. Even then, the results will include errors from the distant reflections.

An alternative method of terminating an FDTD grid is by using absorbing boundary conditions. By matching the impedance of the absorbing boundary to the impedance of free space, there are theoretically no reflections at this interface. Loss mechanisms, conductivity and magnetic resistivity are introduced to reduce the amplitude of the wave in the ABC region. Until 1994, techniques such as matched layers and Mur's absorbing boundary [5] gave reflections of the order of -40dB [1]. Berenger then introduced the perfectly matched layer (PML) [8] that improved the reflections by about 40dB to -80dB [1]. This improvement is due to the fact that Berenger introduced an extra degree of freedom by splitting each field component into two field components, e.g., Hz into Hzx and Hzy. This allowed the waves to be absorbed at different angles of incidence, not just at the normal, as was the case previously. Thus PML boundaries have been used in this research. The split field equations for E_{zx} and E_{zy} are shown in (2-22) and (2-23). The other ten equations are shown in Appendix D.

$$\varepsilon \frac{\partial E_{zx}}{\partial t} = \frac{\partial (H_{yz} + H_{yx})}{\partial x} - \sigma_x E_{zx} \tag{2-22}$$

$$\varepsilon \frac{\partial E_{zy}}{\partial t} = -\frac{\partial (H_{xy} + H_{xz})}{\partial y} - \sigma_y E_{zy} \tag{2-23}$$

Berenger [8], showed in 2-D and extended the idea to 3-D [16], that there is zero reflection when a wave is travelling, in the x direction, from free space to a PML medium with matched x components, $\sigma_x \quad \rho_x^{'}$. Thus there is zero reflection when condition (2-24) applies.

$$\frac{\sigma_x}{\varepsilon_0} = \frac{\rho'_x}{\mu_0} \tag{2-24}$$

Berenger used the notation PML(σ_x, ρ'_x, σ_y, ρ'_y, σ_z, ρ'_z) for a PML layer with those conductivities and magnetic resistivities. The same principle of a reflection null can be applied in the *y* and *z* directions and equation (2-24) must be applied to all three Cartesian components. Applying this to a 3-D problem space surrounded by PML allows the conductivities and magnetic resistivities to be known in all positions in the PML region, as shown in Figure 2.5 [16].

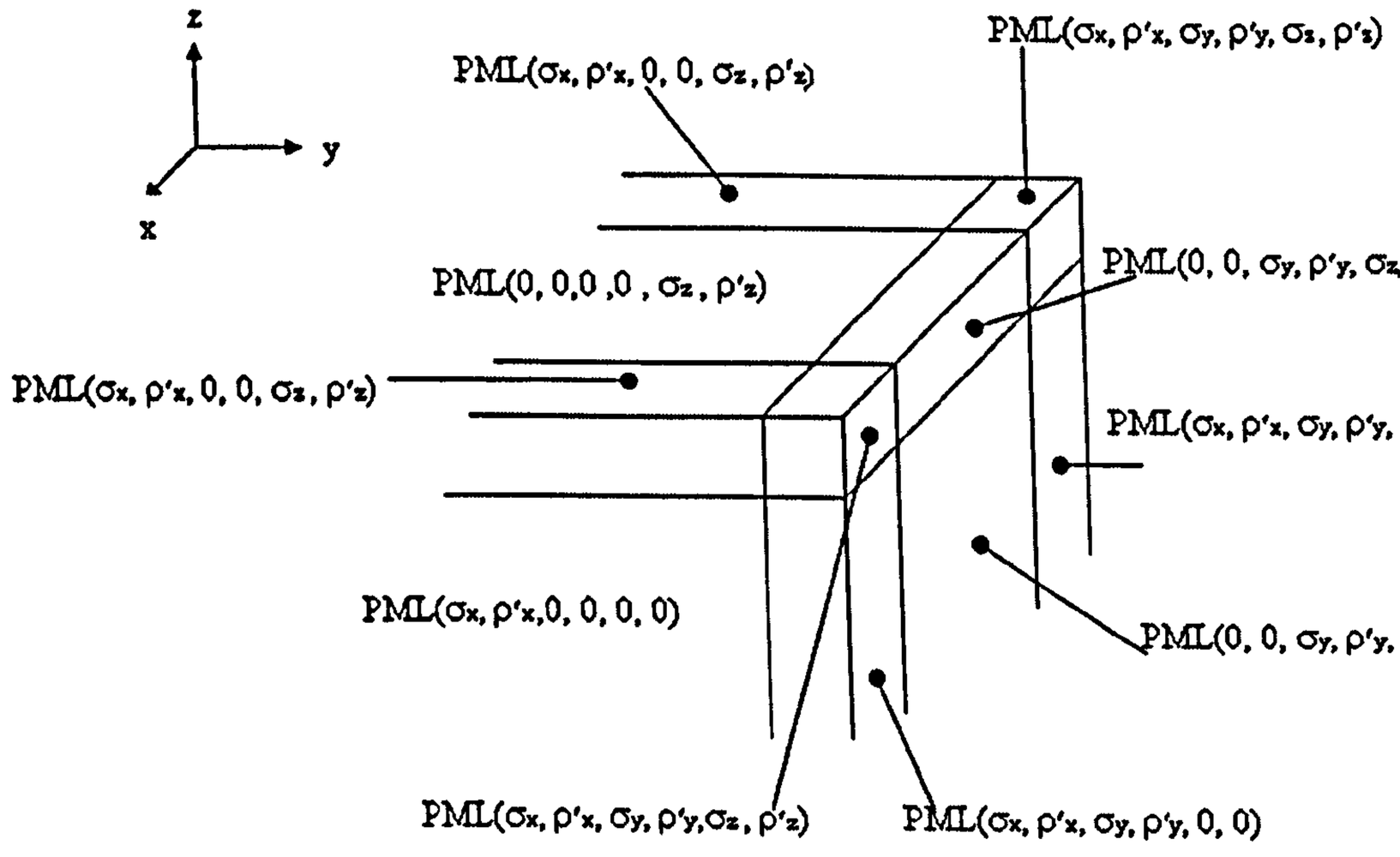

Figure 2.5. The location of conductivities and magnetic resistivities in the PML regions surrounding a corner of the FDTD grid.

It can be shown that the magnitude of the wave at distance *d*, inside a PML layer, can be given by (2-25) [8].

$$\psi(d) = \psi(0)\exp(-(\sigma\cos\vartheta/\varepsilon_0 c)d) \tag{2-25}$$

Here θ is the angle of incidence σ is the conductivity component in that region of PML and c is the speed of light. The PML region is terminated with a PEC which reflects the small fraction of the wave that has not been absorbed back through the PML region. The wave must make two traverses through the PML region, of thickness δ, before it is reflected back into the problem space. This results in a reflection factor [8] given by (2-26).

$$R(\vartheta) = \exp(-2(\sigma\cos\vartheta/\varepsilon_0 c)\delta) \tag{2-26}$$

Equation (2-26) exhibits one of the features of the PML technique, that if the incident wave is nearly parallel to the FDTD/PML interface, i.e. $\theta \approx \pi/2$, then the reflection factor is close to 1. This means that the wave is reflected back into the problem space before it has been absorbed by the PML. However, this does not create problems for the technique, as a wave incident nearly parallel to one boundary will be normal to the next boundary it encounters and will be consequently absorbed by it. This may, however, result in slight errors very close to the PML region.

A further point from regarding equation (2-26) is that the reflection factor is dependent on the product of the conductivity and the thickness of the PML region, so theoretically the PML can have any thickness. However, Berenger [8] noticed that there were reflections at the interface when there were sudden increases in the conductivity. This leads to the conclusion that the PML should be several cells thick with the conductivity increasing within the depth of the PML region. One solution to this is to use a linear conductivity profile, where the conductivity increases by a constant amount for each

cell into the PML region. An alternative to linear conductivity grading is geometric conductivity grading [17]. The conductivity profile of geometric grading is shown in (2-27). The equation is in terms of σ_x and Δx, which relate to the x-axis and are transposable to σ_y and σ_z in the other two dimensions.

$$\sigma_x(d) = \sigma_0\left(g^{1/\Delta x}\right)^d \tag{2-27}$$

σ_0 is the conductivity at the FDTD/PML interface, g is the ratio of conductivity from one cell to the next. This gives a reflection factor for an N layer PML region at normal incidence of (2-28).

$$R(0) = \exp(-(2/\varepsilon_0 c)((g^N - 1)/\ln g)\sigma_0 \Delta x) \tag{2-28}$$

Equation (2-28) can then be rearranged to find σ_0 as shown in (2-29).

$$\sigma_0 = -\frac{\varepsilon_0 c \ln g \ln R(0)}{2\Delta x(g^N - 1)} \tag{2-29}$$

The conductivity at the mesh points were implemented as the average value in the cell around grid point L as in (2-30).

$$\sigma_x(L) = \frac{1}{\Delta x}\int_{l(L)-\Delta x/2}^{l(L)+\Delta x/2}\sigma(u)du \tag{2-30}$$

From (2-27), (2-28) and (2-30) the conductivity at each grid position L inside the PML region where $L = 0, 0.5, 1, 1.5$ etc can be found from the equations (2-31) and (2-32). The conductivities are represented by three variables, reflectivity at normal incidence (%), $R(0)$, geometric factor, g and the number of layers in the PML region, N.

$$\sigma_x(0) = \sigma_0 \frac{\sqrt{g}-1}{\ln g} = \frac{\varepsilon_0 c(1-\sqrt{g})\ln R(0)}{2\Delta x(g^N-1)} \tag{2-31}$$

$$\sigma_x(L>0) = \sigma_0 \frac{g-1}{\sqrt{g}\ln g} g^L = \frac{\varepsilon_0 c(1-g)\ln R(0)}{2\Delta x\sqrt{g}(g^N-1)} g^L \tag{2-32}$$

Remembering from (2-24) that the magnetic resistivities still need to be matched to the conductivities by multiplying them by the ratio of the magnetic permeability divided by the electrical permittivity, μ_0 / ε_0. The magnetic resistivity must be calculated from the conductivity value offset in L by 0.5 from the electric field mesh points.

Berenger [1, 8, 18, 19] considered that the attenuation of the wave inside the PML layer was too rapid for standard time stepping to be used, and proposed the use of exponential time stepping. Using exponential time stepping gives twelve new equations for the PML region. The equation for E_{xy} is shown in (2-33). All twelve equations are listed in Appendix E.

$$E_{xy}\big|_{i,j,k}^{n+1} = \exp(-\sigma_y(j)\Delta t/\varepsilon)E_{xy}\big|_{i,j,k}^{n} + \frac{1-\exp(-\sigma_y(j)\Delta t/\varepsilon)}{\sigma_y(j)\Delta y}\begin{pmatrix} H_{zx}\big|_{i,j+1/2,k}^{n+1/2} + H_{zy}\big|_{i,j+1/2,k}^{n+1/2} \\ -H_{zx}\big|_{i,j-1/2,k}^{n+1/2} - H_{zy}\big|_{i,j-1/2,k}^{n+1/2} \end{pmatrix}$$

(2-33)

Note that the equation set (2-33) is similar to the FDTD set (2-14). Each new field component is calculated from its value at the previous time step and the nearest neighbour components. Also note that the split field components, e.g. Hzx and Hzy, are assumed to be at the same position in space. The E and H fields still leapfrog each other in time. There are also further points to consider for the field components on the

boundary between FDTD and PML regions. This can be most easily visualised and understood by referring to Figure 2.6.

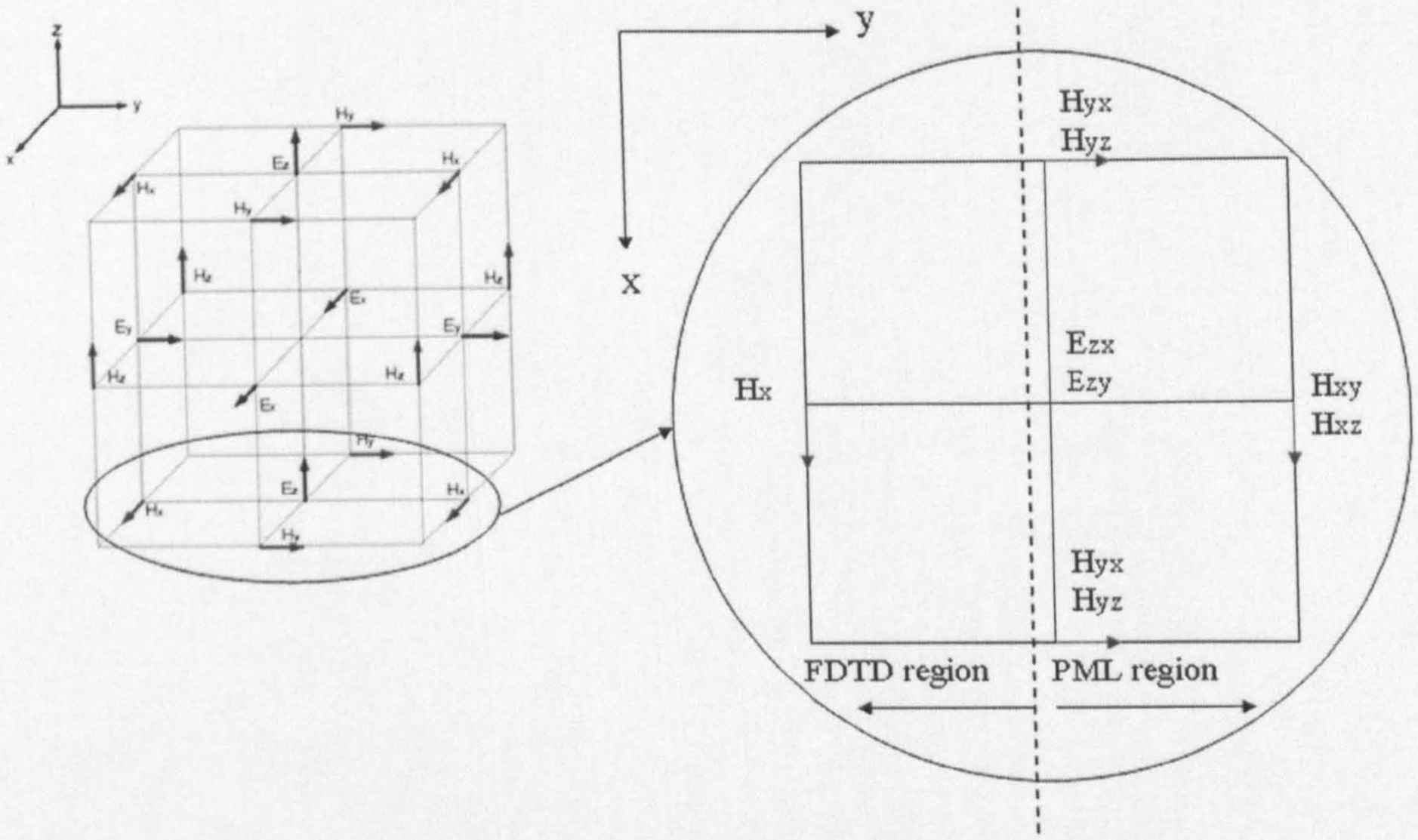

Figure 2.6. A 2-D section, of the Yee cell in Figure 2.1, in the *x*-*y* plane containing *Ez*, showing the components at the border between the FDTD problem space and the PML region in the *y* direction.

Figure 2.6 shows a 2-D section of a Yee cell at the FDTD/PML boundary when approached in the *y* direction. The split field components, E_{xy}, E_{zy}, H_{xy} and H_{zy}, calculated at positions where σ_y and $\rho_y^{'}$ are greater than zero, are calculated with the PML equations of (2-33). The other split field components in the PML region are calculated with the standard FDTD equations of (2-14) but with two sub-components, e.g. replacing H_z with $H_{zx} + H_{zy}$. Note that the equations contain the standard FDTD conductivities and magnetic resistivities. These are set to zero inside the PML region as

it is assumed that all materials are inside the problem space and not the PML region and hence the coefficients are simplified. Therefore the E_{zx} component in Figure 2.6 is calculated as in equation (2-34).

$$E_{zx}\Big|_{i,j,k}^{n+1} = E_{zx}\Big|_{i,j,k}^{n} + \frac{\Delta t}{\varepsilon_{i,j,k}} \left(\frac{H_{yx}\Big|_{i+1/2,j,k}^{n+1/2} + H_{yz}\Big|_{i+1/2,j,k}^{n+1/2} - H_{yx}\Big|_{i-1/2,j,k}^{n+1/2} - H_{yz}\Big|_{i-1/2,j,k}^{n+1/2}}{\Delta x} - \frac{H_{xy}\Big|_{i,j+1/2,k}^{n+1/2} + H_{xz}\Big|_{i,j+1/2,k}^{n+1/2} - H_{x}\Big|_{i,j-1/2,k}^{n+1/2}}{\Delta y} \right) \tag{2-34}$$

2.10 Testing the effectiveness of the PML technique.

One method of evaluating the reflections from the PML is by using two similar grids, one small PML bounded grid and one larger PEC backed grid. If the code is run for a limited number of time steps, the waves in the larger grid do not reach the PEC boundaries and therefore are not reflected. A small grid of size 50 x 50 x 50 cells including PML was compared to a larger PEC backed grid of size 100 x 100 x 100 cells. The frequency of excitation was 1.5GHz and the cell size was one twelfth of a wavelength. A half-wave dipole was positioned at the centre of both grids and was excited with a continuous sinusoidal source as in (2-18). The fields in the grid were calculated for 100 time steps to ensure the waves from the larger PEC grid are not reflected back into the problem space. The percentage error averaged over the whole problem space, P, was calculated at $n = 100$, using (2-35). Note Ez_{PEC} and Ez_{PML} are the electric field values in the large and small grids respectively.

$$P = \frac{1}{27000} \sum_{i=10}^{i=40} \sum_{j=10}^{j=40} \sum_{k=10}^{k=40} \frac{abs(Ez_{PML}\Big|_{i,j,k}^{100} - Ez_{PEC}\Big|_{i,j,k}^{100}) * 100}{Ez_{PEC}\Big|_{i,j,k}^{100}} \tag{2-35}$$

By varying g and $R(0)$, an average percentage error over the entire problem space of 0.023% was found with $g = 2.55$ and $R(0) = 0.00008$. The thickness of the PML was eight cells. This is a reasonable level of error and is likely to be much smaller than errors due to discretization of the problem space into cells and other FDTD errors [20]. Note that, if necessary, these errors can be reduced by increasing the number of layers, N, in the PML region at the expense of computational resources. The effects of reducing the thickness of the PML can be seen in Figure 2.7.

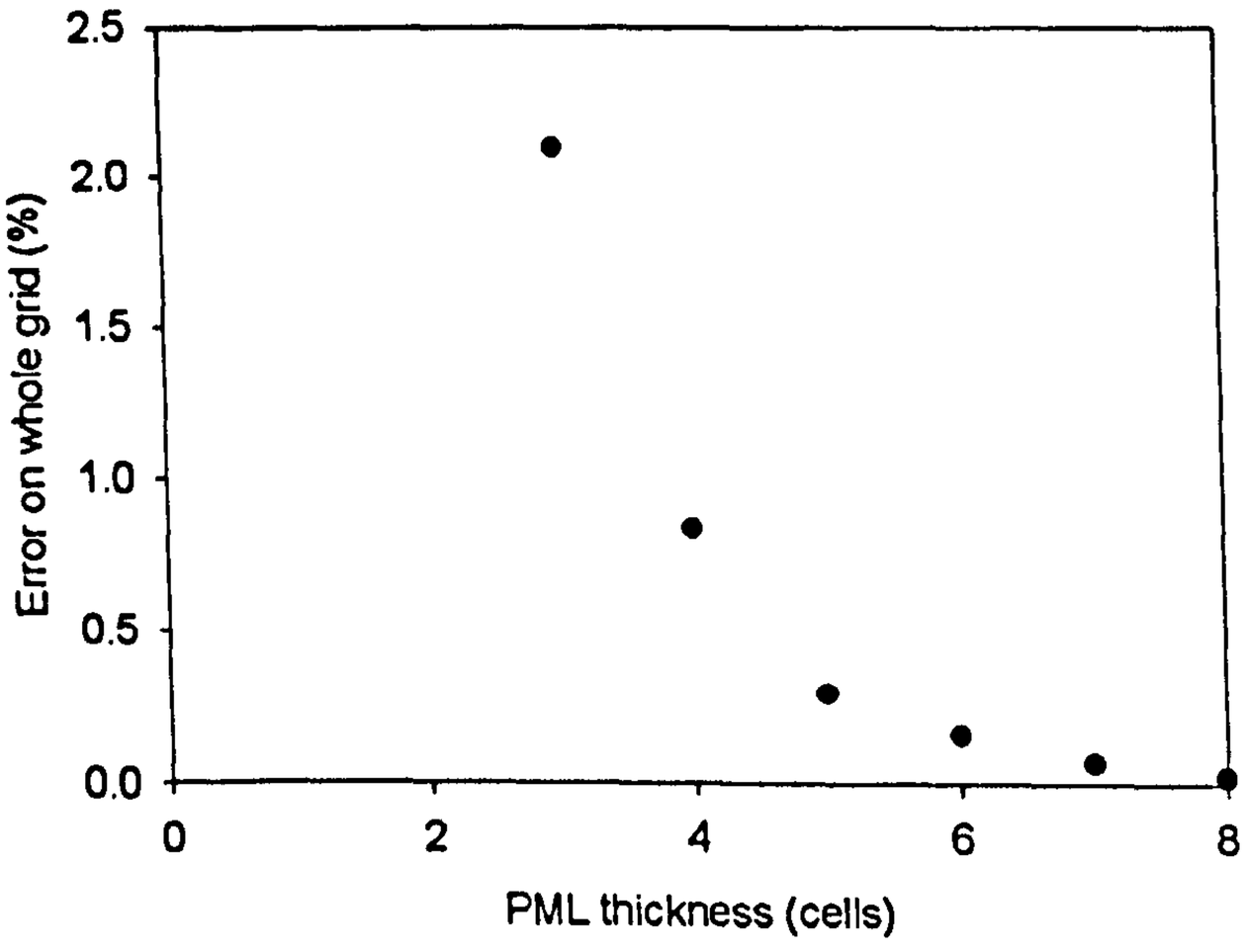

Figure 2.7. The Percentage error on the whole problem space as a function of the PML thickness. The PML uses g=2.55 and R(0)=0.00008.

The effectiveness of the PML absorbing boundary is reduced by reducing the depth, N, of the PML region. A compromise must be found between the amplitude of the reflections and the computational memory and time needed to calculate the fields in the region. Comparing the results from the PML testing program and a general comparison

with various thicknesses used in published papers [21, 22], eight layers was decided to be a reasonable compromise.

2.11 Total field / scattered field approach for plane wave excitation

An alternative excitation to the simple dipole model outlined above is a plane wave excitation. This choice of excitation is common as there are errors associated with modelling an individual source [20]. The plane wave is a well understood excitation and represents a source in the far-field. The total field / scattered field (TFSF) technique is an advantageous method of inserting an excitation into the grid, requiring minimal memory and computation space. The TFSF technique is outlined by Taflove [1]. The method relies on the linearity of Maxwell's equations and the fact that the electric and magnetic fields can be expressed as in (2-36) and (2-37)

$$\vec{E}_{tot} = \vec{E}_{inc} + \vec{E}_{scat} \tag{2-36}$$

$$\vec{H}_{tot} = \vec{H}_{inc} + \vec{H}_{scat} \tag{2-37}$$

This means the total E and H fields can be broken down into two components, the incident wave and the scattered wave. This property can be used to separate the grid into two distinct regions as shown in Figure 2.8.

The interacting structure lies entirely in the total field region. Region 2 contains only scattered fields and is terminated by PML to stop the scattered waves re-entering region 1. Regions 1 and 2 are separated by a virtual surface and are connected by twenty four equations, known as the connecting conditions. These are calculated at the interface

between the two regions, at i0, i1, j0, j1, k0 and k1 as in Figure 2.8. This thesis only uses a vertically polarised plane wave travelling in the x direction, with only E_z and H_y components. Therefore, there are no E_x, E_y, H_x or H_z incident field components and the connection conditions are reduced to the eight equations, listed in Appendix F.

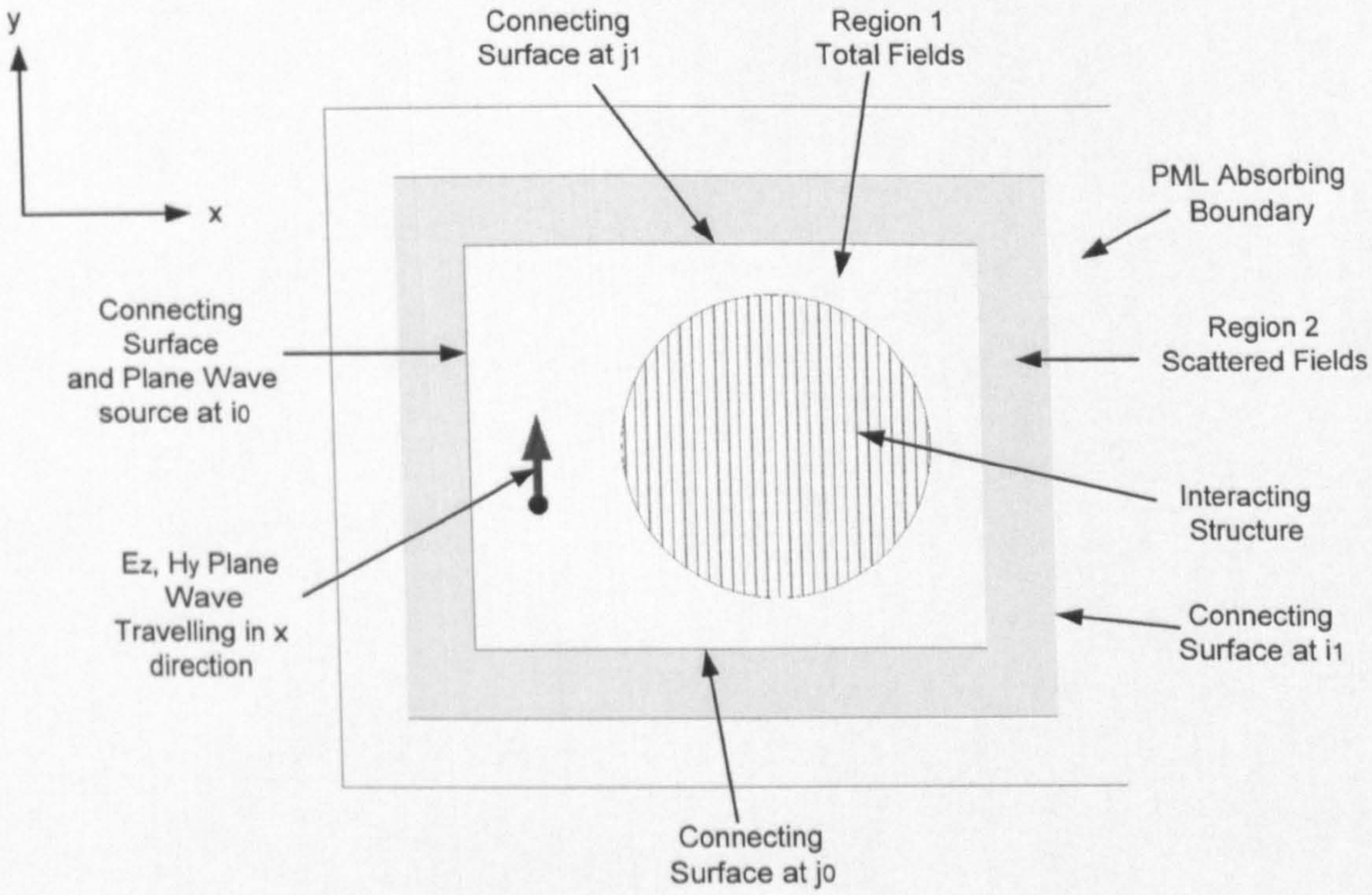

Figure 2.8. Total field and scattered field regions separated by a virtual connecting surface (plane wave source).

2.12 Applying symmetry

The work written up in this thesis attempts to model RF distributions in the head. The human head can be approximated as being symmetric and therefore it is advantageous to model only half the head. This research uses a half head mirrored across a centre plane that bisects the head vertically between the eyes through the nose, mouth and chin and extends all the way to the back of the head. Note that, in general, actual human

heads are not symmetric about this plane. For example, one eye may be slightly higher than the other and a nose may be somewhat bent. Recently, researchers also have evidence of brain torque (i.e. rightward frontal and leftward occipital asymmetry) in humans.

However, in FDTD models where the head is modelled as two identical mirrored halves, the two halves of the head are assumed to be identical. By this method the field values need not be calculated twice, thereby reducing computation time and memory requirements. This line of symmetry in the FDTD problem space can be achieved by replacing the mid-plane of the grid with a magnetic wall. Hirata has previously used this technique in published journals [23, 24].

2.13 Conclusions

This chapter has provided details of the independent FDTD code written for this research and referenced sources that provide more specific information. The derivation of the six FDTD equations from Maxwell's equations has been shown. The code will be validated in Chapter 3. Details of two stimulus conditions, plane wave and dipole, have been included, allowing a wave to propagate throughout the grid. In the model, dielectric materials can be inserted into the grid which represent the human body. Details of the power absorption algorithm have been discussed. PML absorbing boundary conditions have been outlined. Such PMLs allow a wave to be absorbed at the edges of the grid and effectively places the object in free space. Details have also been provided on how to utilise symmetry in the problem space.

2.14 References

1. Taflove, A., *Computational electrodynamics. The finite-difference time-domain method.* 1995: Artech House, Inc.
2. Yee, K.S., *Numerical solution of initial boundary value problems involving Maxwell's equations in isotropic media.* IEEE Trans. Antennas and Propagation, 1966. **14**: p. 302-307.
3. Taflove, A., *Numerical solution of steady-state electromagnetic scattering problems using the time-dependent Maxwell's equations.* IEEE Trans. Microwave Theory Technology, 1975. **23**: p. 888-896.
4. Taflove, A., *Application of the finite-difference time-domain method to sinusoidal steady-state electromagnetic penetration problems.* IEEE Trans. Electromagnetic Compatibility, 1980. **22**: p. 191-202.
5. Mur, G., *Absorbing boundary conditions for the finite-difference approximation of the time-domain electromagnetic field equation.* IEEE Trans. Electromagnetic Compatibility, 1981. **23**: p. 377-382.
6. Maloney, J.G., *Accurate computation of the radiation from simple antennas using the finite-difference time-domain method.* IEEE Trans. Antennas and Propagation, 1990. **38**(7): p. 1059-1068.
7. Katz, D.S., *FD-TD analysis of electromagnetic wave radiation from systems containing horn antennas.* IEEE Trans. Antennas and Propagation, 1991. **39**: p. 1203-1212.
8. Berenger, J.P., *A perfectly matched layer for the absorption of electromagnetic waves.* Journal of Computational Physics, 1994. **114**: p. 185-200.
9. Kunz, K., *The Finite-difference time-domain method in electromagnetics.* 1993.
10. Tinniswood, A.D., C.M. Furse, and O.P. Gandhi, *Computations of SAR distributions for two anatomically based models of the human head using CAD files of commercial telephones and the parallelized FDTD code.* IEEE Transactions on Antennas and Propagation, 1998. **46**(6): p. 829-833.
11. Hirono, T., Y. Shibata, W. Lui, S. Seki, and Y. Yoshikuni, *The second-order condition for the dielectric interface orthogonal to the Yee-lattice axis in the FDTD scheme.* IEEE Microwave and Guided Wave Letters, 2000. **10**(9): p. 359-361.
12. Marrocco, G., M. Sabbadini, and F. Bardatti, *FDTD Improvement by dielectric subgrid resolution.* IEEE Trans. Microwave Theory Techniques, 1998. **46**(12): p. 2166-2169.
13. Caputa, K., M. Okoniewski, and M.A. Stuchly, *An algorithm for computations of the power deposition in human tissue.* IEEE Antennas and Propagation Magazine, 1999. **41**(4): p. 102-107.
14. Stevens, N. and L. Martens, *Comparison of averaging procedures for SAR distributions at 900 and 1800 MHz.* IEEE Transactions on Microwave Theory and Techniques, 2000. **48**(11): p. 2180-2184.

15. Wainwright, P., *Thermal effects of radiation from cellular telephones.* Physics in Medicine and Biology, 2000. **45**: p. 2363-2372.

16. Berenger, J.P., *Three-dimensional perfectly matched layer for the absorption of electromagnetic waves.* Journal of Computational Physics, 1996. **127**: p. 363-379.

17. Berenger, J.P., *Perfectly matched layer for the FDTD solution of wave-structure interaction problems.* IEEE Transactions on Antennas and Propagation, 1996. **44**(1): p. 110-117.

18. Berenger, J.P., *Validation and extension to three dimensions of the Berenger PML absorbing condition for FDTD meshes.* IEEE Microwave and Guided Wave Letters, 1994. 4(8): p. 268-270.

19. Holland, R., *Finite-difference solution of Maxwell's equations in generalised nonorthogonal coordinates.* IEEE Trans. Nucl. Sci, 1983. **NS 30**: p. 4589-4591.

20. Nikita, K.S., M. Cavagnaro, P. Bernardi, N.K. Uzunoglu, S. Pisa, E. Piuzzi, J.N. Sahalos, G.I. Krikelas, J.A. Vaul, P.S. Excell, G. Cerri, S. Chiarandini, R. De Leo, and P. Russo, *A study of uncertainties in modeling antenna performance and power absorption in the head of a cellular phone user.* IEEE Transactions on Microwave Theory and Techniques, 2000. **48**(12): p. 2676-2685.

21. Lazzi, G. and O.P. Gandhi, *Inversion theory as applied to the optimisation of conductivity profile for PML absorbing boundary condition for FDTD code.* Electronics Letters, 1997. **33**(6): p. 502-503.

22. Gandhi, O.P., G. Lazzi, A. Tinniswood, and Q.S. Yu, *Comparison of numerical and experimental methods for determination of SAR and radiation patterns of handheld wireless telephones.* Bioelectromagnetics, 1999: p. 93-101.

23. Hirata, A., S. Matsuyama, and T. Shiozawa, *Temperature rises in the human eye exposed to EM waves in the frequency range 0.6-6 GHz.* IEEE Transactions on Electromagnetic Compatibility, 2000. **42**(4): p. 386-393.

24. Hirata, A., H. Watanabe, and T. Shiozawa, *SAR and temperature increase in the human eye induced by obliquely incident plane waves.* IEEE Trans. Electromagnetic Compatibility, 2002. **44**(4): p. 592-594.

Chapter 3

VALIDATION OF FDTD MODEL AND APPLICATION TO HUMAN HEAD DATA

3.1 Introduction

Since this work uses an independent 3-D FDTD code that was written specifically for this research, a first stage was to compare the results it produces with controls. A selection of validations that verify different aspects of the code is included in this chapter. Validation begins using a geometric model of a head. This shows that the code itself and its PML boundaries are valid. As stated in Chapter 1, one of the main advantages of using the FDTD technique is that it can handle complex heterogeneous structures, such as the human head. Several digital phantom heads exist that have been created from MRI scans of a human body. This allows the structure of the head to be modelled relatively accurately. Current MRI scans allow modelling with around 1mm blocks. It is not a straightforward task to replicate results as different heads vary in size and have different types and quantities of tissues [1]. Discrepancies also exist in the dielectric properties of the tissues [2, 3]. However, Nikita [4] noted that the difference between different heads is small compared to other variables such as the modelling of the source. Special consideration will be given to the validation of SAR in the eyes. Details of the assumptions made about the head models will also be explained in this chapter.

3.2 Validation of dipole near a 3-layered sphere

To check different aspects of the model several controls were used, including: the current along a half-wave dipole [5]; the input resistance and reactance of a fixed length dipole at different frequencies [6]; SAR in square [7], spherical and realistic phantoms excited by plane waves [8] and by dipoles [7].

As mentioned in Chapter 1, early work simulated the human head as a sphere composed of one or two materials. These simple models give rough approximations to a real head. Meier [9] modelled a three-layered spherical phantom. The outer layer, skin, had a diameter of 200mm, the bone layer diameter was 190mm and the inner brain layer diameter was 170mm. Meier used a 0.45λ dipole positioned 15mm from the three-layered sphere to represent a very simple model of a mobile device near a head. It has been shown that the body does not affect the SAR in the head if the frequency is above 600MHz, therefore the body does not need to be included in the model [10]. Note that the further assumption of no hand was made. The excitation frequency was 1.8GHz. Meier calculated this with the three-dimensional multiple multipole (MMP) method and considered his results to be accurate within 1%. The electrical properties of skin, bone and brain are shown in Table 3.1.

Table 3.1. The electrical properties and specific gravities of the tissues used in a spherical head compared with Meier.

	Relative Permittivity, ε_r	Conductivity, σ (S/m)	Density, ρ (Kg/m^3)
Skin	32.5	1.98	1100
Bone	13.4	0.30	1850
Brain	41.0	2.26	1030

The parameters in Table 3.1 were replicated in an FDTD program with a cell size of 2.5mm. And the head was positioned ten cells from the PML absorbing boundary layer. An amplitude of 1V/m was used and the results were then scaled relative to the current around the centre of the dipole. Results of the SAR into the sphere in a direction away from the dipole are plotted in Figure 3.1. There is good agreement between the FDTD code and Meier. Figure 3.1 shows a typical SAR versus depth profile in a human head: there are peaks in the skin and the brain, which have high conductivities. The bone section generally has a lower SAR than the brain due to the higher density and lower conductivity [7]. As the depth into the head increases the SAR decreases.

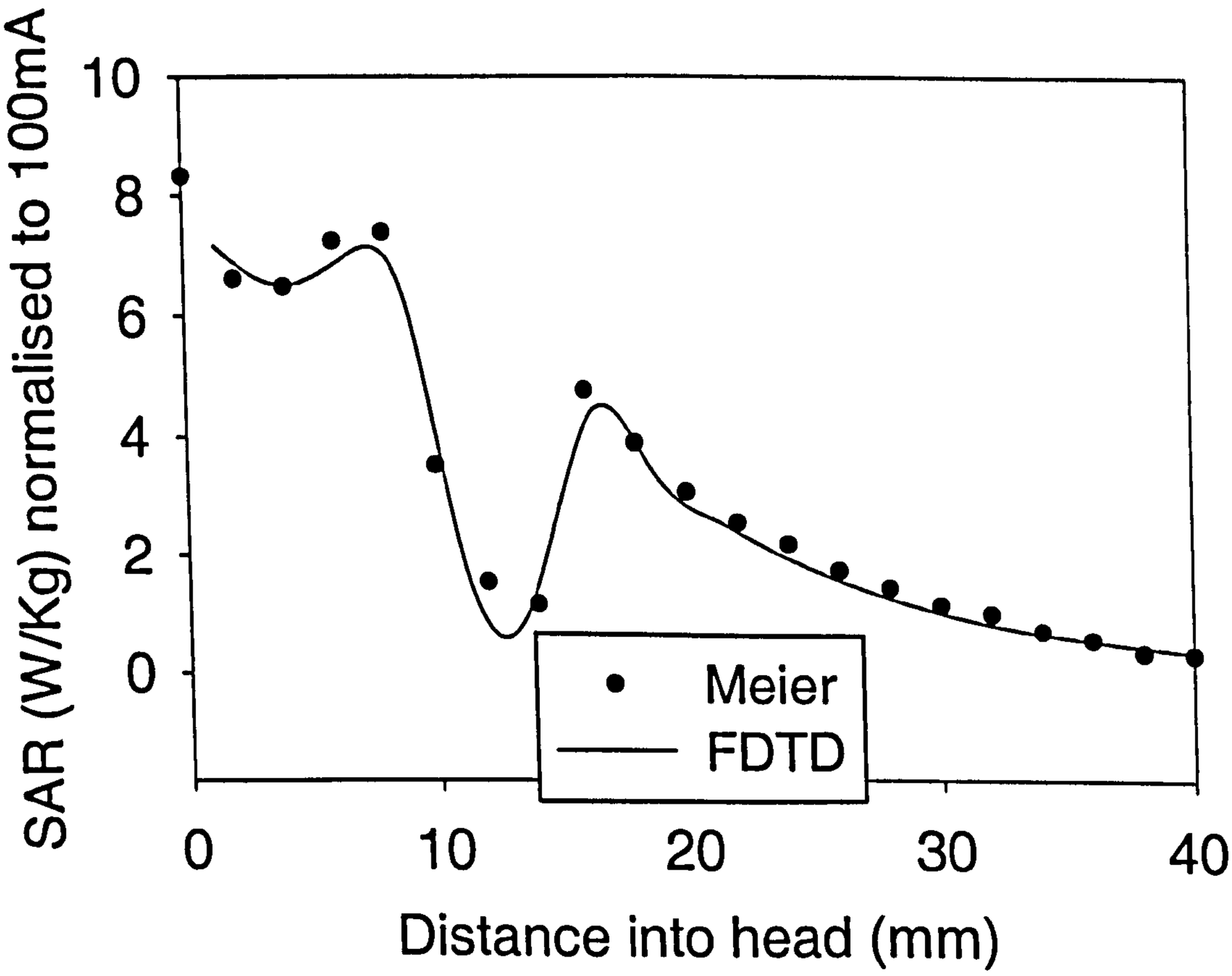

Figure 3.1. The SAR as a function of distance into a three layered sphere, composed of skin, bone and brain, excited by a 0.45λ dipole at 1.8GHz at a distance of 15mm. Results are validated against a published journal.

3.3 Techniques for creating digital phantoms

Three different phantoms have been considered in this research. A tissue-classified high-resolution voxel image of a human head has been created by Bradford University [11] and will be referred to as the Bradford head in this thesis. The exterior shape and resolution of the Bradford head is shown in Figure 3.2.

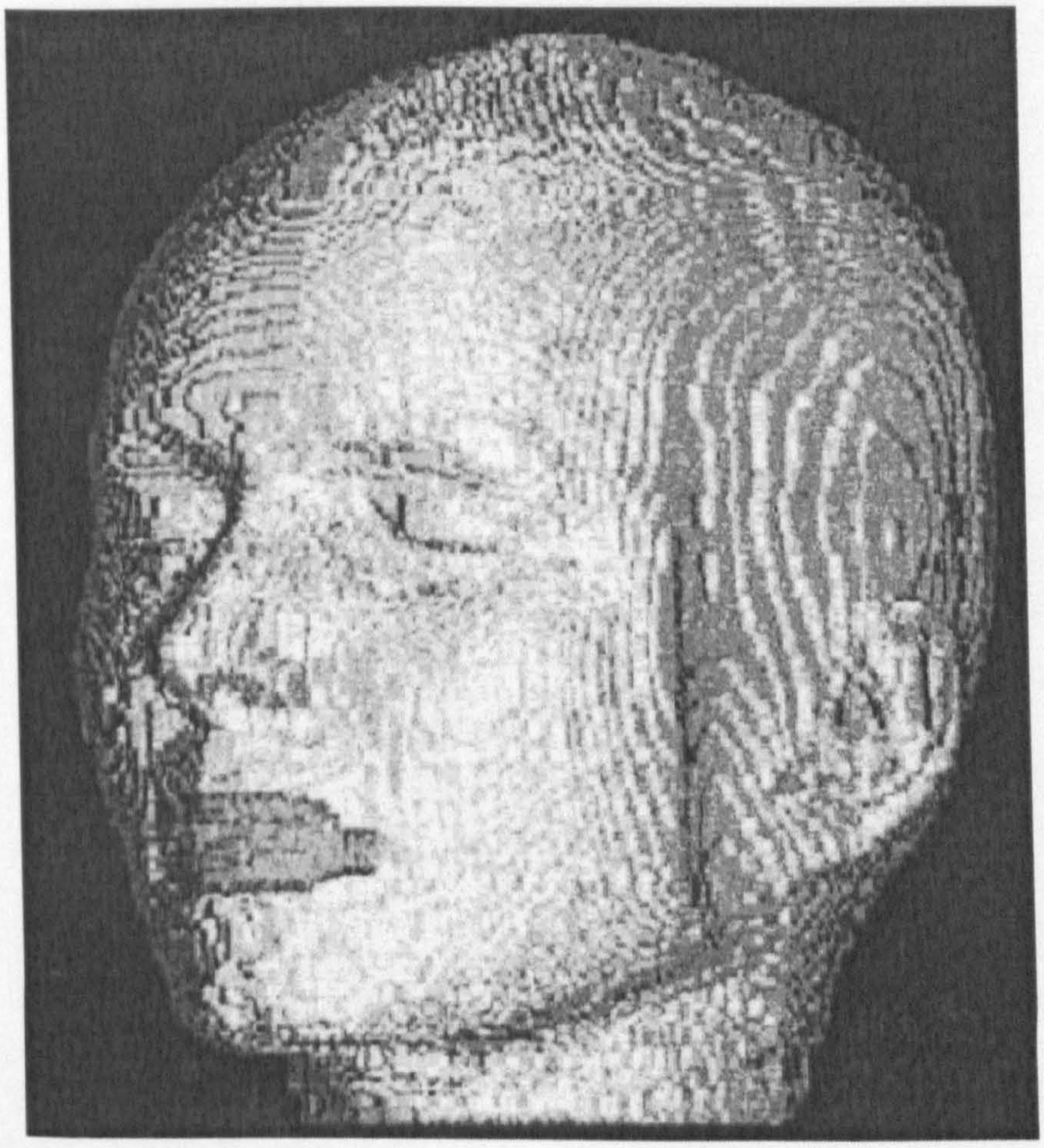

Figure 3.2. The exterior of the Bradford head model after classification [11].

This was created from MRI data taken with permission from Siemens Medical Inc. The raw MRI data was not in a useable format, and had to be modified and enhanced by Bradford University. Noise from the imaging process was removed. The image was also

faded towards the neck. This was corrected with gain equalisation. A Laplacian method was used to enhance the sharpness of the image. Software was implemented to automatically identify different tissues. The MRI values of skin and brain (grey and white matter) are very different from other tissues and these tissues can be identified automatically. All other tissues were identified manually by medical experts. Fifteen different tissues were identified and assigned an integer identification number. An algorithm was then used to reduce the discontinuity between slices. The resolution of the grid is 0.909 x 0.909 x 1.480mm in the *x*, *y* and *z* dimensions. The image can be resampled by writing a program to assign the tissue type at the nearest point in the source dataset to each point in the new dataset [11].

Zubal [12] created another digital head dataset and this will be referred to as the Zubal head in this thesis. A living subject, of average height and mass, was imaged to study a diffuse disease. Seventy-eight slices from mid thigh to neck were imaged using transmission computerized x-ray tomography (CT). Fifty-one slices of his head were also made, at 5mm intervals and with a pixel size of 0.5mm. This series of 2-D images were made into a 3-D matrix. Medical staff then manually outlined the different tissues. 3-D modal filtering was employed to reduce lack of continuity between slices. The data was then resampled. Data of the whole body and just the head, with a resolution of 1.1 x 1.1 x 1.4mm, are available on the internet [13]. The Zubal head is classified into parts of the brain by name and not tissue type and is not directly applicable to electromagnetics. Therefore, the tissues were reclassified by a Neurology lecturer and medics at Sheffield University and the complete list is shown in Appendix G.

Brooks Air Force base has a further head model freely available on the internet [14], based on work by the Visible Human Project [15]. The donated body of a recently

executed 38 year old male was scanned using four methods [16]. X-ray and CT scans were used to visualise bone with a resolution of 0.94 x 0.94 x 1.00mm. An MRI scan of the body was made for soft tissue. Colour photographs, with a resolution of 0.33 x 0.33 x 1.00mm were taken, after each 1mm slice was shaved off. Figure 3.3, taken from Xu [16], shows a cross-section through the eyes using photographs, CT and MRI scans.

Figure 3.3. Images from the Visible Human Project: (Left) Transversal colour photography at 2048 x 1216 pixel resolution; (Middle) CT images at 512 x 512 pixel resolution; and (Right) MR images at 256 x 256 pixel resolution [16].

Brooks Air Force [14] took the data from the Visible Human Project and resampled it to produce cubic grids of both 1 and 2mm. The different tissues were identified and were labelled with an integer number. There have been many visualization and animation tools applied to the Visible Human Project data. Tiede [17] produced an image that provides great insight into the external and internal anatomy of the Visible Human Project data, as shown in Figure 3.4. The figure shows that the man has a high fat content, which is confirmed by the man's mass of 104Kg [16, 17], that the eyelids are shut and that the internal structure including the eyes and brain are clearly defined.

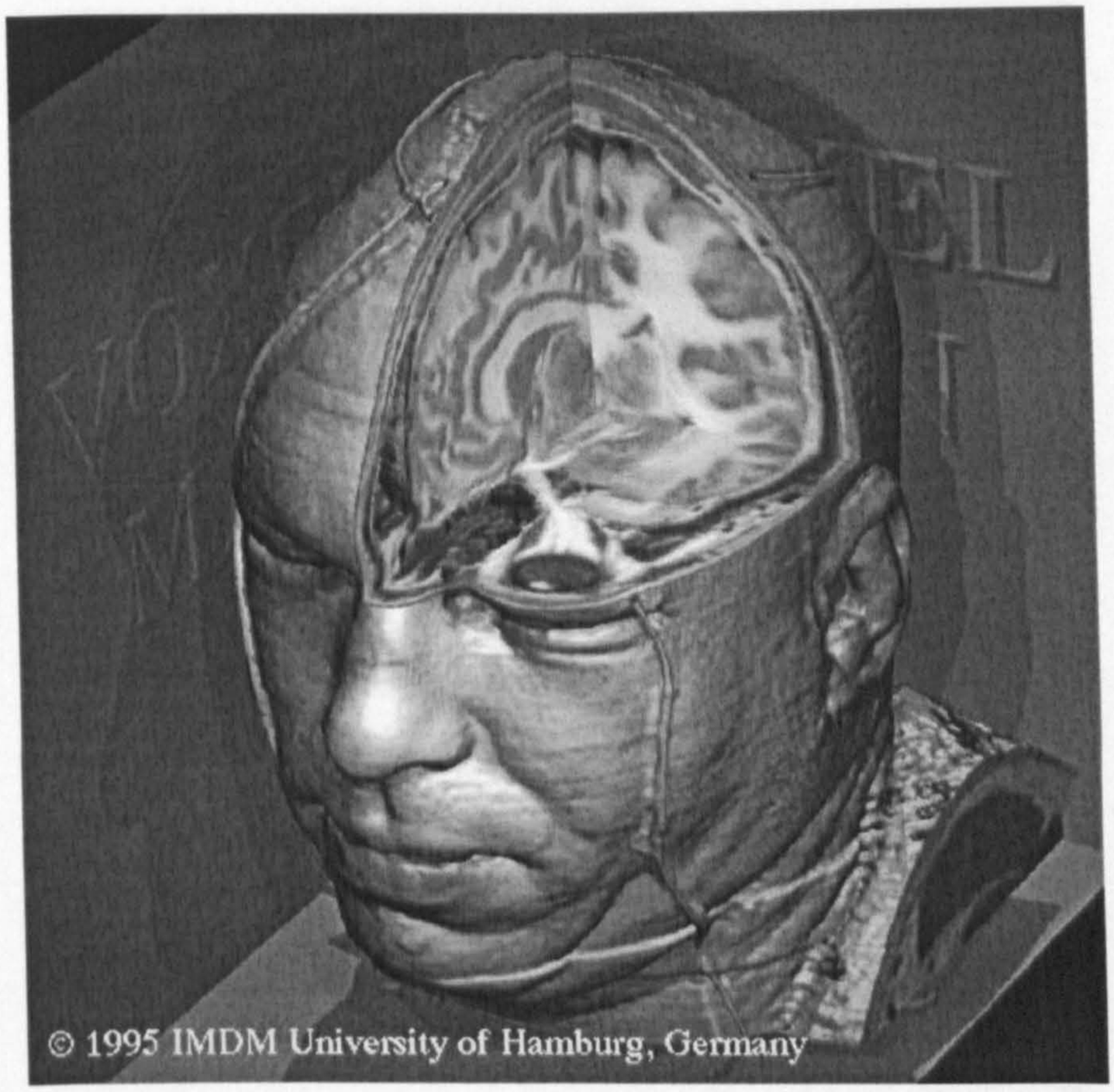

Figure 3.4. Reconstruction of the outer surface of the Visible Human head with three orthogonal cuts to reveal the interior of the head [17].

3.4 Comparison of Brooks, Bradford and Zubal heads

The Brooks [14], Bradford [11] and Zubal [12] heads were carefully compared to see which would be the most suitable to use. All three heads are based on adult males, yet exhibit different shapes, sizes, and internal structure. Gandhi [1] also noted that different heads have very different percentage volumes of the different tissues, that the Brooks model was taken from a 'husky' man of mass 104kg and the model had a higher fat content and a smaller brain than their own digital phantom. To illustrate that different MRI scanning and tissue assigning analysis have different results, the Bradford

head contains no fat or blood. The pixel size of the Zubal head in the x, y plane is 1.1mm and the resolution in the z-axis is 1.4 mm. The Bradford head has a resolution of 0.909 x 1.480 x 0.909mm. The heads were rescaled to have a cubic resolution of both 1 and 2mm. The image clarity of all three heads is excellent. The brain and the ears are very clear and well defined, and all three heads are suitable to use with a source positioned at the side of the ear. However, the Zubal head is not well defined in the region including and surrounding the eyes, as the Zubal study was more interested in the anatomy of the brain. The eyes of the Zubal head have a combined mass of 28.74g. The Bradford head is very clear and well defined but on closer analysis the mass of the eyes are smaller than normal. With a cell size of 2mm, both eyes have a mass of 7.45g, compared to 14.4g ± 6.5g for the mass of both eyes of the ICRP Reference Man [18]. The eyes of the revised MIRD head, a simplified mathematical model, have a similar mass of 15.20g [18]. Wolff's anatomy of the eye [19], quotes three sources for the mass of the eyes; 14.28g, 14.90g and 15.00g. Both of the Brooks eyes, at 2mm resolution, have a mass of 16.67g, which is within the error bars of Reference Man. As the focus of this research will be on the effects on the eyes, it was considered important to use a model of the eye with a mass within the normal range. The majority of the work in this thesis will therefore be carried out with the Brooks head with a resolution of 2mm unless stated otherwise. There have been several journals published about RF interaction with humans which use the Brooks model [1, 20-24]. Chapter 5 will include results with the Bradford head to show that, while the different heads give different results, the addition of metallic spectacles has similar effects. Cross-sections through the eyes of the Brooks, Bradford and Zubal heads at 1mm resolution, together with the tissues they contain, are shown in Figure 3.5, Figure 3.6 and Figure 3.7.

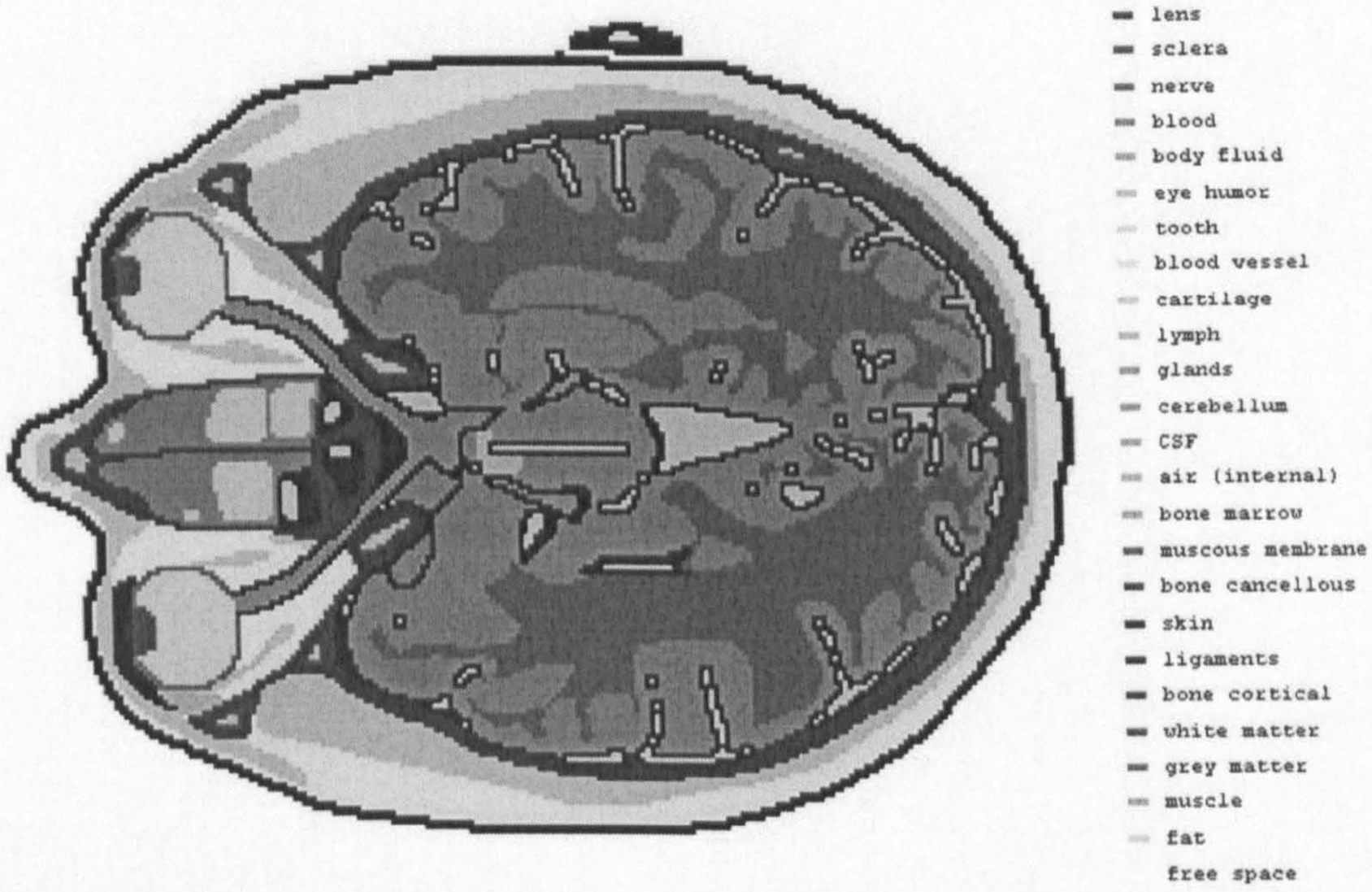

Figure 3.5. A cross-section of the Brooks head through the eyes and a list of the tissues in the model. Resolution is 1mm.

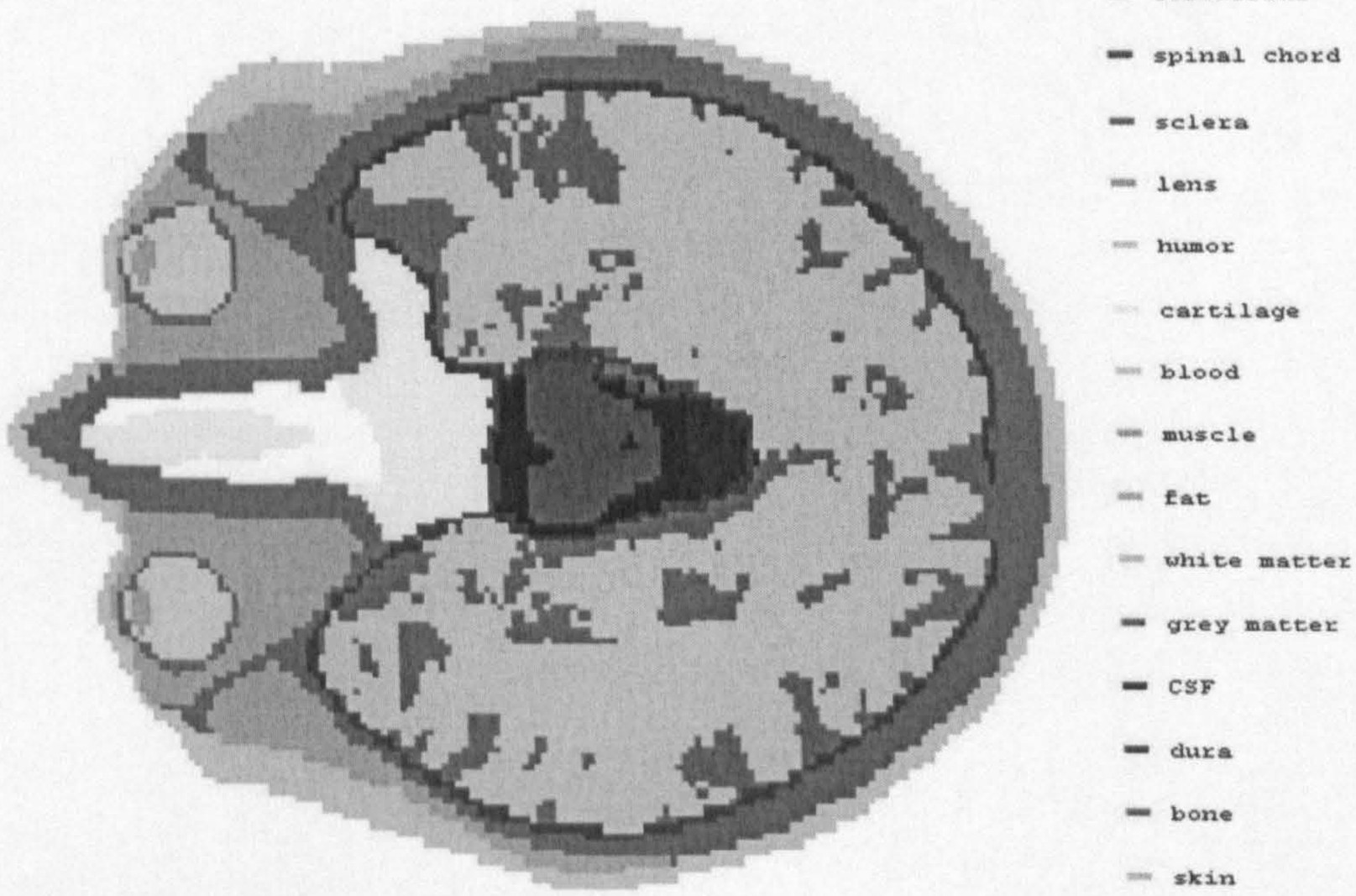

Figure 3.6. A cross-section through the eyes of the Bradford head and a list of the tissues in the model. Resolution is 1mm.

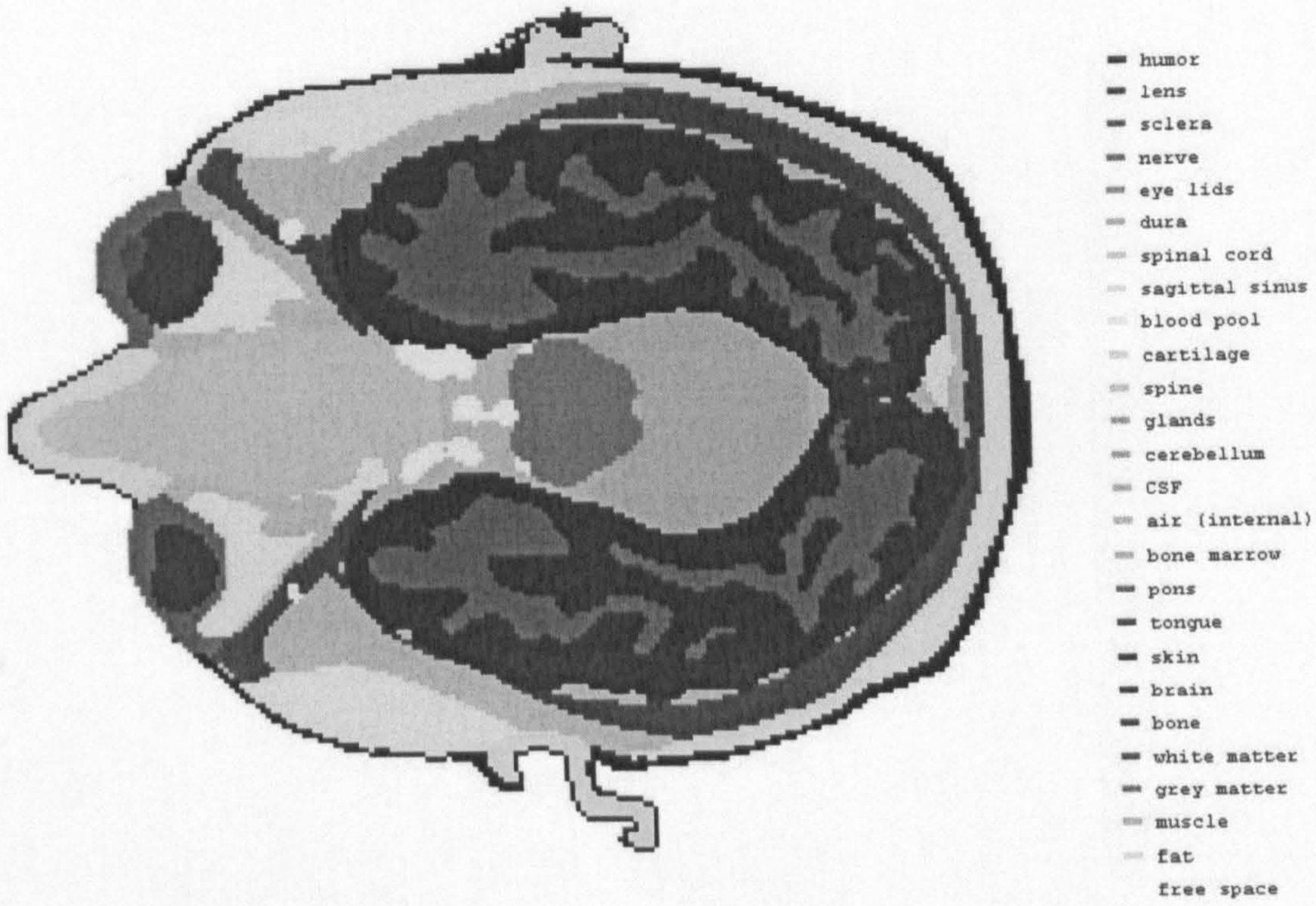

Figure 3.7. A cross-section though the eyes of the Zubal head and a list of tissues in the model. Resolution is 1.1mm.

3.5 Cell size, tissues and electrical properties

The cell size used in FDTD depends on the Courant sampling condition and there should be at least ten cells per wavelength [25], although reasonable results have been achieved with only four cells [26] and fairly accurate results can be achieved with five [27]. The cell size must also allow the shape of the head to be adequately modelled to reduce stair-casing approximations, yet the size of memory and computation time rise rapidly with the number of cells needed. Added to this, making the cell size too small does not necessarily increase the accuracy as there are compound errors that arise from having to do more calculations over more time steps [25]. Therefore a compromise must be found.

Non-cubic Yee cells can be used but in this work the cells are always cubic (i.e. $\Delta x = \Delta y = \Delta z$). As the wavelength is related to the frequency, the number of cells per wavelength decreases as the frequency increases. The head is made of dielectric tissues with ε_r greater than unity, thus the wavelength in these tissues will decrease by the square root of the relative permittivity. Some body tissues have permittivities of about 64, hence the cell size in the grid must be decreased by a factor of roughly eight compared to the cell size required in free space.

If a 2mm Yee cell is used then there are at least six cells per wavelength in any tissue at 3.0GHz. At 1mm resolution, the sampling always exceeds twelve cells per wavelength at 3.0GHz.

The dielectric properties of each tissue are calculated with aid of the 4-Cole-Cole extrapolation [28] and are frequency-dependent. At the interface between two materials, the average values of conductivity and permittivity are used as in Section 2.7. The densities of the different materials are the same as used by Mason [2]. Dielectric properties of the Brooks head at 1.8GHz are listed in Table 3.2.

The Brooks head contains twenty-five tissue types including internal air. The Bradford head contains fifteen tissues which are listed in Table 3.3, along with their dielectric properties at 1.8GHz.

The dielectric properties of the tissues are frequency-dependent. The relative permittivity decreases and the conductivity increases with frequency. Therefore, different values have been used when a frequency band has been considered.

Table 3.2. DIELECTRIC PROPERTIES AND SPECIFIC GRAVITIES OF THE BROOKS HEAD AT 1.8GHz.

Tissue	Conductivity (S/m)	Relative Permittivity	Density (Kg/m³)
Fat	0.078	5.349	920
Muscle	1.341	53.549	1050
Brain Grey Matter	1.391	50.079	1040
Brain White Matter	0.915	37.011	1040
Bone Cortical	0.275	11.781	1990
Tendon	1.201	44.251	1220
Skin (Dry)	1.185	38.872	1130
Bone Cancellous	0.588	19.343	1920
Mucous Membrane	1.232	43.850	1040
Bone Marrow	0.068	5.372	1040
Air (Internal)	0.000	1.000	0
Cerebrospinal fluid (CSF)	2.924	67.200	1010
Cerebellum	1.709	46.114	1040
Gland	1.501	58.142	1050
Lymph	1.501	58.142	1040
Cartilage	1.287	40.215	1100
Blood Vessel	1.066	43.343	1040
Tooth	0.275	11.781	2160
Vitreous Humor	2.033	68.573	1010
Body Fluid	2.033	68.573	1010
Blood	2.044	59.372	1060
Nerve	0.843	30.867	1040
Eye Sclera	1.602	53.568	1030
Lens	1.147	45.353	1050
Cornea	1.858	52.768	1080

Table 3.3. DIELECTRIC PROPERTIES AND SPECIFIC GRAVITIES OF THE BRADFORD HEAD AT 1.8GHz.

Tissue	Conductivity (S/m)	Relative Permittivity	Density (Kg/m³)
Air	0.000	1.000	0
Skin (Dry)	1.185	38.872	1130
Bone	0.380	14.302	1950
Dura	1.320	42.894	1040
Cerebrospinal fluid (CSF)	2.924	67.200	1010
Grey Matter	1.391	50.079	1040
White Matter	0.915	37.011	1040
Fat	0.078	5.349	920
Muscle	1.341	53.549	1050
Blood	2.044	59.372	1060
Cartilage	1.287	40.215	1100
Humor	2.033	68.573	1010
Lens	1.147	45.353	1050
Sclera	1.602	53.568	1030
Spinal Cord	0.843	30.867	1400
Cerebellum	1.709	46.114	1040

3.6 Symmetry

Although the two heads are not exactly symmetric, a line of symmetry (in the x-z plane) has been included in this model to save memory and computational time. This plane of symmetry runs vertically down the centre of the nose and extends to the back of the head. Previously, Hirata [20] made the assumption that the head could be approximated as being symmetric. This use of symmetry was found to have negligible effect on SAR results. The effects of symmetry on the SAR in the eye are shown in Figure 3.8. The

Brooks head, with a resolution of 2mm, is excited from the front with a 50W/m² E_z plane wave.

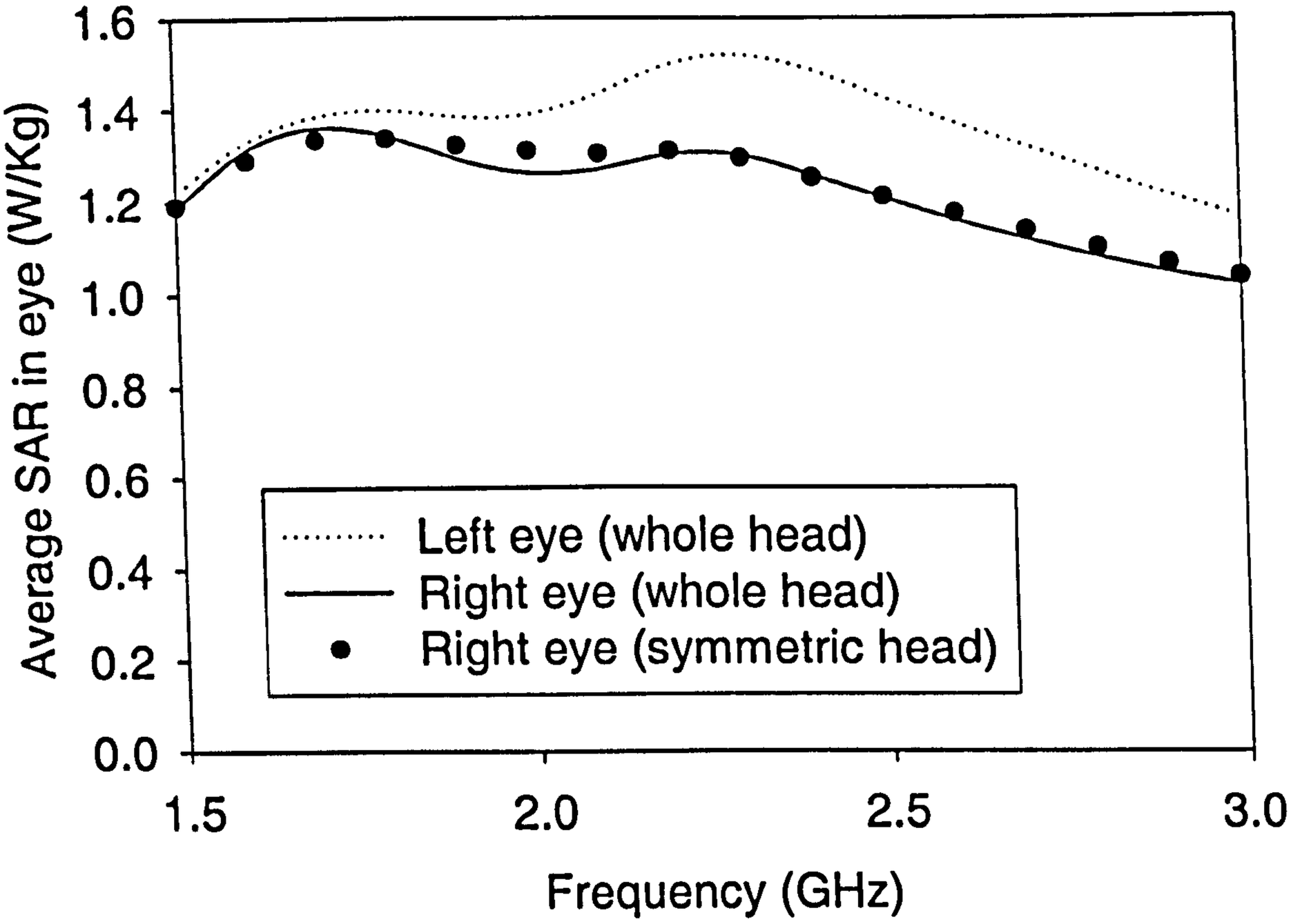

Figure 3.8. The effects of using a line of symmetry in the model to reduce computational time. (2mm Brooks head eyelids closed).

The Brooks head is not symmetric as demonstrated by the left eye having a different average SAR from the right one. In this research only the right eye (as seen from the front) has been modelled. There is little change in the average SAR in this eye when the whole head is modelled. The assumption of using a vertical plane of symmetry in the head is shown to be valid and reduces the computational run time and memory requirements with negligible loss of accuracy in the results. This thesis will contain results using only half the head unless clearly stated otherwise.

3.7 Validation of average SAR in head versus frequency

By comparing the average SAR in the head illuminated with E_z and E_y plane waves with results from Hirata [29], the plane wave incidence, the digital head model and the dielectric properties were validated - see Figure 3.9. Note the E_y plane wave excitation is modelled by rotating the head 90 degrees relative to the x-z plane.

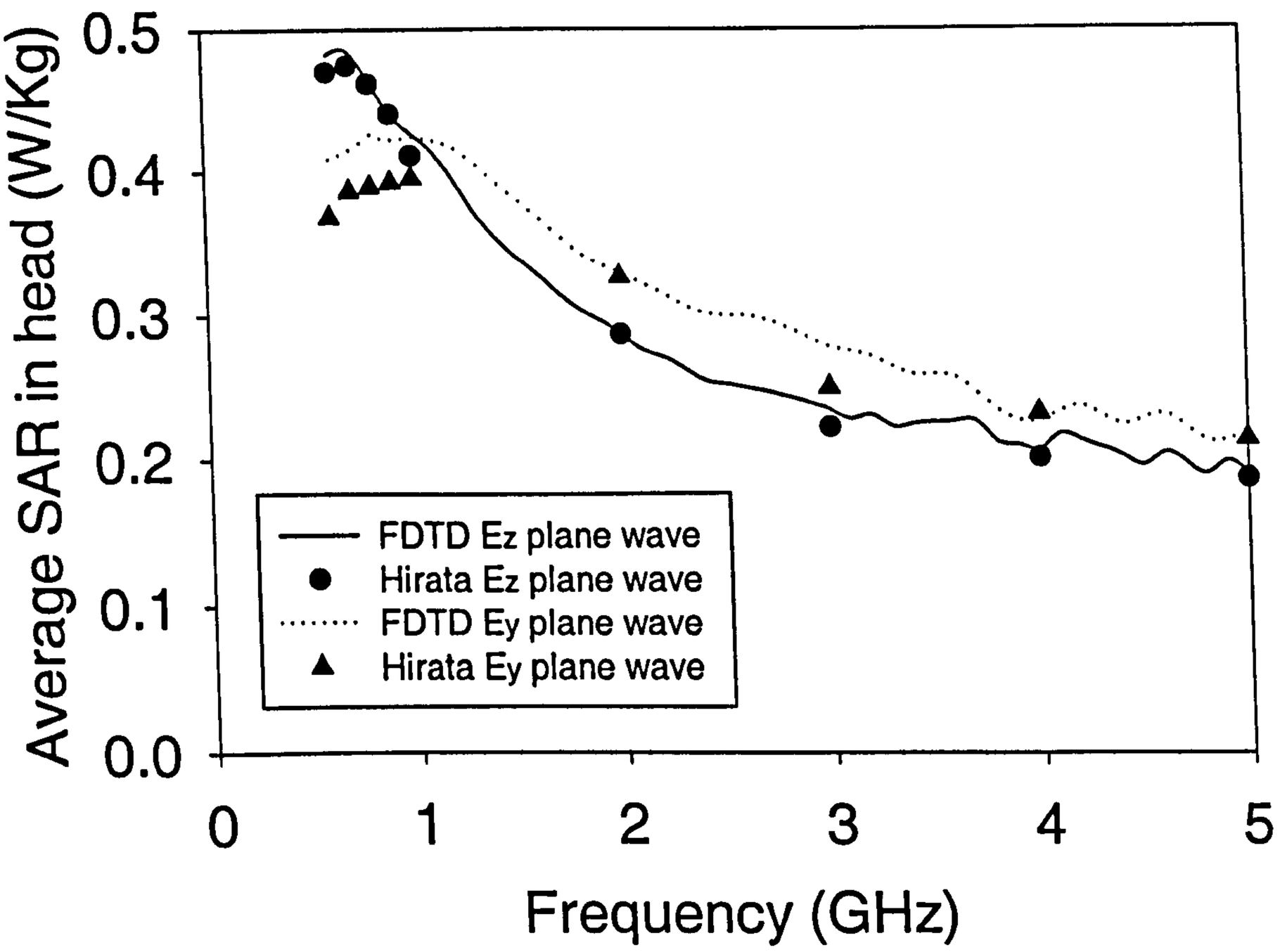

Figure 3.9. The average SAR in a head illuminated by a 50W/m² E_z and E_y plane wave, compared to published paper [29].

The code shows a good level of agreement with both orientations of plane wave excitation. It should be noted that Hirata used a different digital head and that both of these heads give very similar results despite differences in external size and internal

tissue. The average SAR in the head is related to the size of the head. The head is taller (z-axis) than it is wide (y-axis) and therefore the maximum average SAR occurs at a higher frequency with an *Ez* polarised plane wave than an *Ey* plane wave. As the frequency increases and the head becomes large compared to the wavelength, the average SAR in the head decreases.

3.8 Effects of removing the eyelids and comparison with Bradford head

As stated earlier, different digital heads will have different compositions, as will different real heads and this will not produce identical SAR levels. Figure 3.10 shows the average SAR in the eye with three different anatomical heads as a function of frequency. Both Bradford and Brooks heads have been modelled using a line of symmetry and a cell size of 2mm with and without eyelids. Also shown on the graph are results from Hirata [29] who used a 3rd anatomical head. The excitation of all the curves is the same vertically polarised plane wave with a power density of 50W/m^2. The graph shows the different results averaged over the eye that the different heads will produce at different frequencies. The Brooks and Bradford heads have been modelled with a 2mm resolution. The lowest number of cells per wavelength is always greater than six at 3.0GHz, and as previously mentioned, reasonable results have been obtained with only four [26]. Hence the results for frequencies above 3.0GHz for the Brooks and Bradford heads are only approximate.

Figure 3.2 to 3.6 show that both the Brooks and Bradford heads originally have closed eyelids and results in this section are included with the eyelids artificially removed.

Skin, fat and muscle tissues were replaced with air in an elliptical region of 30mm by 12mm in front of the eye. It should be noted that the eyelids were removed and were not opened, as would be the case in a real human. Hirata showed [29] that opening the eyelid increased the average SAR in the eye by 15% at 5.0GHz. Bernardi [23] showed that the modelling of eyelids is far more important at higher frequencies. At an excitation frequency of 30GHz, Bernardi showed that the SAR in the eye increased by a factor of five and the SAR in the lens increased by a factor of fifty, when the eyelids were opened.

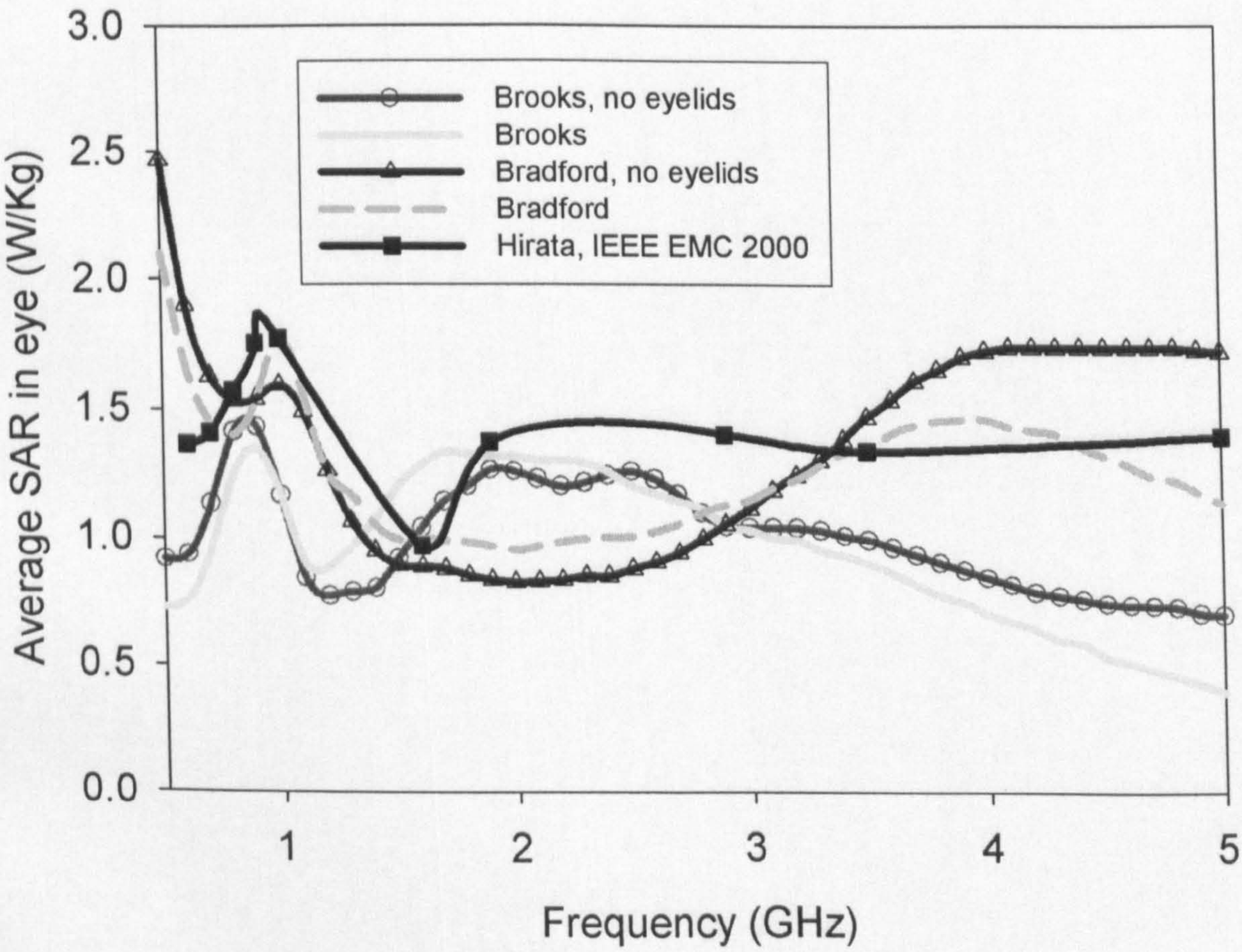

Figure 3.10. The average SAR in the eye with Brooks and Bradford heads with and without eyelids compared to a 3rd model used by Hirata. Excitation is a vertically polarised plane wave.

Figure 3.10 shows that the three heads have similar magnitudes of average SAR in the eye. The FDTD code provides reasonable agreement with published results, across the frequency band. The differences in the three curves are likely to be due to the three different head models used. Removing the eyelids decreases the average SAR in the eye in the range 1.3 to 2.5GHz and increases it at higher frequencies. Therefore, at 1.8GHz, the worst-case scenario, with the highest SAR in the eye, is with the eyelids kept shut.

3.9 Validation of average SAR in eye as head is rotated in a horizontal plane.

To allow further comparison of the model and especially the eye, a simulation by Hirata [20] has been replicated. The whole of the Brooks head, with no symmetry, was excited by a 50W/m² vertically polarised E_z plane wave. The eyelids were manually opened as explained in Section 3.8. A cell size of 2mm was used and the excitation frequency was 1.5GHz. The angle of incidence was changed, by rotating the head in the x-y horizontal plane. Hence a VP plane wave was incident on the head, from the right ear to the left ear passing in front of the head. These results are shown in comparison to Hirata's results in Figure 3.11. The angle 0 degrees represents the scenario when the plane wave excitation is positioned in front of the eyes. Moneda [30] noted the total power absorbed by the eyes set in a geometric head is increased if the excitation is from the front as opposed to the side. However, Figure 3.11 shows that the maximum average SAR in an eye in a realistic head occurs when the incident plane wave is at approximately 45 degrees.

The independent FDTD code (Brooks head) shows good agreement with Hirata's results in Figure 3.11 and can be used with confidence to investigate SAR in the head and the

eye. Possible discrepancies between the results could be due to differences in how the eyelids were removed or errors due to rotating the head. When the excitation is from the front, the model shows good agreement. However, when the excitation is from the side, the agreement is less good. This would suggest that the eyelids have been removed in different ways at the side of the head.

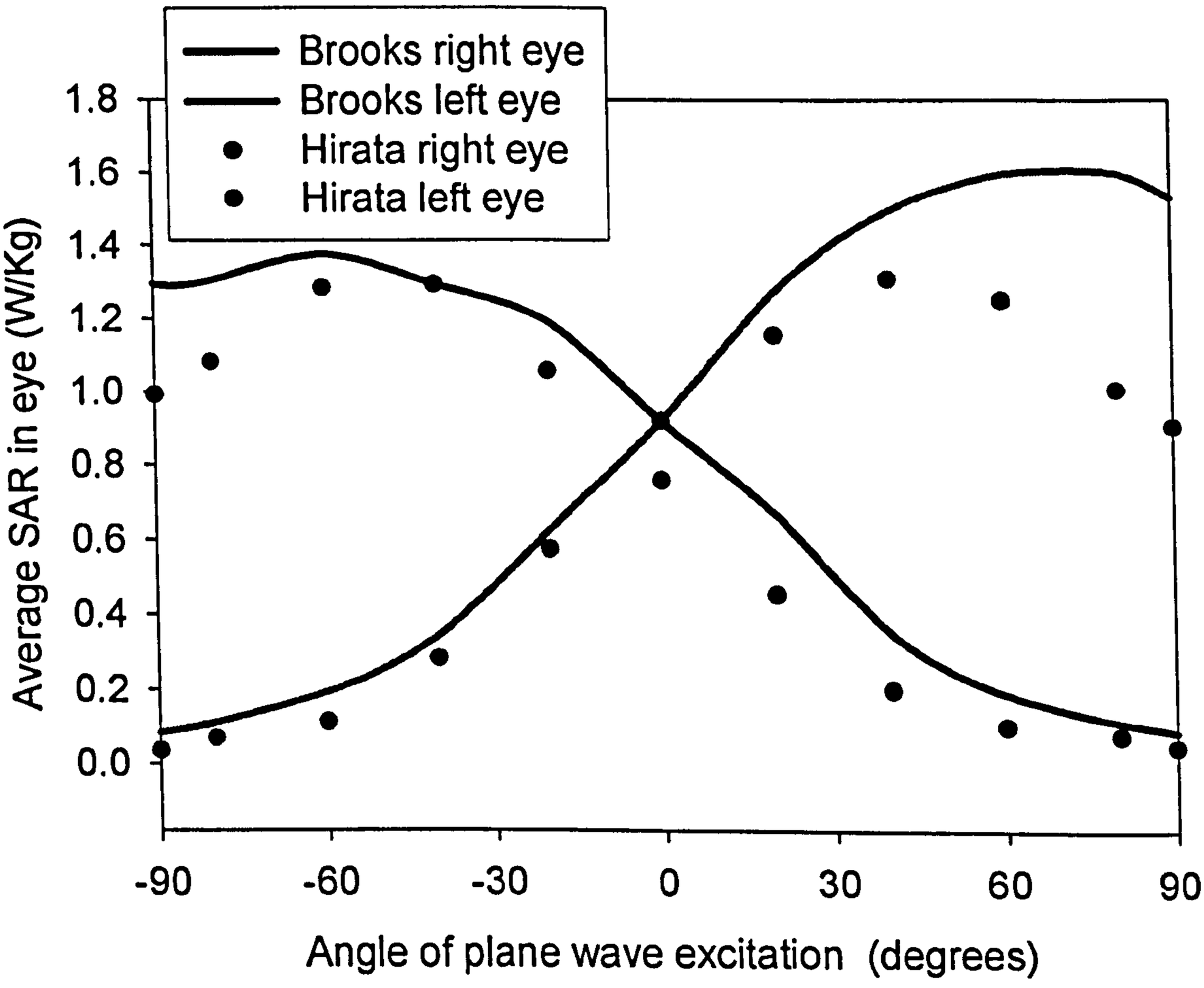

Figure 3.11. The angle dependence of the SAR averaged over the eye for a vertically polarised plane wave with a power density of 50W/m^2 at 1.5GHz.

Removing the eyelids is not a simple task and is arbitrary to some extent. There are many parameters such as the thickness of the tissue, the size of the eyelids and how

open the eyelids are, which make repeating the procedure very difficult. Removing the eyelid is difficult, but opening the eyelid to model a real scenario is even more prone to error. For these reasons the eyelid will be kept shut throughout this thesis.

3.10 Conclusions

An independent 3-D FDTD code has been written especially for this research project. The code has been validated against results in published journals, firstly by using a simple geometric head. Data from three heterogeneous head models was successfully implemented into the code and have been validated. Therefore, all aspects of the code, the implementation of the head and the dielectric properties of the head have been validated. Special attention has been given to validating results in the eye, as this will be an area of focus in this thesis. Both plane wave and dipole excitations have been validated.

It has previously been shown that the presence of the body does not affect the SAR in the head above 600MHz [10] and the body has not been included in this model. Three different heads have been compared. The Brooks head will be used for the bulk of this thesis, as the mass of the eye is within the normal range and the results for the eye show closer agreement with other published results. The Bradford head will be compared to the Brooks head in Chapter 5. The Zubal head is not well discretised around the eyes and care should be taken when exciting this head from the front.

The head is assumed to be symmetric to reduce computation time. This assumption has been shown to be valid with negligible effect to the SAR in the eye. A cell size of 2mm

gives good results compared to published journals, adequately sampling the head but without causing overly long run times. The effects of the eyelids have been investigated and, generally within the frequency range of 1.5 to 3.0GHz, removing the eyelids decreases the SAR in the eye. Thus, keeping the eyelids closed represents a worst-case scenario and avoids creating uncertainty as to how the eyelids should be removed.

Unless clearly stated to the contrary, results in this thesis assume that the Brooks head has been used, that symmetry has been implemented, that the eyelids are kept shut, that the cell size is 2mm and that the cells are cubic.

3.11 References

1. Gandhi, O. and G. Kang, *Some present problems and a proposed experimental phantom for SAR compliance testing of cellular telephones at 835 and 1900 MHz.* Physics in Medicine and Biology, 2002. **47**: p. 1501-1518.

2. Mason, P.A., W.D. Hurt, T.J. Walters, J.A. D'Andrea, P. Gajsek, K.L. Ryan, D.A. Nelson, K.I. Smith, and J.M. Ziriax, *Effects of frequency, permittivity and voxel size on predicted specific absorption rate values in biological tissue during electromagnetic-field exposure.* IEEE Trans. Microwave Theory Technology, 2000. **48**(11): p. 2050-2058.

3. Hurt, W.D., J.M. Ziriax, and P.A. Mason, *Variability in EMF permittivity values: Implications for SAR calculations.* IEEE Trans. Biomedical Engineering, 2000. **47**(3): p. 396-401.

4. Nikita, K.S., M. Cavagnaro, P. Bernardi, N.K. Uzunoglu, S. Pisa, E. Piuzzi, J.N. Sahalos, G.I. Krikelas, J.A. Vaul, P.S. Excell, G. Cerri, S. Chiarandini, R. De Leo, and P. Russo, *A study of uncertainties in modeling antenna performance and power absorption in the head of a cellular phone user.* IEEE Transactions on Microwave Theory and Techniques, 2000. **48**(12): p. 2676-2685.

5. Dimbylow, P.J., *FDTD calculations of the SAR for a dipole closely coupled to the head at 900MHz and 1.9GHz.* Physics in Medicine and Biology, 1993. **38**(3): p. 361-368.

6. Hockanson, D.M., J.L. Drewniak, T.H. Hubing, and P. Van Doren, *FDTD modeling of common-mode radiation from cables.* IEEE Trans. Electromagnetic Compatibility, 1996. **38**(3): p. 376-387.

7. Okano, Y., K. Ito, I. Ida, and M. Takahashi, *The SAR evaluation method by a combination of thermographic experiments and biological tissue-equivalent phantoms.* IEEE Transactions on Microwave Theory and Techniques, 2000. **48**(11): p. 2094-2103.
8. Guy, A., C.K. Chou, and J.A. Mcdougall, *A quarter century of in vitro research: a new look at exposure methods.* Bioelectromagnetics, 1999. **20:21-39**: p. 21-39.
9. Meier, K., V. Hombach, R. Kastle, R. Tay, and N. Kuster, *The dependence of electromagnetic energy absorption upon human-head modelling at 1800MHz.* IEEE Trans. Microwave Theory Techniques, 1997. **45**(11): p. 2058-2062.
10. Dimbylow, P.J., *Finite difference calculations of current densities in a homogenous model of a man exposed to extremely low frequencies.* Bioelectromagnetics, 1987. **8**: p. 355-377.
11. Olley, P. and P.S. Excell. *Classification of a High-Resolution Voxel Image of a Human Head. 'Voxel Phantom Development', Proceedings of an International Workshop at the National Radiological Protection Board.* 1995. Chilton, UK. p. 16-23
12. Zubal, I.G., C.R. Harrell, E.O. Smith, Z. Rattner, and G. Gindi, *Computerized three-dimensional segmented human anatomy.* Med. Phys, 1994. **21**(2): p. 299-302.
13. Zubal, I.G., *The Zubal Phantom.* http://noodle.med.yale.edu/zubal/index.htm.
14. Brooks-Airforce. http://www.brooks.af.mil/AFRL/HED/hedr/hedr.html.
15. NLM, *The Visible Human Project.* http://www.nlm.nih.gov/research/visible/visible_human.html.
16. Xu, X.G. and T.C. Chao, *VIP-Man: An image-based whole-body adult male model constructed from color photographs of The Visible Human Project for multi-particle Monte Carlo calculations.* Health Phys, 2000. **78**(5): p. 476-486.
17. Tiede, U., T. Schiemann, and K.H. Höhne, *Visualizing the Visible Human.* IEEE Comput. Graphics Appl., 1996. **16**(1): p. 7-9.
18. ICRP, *Report of the task group on reference man.* ICRP Report. Vol. 23. 1975: Pergamon Press, New York, NY.
19. Bron, A., *Wolff's anatomy of the eye and orbit.* 8th ed. 1997, London: Chapman and Hall Medical.
20. Hirata, A., H. Watanabe, and T. Shiozawa, *SAR and temperature increase in the human eye induced by obliquely incident plane waves.* IEEE Trans. Electromagnetic Compatibility, 2002. **44**(4): p. 592-594.
21. Hirata, A. and T. Shiozawa, *Correlation of maximum temperature increase and peak SAR in the human head due to handset antennas.* IEEE Trans. Microwave Theory Techniques, 2003. **51**(7): p. 1834-1840.
22. Rowley, J.T. and R.B. Waterhouse, *Performance of shorted microstrip patch antennas for mobile communications handsets at 1800MHz.* IEEE Trans. Antennas and Propagation, 1999. **47**(5): p. 815-822.

23. Bernardi, P., M. Cavagnaro, and S. Pisa, *Assessment of the potential risk for humans exposed to milimetre-wave wireless LANs: the power absorbed in the eye.* Wireless Networks, 1997. **3**: p. 511-517.

24. Bernardi, P., M. Cavagnaro, S. Pisa, and E. Piuzzi, *SAR distribution and temperature increase in an anatomical model of the human eye exposed to the field radiated by the user antenna in a wireless LAN.* IEEE Transactions on Microwave Theory and Techniques, 1998. **46**(12): p. 2074-2082.

25. Taflove, A., *Computational electrodynamics. The finite-difference time-domain method.* 1995: Artech House, Inc.

26. Dimbylow, P.J. and O.P. Gandhi, *Finite-difference time-domain calculations of SAR in a realistic heterogeneous model of the head for plane-wave exposure from 600MHz to 3GHz.* Physics in Medicine and Biology, 1991. **36**(8): p. 1075-1089.

27. Lazzi, G., *Realistically tilted and truncated anatomically based models of the human head for dosimetry of mobile telephones.* IEEE Trans. Electromagnetic Compatability, 1997. **39**(1): p. 55-60.

28. Gabriel, S., R.W. Lau, and C. Gabriel, *The dielectric properties of biological materials: 2. Measurements in the frequency range 10Hz to 20GHz.* Physics in Medicine and Biology, 1995. **41**: p. 2251-2269.

29. Hirata, A., S. Matsuyama, and T. Shiozawa, *Temperature rises in the human eye exposed to EM waves in the frequency range 0.6-6 GHz.* IEEE Transactions on Electromagnetic Compatibility, 2000. **42**(4): p. 386-393.

30. Moneda, A.P., M.P. Ionnidou, and D.P. Chrissoulidis, *Analytical study of radiowave absorption by the brain and the eyes in an eccentric spheres model of the human head.* 11th International Conference on Antennas and Propagation, 2001: p. 774-778.

Chapter 4

MODELLING OF METALLIC SPECTACLES

4.1 Introduction

As explained in Section 1.9, metallic spectacles at the side of the head can have a significant effect on the SAR in the eye. This chapter will give details of how spectacles can be modelled and show results for excitation from the front of the head. Results are presented for different compositions of materials used for both the frames and lens. Some simple geometric shapes of spectacles will be considered. A selection of realistic spectacles is also considered.

4.2 Modelling of spectacles

In this chapter a plane wave is injected into the grid using the total field / scattered field approach [1]. The incident wave is z polarised, plane and propagates in the x direction (from the nose to the rear of the head). The power density used is 50W/m², being the maximum permissible exposure limit for controlled environments [2].

The spectacles were modelled using metallic Yee cells and were achieved by setting the conductivity of the cells equal to the conductivity of copper. Nikita [3] and Bernardi [4] both used this technique to model metal shapes. Wang [5] modelled metallic spectacles by setting the conductivity of the Yee cells in the frames equal to titanium. Four

arbitrary but representative frame types were researched: square, circular, rectangular and elliptical. See Figure 4.1 for orientation and geometry.

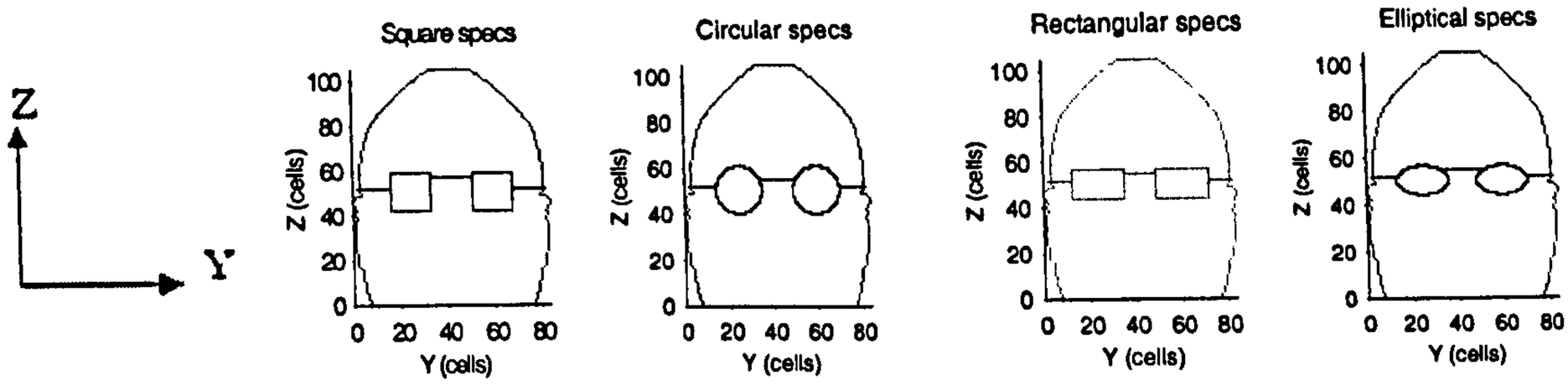

Figure 4.1. The Orientation and coordinate system used. The four types of spectacles: square, circular, rectangular and elliptical are shown relative to the outline of the head.

In each case, the centre of the lens was positioned at the centre of the eye in the *y*–*z* plane and 26mm in front of the cornea. The cells between the frames were assigned a relative permittivity of 2.56; thereby including a realistic Perspex lens 2mm thick. In addition to these basic geometric shapes, a nosepiece and a strut to the arm were included - see Figure 4.1. Care was taken to ensure that the frames did not lie inside the head or touch the skin. Spectacle arms were modelled as a line of single metallic Yee cells, extending 140mm in the *x* direction, touching the head above the ear.

4.1 Using different materials

Spectacles, with copper frames and a 2mm Perspex lens are assumed to be the default spectacles used in this thesis, unless stated otherwise. This section shows the effects of varying both the material of the frame and of the lens.

Spectacle frames are commonly made of many materials including plastic and various metals. The range of conductivities of materials varies from $1x10^{-17}$ S/m for insulators such as quartz, to $6.1x10^{7}$ S/m for silver [6]. Figure 4.2 shows the average SAR in the eye with a vertically polarised plane wave at 1.8GHz, as a function of the conductivity of the frames of the spectacles. The size of the spectacles was arbitrarily chosen to be 34mm square, positioned 26mm in front of the eye, with a 2mm Perspex lens.

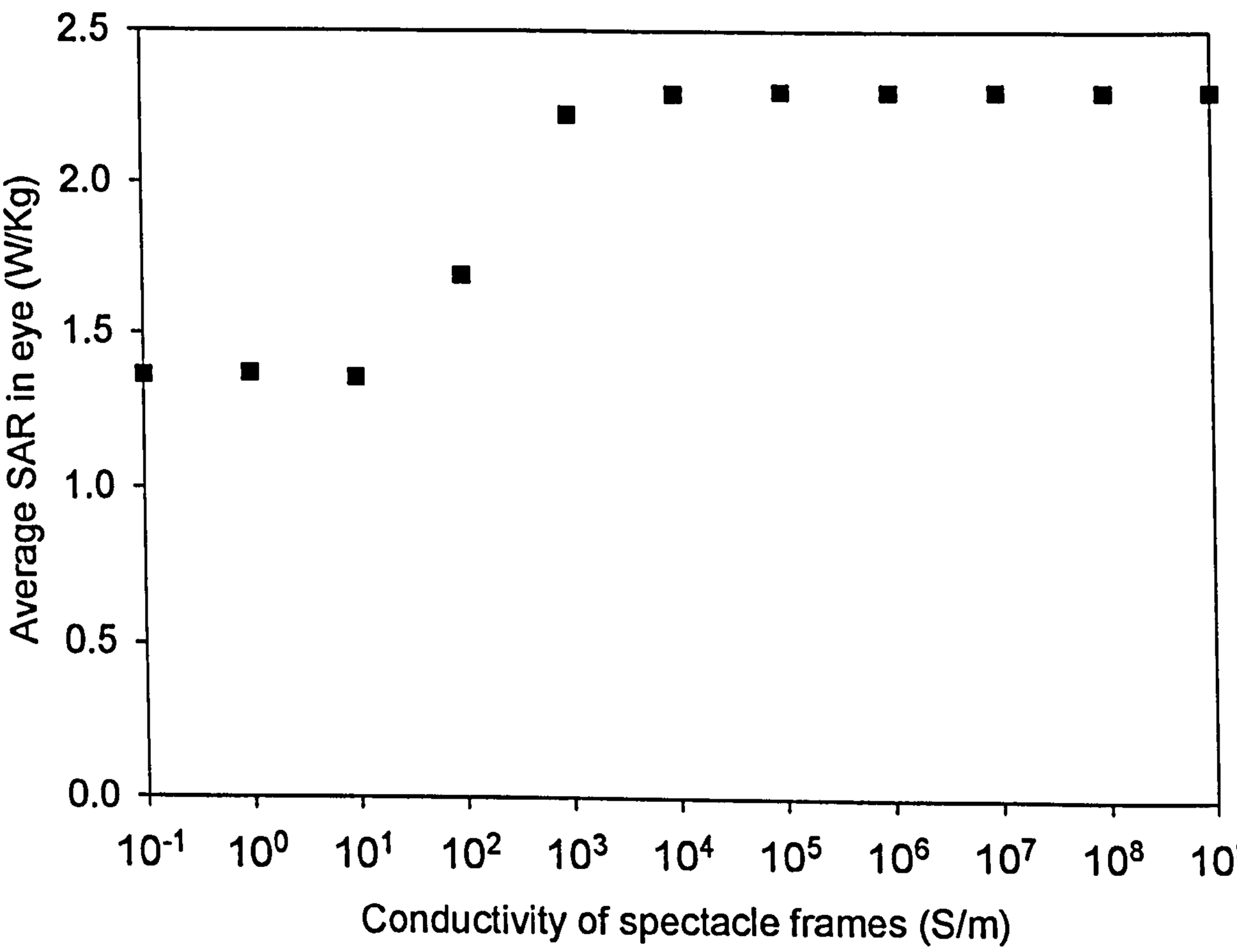

Figure 4.2. Varying the conductivity of the material in the frames. Using a vertically polarised plane wave at 1.8GHz and 34mm square spectacles with a 2mm thick Perspex lens.

If the frames have a low conductivity, then their impact is negligible. The case with just a 2mm Perspex lens with no frame, gives an average SAR in the eye of 1.37W/Kg. The frames have little effect until the conductivity increases to the order of 100S/m. As the conductivity of the frames increases, the average SAR in the eye increases. This is true until the conductivity reaches a value of approximately 10000S/m. Further increases to the conductivity of the material, have negligible effect. This means that the effects of spectacles, with frames made of insulating materials, will be largely dependent on the lens. Carbon, a conducting material, has a conductivity of 30000S/m and all metals have a higher conductivity [6]. Figure 4.2 shows the effects of spectacles on the eye are virtually identical for all conductors including metals and carbon. The rest of this thesis will assume the spectacle frames are made of copper with a conductivity of 57MS/m [6]. Copper was chosen as it has a very high conductivity and therefore simulates a worst case scenario.

Figure 4.2 shows that spectacles, composed of 34mm conducting frames and a Perspex lens, have a significant effect on the average SAR in the eye at 1.8GHz. However, it does not provide any details on the behaviour of the lens.

Figure 4.3 shows results of various different frame and lens combinations across a frequency range. The size of the frames is 34mm square and the excitation is a vertically polarised plane wave. Eight combinations of frame and lens are shown, including frames and lenses separately. To aid understanding, plots that represent frames are shown as lines and plots that represent lenses are shown as symbols. Hence a line with symbols represents a metal frame and lens. Also included are metal frames without arms represented by a broken cyan line. Plastic frames with a conductivity of 0S/m and a relative permittivity of 2.56 have been shown as a dashed yellow line.

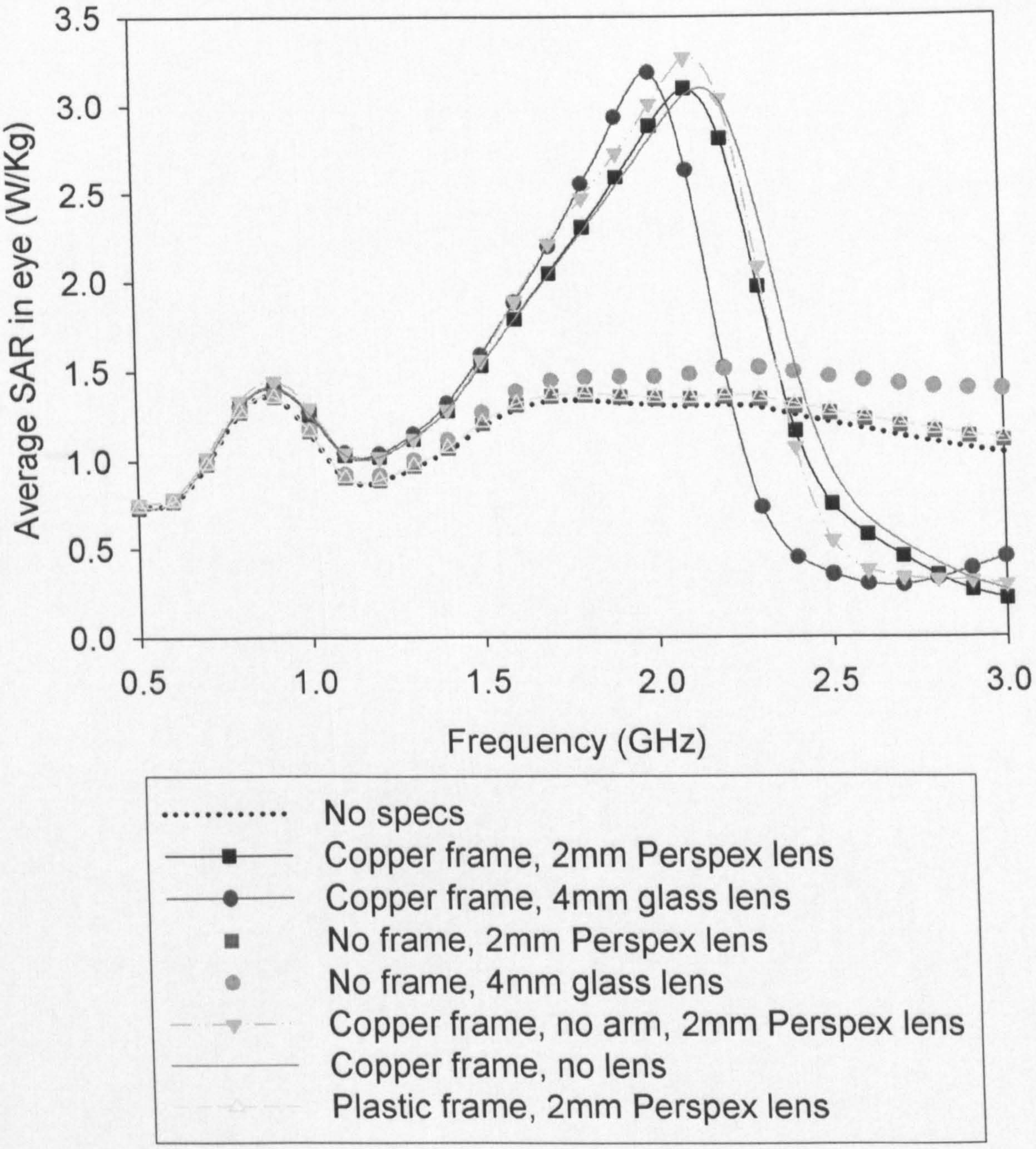

Figure 4.3. 34mm square spectacles with different frames and lenses.

Figure 4.3 provides information to explain how the frame and lens of spectacles affect the SAR in the eye at different frequencies. The lens has a small effect compared to the frame; however the effect of the lens increases with frequency. The 2mm Perspex lens,

with no frame, marginally increases the SAR in the eye. The 4mm glass lens, which has a higher permittivity of 5.00 as opposed to 2.56 for Perspex, causes a larger increase in the SAR in the eye. Figure 4.3 also shows that if the frames are made of Perspex with zero conductivity but with a relative permittivity of 2.56, the change in SAR in the eye will be largely due to the lens. Plastic frames increase the SAR in the eye by very small, insignificant amounts.

It is clear from Figure 4.3 that if the frames are metallic then the SAR in the eye is altered significantly. Generally there was an increase in SAR at around 2GHz and decreases in SAR at higher frequencies for the 34mm square spectacles investigated in this case. All cases with metallic frames cause a resonance in the eye, with similar amplitudes regardless of the lens. The inclusion of the lens can alter the resonant frequency, hence the SAR at a specific frequency e.g. 1800MHz, could be very different with a different lens. It is important, therefore, that the lens is included in the model. In this example adding a lens and increasing its permittivity decreases the resonant frequency. The graph also includes the same spectacles without an arm. The absence of the arm marginally increases the SAR in the eye and it is important that the arm is modelled. As the plot with the arm is similar to that without the arm, it is assumed that the increase of SAR in the eye is mainly due to the frames in front of the eye, and that the arm is of less significance.

Neither the frames nor the lens have a significant effect between 0.5 and 1.0GHz. These results strongly suggest that spectacles will also have little effect at 400MHz as it is considered likely that spectacles will be less likely to cause resonance effects when the wavelength is increased. This means that spectacles are unlikely to be significant to the average SAR level in the eye at the Tetra frequency ≈ 400MHz, the Nordic Mobile

Telephone system, ≈ 450MHz used in Scandinavia, and the GSM communication frequency ≈ 900MHz. This thesis will concentrate on the frequency range 1.5 to 3.0GHz. This range includes the Japanese mobile telephone system frequency ≈ 1.5GHz, the mobile phone frequencies ≈ 1800 used in Europe, ≈ 1900MHz, used in USA, Canada, Mexico, Taiwan and Japan, and the Bluetooth frequency ≈ 2.4GHz.

4.2 Results of square, rectangular, elliptical and circular spectacles with vertically polarised plane wave excitation.

In this section the excitation is a vertically polarised plane wave and the four geometric spectacles investigated, are shown in Figure 4.1. Their shapes and sizes are square (external dimensions of 36mm x 36mm in y and z dimensions), circular (44mm x 44mm), rectangular (48mm x 28mm) and elliptical (48mm x 28mm). The frames and arms of the spectacles are made of copper and the lens is 2mm thick and composed of Perspex. To examine the effect of adding metallic spectacles, four different criteria were investigated; the maximum local SAR in a single cell in the head, the maximum local SAR in a single cell in the eye, the SAR_{1g} averaged over 1g of the eye and the average SAR in the eye.

Figure 4.4 shows the maximum local SAR in any one Yee cell in the head as a function of frequency over the important range of 1.5 to 3.0GHz. The dotted line shows SAR in the head without any spectacles. It can be seen from the figure that all of the four shapes of spectacle investigated give similar effects in local SAR but that this effect is shifted in frequency. Rectangular and elliptical spectacles approximately double the maximum local SAR in any one Yee cell in the head at 2.2GHz and 2.6GHz respectively. The

addition of metal spectacles generally gives an increased maximum local SAR over the frequency range considered. However, elliptical spectacles can decrease the maximum SAR in any cell at some frequencies. In terms of location it was found that the position of the maximum SAR shifts from the skin at the front of the nose when no spectacles are present, to the skin close to the metal edges of the spectacles; either on the side of the nose or on the side of the head next to the metallic arms.

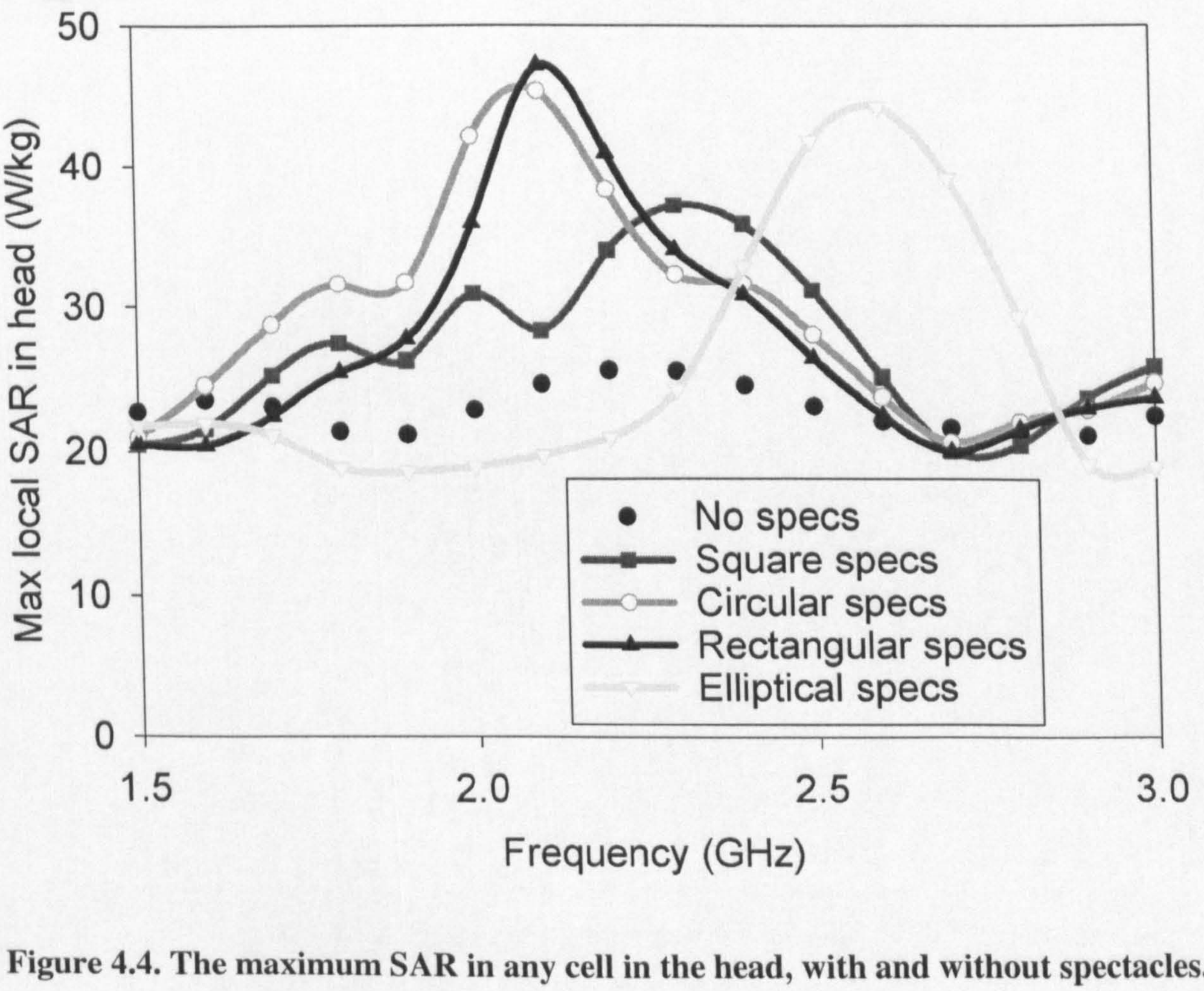

Figure 4.4. The maximum SAR in any cell in the head, with and without spectacles.

Figure 4.5 shows that the maximum local SAR in the eye is generally increased by the addition of metal spectacles below 2.2GHz and decreased above this frequency.

Elliptical frames however make the eye resonate at 2.3GHz. The existence of both increases and decreases in maximum SAR is due to the constructive and destructive interference of the electromagnetic waves interacting with the metal frames. The position of the maximum is relatively unchanged, and is located in the sclera or humor, centrally in the *x-y* plane and towards the top of the eye.

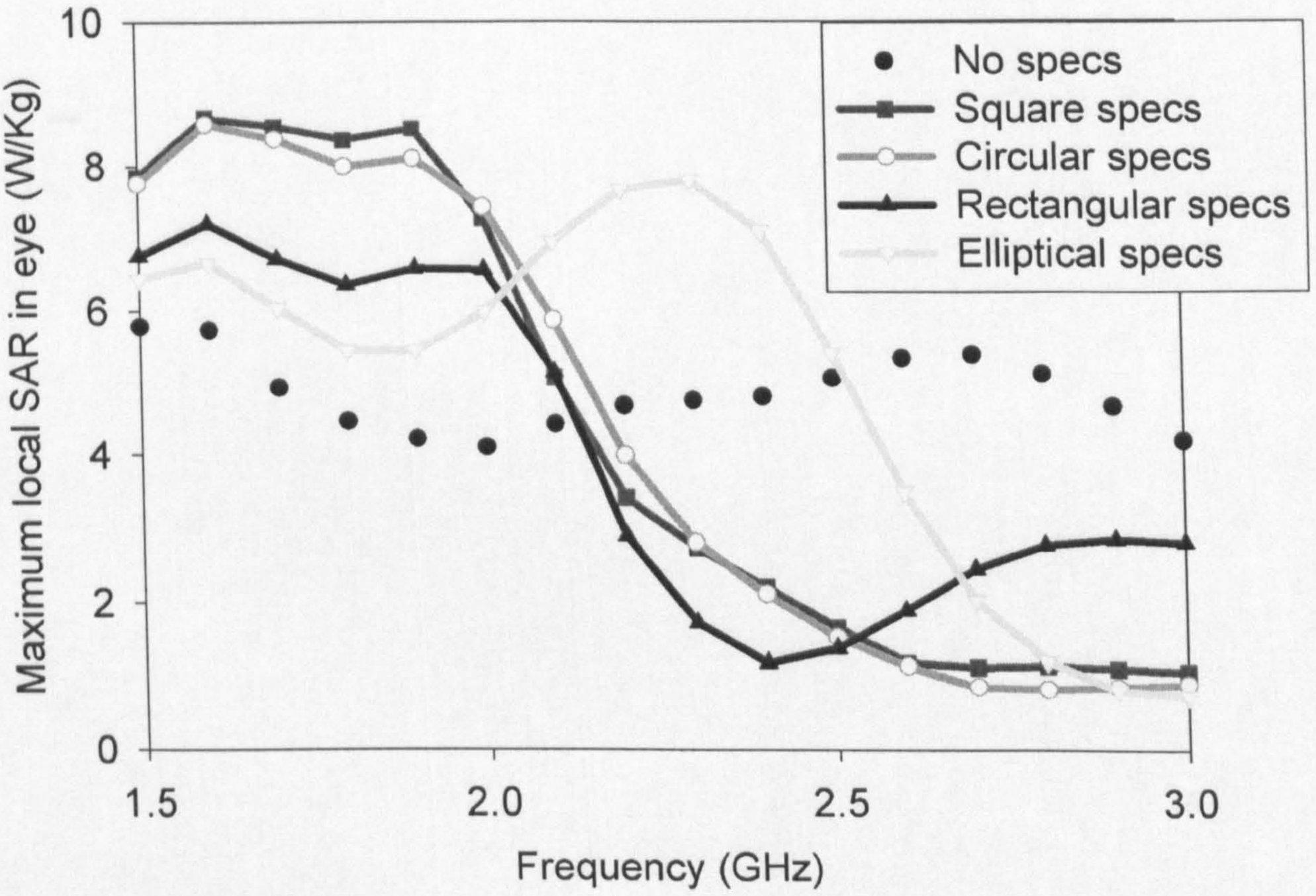

Figure 4.5. The maximum SAR in any cell in the eye with and without spectacles.

The maximum SAR_{1g} in the eye has similar characteristics to the maximum local SAR in the eye – see Figure 4.6. The square, circular and rectangular metallic spectacles modelled, increase the SAR_{1g} below 2.2GHz and decrease it above this frequency. Elliptical spectacles again cause resonance at a slightly higher frequency. The amplitude

of the SAR_{1g} is lower than the maximum SAR in any one cell in the eye by a ratio of approximately 1.5.

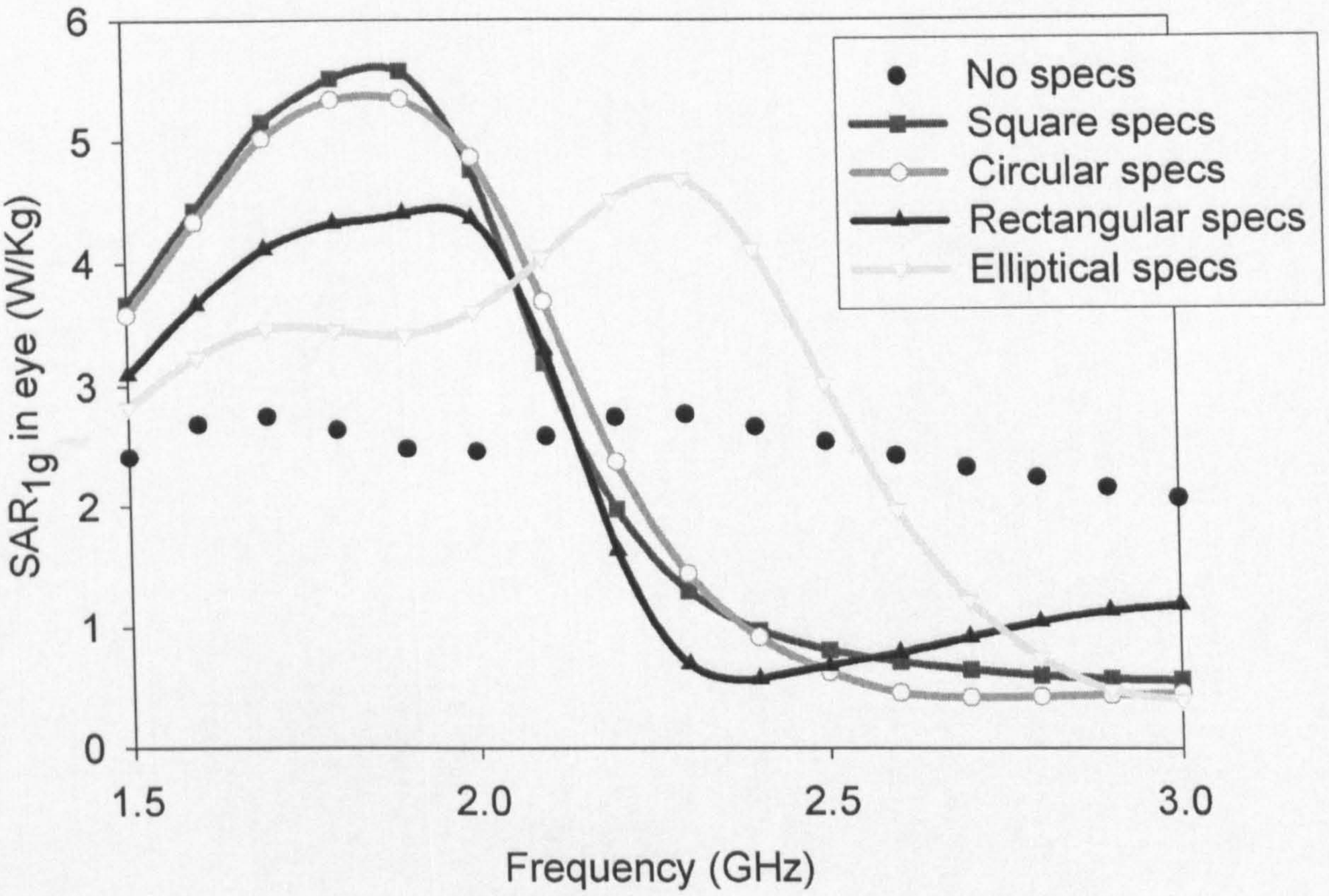

Figure 4.6. The maximum SAR averaged over 1g in the eye.

Figure 4.7 shows the SAR averaged over the whole of the eye. The eye in this model has a mass of 8.37g and is comparable to the ICNIRP [7] safety standard of 2W/Kg averaged over 10g. The average SAR in the eye exhibits similar behaviour to the values of SAR_{1g} in Figure 4.6, except that the amplitude of the SAR averaged over the eye is very closely equal to half SAR_{1g}.

The maximum effect of metallic spectacles on the average SAR in the eye is with square frames at 1.9GHz, which result in an increase of approximately 120% compared with no spectacles. However, adding spectacles can also decrease the average SAR in

the eye for the spectra considered here, particularly at higher frequencies. Elliptical spectacles at 3.0GHz reduce the power absorbed in the eye by approximately 80%.

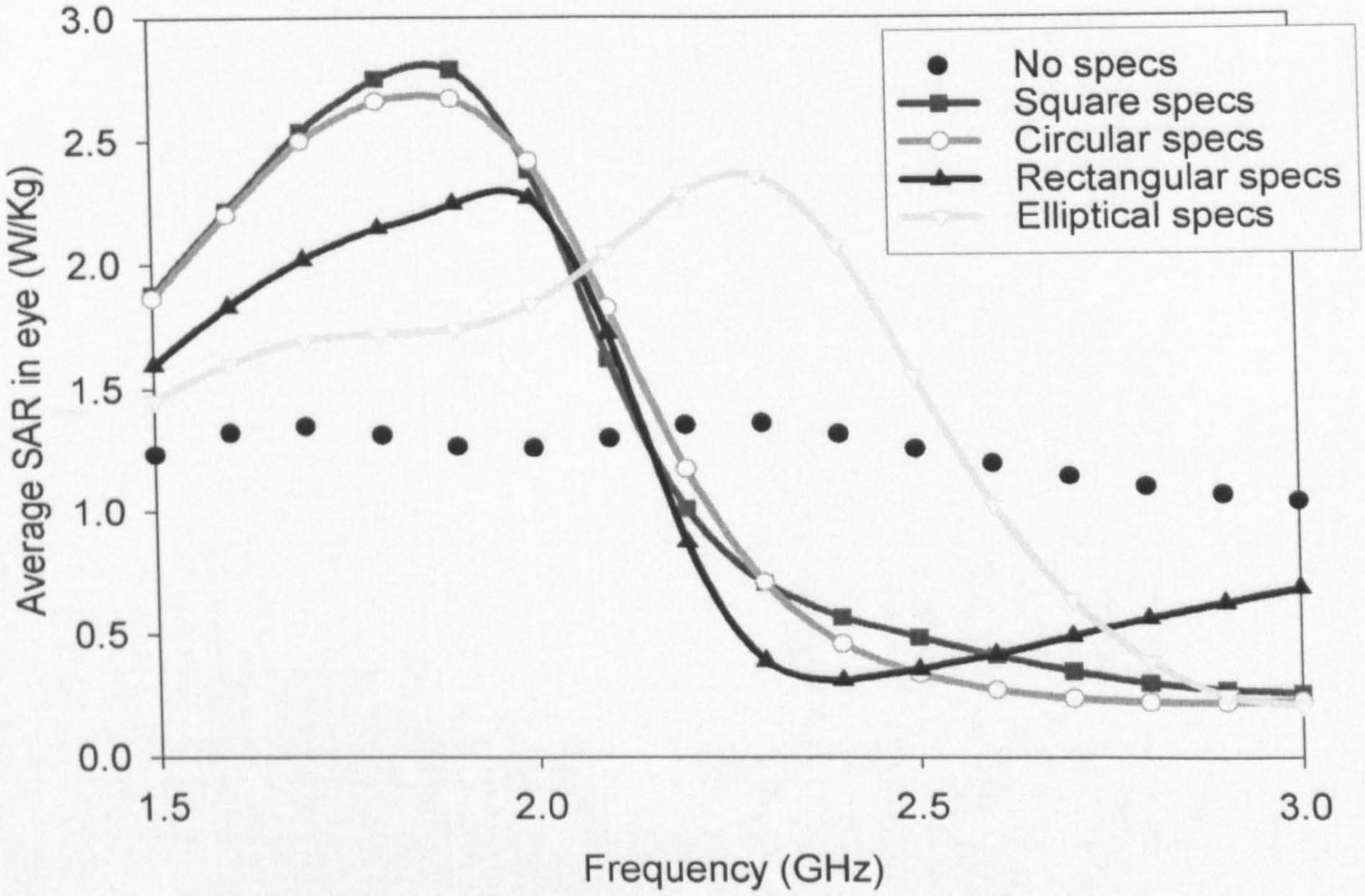

Figure 4.7. SAR averaged over the eye with and without spectacles.

All four frames examined increase and decrease (depending on the frequency) the power absorbed in the whole head by approximately 10%. The maximum increase in the power absorbed in the head is with square frames at 1.9GHz, which produced an increase of approximately 13%.

Figure 4.8 represents the difference that square spectacles make to the SAR at 1.9GHz, the frequency that produced the largest SAR in the eye, in three cross-sections through the centre of the eye. The red parts of the plot represent areas where adding spectacles increased the SAR and blue areas indicate areas where the SAR is decreased by adding

spectacles. Green represents areas where spectacles have no or negligible effect on the SAR, e.g. internal air which fill the sinuses and mouth cavities. These cavities can be clearly seen in the figure.

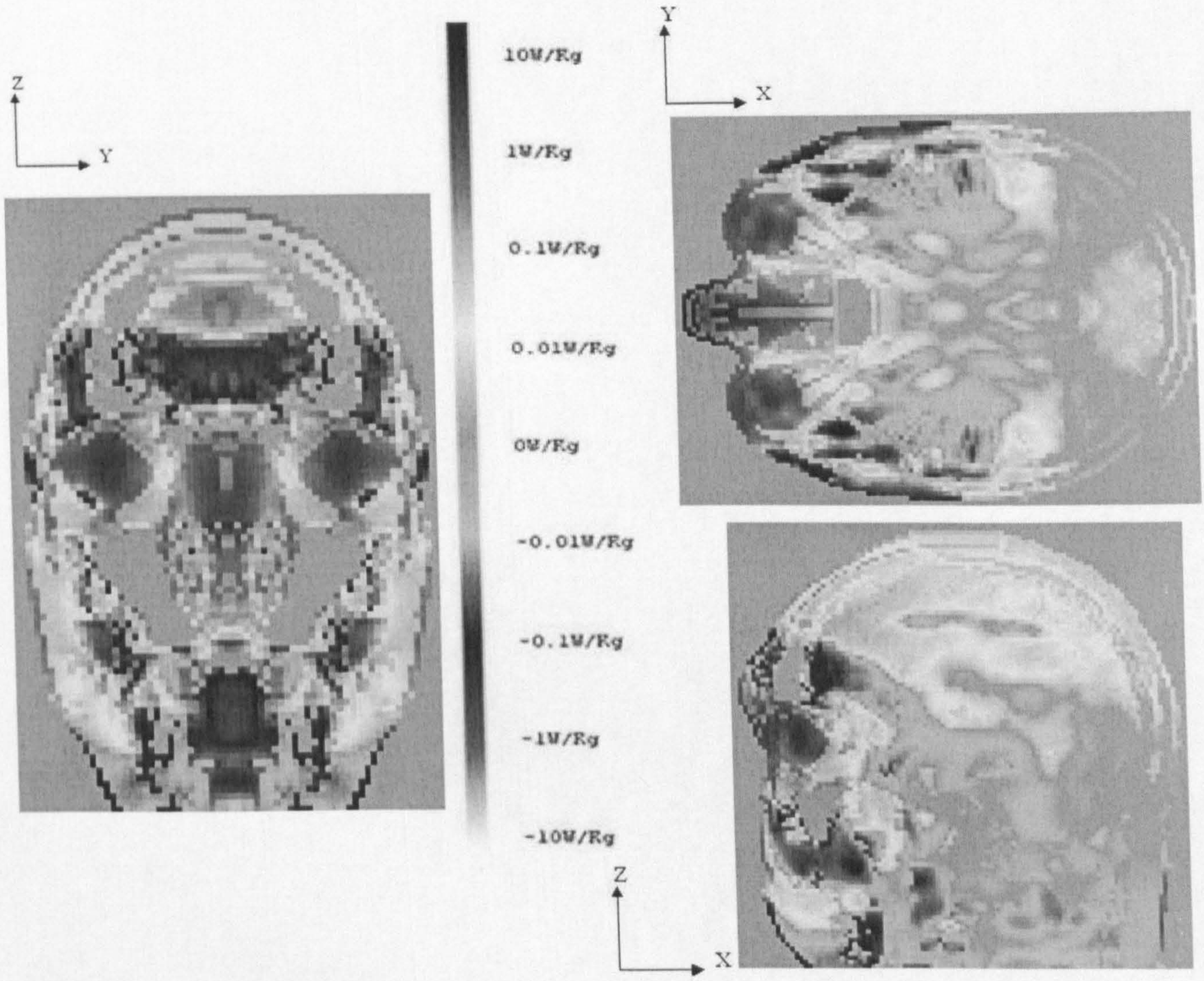

Figure 4.8. A logarithmic plot to show the increase (and decrease) in SAR, when adding square spectacles at 1.9GHz compared to no spectacles, shown as three cross-sections through the middle of the eyes. Only half the head has been modelled and the results have been mirrored to aid visual understanding.

Figure 4.5 to Figure 4.7 show there is a large increase in SAR in the eyes, but the greatest increase due to the spectacles is in the nose, as shown in Figure 4.8. This is

explained due to the nose containing tissues with relatively high conductivity, notably skin, muscle and mucous membrane. At the cross-section through the eyes, the effects of spectacles are relatively superficial and they make little difference in the region located behind the eyes and the nose. The effects decrease towards the back of the head. Figure 4.8 shows that the square spectacles at 1.9GHz generally increase the SAR throughout the head. However, there are areas of decreased SAR in the head due to the constructive and destructive interference nature of waves. The centre of the eye shows a higher increase in SAR than the surrounding tissue. Generally the SAR decreases, in a specific tissue type, with distance away from the source, as shown in Figure 3.1. The position of the maximum increase being at the centre of the tissue is an indication that the eye is resonating [2, 8].

Figure 4.9 represents a similar set of plots to Figure 4.8, except that it shows the effect of adding circular spectacles at 2.4GHz. This configuration produced the lowest average SAR in the eye. Figure 4.9 shows that the SAR is decreased significantly in the eyes and there is also a general decrease in most of the head. The possibility of decreasing the SAR in the head is of course an interesting area. However, the figure shows that care should be taken, as even though the SAR in both the eye and in the head are reduced, there are areas where the SAR is increased. Assuming any possible health risks are related to the value of the SAR, these circular spectacles could reduce the risk of damage to the eye and other specific locations in the head, but they increase the SAR in other parts of the head, and increase the maximum SAR in any cell in the head, as shown in Figure 4.4. Therefore the possible risk may be increased.

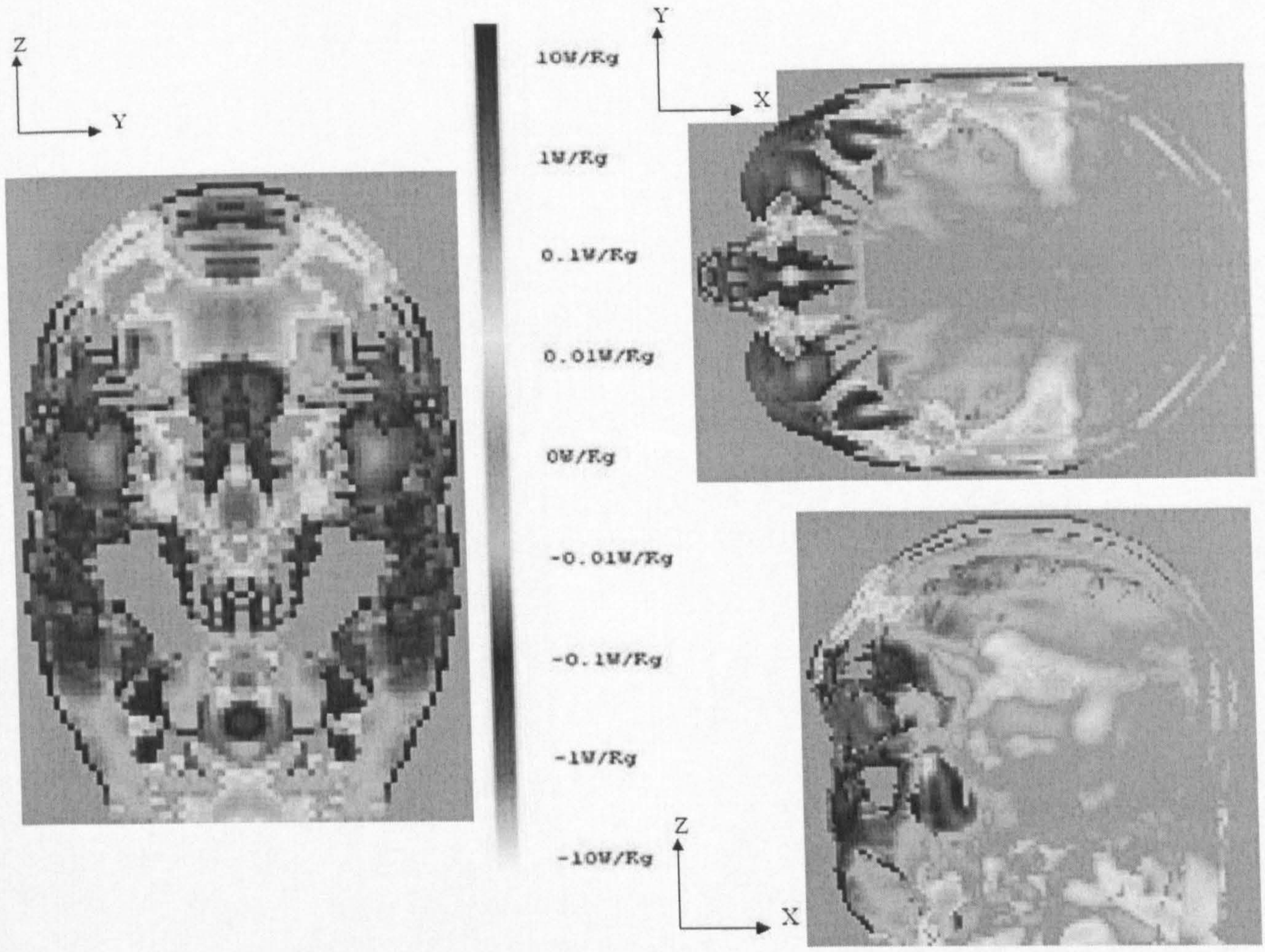

Figure 4.9. A logarithmic plot to show the decrease (and increase) in SAR, when adding circular spectacles at 2.4GHz compared to no spectacles, shown as three cross-sections through the middle of the eyes. Only half the head has been modelled and the results have been mirrored to aid visual understanding.

4.3 Realistic spectacles

The simple geometric spectacles, in Section 4.2, have been shown to have significant effects on the SAR in the eyes. Although these geometric spectacles are representative of real spectacles, real spectacles will have different shapes and sizes. Clearly there are thousands of different shapes and sizes of metallic spectacles, and it is impossible to model them all. In this section, seven different real spectacles are modelled.

The procedure to sample real spectacles is outlined briefly below. The spectacles were scanned to create a digital image of the frames. This image was converted to a raw data file, then read into the FDTD code, so the shape and size of the frames were known. Care was taken to ensure that the frames were positioned in the right location. To model the spectacles as accurately as possible a 1mm resolution of the head and a 1mm cell size are used in this section. This extra accuracy and resolution comes at the price of increasing the run time by approximately twelve times. The arms are modelled by using a line of metallic Yee cells extending from the arm strut 140mm in the x direction, as in Section 4.2. Figure 4.3 showed that the arms are not as significant as the shape and size of the metallic frames, so the simplistic modelling of the spectacles does not substantially degrade the realism of the frames. A 6mm long metal nosepiece directed in the x direction was attached to the frames, so the spectacles rested on the nose. The metal did not touch the nose but was insulated from it with 2mm Perspex pads. A 2mm thick Perspex lens has been included. The head has been considered to be symmetric.

Figure 4.10 and Figure 4.11 show the maximum SAR_{1g} in the eye and the average SAR in the eye with a 1mm resolution head and spectacles. Results are very similar to the results using a 2mm cell size for the case without spectacles. This shows that using a 2mm cell size is valid, and that the extra level of detail of the head and the increased sampling with a 1mm resolution model does not make significant changes to the SAR distribution in the eyes.

Figure 4.10 and Figure 4.11 show that adding 1mm resolution realistic metallic spectacles can significantly increase and decrease the SAR in the eye depending on the frequency and the size and shape of the frame. 1mm resolution realistic spectacles give similar results compared to 2mm resolution geometric spectacles. Both sorts of

spectacles generally increase the maximum SAR_{1g} and the average SAR in the eye by approximately 100% at frequencies around 1.8GHz and decrease the SAR in the eye at higher frequencies. Five of the seven realistic spectacles increase the SAR in the eye by approximately 100%, while spectacles 3 and 5 cause only very small increases in the frequency range considered.

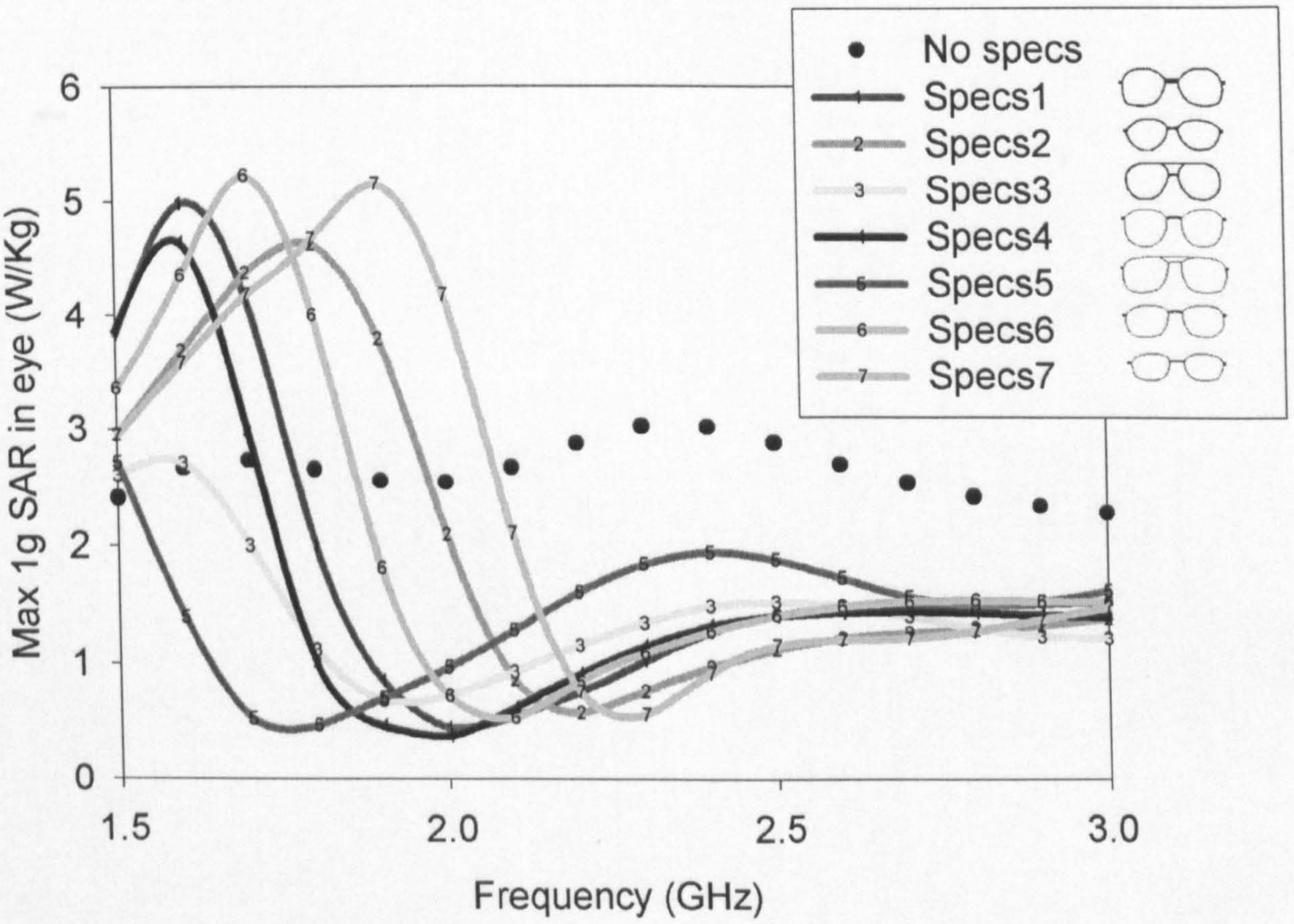

Figure 4.10. The maximum SAR in any 1g of the eye with seven different 1mm resolution realistic metallic spectacles, shown inset in the legend.

Five of the seven spectacles, shown in Figure 4.10 and Figure 4.11, produce similar magnitudes of SAR in the eye at frequencies varying from 1.6 to 1.9GHz. This frequency range includes the 1.8GHz telecommunication frequency. The Q of the

resonance means that different pairs of spectacles could have very different effects at a specific frequency. The resonance frequency appears to be inversely proportional to the height, with shorter (in the *z* direction) spectacles producing a resonance at a higher frequency. Again the maximum SAR averaged over 1g of the eye is very closely equal to twice the average SAR in the eye. Comparing the amplitudes and resonant frequencies of both realistic and geometric spectacles indicates that their behaviour is similar. Therefore, it is considered reasonable to continue to model spectacles using simple geometric shapes.

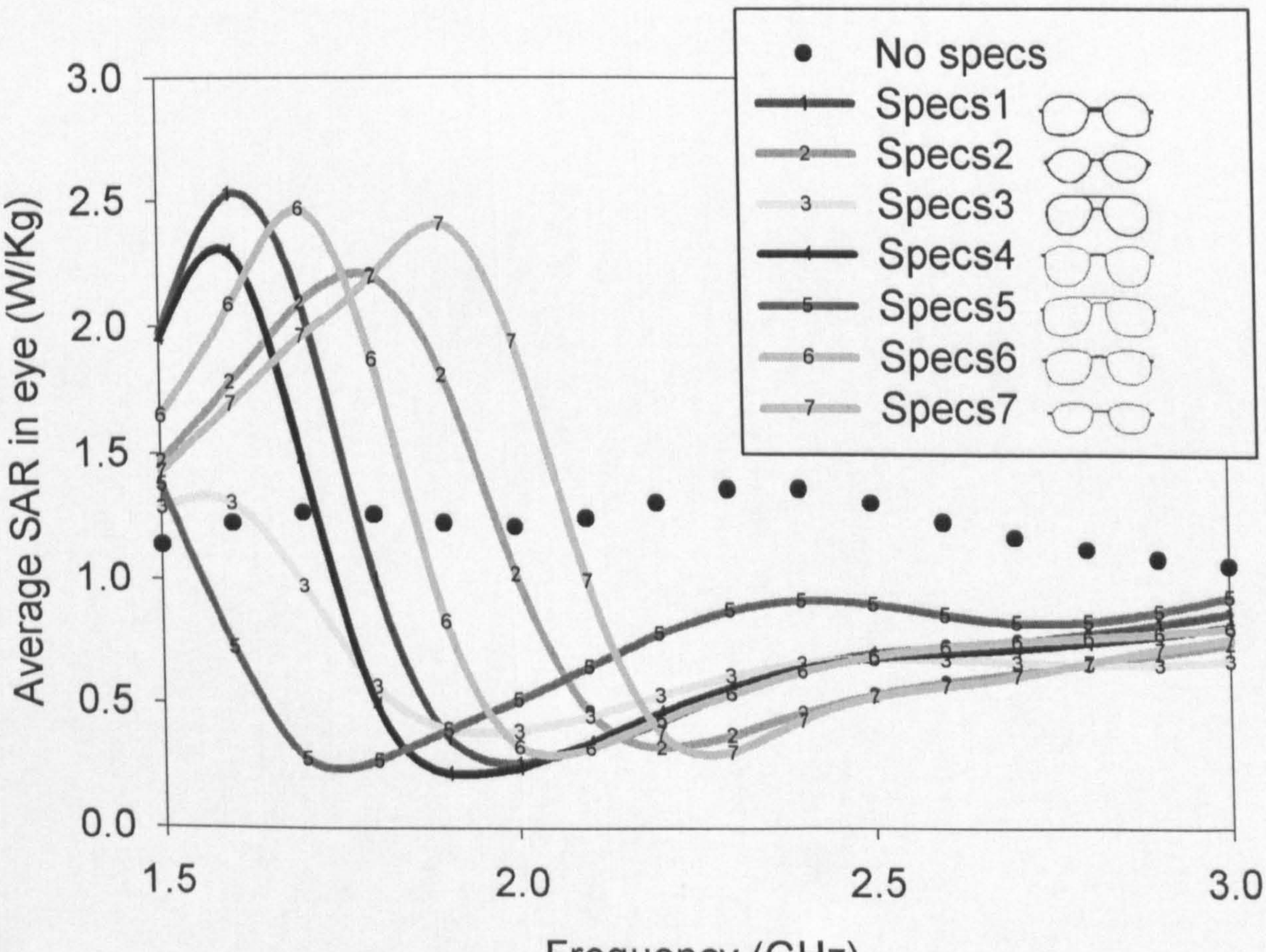

Figure 4.11. The average SAR in the eye with seven different 1mm resolution realistic metallic spectacles, shown inset in the legend.

Figure 4.12 shows the effect of adding spectacles 1 at 1.6GHz. This combination was chosen as it gave the highest average SAR in the eye. At the cross-section shown the addition of spectacles generally increased the SAR in the head. Again effects are similar to the square spectacles at 1.9GHz shown in Figure 4.8. The spectacles cause large increases in the SAR in the eyes and the front of the head. The levels decrease towards the back of the head. Note that the logarithmic scale tends to exaggerate the perturbations in SAR caused by the spectacles at the back of the head. At certain locations throughout the head the addition of metallic spectacles decreases the local SAR. Again the sinuses in the nose are clearly visible as areas of no change in the SAR. The higher resolution of the model can also be seen. The symmetry in Figure 4.12 is because only half the head has been modelled and the results have been mirrored.

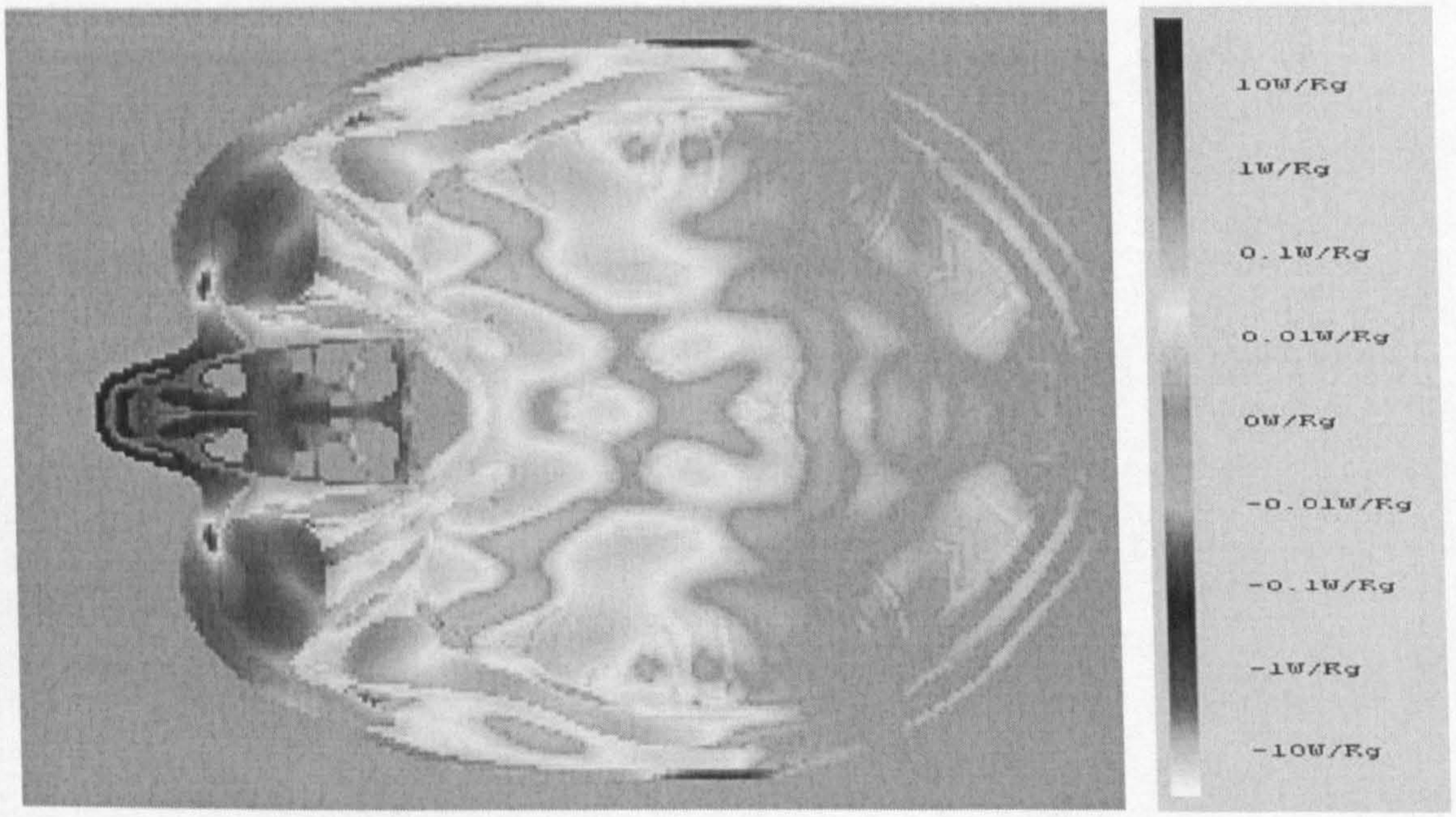

Figure 4.12. A logarithmic plot to show the increase (and decrease) in SAR in a cross-section through the eyes. Spectacles 1 have been added with a plane wave excitation of 1.6GHz. N.B. only half the head has been modelled and the results have been mirrored to aid visual understanding.

4.4 Conclusions

This chapter has provided accurate details of the modelling of the metallic spectacles. Metallic arms and lenses have also been modelled. The effect of metallic spectacles is strongly dependent on the excitation frequency and spectacles have little effect below 1.0GHz. This allows the frequency range investigated, to be narrowed to 1.5 to 3.0GHz.

Metallic spectacles have been shown to have a significant effect on the head and especially on the eye. The materials that the spectacles are made of is important. Generally frames made of insulating materials will have little effect, whereas all conductors could have a potentially large effect. Yet the specific conducting material is less significant. The lens has a small effect on its own, but can also alter the resonance frequency of the peak interaction. Metallic spectacles can produce a resonance in the eyes at a particular frequency that is dependent on the size of the frames and particularly on the height. Increases of approximately 100% in the average SAR in the eye have been found, as well as decreases of 80%. Generally, metallic spectacles increase the maximum SAR in any cell in the head at all frequencies considered. Representative shaped spectacles have also been considered and give similar amplitudes of SAR in the eye, resonance frequencies and locations of maximums, as geometrical spectacles.

4.5 References

1. Taflove, A., *Computational electrodynamics. The finite-difference time-domain method.* 1995: Artech House, Inc.
2. Hirata, A., S. Matsuyama, and T. Shiozawa, *Temperature rises in the human eye exposed to EM waves in the frequency range 0.6-6 GHz.* IEEE Transactions on Electromagnetic Compatibility, 2000. **42**(4): p. 386-393.

3. Nikita, K.S., M. Cavagnaro, P. Bernardi, N.K. Uzunoglu, S. Pisa, E. Piuzzi, J.N. Sahalos, G.I. Krikelas, J.A. Vaul, P.S. Excell, G. Cerri, S. Chiarandini, R. De Leo, and P. Russo, *A study of uncertainties in modeling antenna performance and power absorption in the head of a cellular phone user.* IEEE Transactions on Microwave Theory and Techniques, 2000. **48**(12): p. 2676-2685.

4. Bernardi, P., M. Cavagnaro, and S. Pisa, *Evaluation of the SAR distribution in the human head for cellular phones used in a partially closed environment.* IEEE Transactions on Electromagnetic Compatibility, 1996. **38**(3): p. 357-366.

5. Wang, J., T. Joukou, and O. Fujiwara, *Localized specific absorption rate in the human head in metal-framed spectacles for 1.5GHz Hand-held mobile telephones.* Trans IEE of Japan, 1998. **118-A**(11): p. 1234-1240.

6. Kraus, J.D., *Electromagnetics*. 4th ed. 1981.

7. ICNIRP, *Guidelines for limiting exposure to time-varying electric, magnetic and electromagnetic fields (up to 300GHz).* Health Phys, 1998. **74**: p. p. 494-522.

8. Taflove, A. and M.E. Brodwin, *Computation of the electromagnetic fields and induced temperatures within a model of the microwave-irradiated human eye.* IEEE Trans. Microwave Theory Technology, 1975. **23**(11): p. 888-896.

Chapter 5

OPTIMISATION OF SPECTACLES FOR SAR USING A GENETIC ALGORITHM

5.1 Introduction

Chapter 4 showed that metallic spectacles can affect the SAR in the eye and the head. In this chapter, a genetic algorithm (GA) was used to search for the maximum effects of adding metallic spectacles at various frequencies. The GA was used to provide a complete definitive range of SAR values that could be produced in the eye in conjunction with various shapes and sizes of spectacles. The algorithm used was that described in [1] and is explained in more detail in Appendix H. The GA had two objectives; the average SAR in the eye and the maximum SAR averaged over any 1g of the eye. Both plane wave and dipole excitations are considered in separate searches. Results are also included for the maximum SAR_{1g} and SAR_{10g} in the whole head.

5.2 GA application to metallic spectacles

Seven different genes describe each pair of spectacles; these are listed in Table 5.1. The results in Chapter 4 indicated that the shape and size of metal frames changes the absorption in the head significantly. Figure 4.3 showed that different lens materials and thicknesses used with the same metal frames can affect the SAR in the eye, thus it is important to consider different lenses. Two possible materials for the lens were chosen. These were Perspex and glass; with relative permittivities of 2.56, and 5.00,

respectively. The position of the spectacles in relation to the head was thought likely to have an effect on the SAR in the head and is also included as a gene.

Table 5.1. The seven different genes used to build each pair of spectacles, including the range of each variable and the number of possible configurations produced.

Gene	Range	No. of possibilities
Distance from spectacles to eye	24 to 34mm, every 2mm	6
Width of spectacle frames	34 to 48mm, every 2mm	8
Height of spectacle frames	20 to 38mm, every 2mm	10
Lens material	Perspex, glass	2
Thickness of lens	2 to 6mm, every 2mm	3
Shape of spectacle frames	Rectangular, elliptical	2
Length of strut to arm	2 to 18mm, every 2mm	9

The position and size of the frames were chosen so that no configuration of spectacles either lay inside the head or touched the surface of the head, thus ensuring that the frames were electrically insulated from the head.

As the Brooks head was thought by the author to be relatively large when compared to other heads in the space from ear to ear the width of the spectacles was also varied. This was done by varying the length of the strut from the frame to the arm. The arms were then tapered to fit the head, touching the sides of the head.

The search space was thus represented as having 51840 discrete points. The GA was run with a population size of eighty of which the best sixteen chromosomes were kept and the worst sixteen were discarded. More chromosomes provide a better sampling of the solution space but slow convergence [2] as the GA has to call the FDTD code more often. Population sizes of 30 to 100 [3] or equal to ten times the number of genes in a

chromosome [2] are typical. Twenty generations of spectacles were used, but no significant change was seen in the Pareto optimal set after twelve generations. The results of the GA can be tested by running the algorithm several times with random real seeds and also by varying the mutation probability and number of chromosomes [2]. This did not produce higher results and therefore the GA is thought to have found a good solution as these subsequent searches failed to better it. There is, however, no guarantee that the global maximum has been found [2]. Searches with smaller populations also converged to the same maximum; therefore the GA could have been run with a smaller population if time constraints were of a higher importance.

5.1 Comparison of Brooks and Bradford heads with fifty random pairs of metallic spectacles

The results in Chapter 4 showed the effects of metal spectacles using the Brooks head. It was considered possible that the same spectacles could have different effects on different heads. The seven parameters outlined in Table 5.1, were chosen randomly from the predefined ranges to produce fifty random spectacles. The same spectacles were then added to both the Brooks and Bradford heads and the effects on the average SAR on the eyes were investigated. The heads were excited with a 1.8GHz vertically polarised plane wave. The results are shown in Figure 5.1.

All fifty spectacles investigated increased the average SAR in the eyes of both heads. All points in Figure 5.1 lie close to the 45° straight line, which represents the same percentage increase of the average SAR in the eyes of both heads. The average SAR in the Brooks eye was higher, but the percentage increase when adding metallic spectacles

was very similar for both heads. The average percentage increases of SAR in the eye for the Brooks and Bradford heads were 54.6% and 50.4% respectively.

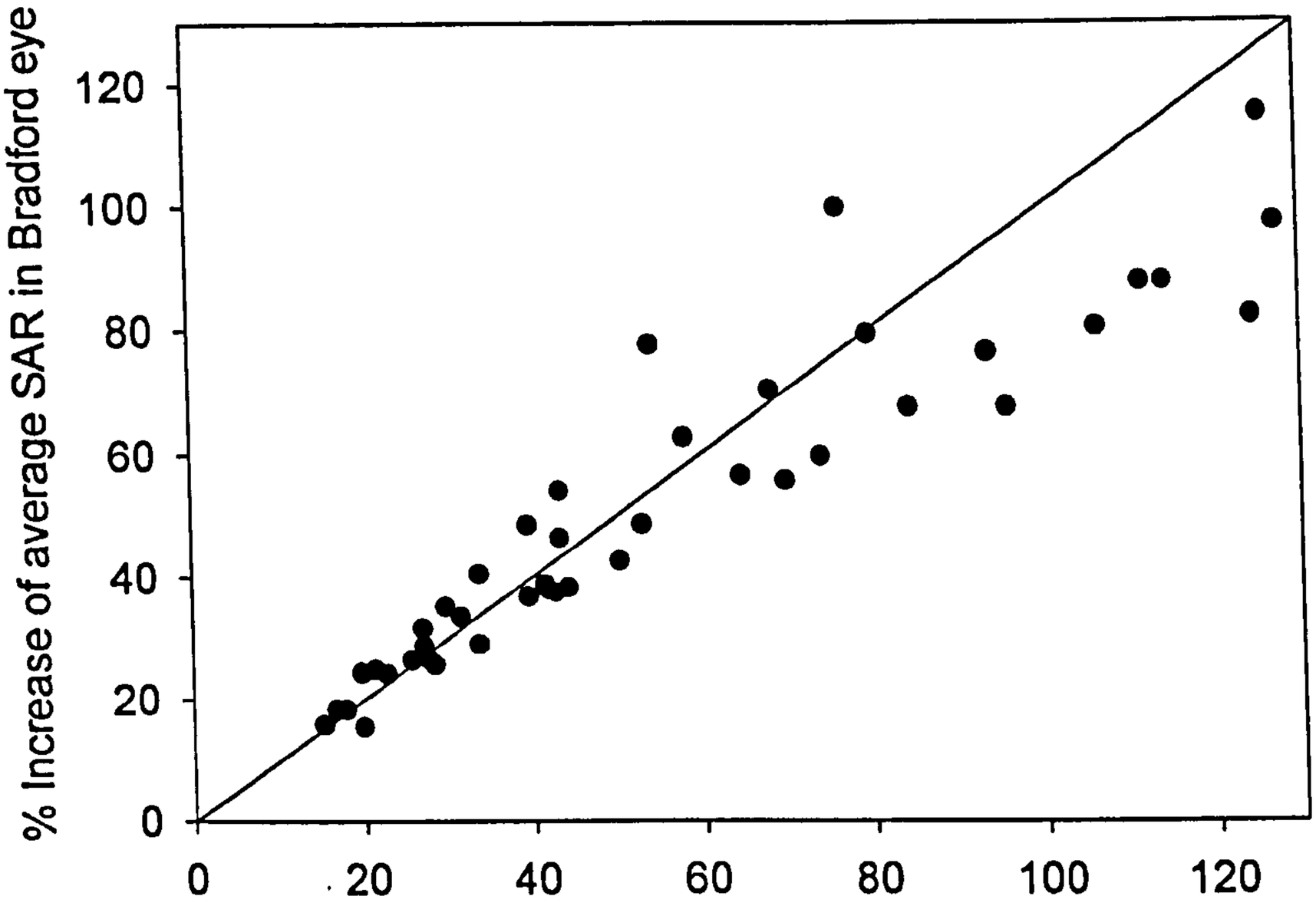

Figure 5.1. The effect of adding fifty random spectacles to both Brooks and Bradford heads at 1.8GHz. The straight line represents pairs of spectacles that increase the average SAR in the eyes in both heads by the same percentage.

Although fifty spectacles is a small sample size, the results indicate that a specific pair of spectacles will have similar effects on different heads, even though the heads are different sizes, are composed of different materials and have different sized eyes. It is therefore likely that a specific pair of real spectacles will have similar effects on different people, and hence it is reasonable to primarily model the effects of spectacles using only the Brooks and Bradford heads and to assume that all heads will be similar.

The results show that the choice of spectacles is more important than the choice of head. If the results in Figure 5.1 had diverged significantly from the 45° straight line, it would be very difficult to estimate the effect of a pair of spectacles on different people.

5.2 GA run with a vertically polarised plane wave at 0.9, 1.5, 1.8, 2.4 and 3.0GHz

This section will use the GA to search for the maximal effects of adding metallic spectacles to the Brooks head at various popular communication frequencies. The excitation used is a 50W/m² vertically polarised plane wave.

Figure 5.2 shows the total range of effects, found by the GA, at various communication frequencies. The GA was used as described above to search for both the maximum and minimum SAR in the eye in two separate searches. The red and green lines represent the highest and lowest average SAR found in the eye. The yellow line represents the average value of 100 random pairs of spectacles.

Figure 5.2 shows the results of the average of 100 spectacles with parameters chosen at random in the predefined ranges as defined in Table 5.1. This is a relatively small sample but represents the likely effect of a real person wearing a random pair of spectacles. On average, spectacles have little effect at 900MHz and 1.5GHz and decrease the SAR in the eye at 3.0GHz. However, at 1.8 and 2.4GHz metallic spectacles are likely to increase the average SAR in the eye. As shown in Chapter 4, realistic spectacles behave similarly to geometric spectacles; hence it is likely that the total range of average SAR in the eye found with geometric spectacles will be similar to the range with real spectacles.

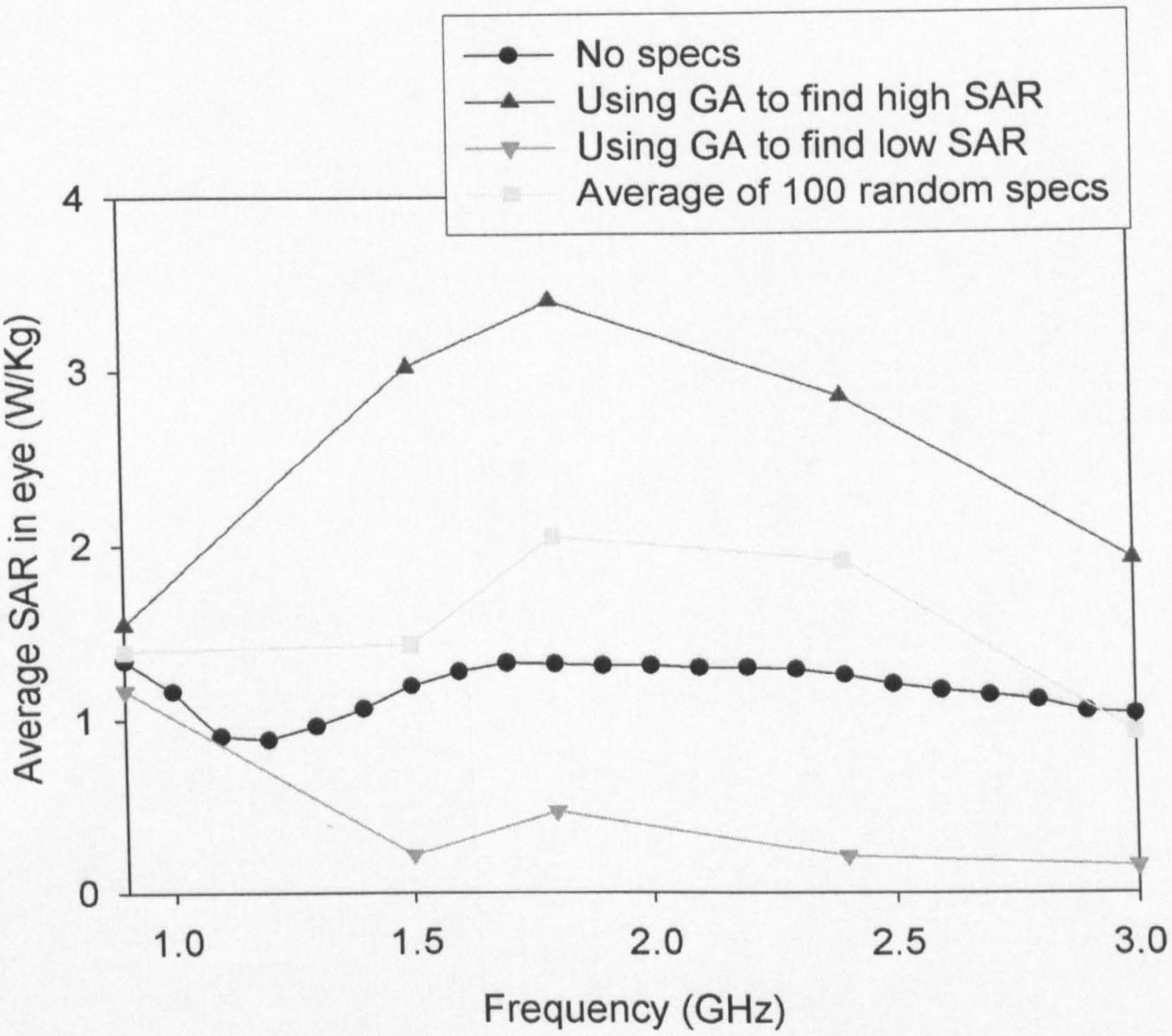

Figure 5.2. The maximum and minimum average SAR in the eye found by the GA, when adding metallic spectacles at different frequencies. Also shown is the average value of 100 spectacles with random parameters in the seven predefined ranges.

Figure 5.2 shows that the effects of metallic spectacles are small at 900MHz. The GA did not find a pair of spectacles that either significantly increased or decreased the average SAR in the eye. This verifies the decision to concentrate on the frequency range between 1.5 and 3.0GHz. At all four frequencies considered in this range, metallic spectacles can significantly increase and decrease the SAR in the eye. The largest average SAR in the eye was found at 1.8GHz. This frequency also showed the largest percentage increase of the average SAR in the eye due to the metallic spectacles.

At 1.8GHz, the GA found a configuration of spectacles with an average SAR in the eye of 3.40W/Kg. Spectacles increased the average SAR in the eye by 2.59 times compared to 1.31 W/Kg, the average SAR in the eye with no spectacles present. The same spectacles increased the maximum SAR averaged over 1g by 2.76 times from 2.64W/Kg to 7.29W/Kg. The genes that describe these spectacles are listed in Table 5.2.

Table 5.2. The parameters of the metallic spectacles that produced the maximum SAR in the Brooks eye with a vertically polarised plane wave at 1.8GHz.

Gene	Value
Distance from spectacles to eye	26mm
Width of spectacle frames	36mm
Height of spectacle frames	38mm
Lens material	Glass
Thickness of lens	4mm
Shape of spectacle frames	Rectangular
Length of strut to arm	18mm

The GA also produced configurations of spectacles that reduced the SAR in the eye at 1.8GHz. The lowest result found for the average SAR in the eye was 0.47W/Kg, a decrease of 64% compared to without spectacles. The SAR_{1g} in the eye was 0.99W/Kg. The spectacles were positioned 28mm from the eye. The frames were rectangular, 46mm wide by 38mm high. A 6mm glass lens was used and the strut length was 6mm. The main difference between the two spectacles, that caused the biggest increase and decrease in the SAR in the eye, was the size of the frames.

5.3 GA run with Bradford head with a vertically polarised plane wave at 1.8GHz.

The GA was run in the same way as in Section 5.2 using the Bradford head with a 2mm resolution. The Bradford head allowed spectacles to be positioned closer to the eye and hence the range of the spectacles-eye distance gene was increased to 12-34mm. The highest average SAR found in the eye was 2.62W/Kg, an increase of 2.66 times. The same spectacles increased the SAR in the eye averaged over 1g by 2.71 times to 3.74W/Kg. These spectacles were very similar to the pair found by the GA with the Brooks head, described in Table 5.2. The frames were the same size and shape; the lens was 6mm thick glass as opposed to 4mm. The frames were 24mm in front of the eye and the strut length was 14mm.

The GA was also used to search for the lowest SAR in the eye with the Bradford head, reducing the average SAR in the eye by 53% to 0.46W/Kg and reducing the maximum SAR averaged over 1g of the eye by 59% to 0.57W/Kg. Again the spectacle frames were the same shape and size as the frames that produced the lowest SAR in the eye of the Brooks head. The lens was 4mm thick glass. The spectacles were positioned 14mm in front of the eye and the strut length was 14mm.

In searching for the minimum and then for the maximum SAR in the eye, the GA found similar spectacles with the two different heads. This result consolidates those in Section 5.1, which suggested that the same spectacles have similar effects on different heads. The results also indicate that the GA has converged to very similar spectacles in different searches, which provides confidence that the GA is finding the global maximum or minimum in each case.

As a further comparison of the Brooks and Bradford heads, the two heads were both modelled with the spectacles that gave the highest average SAR in the eye at 1.8GHz with the Brooks head, as described in Table 5.2. These results, as a function of frequency of the vertically polarised plane wave excitation, are shown in Figure 5.3. The effects of the same spectacles, on the two different heads, are similar across the whole frequency range considered. The spectacles cause an increase in the SAR in the eye at 1.8GHz and decrease the SAR above 2.0GHz.

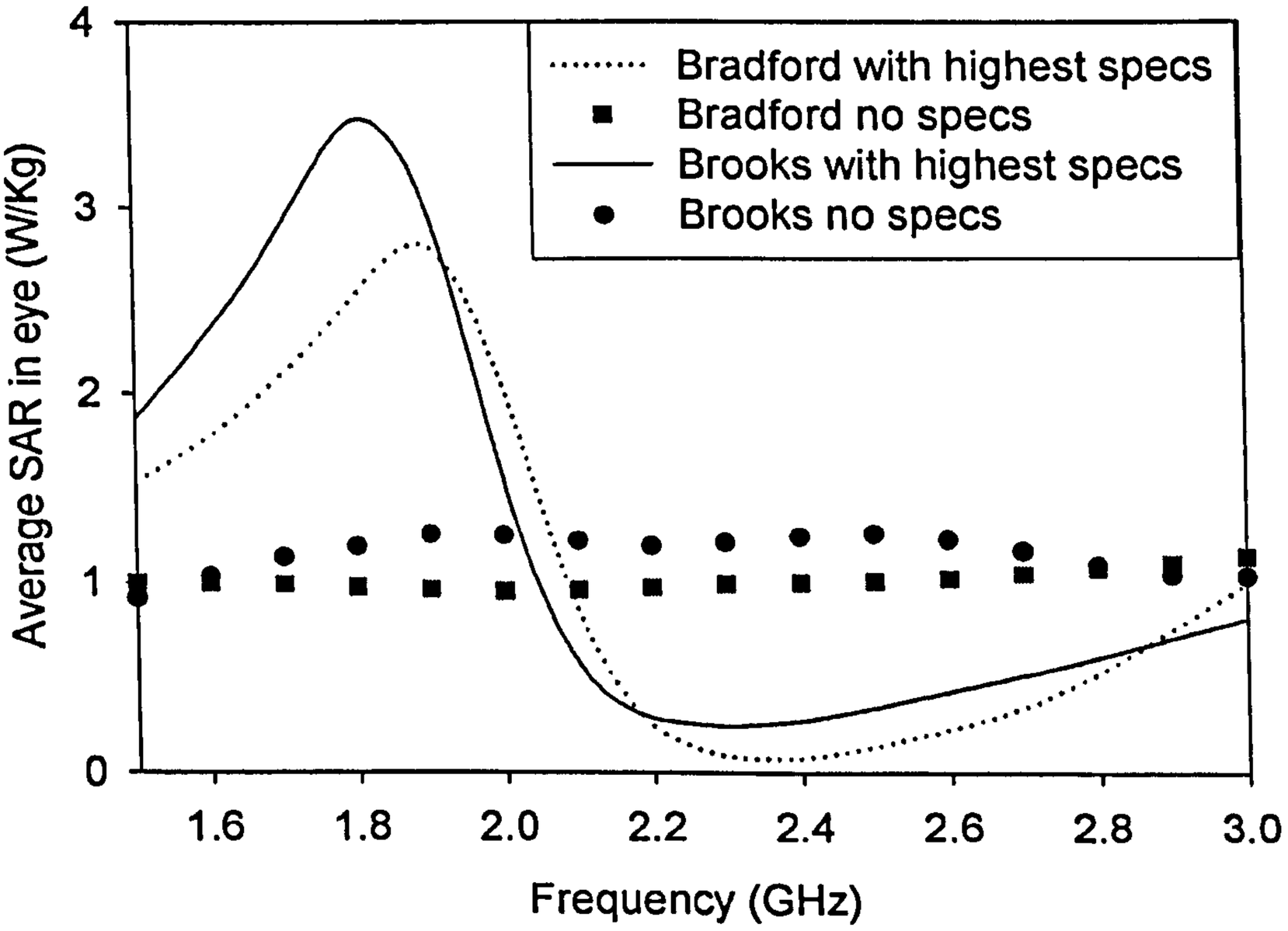

Figure 5.3. The average SAR in the eye at 1.8GHz with both Bradford and Brooks heads in conjunction with the spectacles described in Table 5.2.

The results earlier in this section and those in Figure 5.1, showed that the effects of a specific pair of spectacles at 1.8GHz is likely to be similar on different people and that the maximum and minimum effects are likely to be found with similar spectacles. Figure 5.3 suggests that the effects of the same spectacles on different people may be similar over a frequency range and not just at 1.8GHz. This suggests that the choice of

primarily only using one digital head, and assuming that the effects of spectacles on different people will be similar, is valid across the frequency range, considered in this thesis, that includes communication spectra.

5.4 Varying the individual parameters of the spectacles

The largest effect of spectacles was at 1.8GHz; hence more detailed analysis will be given to spectacles at this frequency. To investigate the effects of the different parameters that describe a pair of spectacles, individual parameters were examined separately. The spectacles were initially the same as the ones described in Table 5.2, and then the individual parameters were varied. It should be noted that Figure 5.4 to Figure 5.8 only show the relationship based on the spectacles with the highest SAR in the eye and are not a general rule.

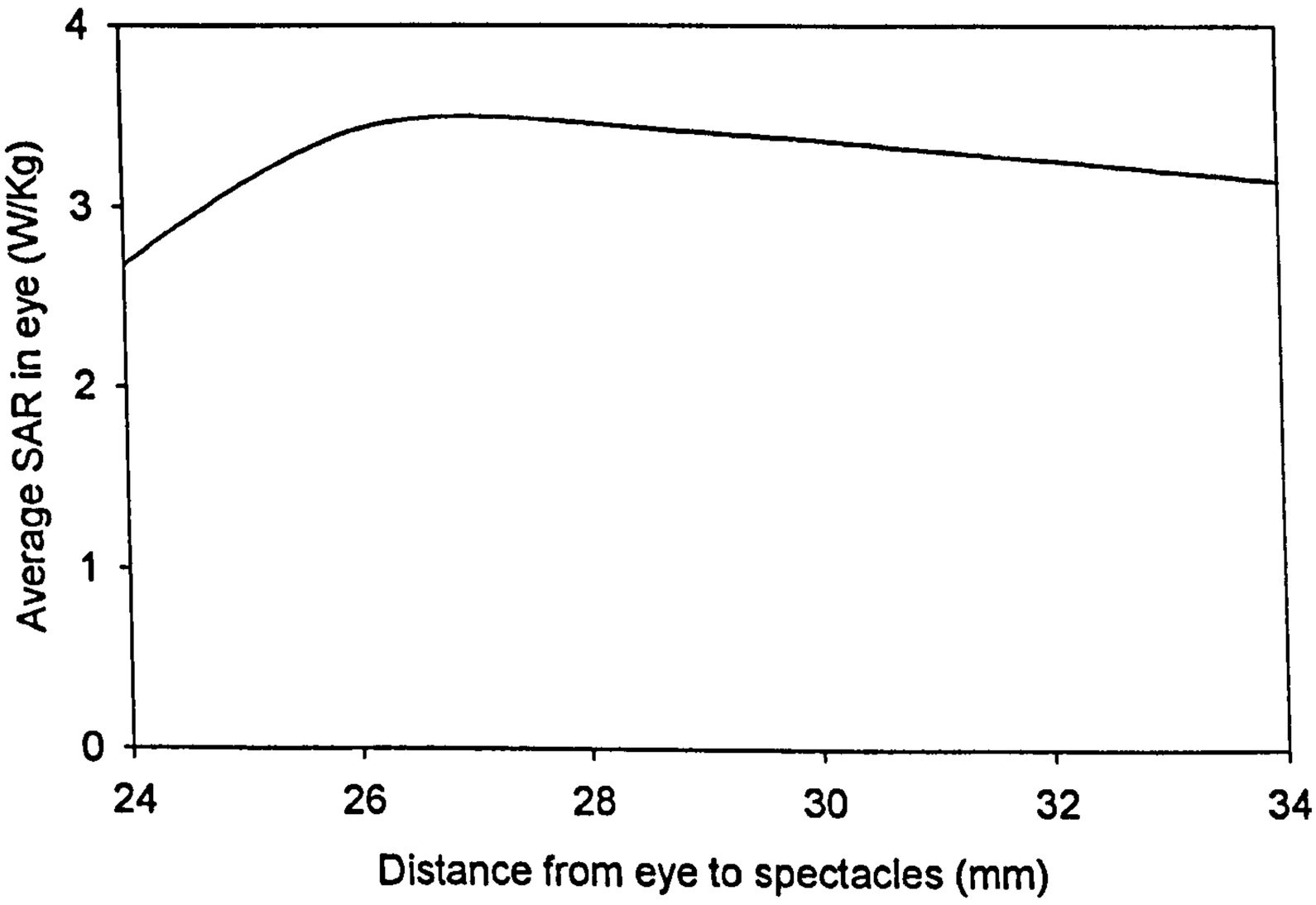

Figure 5.4. Varying the distance from the front of the eye to the frames of the spectacles in Table 5.2.

Figure 5.4 shows that the SAR in the eye is at a maximum when the frames are 26mm away from the eye. Note that the spectacles could not be moved closer than 24mm from the front of the eye without the frames lying inside the head. As the spectacles-eye distance increases above 26mm the SAR in the eye decreases marginally. Moving the spectacles closer to the eye from the maximum distance of 26mm may decrease the average SAR in the eye.

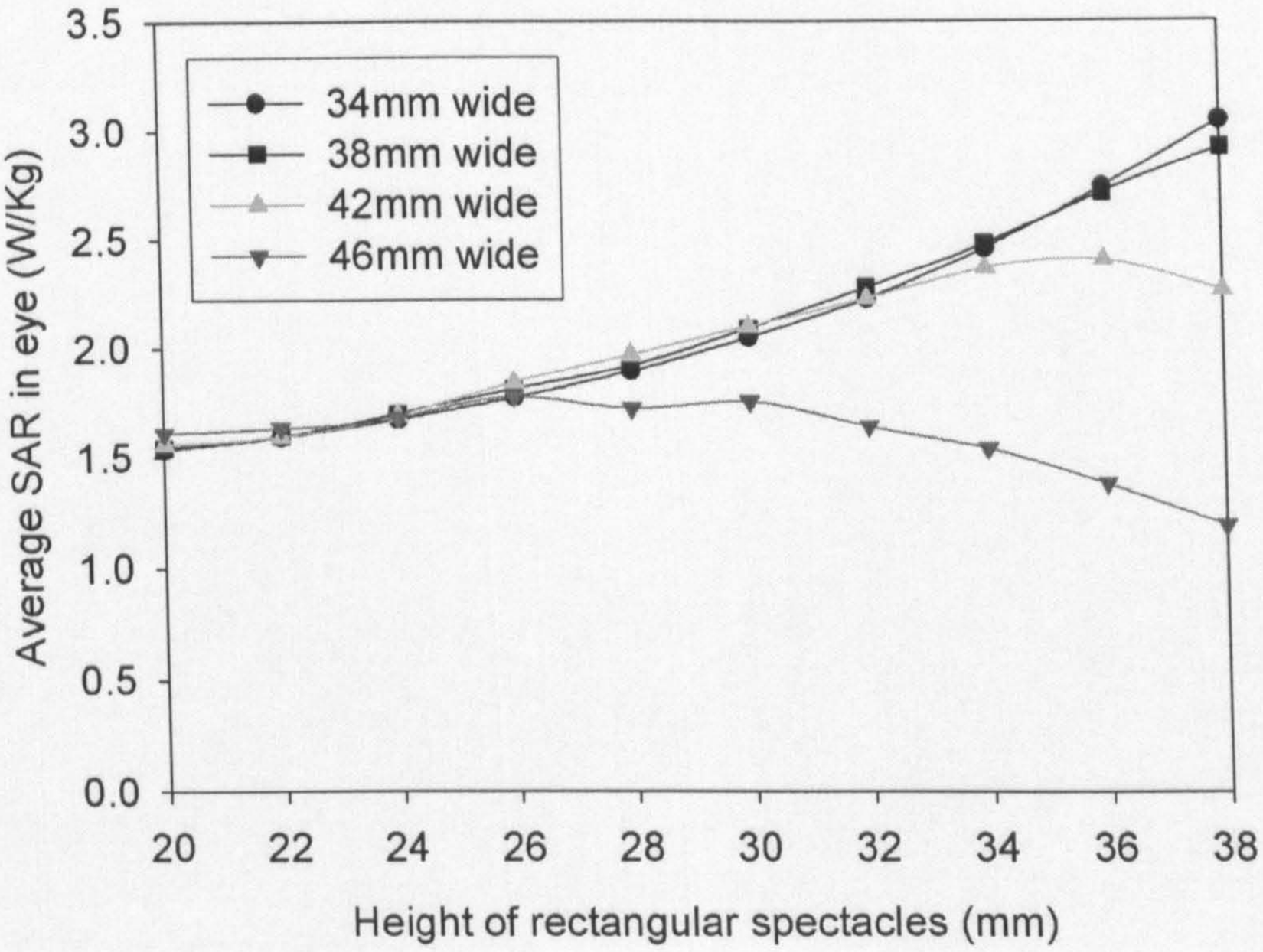

Figure 5.5. Varying the size of rectangular frames of the spectacles in Table 5.2.

Figure 5.5 shows the average SAR in the eye as a function of the size of the frames for rectangular spectacles. The SAR increases as the height of the frames increases. For frames that have large heights, the average SAR in the eye decreases as the width of the frames increases. Figure 5.5 indicates that the effect of rectangular metallic spectacles on the eye is likely to be less significant with frames that are small in the vertical z

direction. If the frames are larger in this dimension, then increases in the SAR in the eye are possible, however the width of the frames becomes an important factor.

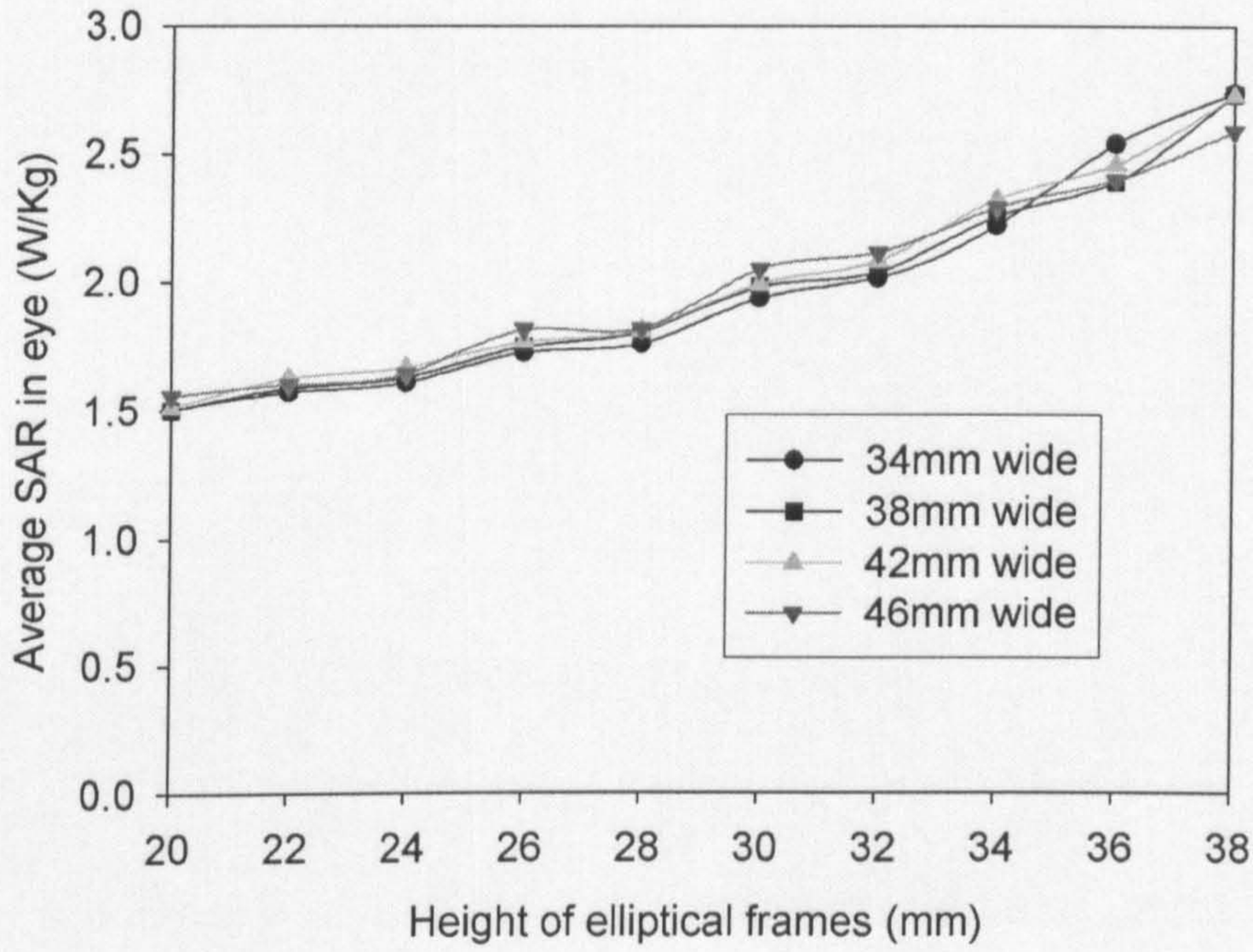

Figure 5.6. Varying the size of elliptical frames of the spectacles in Table 5.2.

Figure 5.6 show the average SAR in the eye as a function of the size of the frames for elliptical spectacles. The graph is similar to Figure 5.5, showing that the SAR increases as the height of the frames increase. The effect of the width of the elliptical spectacles has less effect on the SAR in the eye than with the rectangular frames in Figure 5.5. Comparing Figure 5.5 and Figure 5.6 also shows that for the original configuration of spectacles, rectangular frames generally give higher SAR in the eye than elliptical frames at 1.8GHz.

The effects of varying the lens are shown in Figure 5.7. This graph also shows the metallic frames with no lens. The addition of the lens increases the SAR in the eye.

Generally the SAR in the eye increases with lens thickness. Results are slightly higher with a glass lens as opposed to a Perspex lens. The different lens configurations give variations of up to 15% to the average SAR in the eye. The lens on its own can act as an adaptor as described by Bernardi [4]. The lens also shifts the resonant frequency of the frames as shown in Chapter 4.

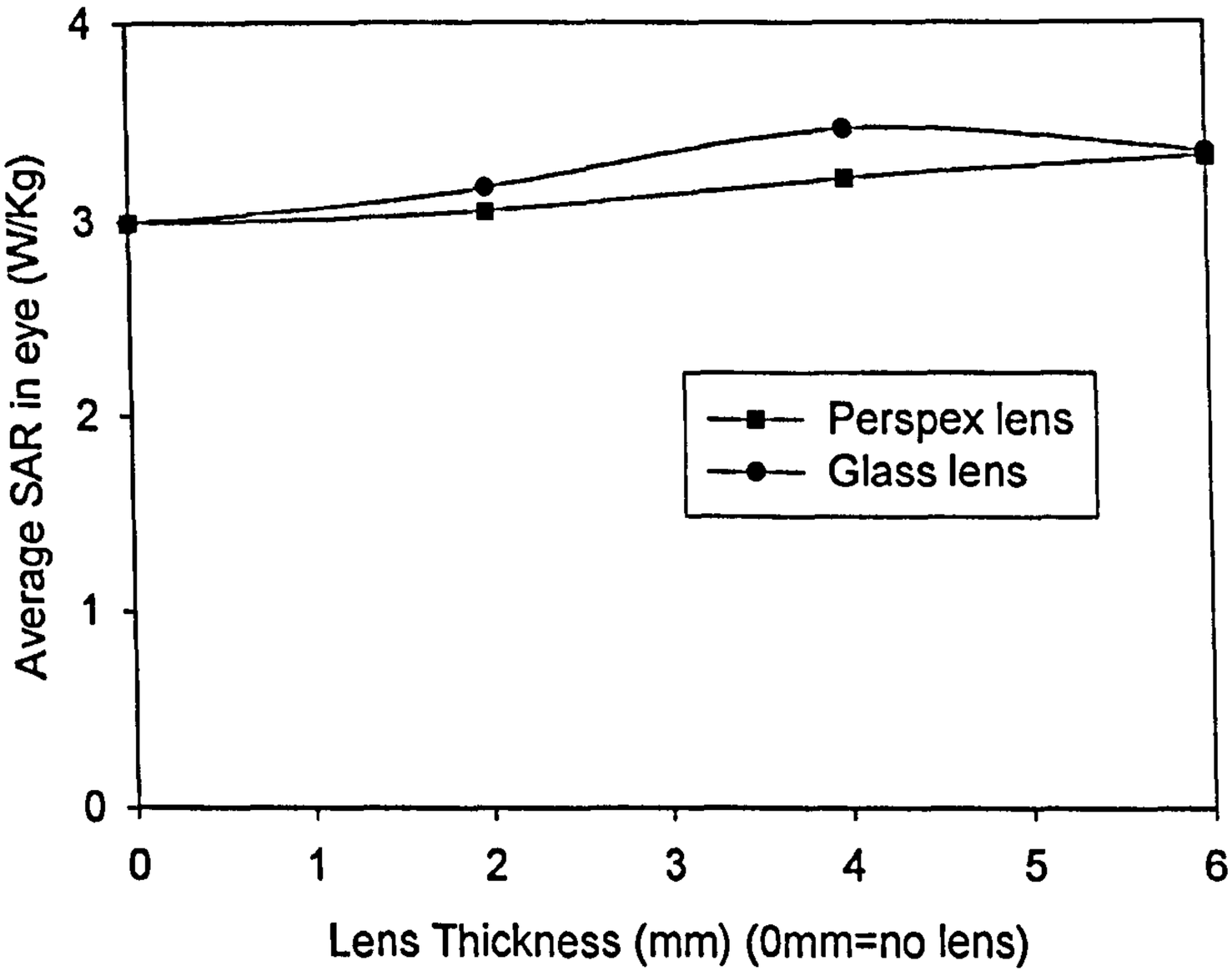

Figure 5.7. Varying the lens of the spectacles in Table 5.2. N.B. The points at 0mm represent the case where no lens exists between the metal frames.

Figure 5.8 shows the effect of varying the length of the strut from the frames to the arms. As the strut length is varied, the total width of the spectacles changes. However, Figure 5.8 shows there is little variation to the SAR in the eye as the strut increases. The average SAR in the eye increases by 2% with the maximum width of spectacles. It should be noted that the strut is orientated in the *y* direction and the source is polarised in the *z* direction. When the strut is 18mm the arms are perpendicular to the frames,

whereas with a smaller strut the arms are tapered to the temple of the head. Figure 5.8, therefore, also shows that the orientation of the arm has negligible significance on the SAR in the eye.

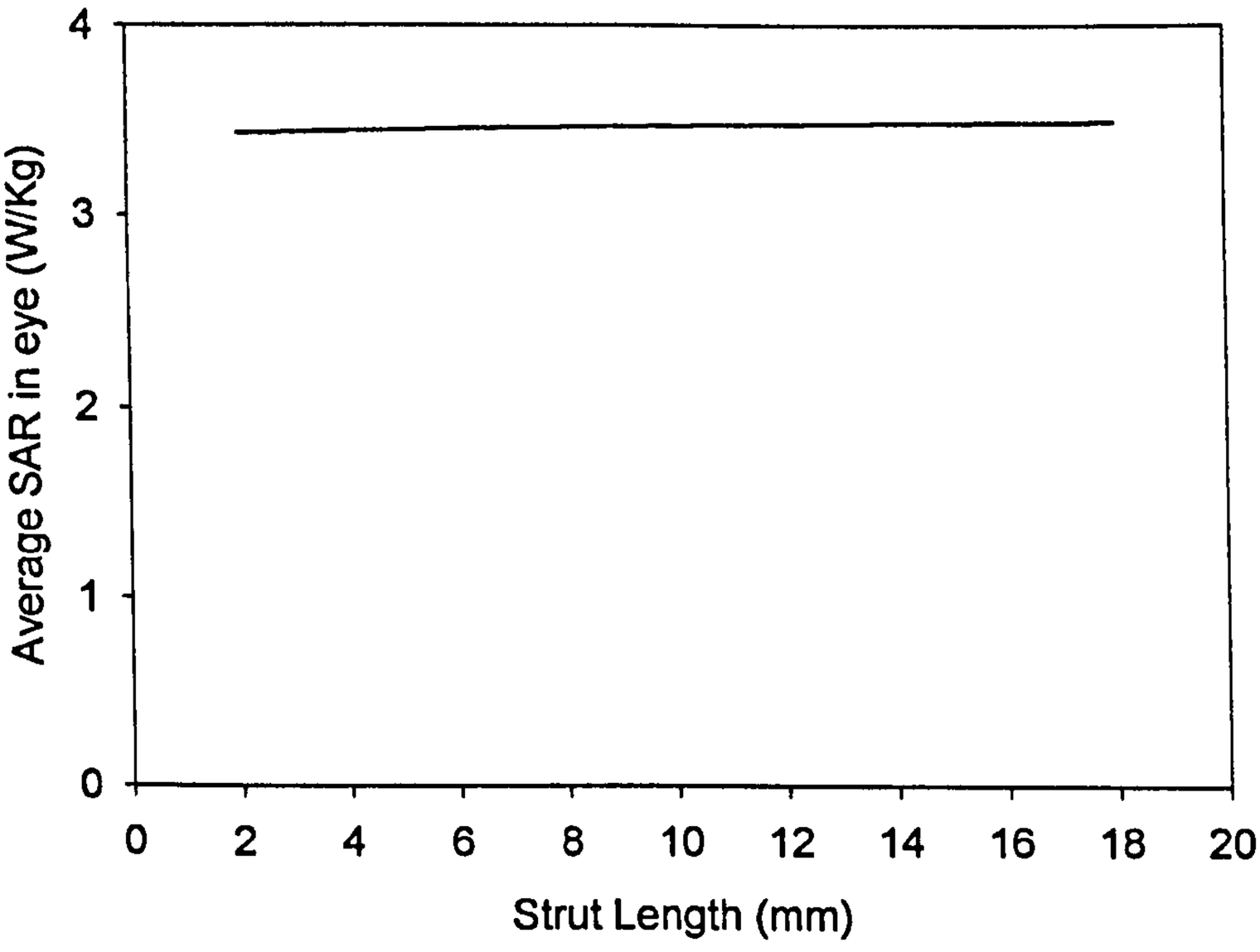

Figure 5.8. Varying the strut length, from the edge of the frame to the arm, of the spectacles in Table 5.2.

5.5 GA run with vertically orientated dipole

In this section the E_z plane wave excitation is replaced by 0.45λ z directed dipole positioned 8cm in front of the nose. The dipole represents a different source and therefore allows the effects of the spectacles to be compared with a different excitation. The dipole positioned in front of the head is representative of a mobile device held in front of the head. The dipole was given an input power of 0.6W to allow comparison with a realistic source. The GA was applied to this stimulus at 1.8GHz with the same parameters as before. The highest average SAR in the eye found by the GA was

0.23W/Kg, an increase of 2.67 times compared to a head without spectacles. The spectacles can be described with the following parameters; frames-eye distance = 28mm, width = 36mm, height = 38mm, 6mm glass lens, rectangular frames with a strut length of 14mm. These spectacles are very similar to the pair that the GA found for the E_z polarised plane wave excitation, in Table 5.2, with only a small difference to the lens thickness and the strut length. The similarity of the spectacles found shows that spectacles behave similarly with a z directed dipole and a z polarised plane wave. Again results suggest that the GA is converging towards a global maximum as it finds very similar spectacles with similar percentage increases with two different excitations.

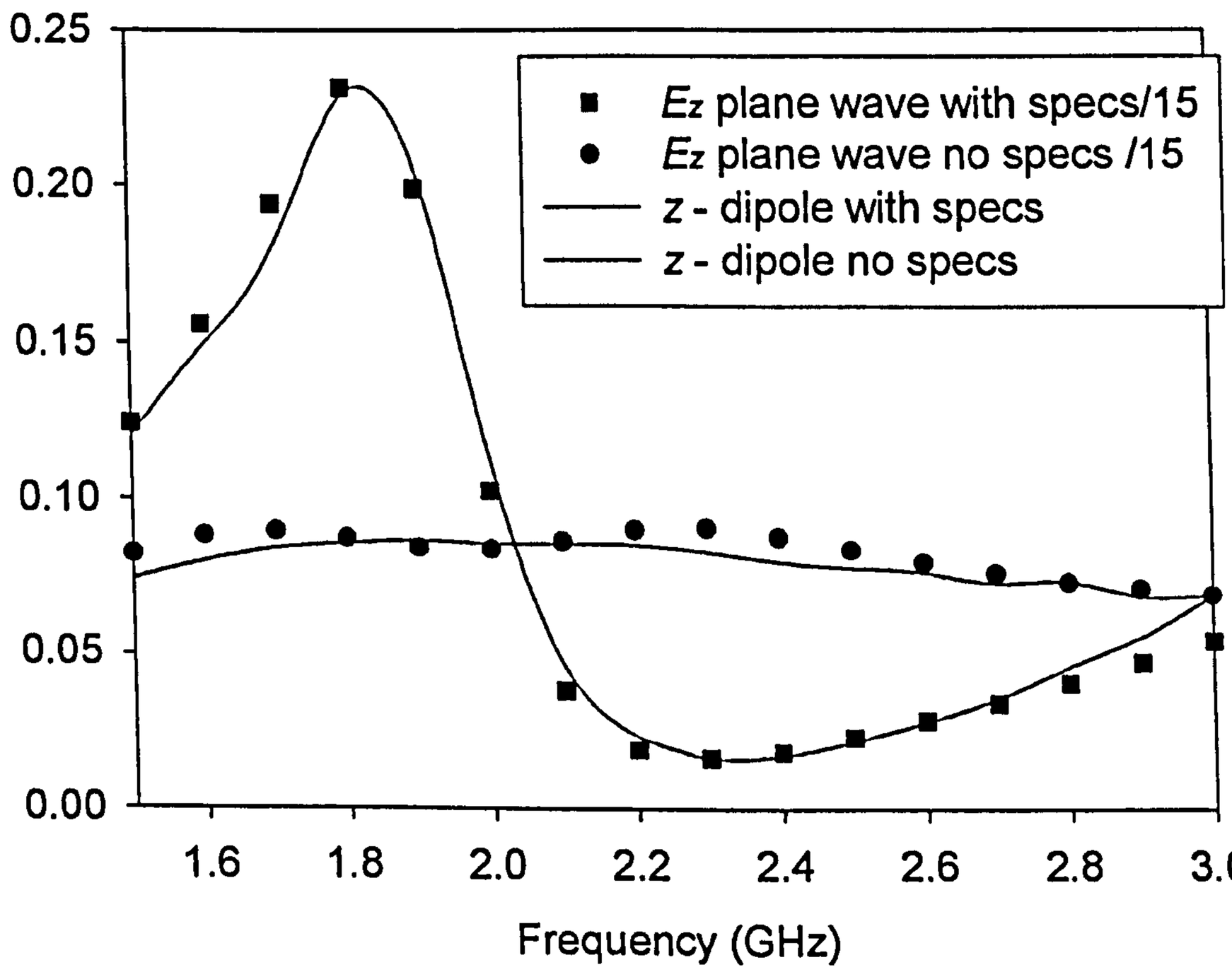

Figure 5.9. Using the spectacles in Table 5.2 with two different excitations: *Ez* plane wave and a *z* directed dipole. N.B. the plane wave results have been scaled by a factor of 1/15.

Figure 5.9 shows the average SAR in the eye for the z directed dipole with the spectacles described in Table 5.2. Figure 5.9 also shows scaled results of the head excited with the E_z plane wave with the same spectacles to allow comparison. It should be noted that the results from the plane wave excitation have been scaled by 1/15 so the amplitudes are comparable. The scaled results are very similar for the two excitations over the frequency range 1.5 to 3.0GHz. The same spectacles give an increase in the average SAR in the eye of approximately 160% at 1.8GHz and a decrease of approximately 80% at 2.4GHz. The results show that the effect of the spectacles is not dependent on the excitation as long as the results are scaled accordingly.

5.6 GA run with horizontally polarised plane wave

In this section the head was rotated so that it was illuminated with an E_y polarised plane wave from the front travelling in the x direction. The power density was kept at 50W/m². The GA was again used to search for the highest average SAR in the eye and the maximum SAR_{1g} in the eye, with the same parameters as outlined in Table 5.1. The GA found no spectacles that increased the SAR in the eye. The maximum average SAR in the eye found was 0.84W/Kg, which corresponds to a decrease of 45%, compared to the same excitation with a head without spectacles. This pair of spectacles were positioned 32mm in front of the eye, had a rectangular frame of 48mm by 38mm, a 6mm glass lens and the strut length was 16mm. Varying the properties of the spectacles was found to be less significant than with an E_z polarised plane wave. Varying the strut length changed the average SAR in the eye by 10%, compared to 2% with an E_z plane wave.

Figure 5.10 shows the spectacles outlined in the paragraph above over the frequency range 1.5 to 3.0GHz. The same spectacles have also been modelled with a 0.6W y orientated 0.45λ dipole, 8 cm in front of the nose. These results are also included and to allow direct comparison the plane wave results have been scaled by a factor of 1/15.

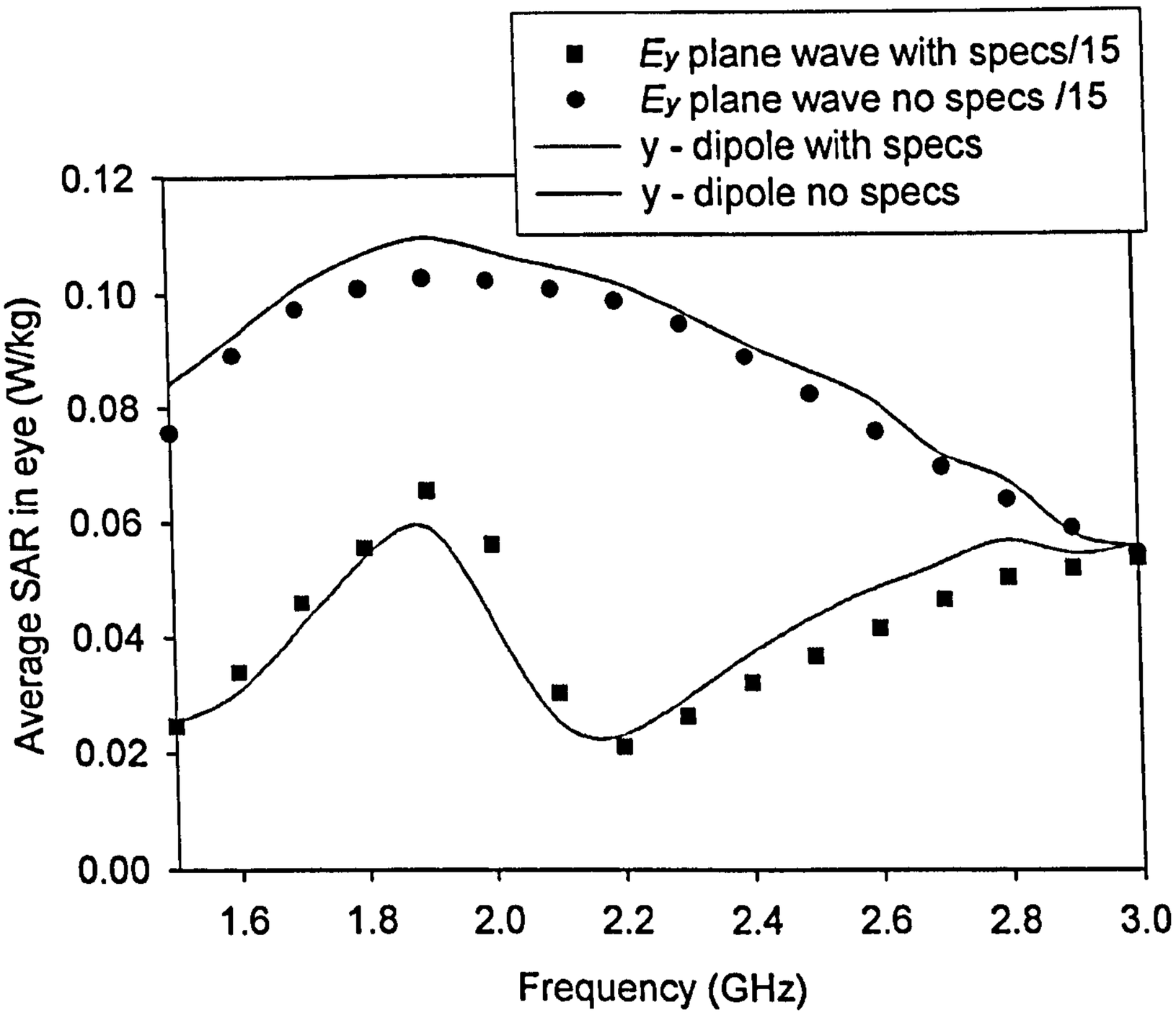

Figure 5.10. Chart of the average SAR in the eye using the spectacles that gave the highest average SAR in the eye at 1.8GHz for the E_y plane wave with two different excitations: an E_y plane wave and a y directed dipole. N.B. the plane wave results have been scaled by a factor of 1/15.

Again the y orientated dipole and E_y plane wave excitations give similar results with and without spectacles across the frequency range considered, assuming the results are scaled to have the same amplitude. This shows that the effects of spectacles are strongly

dependent on the polarisation of the excitation and less dependent on the excitation itself. At all frequencies considered, this pair of spectacles reduced the average SAR in the eye with both the plane wave and dipole excitations. Figure 5.10 only includes results up to 3.0GHz, however the trend of the curves indicates that metallic spectacles could potentially increase the SAR in the eye above 3.0GHz if the excitation is orientated in the *y* direction.

5.7 GA optimisation of spectacles for maximum and minimum SAR in the head

Thus far in this chapter, the GA has been used to find the maximum and minimum SAR in the eye. This section will find the maximum and minimum SAR in the head when metallic spectacles are added. The GA will be run in a similar way as in Section 5.2 except that the two objectives; are the maximum SAR averaged over 1g, and the maximum SAR averaged over 10g of the head. The excitation is a 50W/m^2 vertically polarised plane wave. Table 5.3 shows the results of using the GA to find the minimum and maximum SAR in the head at 900 and 1800MHz.

Results in Table 5.3 show that the effect of adding metallic spectacles on the SAR in the head is greater at 1.8GHz than at 900MHz. At 1.8GHz the maximum SAR_{10g} in the head was found to increase by 257%. Note that a 257% increase here is equivalent to spectacles increasing the SAR by 3.57 times the value found without spectacles.

The spectacles that produced the highest SAR in the head were different from the spectacles that produced the highest SAR in the eye. Generally the maximum SAR in

the head was found to be proportional to the sum of the height and the width of the frames. No spectacles were found by the GA that decreased the SAR in the head at either frequency. This result is complimentary to the discussion of Figure 4.9. Although it is possible for metallic spectacles to reduce the SAR in certain localities, for example in the eye, spectacles are likely to increase the SAR at other locations. The results in Table 5.3 confirm that the GA only found spectacles that increased the maximum SAR in the head.

Table 5.3. Using the GA to search for maximum and minimum SAR in the Brooks head averaged over 1 and 10g at 900 and 1800MHz.

	SAR_{1g} (W/kg)	% change in SAR_{1g}	SAR_{10g} (W/kg)	% change in SAR_{10g}
No spectacles at 1800MHz	6.45		2.83	
36 x38mm spectacles in Table 5.2	14.58	126%	6.99	147%
Maximum SAR in head at 1800MHz	21.04	226%	10.08	257%
Minimum SAR in head at 1800MHz	6.48	0.4%	2.93	4%
No spectacles at 900MHz	3.71		2.09	
Maximum SAR in head at 900MHz	7.61	105%	3.50	67%
Minimum SAR in head at 900MHz	3.92	6%	2.12	1%

5.8 Conclusions

This chapter has applied a GA to search for maximal and minimal effects in the eye when metallic spectacles are added. Although there are many shapes and sizes of spectacles that have not been considered in this search, by varying many of the parameters, it is thought likely that the range of results will correspond to those that

would be produced with real spectacles. At 1800MHz, the addition of metallic spectacles can decrease the SAR in the eye by 60% or increase it by 170%. Therefore, one pair of spectacles could produce SAR levels in the eye seven times higher than with another pair of spectacles. The size and shape of the frames was found to be more significant than the lens.

The effects of a particular size and shape of spectacles was found to be similar on two different heads, both in terms of amplitude and frequency. The maximum and minimum effects in the eyes of both heads were produced by spectacles with very similar parameters and the same spectacles generally produced similar effects on the two heads across the frequency range considered. This shows that the effects of the spectacles are relatively independent of the shape and geometry of the head. This is important as it allows the effects of spectacles to be investigated using a single head, and assume the effect of each pair of spectacles will not differ significantly between different people. The GA also found that similar spectacles produced the maximum SAR in the eye with a vertically polarised dipole. Similar percentage increases were found for both excitations. Thus it is considered likely that other vertically polarised sources will have similar effects. The fact that the GA is converging to very similar points with different model parameters suggests the GA succeeding in finding the global maximum.

When a horizontally polarised source was used, no spectacles were found that increased the SAR in the eye at 1.8GHz. Results were similar with the horizontally polarised plane wave and the horizontally directed dipole, when scaled for amplitude. With this polarisation of source the average SAR in the eye was decreased by at least 45% and was relatively independent of the size and shape of the frames.

The maximum and minimum SAR in the head, using a vertically polarised plane wave excitation, was also searched for using the GA. At both 900MHz and 1.8GHz, no spectacles were found that decreased the maximum SAR in the head. The SAR averaged over both 1 and 10g could be substantially increased even at 900MHz where no significant increase in the SAR in the eye was found. The effects were larger at 1.8GHz than 900MHz.

Figure 5.2 showed that metallic spectacles can decrease the SAR in the eye. However, the results in Table 5.3 suggest that the maximum SAR in the head may always be increased. This highlights the dangers of attempting to engineer spectacles that reduce the SAR in the eye, as the advantages of this possible reduction may be offset by increases in the maximum SAR in the head. The net advantage may become significant if the biological researchers find evidence that specific locations such as the eye may be especially vulnerable to RF interaction.

5.9 References

1. Edwards, R.M. and G.G. Cook. *3G tri band probe fed printed eccentric spiral antenna for nomadic wireless devices using optimal convergence for Pareto ranked genetic algorithm. Proc. ICAP 2001. Eleventh International Conference on antennas and propagation.* 2001. Manchester, UK. p. 537-541
2. Haupt, R.L., *An introduction to genetic algorithms for electromagnetics.* IEEE Antennas and Propagation Magazine, 1995. **37**(2): p. 7-15.
3. Johnson, J.M. and Y. Rahmat-Samii, *Genetic algorithms in engineering electromagnetics.* IEEE Antennas and Propagation Magazine, 1997. **39**(4): p. 7-25.
4. Bernardi, P., M. Cavagnaro, S. Pisa, and E. Piuzzi, *SAR distribution and temperature increase in an anatomical model of the human eye exposed to the field radiated by the user antenna in a wireless LAN.* IEEE Transactions on Microwave Theory and Techniques, 1998. **46**(12): p. 2074-2082.

Chapter 6

MEASUREMENTS OF EFFECTS OF METALLIC SPECTACLES ON SAR IN THE HEAD

6.1 Introduction

It is hypothesised that metallic spectacles will have a measurable effect on the electric fields inside a head. This chapter discusses measurements which investigate the effects of metallic spectacles and validate results from the FDTD code. The code itself has been validated as shown in Chapter 3, however the novel area of the effects on SAR in the head by the addition of metallic spectacles, can not be validated by published controls. Measurements on a phantom were, therefore, used to support our simulations with FDTD and showed good agreement. Measurements have been used to examine both the phone's performance [1, 2] and also to investigate the SAR produced in the head with RF devices [3-6].

Cleveland [7] measured the SAR in the head from portable radios held in front of the head at 800MHz. Both a real skull and an artificial skull were used to simulate heterogeneous phantoms composed of brain, muscle and eye tissues. The maximum SAR was found in the eye or the forehead depending on the antenna type and position.

Griffin [8] illuminated half a phantom near a conducting metal plate wearing an actual pair of spectacles with a plane wave excitation from various angles of incidence. A monopole was used to probe one component of the electric field in a single location in

the eye. Metallic spectacles increased the electric field in the eye by 20dB with both a vertically polarised plane wave at 2GHz and also a horizontally polarised plane wave at 3.6GHz.

Anderson [9] has also performed measurements with a phantom with a real pair of metallic spectacles. Different phones were positioned by the ear. The spectacles increased the SAR in the eye by 9 to 29% with different phones. Anderson noted that different phones produced SAR in the eye that varied by a factor of thirty.

The measurement technique generally involves a tri-axial probe, which can be positioned very accurately with the use of a robot. The DASY4 system [10] has become a commercially available industry standard and has been frequently used to investigate the interaction of mobile phones with humans [2, 4, 5]. The measurements in this chapter are made with the DASY4 automated SAR measurement system. The frequency of the measurements was 1.8GHz as this gave the largest increase in the SAR in the eye. This frequency lies within the dynamic range of the DASY4 system [10]. Further measurements are reported near the end of this chapter, using a crude measurement system made at Sheffield University.

6.2 Modelling the measurement set up with FDTD

Different geometries and phantoms were investigated with the FDTD code before the measurements were made. Initially digital phantoms were considered that were composed of two tissues; eye and brain. However, very similar percentage increases in the SAR in the eye location were found when the eye was replaced with brain tissue.

The use of a homogenous phantom is advantageous as it simplifies the measurement procedure and increases the repeatability of the results. Therefore, in this thesis, the phantom used is homogeneous.

To compare the measurement set up with the FDTD code, the measurement geometry was replicated as closely as possible. Careful measurements of the size of the phantom were made. Figure I.1 in Appendix I shows that the DASY4 [10] phantom consists of a torso with two heads allowing the phone to be positioned on both the right and left side of the head. In this research the right side of the head was arbitrarily chosen. This side of the head is shown in Figure 6.1. The shape of the phantom is similar to a whole head that has been cut in half and has then had the middle of the face stretched so the phantom effectively has a very wide nose.

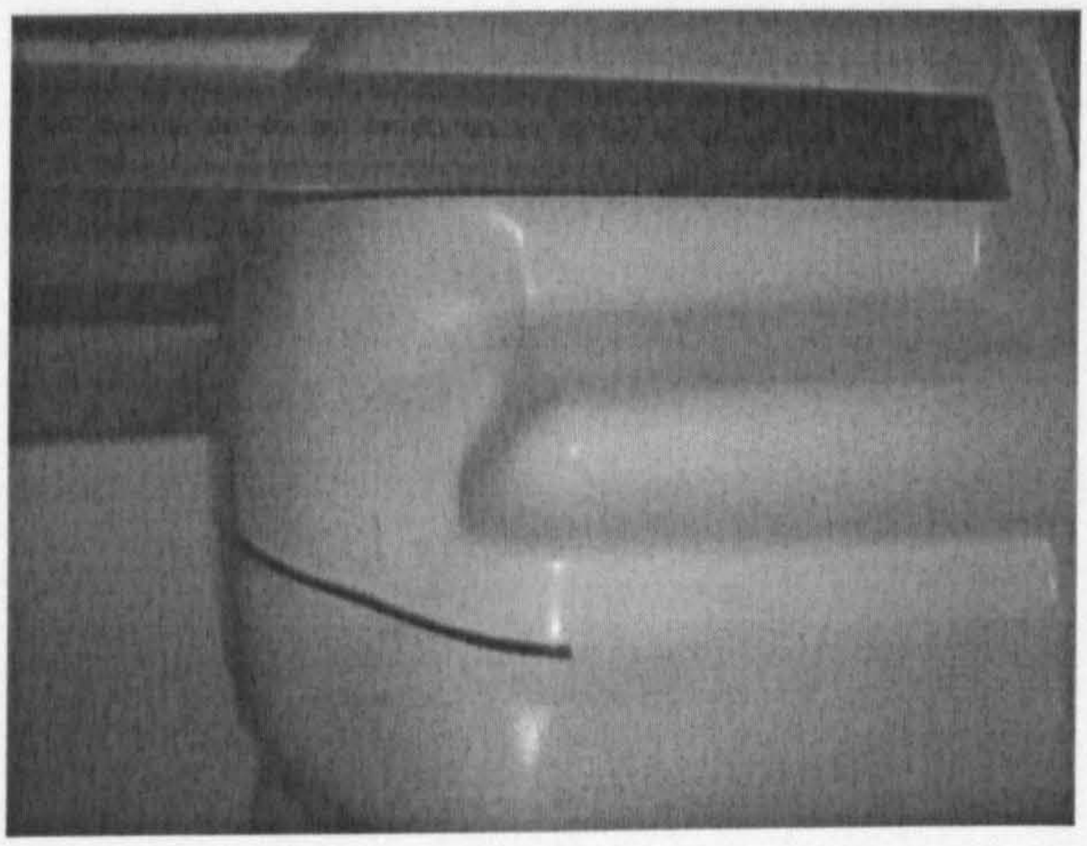

Figure 6.1. The shape of the 'right hand' head of the DASY4 phantom.

To recreate the phantom, the Bradford head was used and modified as below. The assumption that the body does not affect the SAR in the head was made, and therefore only the head needed to be modelled. The cell size of the model was 2mm. Half of the

head was used and the centre of the head in the *y*-axis was stretched to replicate the wide nose of the DASY4 phantom. The nose was stretched by 76mm to replicate the height of the fluid in the phantom. The side of the head by the ear was flattened. The external shape of the head was replaced by 2mm thick fibre glass shell, with $\sigma = 0$S/m and $\varepsilon_r = 3.5$. All tissues inside the head including internal air were replaced with brain simulating material with $\sigma = 1.37$S/m and $\varepsilon_r = 40.48$ to replicate the fluid used in the phantom. The Yee cells that were originally composed of eye tissues were labelled in the code and in this thesis will be referred to as the *'eye'* in inverted commas. This allowed the SAR, averaged over cells in the original eye location, to be calculated. The excitation in the FDTD simulation was a vertically orientated half-wave dipole with a radiating power of 0.1W. The centre of the dipole was located in front of the original eye location.

6.1 Selecting and making the spectacles

As shown in Chapters 4 and 5, different sizes of spectacle frames, produce different results with an anatomical head. To allow comparisons of the results of measurements and the FDTD code, the same spectacles had to be modelled and built accurately. To facilitate this procedure the spectacles were simplified; no lens was used, the spectacles were rectangular and were positioned 20mm in front of the cornea. The arms were straight, extending 140mm in the *x* direction and were perpendicular to the frames. This reduced the description of the spectacles to two of the seven parameters used in Chapter 5; the width and the height of the frames. It has been shown in Chapter 4 that the metallic frames are more significant than the lens or the arm. Thus these simplified

spectacles provide a reasonable approximation to real spectacles. Note that due to the width of the nose only half a pair of spectacles was added to the digital model.

Initially, rectangular spectacles were chosen with frame dimensions of 36x38mm, as this was the size that gave the highest SAR in the eye when the excitation was a vertically polarised dipole at 1.8GHz. The distance from the tip of the nose to the dipole was then increased to obtain the variations of the SAR in the head. Figure 6.2, show results of the percentage increase in the average SAR in the whole head and also in the *'eye'* which is an average of the Yee cells that were originally eye materials.

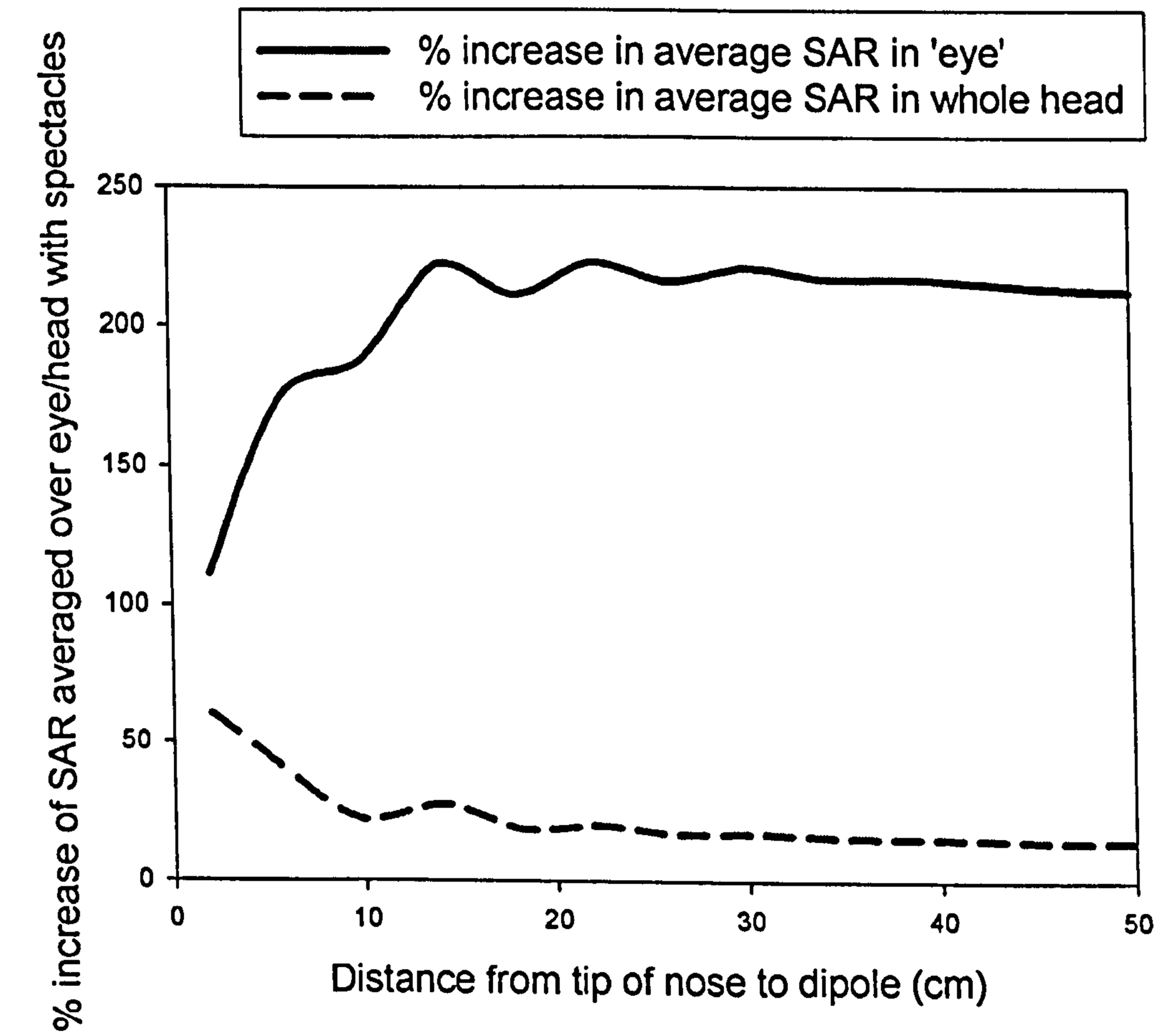

Figure 6.2. FDTD analysis of the measurement phantom. The excitation is a *z* directed dipole with the source positioned in front of the *'eye'*. The spectacles are 36x38mm rectangular frames with no lens.

Figure 6.2 shows that the effect of the spectacles is different depending how far the source is from the head. The 36x38mm spectacles increase the average SAR in the *'eye'* and in the whole head at all dipole-head distances. Generally as the distance increases, the percentage increase in the average SAR in the *'eye'* increases and the percentage increase of the SAR averaged over the whole head decreases. If the dipole is close to the face, the increase in the total power absorbed in the head can be greater than 60%. The increase of SAR in the *'eye'* and the head is similar to the effects of the whole pair of spectacles as modelled when the head is assumed to be symmetric, thus showing that the effect of spectacles is largely dependent on the shape of the rectangular frame of half the spectacles and not on the whole pair of spectacles.

The percentage increase of the SAR in the head and *'eye'* become relatively constant when the dipole is at least 14cm from the head, although the magnitude of the SAR decreases with distance. With the dipole 14cm in front of the tip of the nose, the average SAR in the *'eye'* increases by 222% when 36x38mm rectangular spectacles are added.

With the dipole positioned 14cm in front of the tip of the nose, a search was made for the spectacles that produced the highest SAR in the *'eye'*. As the description of the spectacles was reduced to two parameters, the width and the height of the frames, the number of possible frames was significantly reduced, hence an exhaustive search was used as opposed to the GA. Results confirmed the initial guess that 36x38mm rectangular spectacles produced the largest SAR in the *'eye'* with the FDTD code modelling the measurement phantom.

Chapter 5 showed that spectacles can both increase and decrease the SAR in the eye depending on the orientation of the excitation. To validate these results, measurements

were also made with a *y* directed dipole. Again an exhaustive search was made for the spectacles that produced the lowest SAR in the *'eye'* with a *y* orientated dipole 14cm in front of the head. At this distance and at 1.8GHz, all sizes of rectangular frames decreased both the average SAR in the *'eye'* and the average SAR in the whole head. Rectangular frames of size 48x22mm decreased the SAR in the *'eye'* by 78% to 0.008W/Kg. This still lies within the dynamic range of the DASY4 system of 1mW/Kg to 100W/Kg [10].

Thus two sizes of rectangular spectacles, 36x38mm and 48x22mm, were chosen for the measurements. These were created by using copper wire of 2mm thickness which was coated in a further thin layer of lacquer. The lacquer was removed by a combination of heating and sanding. The copper wire was straightened to remove the kinks and was cut up into lengths. These were then carefully soldered together to provide both a structural and an electrical connection. This method allowed the corners of the frames to be perpendicular, which would not have been achieved if the wire had been bent into shape. The wire was also used to create a 140mm arm, perpendicular to the frames.

6.2 Experimental technique using the DASY4 system

As previously mentioned, the measurements were performed with the automated near field scanning system DASY4 [10]. The system uses a six-axis robot; see Figure I.1 in Appendix I, which can position a probe with an accuracy of 0.2mm. The robot moves the probe inside a phantom, representing two heads and a torso filled with a liquid simulating the electromagnetic properties of brain. The right hand head was used.

The SAR measurements were made with three small dipoles, each 3mm in length, designed in a triangular formation. This provides a more compact shape than the rectangular formation with the centres of the dipoles less than 2mm apart [10]. This distance is small compared to the dimensions of the field gradients induced by mobile phones below 3GHz [11]. The triangular formation also allows the position sensor to be at the centre of the probe [10]. Each dipole is directly loaded with a Schottky diode and connected to the acquisition unit with resistive lines. The DASY4 system has a repeatability of less than 5% [10]. The uncertainty related to SAR measurements is considered to be approximately 25% [5]. The overall uncertainty with the normal DASY4 set up is better than +/- 1dB [4].

The DASY4 system requires the probe to be perpendicular to the phantom surface; therefore measurements can not be made in the eye region of the phantom. This problem was overcome by placing the frames of the spectacles by the ear and the spectacle arm along the extended nose of the phantom. This geometry is shown in Figure 6.3. This new geometry was carefully replicated in the FDTD model, see Figure 6.3. Measurements were made with both vertical and horizontal half-wave dipoles at 1800MHz. Further specific details of the measurements are included in Appendix I.

Three sets of measurements were made for each dipole geometry: no spectacles, 36x38mm frames, and 48x22mm frames. The dipole was positioned 10cm from the centre of the frames of the spectacles. Measurements involved an initial course scan to find the position of the local maximum SAR, and then a second fine scan to determine the SAR averaged over both 1g and 10g. The whole process takes approximately fifteen minutes. The input to the dipole was a continuous wave source at 1.8GHz. The amplitude of the source was measured with a power meter to be 19.45mW.

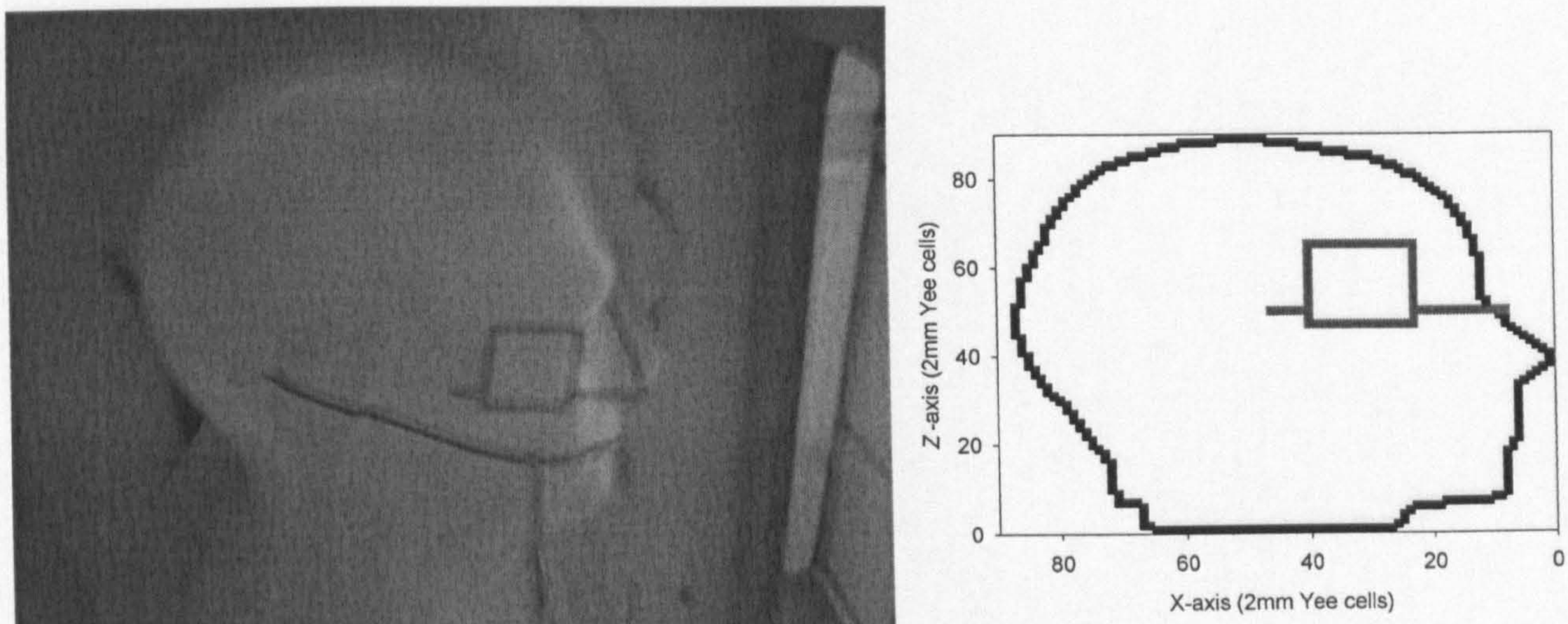

Figure 6.3. A photograph (left) of the measurement phantom. The dipole is orientated vertically, relative to the head, and the spectacles are 36x38mm. Note the diagonal line from the ear to the mouth has been previously drawn on the phantom to aid the positioning of mobile phones. The spectacle frames relative to the outline of the digital head in the FDTD simulation is also shown (right).

The FDTD code used an excitation of 100mW. At the end of the calculations the results were scaled to 19.45mW. Figure 6.4 and Figure 6.5 show the maximum SAR_{1g} and SAR_{10g} in the head with the dipole orientated horizontally relative to the head. There is agreement between the modelled and the measured results. With this geometry the addition of 36x38mm spectacles have little effect on the maximum SAR_{1g} and SAR_{10g} in the head.

Comparing the effects of the 48x22mm frames, on the SAR_{1g} in Figure 6.4, shows a discrepancy. The measurement results are decreased while the maximum SAR_{1g} in the head is increased in the FDTD simulation with 48x22mm frames. Analysis of the results revealed that the FDTD code found the maximum SAR_{1g} in the nose by the arms of the

frames, yet this area was not scanned by the DASY4 system. Therefore, to compare similar geometries, the FDTD maximum SAR_{1g} near the 48x22mm frames is also shown in Figure 6.4 as the green section of the graph. The maximum SAR_{1g} by the frames was found to decrease with both methods. The decrease is more significant in the measurement results than the FDTD results.

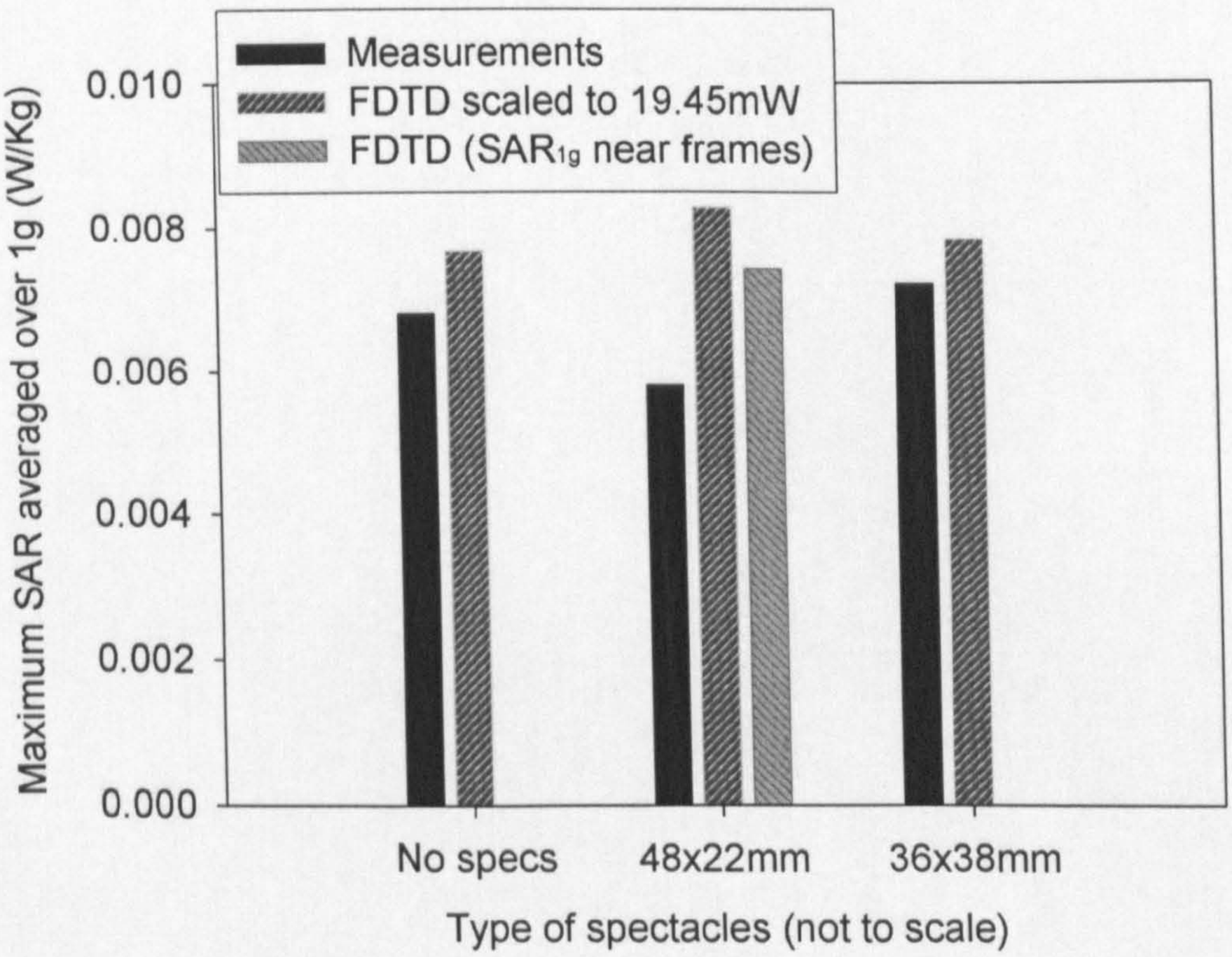

Figure 6.4. The maximum SAR_{1g} of the horizontal dipole positioned 10cm from the side of the head. Measurements are compared to normalised FDTD values.

The SAR_{10g} in Figure 6.5 show a better correlation than the SAR_{1g} in Figure 6.4. This is expected as the 10g averaging mass contains more Yee cells and is therefore less sensitive. Figure 6.5 shows that with a dipole orientated horizontally compared to the head, the addition of spectacles does not significantly affect the SAR in the head. The maximum SAR_{10g} is marginally decreased with the addition of the 48x22mm frames.

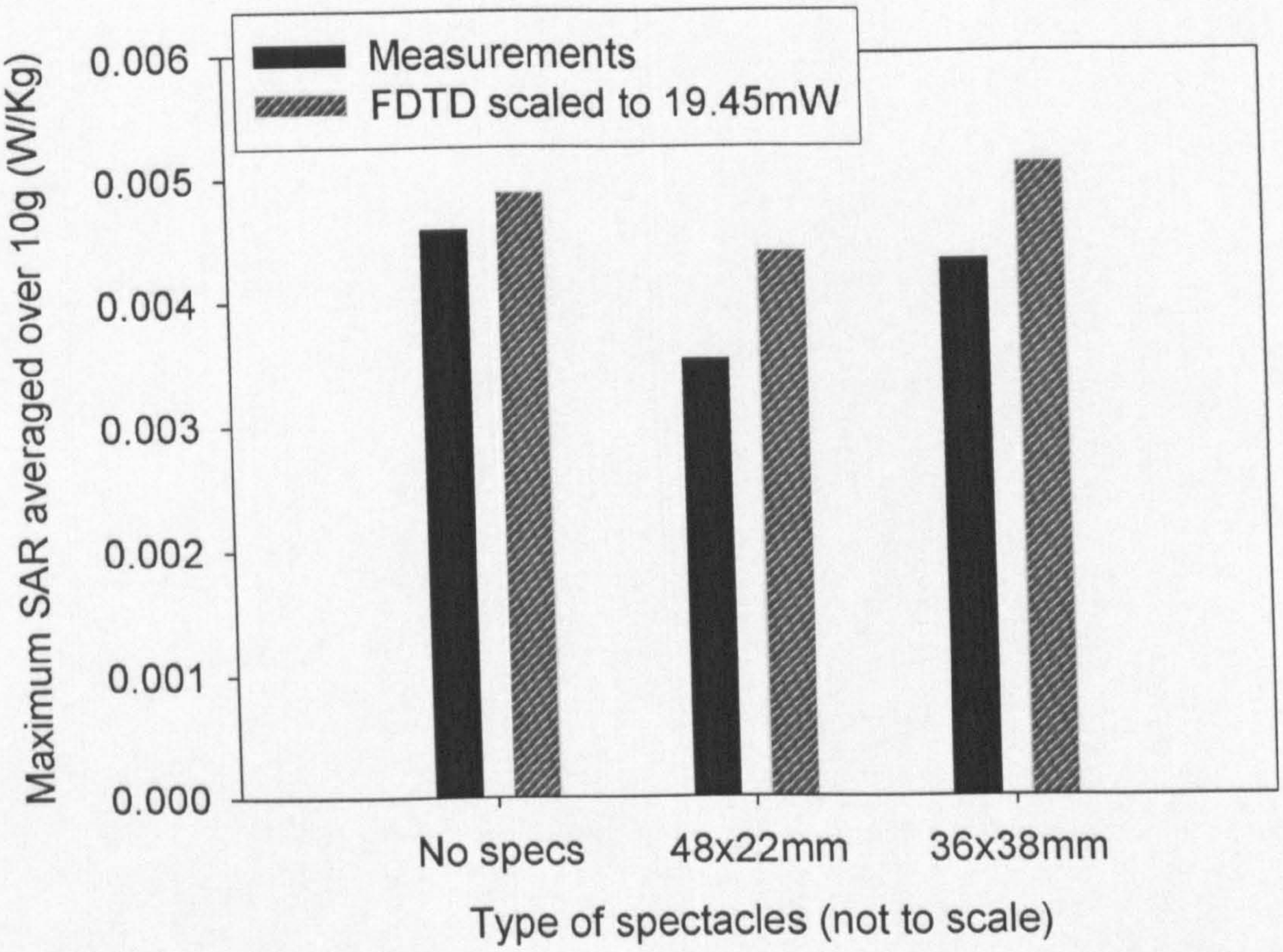

Figure 6.5. The maximum SAR_{10g} of the horizontal dipole positioned 10cm from the side of the head. Measurements are compared to normalised FDTD values.

The SAR_{1g} and SAR_{10g} results with the vertical dipole are shown in Figure 6.6 and Figure 6.7. Both figures produce similar sets of results and will be analysed together. Both the 48x22mm and the 36x38mm frames increase the maximum SAR in the head. As predicted by the FDTD code, the effects with the 36x38mm frames are much greater than with the 48x22mm frames. The measurement results increase the SAR_{1g} by 5.4 times and the SAR_{10g} by 4.27 times with the 36x38mm frames. The same size frames in the FDTD simulation increase the SAR_{1g} by 3.3 times and the SAR_{10g} by 3.24 times compared to the case with no spectacles. The measurements, therefore, produced greater percentage increases than the computer simulation. The measurements show agreement with the FDTD results.

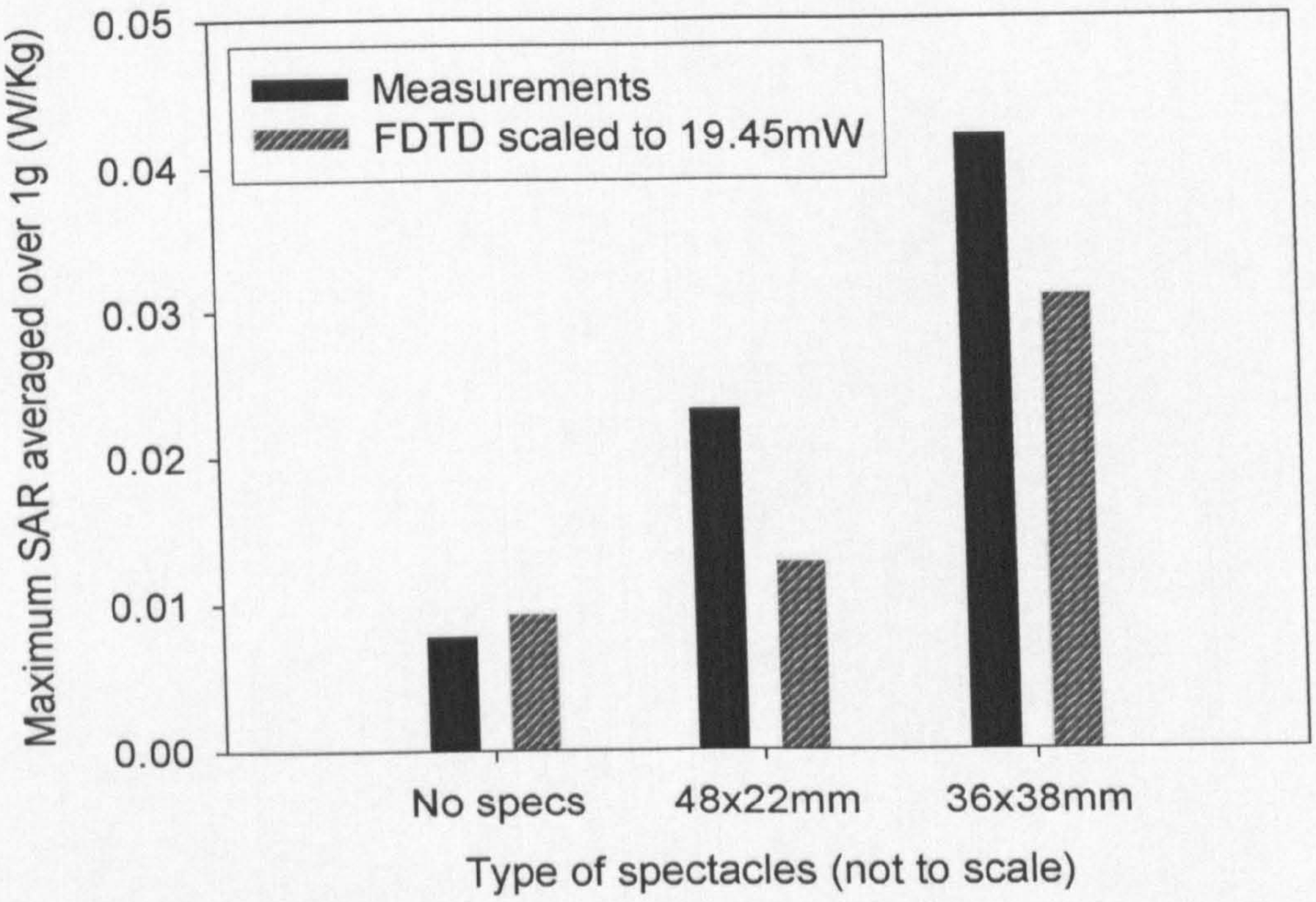

Figure 6.6. The maximum SAR_{1g} of the vertical dipole positioned 10cm from the side of the head. Measurements are compared to normalised FDTD values.

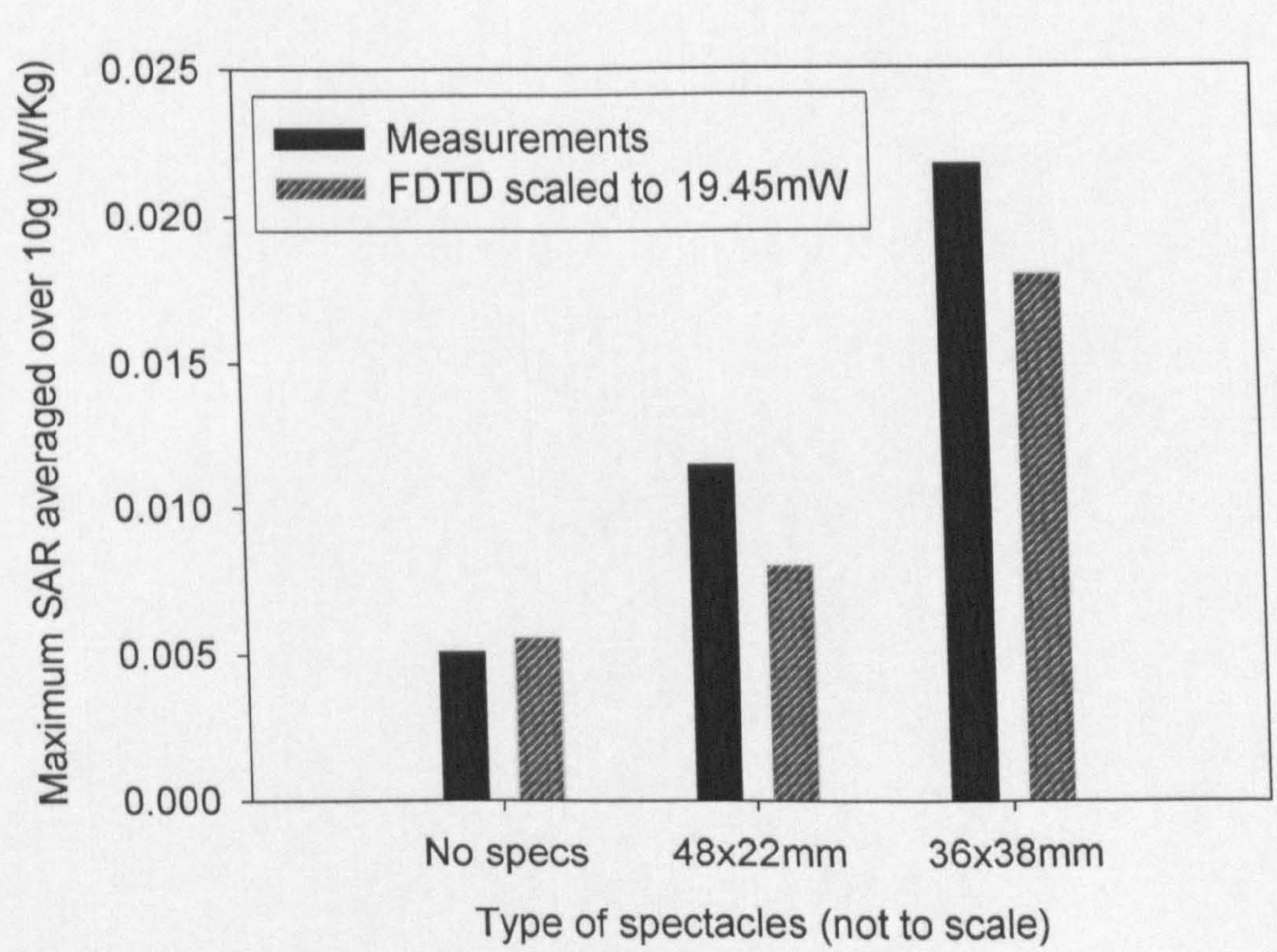

Figure 6.7. The maximum SAR_{10g} of the vertical dipole positioned 10cm from the side of the head. Measurements are compared to normalised FDTD values.

6.3 Analysis of measurements

In general the measurements show agreement with the FDTD results (see Figure 6.4 to Figure 6.7). The trend of the effects of the frames is very good, and the amplitude of the SAR values is reasonable. The discrepancies between the two methods is within 25% which is often considered to be the uncertainty related to SAR measurements [5].

However, there are differences between the measured and the simulated results which need to be explained. Generally the effects of metallic spectacles are larger within the measured set of results than the FDTD results.

This section will discuss possible reasons for these discrepancies. The standard anthropomorphic model (SAM) phantom used in the measurements is a different shape and size from the modified Bradford head used in the computer simulations. Figure 3.10 highlighted the difference in SAR values when three different heads were modelled using the same method. It is therefore considered likely that different heads will produce different results using different methods. The differences to the external shape of the phantom could cause discrepancies in the results, as the location of the averaging volume will be different in both methods. Slightly different averaging volumes can also produce different results. The DASY4 system allows the cubic volume to contain 10% air. The internal structures, although homogeneous may be different as the electrical properties of the brain-simulating-fluid inside the phantom varies with temperature.

The different external shape of the phantom also means that the position of the spectacles, relative to the head, will differ. The dimensions of the frames only have an accuracy of ±1mm, and it was shown in Chapters 4 and 5 that different sizes of spectacles have different effects. Another possible factor is that the measurement

spectacles were made of cylindrical wire, whereas the FDTD method creates the metallic frames from cubic cells.

Nikita [12] stated that the position of the dipole relative to the head is important. The accuracy of the dipole's position relative to the head is estimated at 4mm. It is difficult to locate the metal frames relative to the head in exactly the same position in the two different methods. Therefore, the dipole is likely to be at different positions relative to both the head and the metallic frames. Chapter 5 showed that the orientation of the dipole, in relation to the spectacles, is very significant. Therefore, discrepancies could arise, if either the dipole or the spectacles, in the measurement set-up was not perfectly aligned.

6.4 Further measurements

The measurement results in this chapter using the DASY4 measurement system, showed good agreement with the FDTD code, however they only provided knowledge of the maximum SAR_{1g} and SAR_{10g} values in the head. A further problem with these results is that the spectacles had to be incorrectly positioned on the side of the phantom. Therefore, a further set of measurements were made with a specially designed measurement kit made at Sheffield University.

A plastic mould of the front of the face of a 29 year old white female was made at Bristol University. The phantom was filled with 4 Litres of dielectric fluid with the properties of brain at 1800MHz. The electrical properties of the fluid vary with temperature and frequency. The conductivity and permittivity are shown in Table 6.1.

Table 6.1. The electrical properties of the brain simulating fluid as a function of temperature and frequency. Relative permittivities are in red and conductivities are in blue.

	Temperature (°C)		
Frequency (GHz)	21.06	21.31	21.97
1.7	40.853 1.284 S/m	40.770 1.286 S/m	40.243 1.273 S/m
1.8	40.386 1.382 S/m	40.305 1.375 S/m	39.791 1.358 S/m
1.9	39.876 1.483 S/m	39.870 1.471 S/m	39.370 1.449 S/m

Care was taken to keep the fluid covered, when it was not in use, to reduce contamination and evaporation. The frequency band of 1710MHz to 1880MHz was investigated. As the electrical properties of the fluid were not known above 22°C, the experiments were done at night so the temperature was kept relatively constant. The temperature range of the experiments was 21.6°C to 22.8°C. Such small variations in temperature cause minimal variation to the electrical properties of the fluid.

A half-wave dipole was used as a source. Both horizontal and vertical orientations relative to the head were investigated. A probe was created using copper wire and a 48cm length of 3.5mm coaxial cable. The probe consisted of two perpendicular sections of copper wire, 1cm in length, that were soldered together to form a cross connected to the end of the stripped semi-rigid coaxial cable. Thus all three Cartesian field components would be measured by the probe and the electrical signal from the probe

would be approximately proportional to the total field strength at that location. The tip of the probe was coated in Perspex to ensure that the conductive brain liquid did not electrically short out the probe. A photo of the probe is shown in Figure 6.8. A quarter wavelength Bazooka balun was added near the tip of the probe using metal tape insulated from the probe by a strip of celotape a quarter of a wavelength long. The balun was used to reduce the currents flowing along the exterior of the probe. High frequency (up to 2GHz) ferrite cores (www.digikey.com) were also added at the other end of the probe to further reduce the exterior currents.

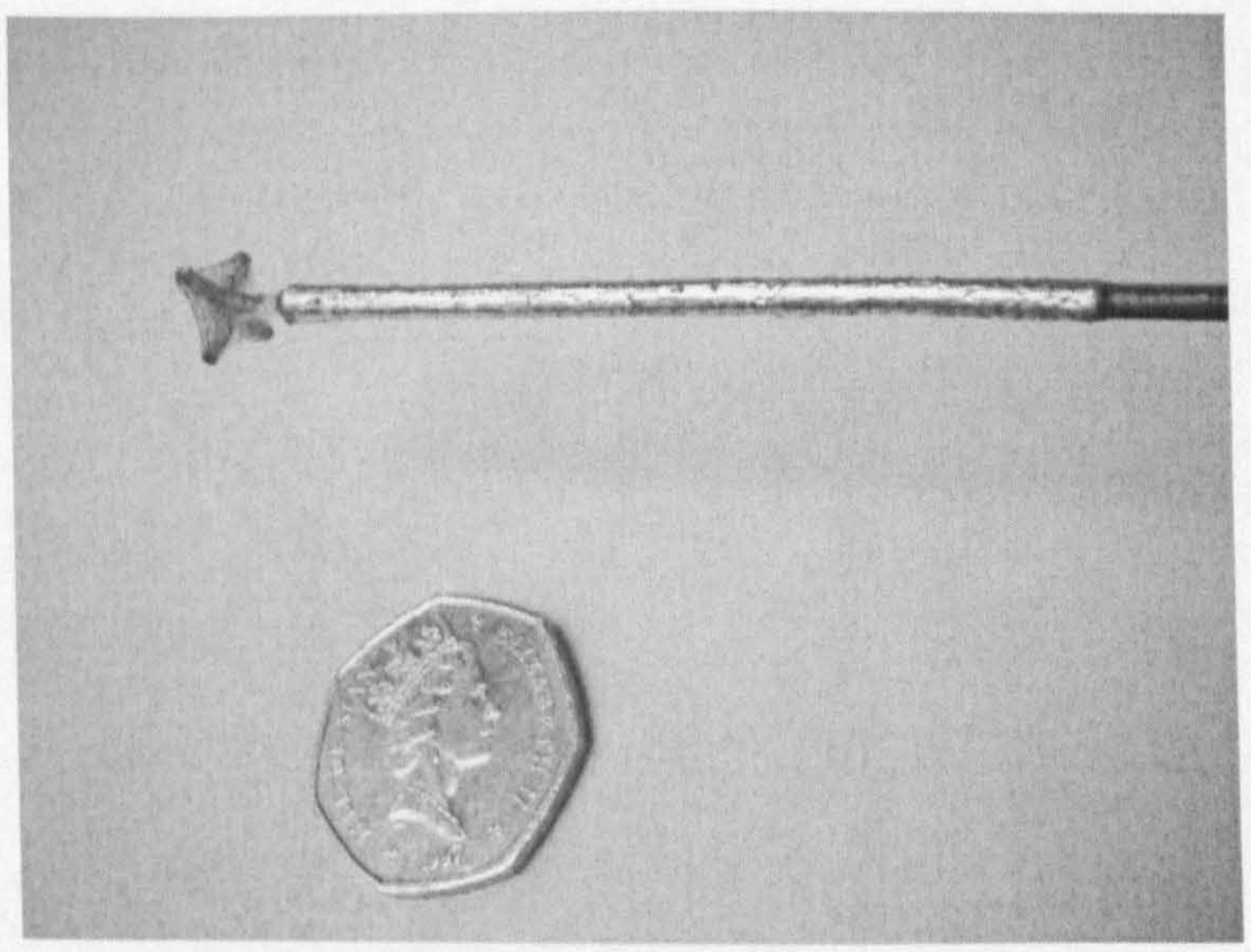

Figure 6.8. Enlargement of the probe showing the scale relative to a British 50 pence coin.

A plastic positioning device was created that allowed the probe to be moved with an accuracy of 3mm in all three axes. Care was taken to ensure that the probe alignment was not changed throughout the experiments, to reduce variations due to the isotropy of

the probe. The probe and the positioning device are shown in Figure 6.9. The probe and the half-wave dipole were connected to an HP 8714B network analyser.

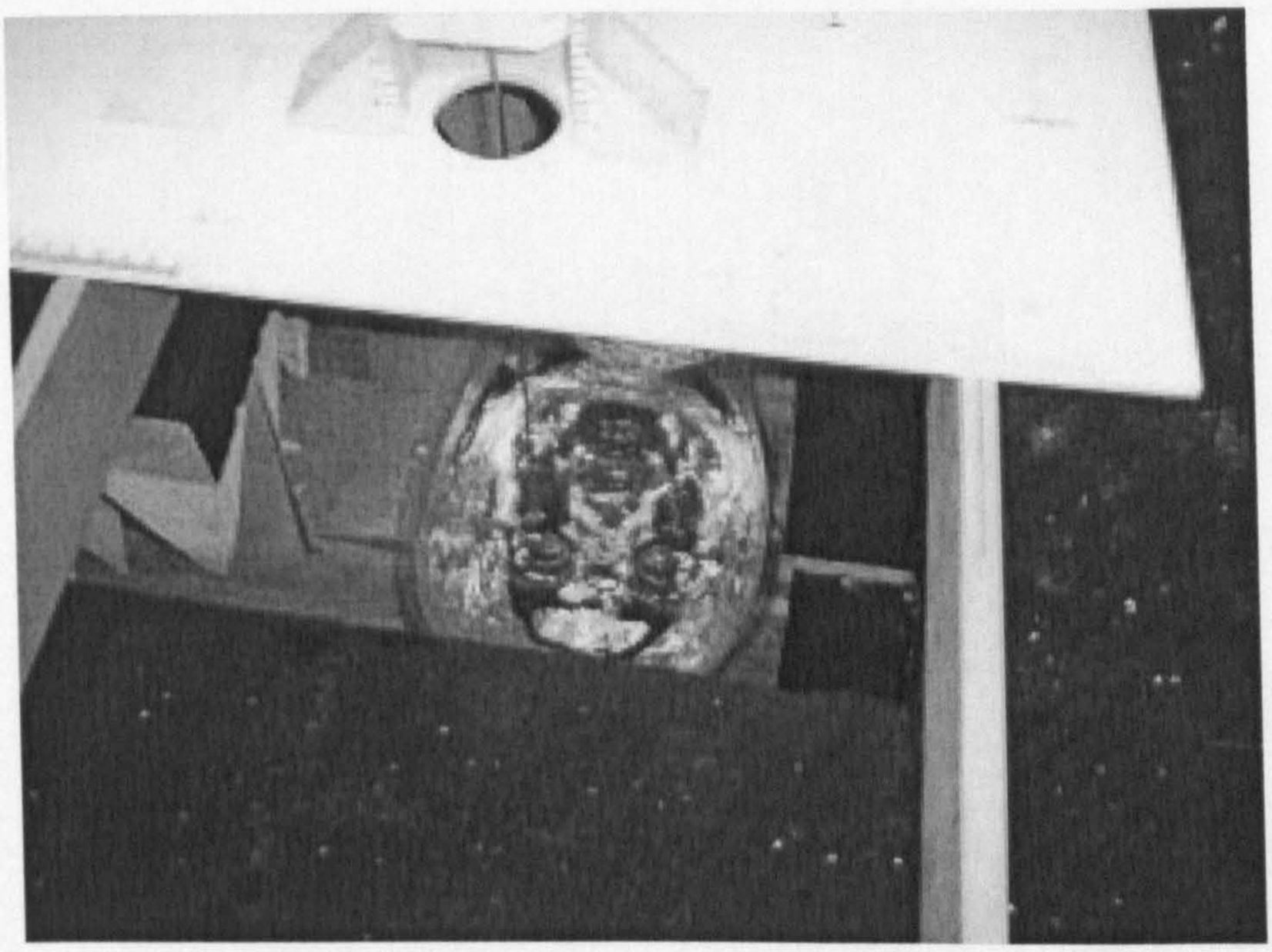

Figure 6.9. The head phantom with spectacles filled with brain fluid and the probe positioning device.

Initially the phantom was positioned inside a small wooden box lined with high frequency radar absorbing material (RAM). This set-up is shown in Figure 6.10. This system proved to be extremely sensitive to any movements in the vicinity, and thus produced a very poor level of repeatability. As an improvement to this system, a second box was made. This box was larger than the original version and had dimensions of 86 x 88cm and was 110cm high. The box was made of metal to shield the system from the movements in the laboratory. The floor and the walls of the box were carefully lined with RAM so that all metal surfaces were covered. The larger size of the box allowed

six inch RAM to be used which is more absorbent at the frequencies considered. The wooden board supporting the phantom, that was carefully kept dry, was covered in RAM, as shown in Figure 6.9.

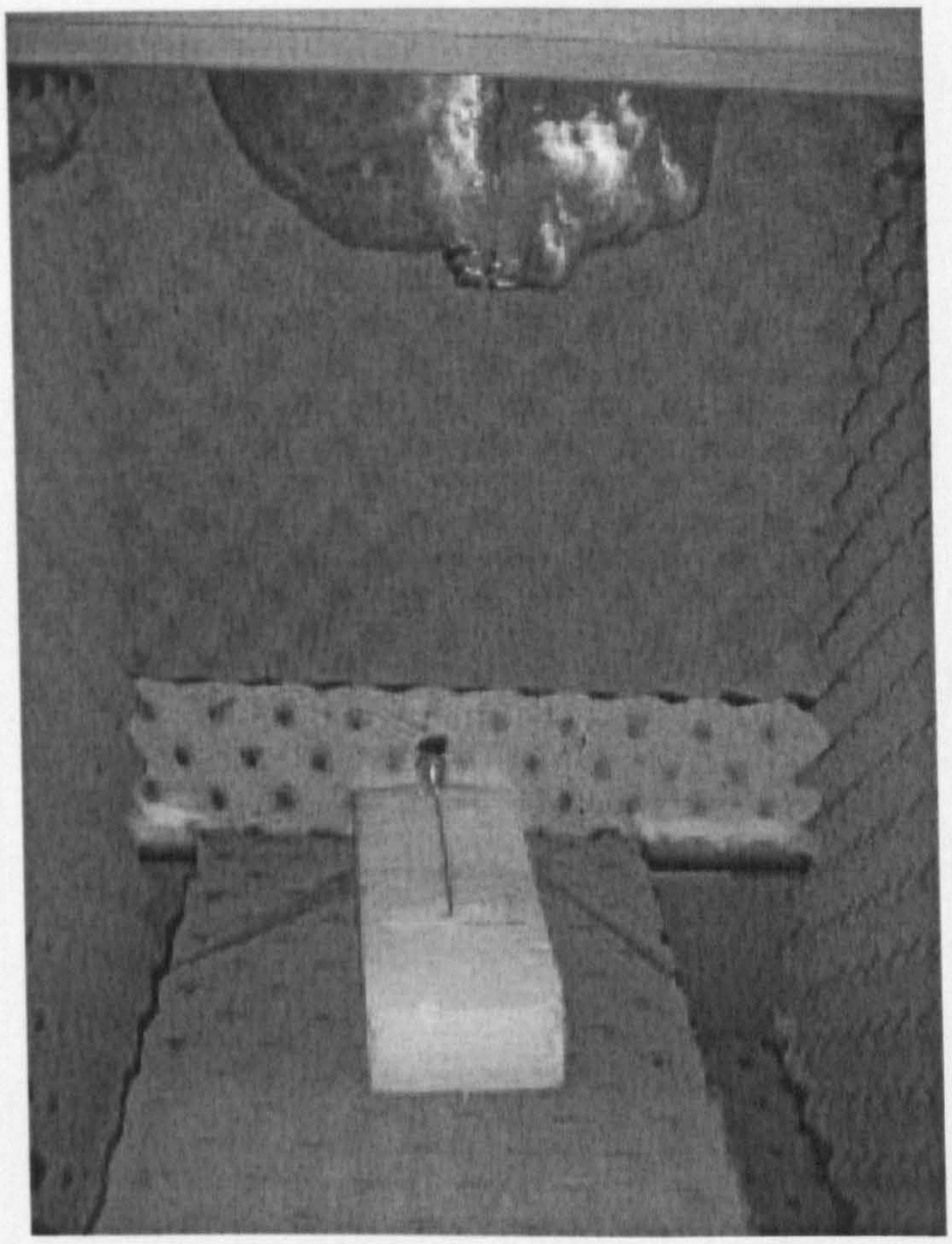

Figure 6.10. The plastic head phantom, with spectacles, inside a wooden box lined with RAM.

The experimental set-up is shown in Figure 6.11. The half-wave dipole was mounted on a physically stable piece of polystyrene which is assumed to be invisible to RF at 1.8GHz, to ensure that the dipole did not move throughout the experiments. One side of the box was removable allowing access to the dipole or to add spectacles to the head.

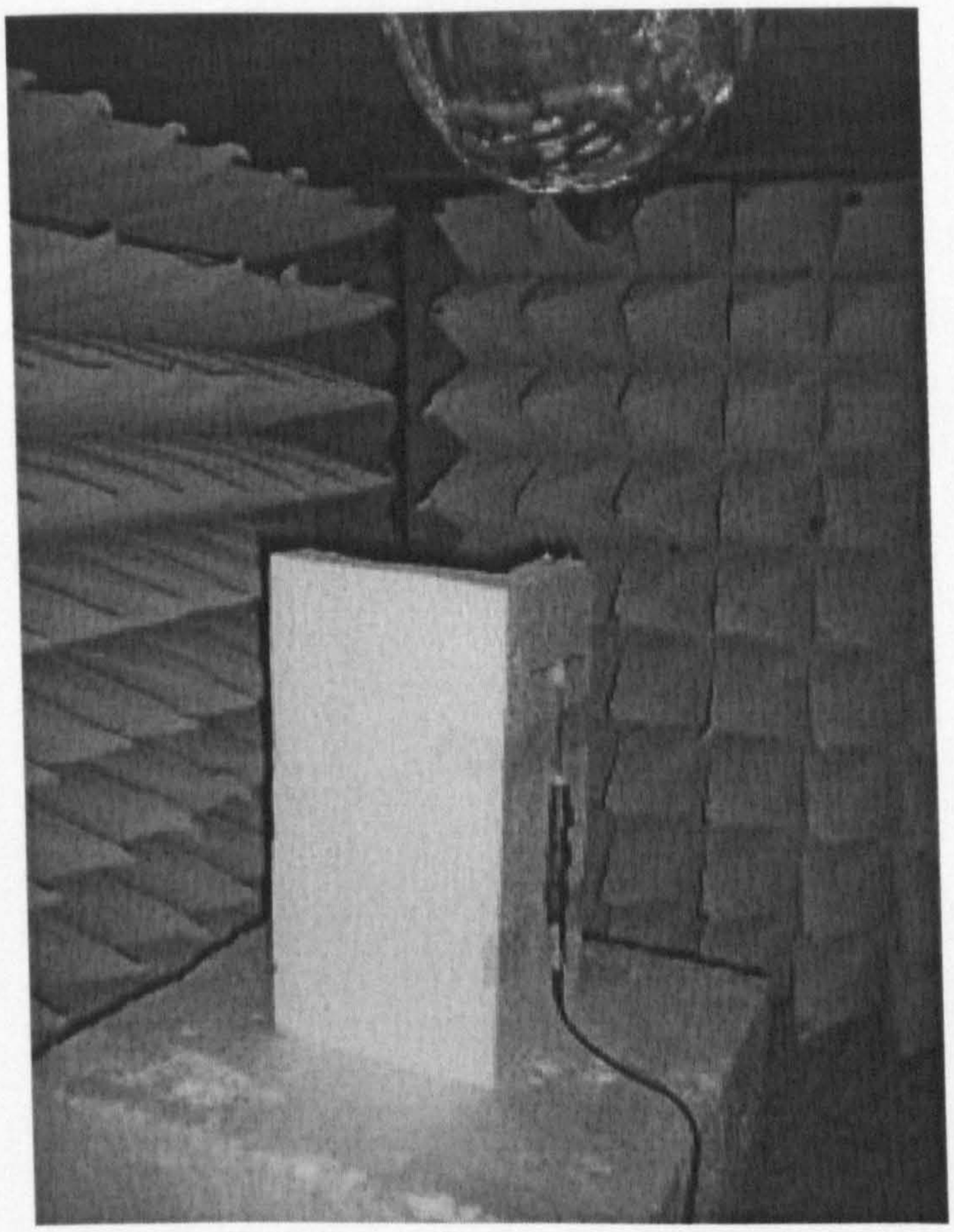

Figure 6.11. A vertically polarised dipole in front of the phantom head, positioned inside the metal box lined with RAM.

The probe was positioned manually as shown in Figure 6.9. The range in the *x*-axis from nose to the back of the head was 0 to 5cm. The 0cm position was located by finding the centre of the eye and raising the probe slightly so that it was not touching the surface of the phantom. The *y* (ear to ear) and *z* (chin to scalp) axes both ranged from 0 to 8cm. Note that with this coordinate system the surface of the eye is at 0, 7, 3 (cm). The centre of the excitation dipole was positioned at -20, 4, 3 ±0.5cm.

Prior to the measurements, the probe was positioned at 5, 4, 3 and the field value at that point was used to calibrate the system. This allowed all subsequent values to be known

relative to this original calibration point, with no spectacles on the head. An alternative calibration technique was also investigated. This involved removing the dipole and probe and replacing the gap between them by a wire and calibrating though the wire. This produced very similar results to calibrating to a standard point in the head; however it was difficult to disconnect the cables without moving the source dipole and hence altering the system. Therefore, calibrating at a point in the head was the technique used.

After calibrating without any spectacles, scans were made in all three directions at the following position coordinates. The x scan was made from $x = 0$ to 5cm, every 0.5cm, at $y = 7$cm and $z = 3$cm. The y scan was made from $y = 0$ to $y = 8$cm, every 0.2cm, at $x =$ 1cm and $z = 3$cm. The z scan was made from $z = 0$ to 8cm, every 0.2cm, at $x = 1$cm and $y = 7$cm. Therefore, the three scans run through the centre of the eye in each direction.

Both vertical and horizontal source dipole orientations were used with an arbitrary selection of real metallic spectacles. The frequency band of 1710MHz to 1880MHz was investigated. A selection of results is shown in Figure 6.12 to Figure 6.15.

Figure 6.12 and Figure 6.13 represent results, in the x and y directions respectively, excited with a vertically orientated dipole, relative to the head, at 1710MHz. Metallic spectacles were found to have a significant effect on the electric fields inside the head. With this excitation the electric fields in the head were both increased and decreased.

In Figure 6.12 and Figure 6.13 the electric fields are generally increased. However, the field distributions with and without spectacles are different from what is intuitively expected, which puts doubt on the measurement procedure. Clearly metallic spectacles

have a significant effect on the fields inside the head, as the difference with spectacles (±20dB) is much larger than the repeatability of the results (±1dB).

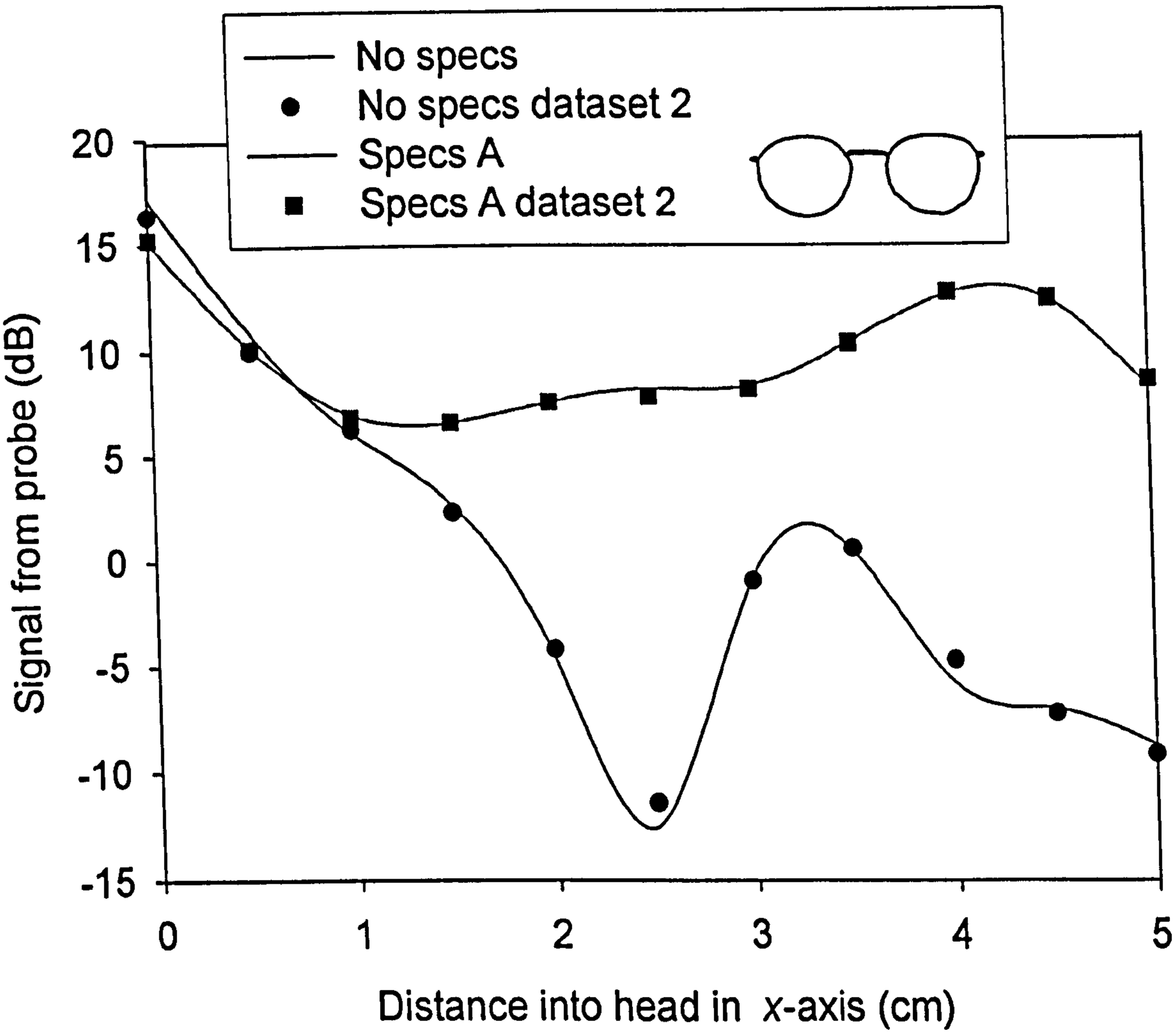

Figure 6.12. The electric fields into the head through the eye position, with and without spectacles (inset). The source is a vertically orientated half wave dipole and the frequency is 1710MHz.

Figure 6.12 shows a typical set of results for a scan in the *x* direction into the head through the eye. In a homogenous material, a smooth exponential decay of the fields inside the head is expected as found in the right hand side of Figure 3.1. However,

Figure 6.12 does not produce this typical result even for the simplified case with no spectacles. Possible explanations are that the probe is not functioning properly, that the probe is coupling to the surface of the phantom or that the metal box is too small and insufficiently lined with RAM so that there were standing waves inside the box. The measurements made with the metallic spectacles produce the added complication of the probe possibly coupling to the metallic frames. Therefore, the results presented are only indicative that metallic spectacles have an effect and further work is needed to investigate the cause of these atypical results with this crude measurement system. Generally the results show a good degree of repeatability (±1dB), both with and without spectacles, as shown in Figure 6.12 to 6.14. This represents a marked improvement over the original wooden box design.

Figure 6.13 shows results with and without an arbitrary pair of metallic spectacles with the dipole orientated vertically with respect to the head. The results are along the *y*-axis, from ear to ear of the head and show that the electric fields can be both increased and decreased by metallic spectacles. The fields at the centre of the head are increased, while the fields at the edge are decreased with the spectacles shown in Figure 6.13. The line without spectacles in Figure 6.13 shows a degree of symmetry in the *y*-axis as would be intuitively expected. A symmetrical result can also be seen in the line with spectacles; however the figure suggests that the central point is shifted in the *y*-axis. This may be due to the excitation dipole not being positioned at the centre of the head. The shift in symmetry may also be due to the spectacles having been aligned at a slight angle relative to the face. However, the effects are repeatable which suggests that the spectacles were positioned in the same position relative to the head in each measurement.

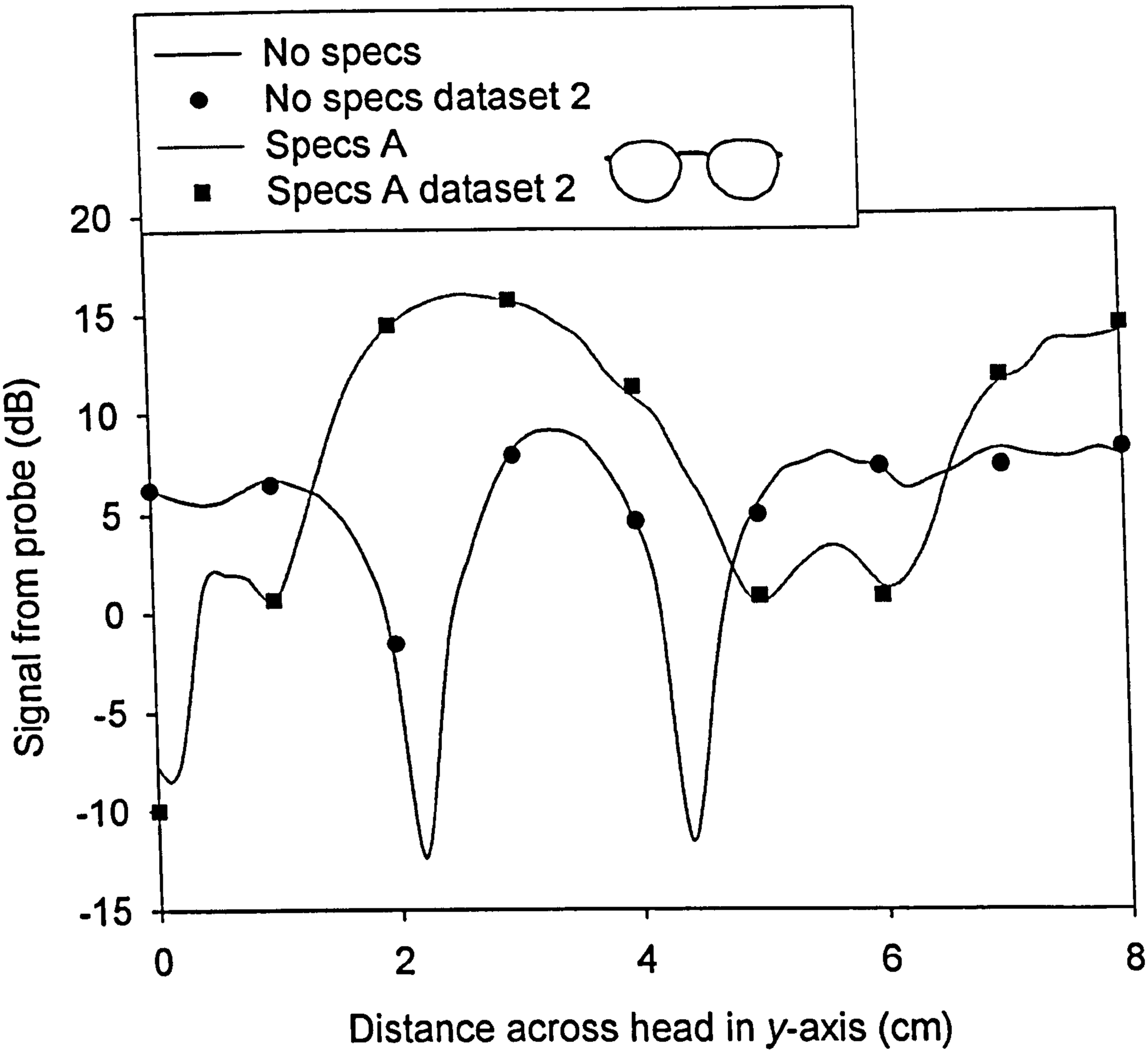

Figure 6.13. The electric fields into the head through the eye position, with and without spectacles (inset). The source is a vertically orientated half wave dipole and the frequency is 1710MHz.

Figure 6.14 and Figure 6.15 represent results, in the *x* and *z* direction respectively, using a horizontally orientated (relative to the head) half-wave at 1800MHz. Results with two different metallic spectacles are included. Both spectacles generally decrease the fields in the head with this orientation of excitation. The two spectacles also produce repeatable but different results, thereby implying that the effects in the head are affected

by the shape and size of the frames. This highlights the dangers of only considering a small selection of spectacles.

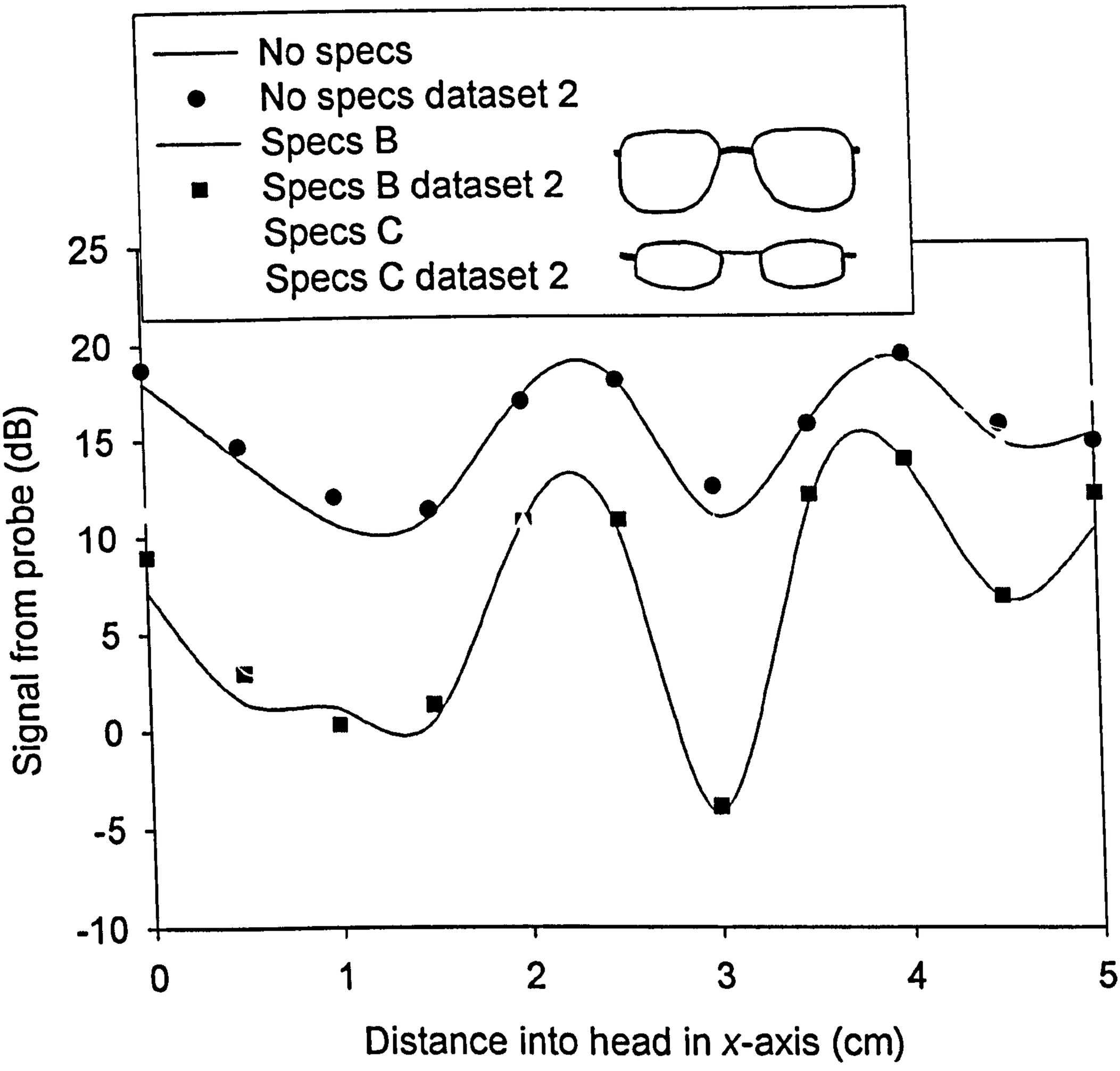

Figure 6.14. The electric fields into the head through the eye position, with and without spectacles (inset). The source is a horizontally orientated half wave dipole and the frequency is 1800MHz.

Figure 6.14 shows the fields as a function of the distance into the head in the x direction with the horizontally orientated dipole (relative to the head). Again this figure does not

produce a smooth exponential decay of the electric fields into the head as is intuitively expected. This further strengthens the conclusion that this measurement system is only useful to indicate that metallic spectacles affect the fields in the head, but can not be used to quantify or accurately locate these effects. The figure shows a series of peaks in the electric fields as the distance is increased. The addition of spectacles, with the horizontally orientated dipole, did not change the location of these peaks but reduced the amplitude of the electric fields measured.

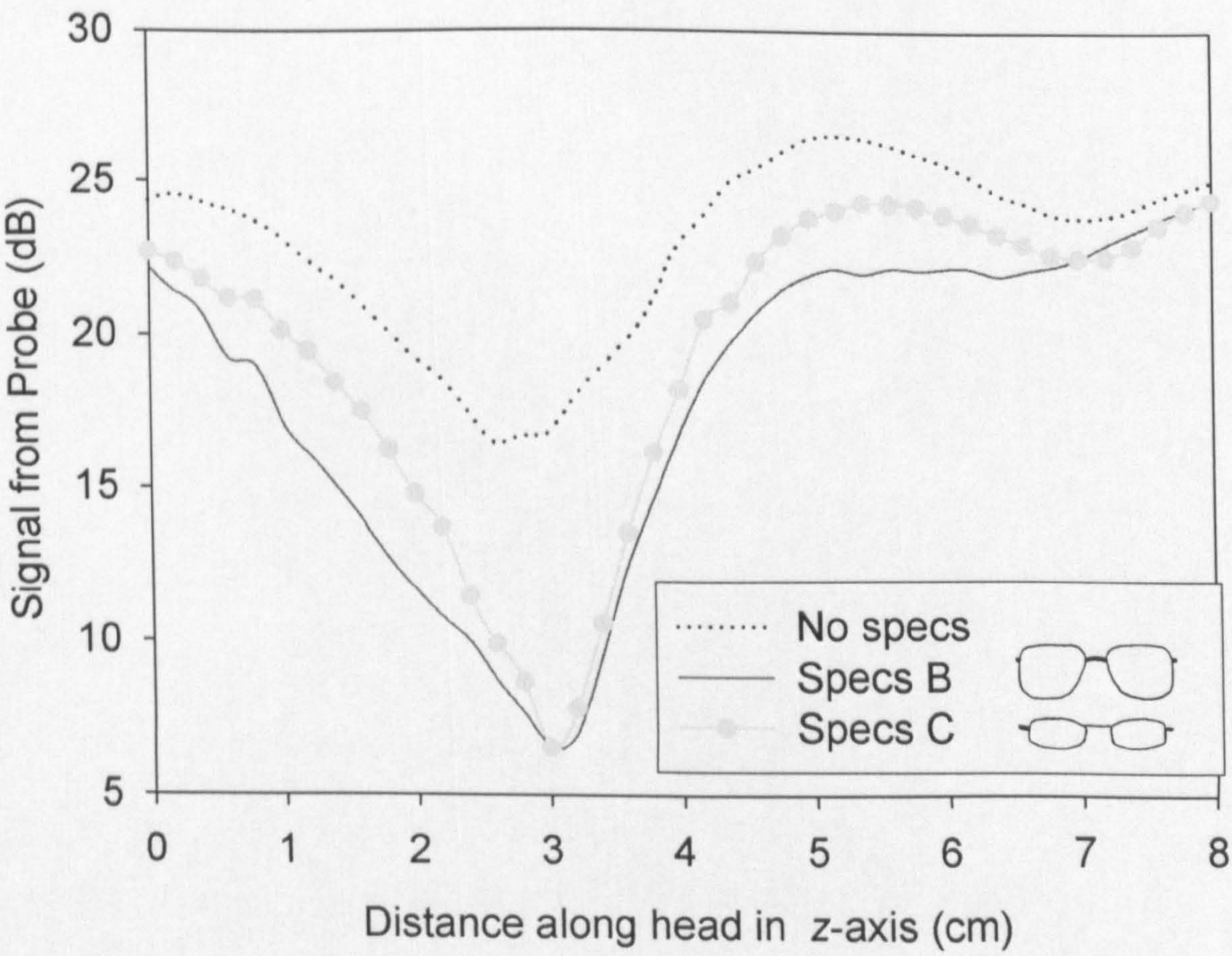

Figure 6.15. The electric fields into the head through the eye position, with and without spectacles (inset). The source is a horizontally orientated half wave dipole and the frequency is 1800MHz.

Figure 6.15 shows the fields in the head in the *z*-axis, moving from chin to scalp. The figure indicates that the fields are reduced along the entire range in the *z*-axis however this reduction is strongest at the centre of the frames. The figure also shows that metallic spectacles cause one null at the centre of the lens as opposed to two with one near the top piece and the other near the bottom section of the metallic frames.

6.5 Conclusions

This chapter has compared results from the FDTD code to measurements. Two different measurement set-ups were used and both found that metallic spectacles had a significant effect on the electric fields in the head. The DASY4 system, an internationally recognised method of measuring SAR in the head, showed good agreement with the FDTD simulation. Geometric metallic half frames, found to optimise the maximum SAR in the head with the computer model, were added to the SAM phantom of the DASY4 system. The measured results showed good agreement with the computer code, both in terms of the trend of the results and the amplitude of the maximum SAR. The metallic spectacles were found to significantly increase the SAR in the head with the vertically orientated dipole. When the dipole was horizontally orientated there was little change in the maximum SAR in the head. This consolidates results in Chapters 4 and 5. Care should be taken when using metallic objects such as spectacles with a measurement phantom, as the maximum SAR in the head may not necessarily be located at a position in the head nearest to the source and may, therefore, not be in an area scanned by the system. The DASY4 measurements showed good agreement with the computer model with both orientations of excitation and both sets of metallic

frames. The measurement also further confirmed the hypothesis of this research; that metallic spectacles can significantly increase the SAR in the head when the excitation is positioned in front of the head.

A further set of measurements were made with a crude measurement system made at minimal financial cost at Sheffield University. This measurement system showed that metallic spectacles have a significant effect on the electric fields in the head. Spectacles caused both increases and decreases to the electric fields at different locations in the head. Different shapes and sizes of spectacles produced different effects. The results showed a good level of repeatability. However, the results appeared to be intuitively incorrect, and therefore the system is only useful to show that metallic spectacles can strongly affect the electric fields in the head. Possible problems with the measurement system are: the probe is not functioning correctly, or is coupling to the surface of the phantom or the spectacles themselves; that the metallic box is too small and is not perfectly lined with RAM and standing waves distort the results. Future work will investigate the causes of these uncertainties, and attempts will be made to improve the system.

6.6 References

1. Lazzi, G., S.S. Pattnaik, C.M. Furse, and O.P. Gandhi, *Comparison of FDTD computed and measured radiation patterns of commercial mobile telephones in presence of the human head.* IEEE Transactions on Antennas and Propagation, 1998. **46**(6): p. 943-944.
2. Siegbahn, M., S. Mazur, and C. Tornevik. *Comparisons of measurements and FDTD calculations of mobile phone electromagnetic far-fields and near-fields. Antennas and Propagation Society International Symposium, 1997. IEEE., 1997 Digest.* 1997. p. 978-981

3. Yu, Q.S., O.P. Gandhi, M. Aronsson, and D. Wu, *An automated SAR measurement system for compliance testing of personal wireless devices.* IEEE Transactions on Electromagnetic Compatibility, 1999. **41**(3): p. 234-245.

4. Bahr, A., S. Pan, T. Beck, R. Kastle, T. Schmid, and N. Kuster, *A comparison between numerical and experimental near-field evaluation of a DCS mobile telephone.* Radio Science, 1998. **33**(6): p. 1553-1563.

5. Schiavoni, A., P. Bertotto, G. Richiardi, and P. Bielli, *SAR generated by commercial cellular phones - Phone modeling, head modeling, and measurements.* IEEE Transactions on Microwave Theory and Techniques, 2000. **48**(11): p. 2064-2071.

6. Balzano, Q., O. Garay, and T.J. Manning, *Electromagnetic energy exposure of simulated users of portable cellular telephones.* IEEE Trans. Vehicular Technology, 1995. **44**(3): p. 390-403.

7. Cleveland, R.F. and T.W. Athey, *Specific absorption rate (SAR) in models of the human head exposed to hand-held UHF portable radios.* Bioelectromagnetics, 1989. **10**: p. 173-186.

8. Griffin, D.W., *A microwave antenna method of measuring the effect of metal-framed spectacles on microwaves near the eye.* Antennas and Propagation Society International Symposium, 1983. **21**: p. 253-256.

9. Anderson, V. and K.H. Joyner, *Specific absorption rate levels measured in a phantom head exposed to radiofrequency transmissions from analog hand-held mobile phones.* Bioelectromagnetics, 1995. **16**(1): p. 60-69.

10. Schmid, T., O. Egger, and N. Kuster, *Automated E-field scanning system for dosimetric assessments.* IEEE Microwave Theory and Techniques, 1996. **44**(1): p. 105 -113.

11. Kuster, N. and Q. Balzano, *Energy absorption mechanism by biological bodies in near field of dipole antennas above 300MHz.* IEEE Trans. Vehicular Technology, 1992. **41**(1): p. 17-23.

12. Nikita, K.S., M. Cavagnaro, P. Bernardi, N.K. Uzunoglu, S. Pisa, E. Piuzzi, J.N. Sahalos, G.I. Krikelas, J.A. Vaul, P.S. Excell, G. Cerri, S. Chiarandini, R. De Leo, and P. Russo, *A study of uncertainties in modeling antenna performance and power absorption in the head of a cellular phone user.* IEEE Transactions on Microwave Theory and Techniques, 2000. **48**(12): p. 2676-2685.

Chapter 7

CONCLUSIONS

7.1 Summary of research and novelty

This thesis has investigated the absorption of electromagnetic energy from RF sources positioned in front of the head. The research was made using a specially developed FDTD code. FDTD is the most common computational method used to analyse RF interactions with biological matter because it is simple to code, intuitive and allows complex inhomogeneous shapes to be modelled. Two common sources, dipoles and plane waves, have been used. The grid has been truncated by PML absorbing boundary conditions. All aspects of the code have been carefully validated against other published results, giving confidence in its use and its application to more complex geometries. An additional analytical validation of the code is included in Appendix J. Three different anatomical heads were implemented into the FDTD grid space, two of which were deemed suitable for excitation from the front and are included in the results of this thesis. The use of two numerical phantoms, of different size and internal structure, allows comparisons to be made. In this work the head has been assumed to be symmetric to reduce computational complexity and this has been shown to have negligible effect. Results with the anatomical head have also been validated, including the SAR in the eyes, using published journals. Eyes have received considerable attention in this thesis due to their vulnerability. The excitation from the front and the microwave frequency range used is also germane to the vulnerability of eyes.

This thesis has shown results of adding metallic spectacles to two anatomically accurate heads. As reviewed in Chapter 1, spectacles have only received limited attention in scientific journals. Previously only specific frequencies had been considered with the excitation predominantly at the side of the head. This thesis has considered the novel area of exciting a head with metallic spectacles from the front. A topical frequency range from 0.5 to 3.0GHz has been considered, thereby including many communication frequencies where the effects of spectacles have received no attention.

Previously, authors had only considered one specific pair of spectacles. This thesis compares many different shapes and sizes. The results show that the effects are very dependent on the shape and size of the frames. This thesis also investigates the novel area of varying the material of both the lens and the frame. Initially geometric spectacles were considered with a nosepiece, a strut to the arm, an arm and a lens included. Further results have been made with a selection of spectacles based on realistic shapes.

Maximal effects of metallic spectacles have been searched for with a genetic algorithm. To the author's knowledge this is the first time a GA has been applied to the absorption of RF in the human head. Seven chromosomes have been used to describe a pair of spectacles. These included the size of the frames, the shape of the frame, the thickness of the lens, the material of the lens, the width of the spectacles and the distance from the eye. These parameters produced a large range of spectacles, which are similar to the range of real spectacles. The GA has been used to search for the maximum and minimum SAR in the eye with different metallic spectacles with a plane wave excitation at various communication frequencies. A dual objective Pareto ranked GA was used to search for both the average SAR in the eye and the maximum SAR averaged over 1g of

the eye. A statistical analysis using a range of random spectacles has also been made to investigate the likely effects of a random pair of spectacles. The GA has also been applied with other sources, including a half-wave dipole and horizontally polarised sources. Plane wave and dipole sources have been compared showing that results are similar when the results are scaled.

Measurements have been made to further validate the FDTD code. The industry standard DASY4 measurement system has been used to investigate the effects of metallic spectacles in the head. To the author's knowledge no SAR measurements have been made using this geometry with metallic spectacle frames positioned between source and the head. The comparison of the results of measurements and computer modelling with metallic spectacles is a novel area. The two techniques showed a good level of agreement. Measurements were also made with an elementary measurement system, built at Sheffield University that provided further evidence that metallic spectacles could affect the distribution of energy in a phantom head with the source positioned in front of the face. A measurement system that can look at the electric fields at different locations in a phantom head wearing metallic spectacles has not previously been investigated. This system potentially allows the effects of real spectacles to be measured in the whole phantom head and not just at a single point in the eye.

7.2 Summary of results

The FDTD code was initially used to model previously researched geometries and the good agreement obtained with results from published journals, proved that the code was valid and could be confidently extended to novel applications. Two different

anatomically realistic heads were implemented into the FDTD code. Results show slight differences between the two different heads. This thesis has largely concentrated on effects in the eye. Opening the eyelids has been found to decrease the SAR in the eye around 1.8GHz – this means the worst case scenario is with the eyelids closed. This effect has not previously been reported in the literature and is potentially useful for future researchers. The head has been shown to be approximately symmetric and a line of symmetry has been shown to have little effect on the SAR in the eye. The use of symmetry has not been previously investigated with an asymmetric anatomical head.

The effect of spectacles has been found to be very dependent on the material of the frames. Generally, results indicate that spectacles made of insulators have very little effect, whereas the effect of conductors, such as carbon or metal, can be significant. There was found to be very little difference between frames made of different conducting materials. The arm is less significant than the front section of the frames. The lens has little effect on its own, at the communication frequencies considered, but can reduce the resonance frequency of the frames. Results show that the lens becomes more significant as the frequency increases, and it is therefore possible that plastic frames with lenses could prove to be significant at higher frequencies. Metallic spectacles can both significantly increase or decrease the SAR in the eye depending on the type of frames and the frequency of excitation. The location of the maximum increases have been plotted in three planar cuts through the eyes, the maximum increases in the SAR in the head are in the eyes, the nose, and the skin by the arms of the spectacles. The effects of spectacles decrease towards the back of the head. The average SAR in the head can increase by up to 13%, and results of modelling the homogenous measurement phantom in Figure 6.2 indicated that this may increase to

60% if the source is positioned close to the head. Realistically shaped spectacles have been investigated and have produced similar effects in terms of frequency and amplitude as geometric spectacles.

A GA was applied to a vertically polarised plane wave excitation at various communication frequencies. Results showed that metallic spectacles could both increase and decrease the SAR in the eye at all frequencies. The effects below 1GHz were relatively small. The largest effect of spectacles was at 1.8GHz, where rectangular frames increased the average SAR in the eye by approximately two and half times. Significant decreases, of up to 85%, were found in the SAR in the eye, at frequencies between 1.8GHz and 3.0GHz. The size and shape of the frames were found to be the most significant factors determining the SAR in the eye.

The effects of adding the same spectacles to a different anatomical head produced similar percentage increases in the SAR in the eye across the frequency range considered. The effects of one hundred different spectacles at 1.8GHz produced similar results in the eyes of both heads. The GA found the maximum and minimum SAR in the eyes of both heads with very similar spectacles and similar percentage increases and decreases were found. This evidence suggests that the same pair of spectacles will produce similar effects on different people. This is important as it shows that it is valid to primarily investigate the effect of metallic spectacles with one anatomical head and assume that the results for different people will be approximately the same. It also allows the effects of a specific pair of spectacles on different people to be predictable.

The GA was also applied to a vertically orientated dipole, again similar percentage increases were found with similar spectacles as with the vertically polarised plane wave.

This shows that the GA is converging. The GA was also used in conjunction with a horizontally polarised plane wave. No spectacles were found that increased the SAR in the eye. Generally varying the parameters describing the spectacles had relatively little effect with this polarisation of source, however varying the total width of the frames increased the SAR in the eye by 10% compared to 2% with a vertically polarised plane wave. Again similar results were found with a horizontally orientated dipole. This suggests that the frequency and the polarisation of the source are more important than the source itself.

The GA was also used to search for the maximum SAR in the head averaged over both 1g and 10g with a vertically polarised plane wave. The GA found configurations of spectacles that marginally decreased the SAR in a single cell, but no spectacles decreased the maximum SAR averaged over 1g or 10g of the head. Substantial increases in the SAR in the head were found. The spectacles that produced the highest SAR in the head were different from those that produced the highest SAR in the eye. Generally the maximum SAR_{10g} in the head was roughly proportional to the height plus the width of the frames.

The FDTD code was used to model a homogeneous asymmetric head to allow comparison to the measurement results. The stretched nose of the phantom meant that real spectacles could not be added to the head; hence the spectacles added had only one rectangular frame. This half pair of spectacles produced similar increases to the SAR in the head as the whole pair of spectacles modelled when using a symmetric head. This shows that the effects are not dependent on the whole width of the frames, but on just half the frame. Results with this measurement geometry showed that the percentage increases in the head and eye were dependent on the distance of the source to the head.

Spectacles increased the power absorbed in the head by approximately 60% with the source positioned close to the head. With the source positioned at least 14cm away from the head, the maximum SAR averaged over the 'eye' increased by a factor of three.

The effects of metallic spectacles were also investigated using the DASY4 measurement system, this system has become an industry standard for SAR measurements. Suitable geometric spectacles were found by simulating the measurement phantom using the FDTD software. Metallic spectacles used in conjunction with a vertically orientated dipole (relative to the head) significantly increased the maximum SAR_{1g} and SAR_{10g} in the head, by up to 5.4 times. Different spectacles produced different results. Metallic spectacles used in conjunction with a horizontally orientated dipole had very little effect on the maximum SAR in the head, although small decreases were found with this geometry. The results showed good agreement with the FDTD code and therefore further validate the results from the computer model.

Further measurements were made with real metallic spectacles positioned in front of the head with a crude measurement system. Metallic spectacles were found to significantly change the electric fields at different positions inside the head. The results showed a good level of repeatability. However, the overall system was very crude and generally did not produce results which were intuitively correct. Therefore, this set of measurement results only verify that spectacles can significantly alter the SAR in the head, but does not provide accurate assessment of the relative increases or the locations of the peaks.

The mechanism for the effects of spectacles is discussed in Appendix K.

7.3 Implications for industry

This thesis has showed that significant increases and decreases in the SAR in the eyes and the head are possible with metallic spectacles and this has implications for many different industrial areas. Many sources estimate that there are approximately one billion mobile phones in the world and the popularity of other communication enabled devices is increasing with the advancement of technology. There are also many millions of spectacle wearers in the world, although not all of these will have metallic frames.

The FCC allows exposure to sources with a power density of 50W/m² at 1.8GHz in controlled conditions. Figure 3.10 showed this power density produces SAR levels in the eye that are very close to the international safety limits.

The manufacturers of mobile phones, PDAs and other mobile devices may wish to research different antennae to reduce the SAR in the head, to safely allow the addition of metallic spectacles. Also antennas with horizontal polarisations may be of interest as spectacle wearers are very common. This may prove to be an interesting idea from both a safety and a marketing viewpoint.

Spectacle manufacturers may also be interested in these results. The effects of spectacles can be made insignificant if the frames are plastic, and spectacle manufacturers may wish to produce a higher percentage of plastic frames. It may be possible to reduce the effects of metallic spectacles by making part of the metal frames out of insulating materials. The shape and size of spectacles may also become a significant factor in their design in light of the results published in this thesis.

Results show that spectacles can be designed to significantly decrease the SAR in the eye. However, care should be taken in pursuing this idea as the maximum SAR in the head is likely to increase and no spectacles have been found that decrease the maximum SAR in the head, with a vertically polarised plane wave. This may become interesting if further research finds that the eyes are particularly vulnerable compared to other tissues in the head. The results in this thesis show that the spectacles can particularly increase the SAR in the eye, the nose and at the sides of the head. This knowledge allows the biologists and chemists researching the effects of RF to concentrate effort into these areas and to use larger power to allow for the worst case of using metallic spectacles.

This thesis has investigated the effects of metallic spectacles when exposed to RF radiation. This may emanate from many sources, such as a mobile phone used to send text messages or video messaging, a PDA, a Bluetooth device, a wireless LAN connection, radiation from base stations, leaking microwave ovens, metal detectors and shop security mechanisms. Metallic spectacles have implications for many sources, and this thesis aimed to show the effects of spectacles for a general rather than a specific source.

7.4 Future work

This thesis has produced many new results; however, as in any area of science, new results leads to more questions and future work that has not been carried out as part of this project. Further work will continue to research the effects of metallic spectacles. Realistic sources will replace the dipole and plane wave sources used this far. The source will be moved to different angles to the side and above and below the head. Thus

the effect of metallic spectacles in more realistic geometries can be investigated thoroughly. Real sources may include a hands-free wire kit or a short range Bluetooth device to a headset. The addition of these possibilities will also be considered.

Further research will be done using the FDTD code and the DASY4 measurement system to allow comparison between the two methods. This will also allow both real and geometric spectacles to be considered. It may also be possible to develop a new phantom for use with the DASY4 system where the spectacles can rest on the nose of the phantom. Further work will be invested into improving the measurement set-up developed at Sheffield University to understand and reduce the uncertainties associated with the results. This will allow spectacles to be placed normally on the face.

With these three different analysis techniques, it will be possible to investigate the mechanism that changes the SAR in the head when spectacles are added. When this is better understood, it may be possible to design spectacles that reduce the SAR in the whole head. For example adding a thin transparent conducting surface to the lens may reflect the energy away from the head. Future technology may produce spectacles that have an inbuilt antenna, used as a communicating device. Thus it may be interesting to investigate how safely an antenna could be added to the frames of spectacles.

A related topic to the effects of metallic spectacles is that of metallic implants and jewellery. Metallic implants in the eye may become more common as a method of improving failing eyesight. Jewellery may include gold teeth, nose rings, eyebrow piercings and rings on the hand holding the communicating device. It is possible that fashion may increase the wearing of large metallic jewellery which may become resonant at communication frequencies.

Appendix A

Six partial differential equations, see (2-9).

$$\frac{\partial E_z}{\partial t} = \frac{1}{\varepsilon}\left(\frac{\partial H_y}{\partial x} - \frac{\partial H_x}{\partial y} - \sigma E_z\right)$$

$$\frac{\partial E_x}{\partial t} = \frac{1}{\varepsilon}\left(\frac{\partial H_z}{\partial y} - \frac{\partial H_y}{\partial z} - \sigma E_x\right)$$

$$\frac{\partial E_y}{\partial t} = \frac{1}{\varepsilon}\left(\frac{\partial H_x}{\partial z} - \frac{\partial H_z}{\partial x} - \sigma E_y\right)$$

$$\frac{\partial H_x}{\partial t} = \frac{1}{\mu}\left(\frac{\partial E_y}{\partial z} - \frac{\partial E_z}{\partial y} - \rho' H_x\right)$$

$$\frac{\partial H_y}{\partial t} = \frac{1}{\mu}\left(\frac{\partial E_z}{\partial x} - \frac{\partial E_x}{\partial z} - \rho' H_y\right)$$

$$\frac{\partial H_z}{\partial t} = \frac{1}{\mu}\left(\frac{\partial E_x}{\partial y} - \frac{\partial E_y}{\partial x} - \rho' H_z\right)$$

Appendix B

Substituting the finite difference expressions, (2-10) and (2-11), into the six partial differential equations, (2-9), results in the formation of six new equations, see (2-12).

$$\frac{H_x\big|_{i,j,k}^{n+1/2} - H_x\big|_{i,j,k}^{n-1/2}}{\Delta t} = \frac{1}{\mu_{i,j,k}}\left(\frac{E_y\big|_{i,j,k+1/2}^{n} - E_y\big|_{i,j,k-1/2}^{n}}{\Delta z} - \frac{E_z\big|_{i,j+1/2,k}^{n} - E_z\big|_{i,j-1/2,k}^{n}}{\Delta y} - \rho'_{i,j,k} H_x\big|_{i,j,k}^{n}\right)$$

$$\frac{H_y\big|_{i,j,k}^{n+1/2} - H_y\big|_{i,j,k}^{n-1/2}}{\Delta t} = \frac{1}{\mu_{i,j,k}}\left(\frac{E_z\big|_{i+1/2,j,k}^{n} - E_z\big|_{i-1/2,j,k}^{n}}{\Delta x} - \frac{E_x\big|_{i,j,k+1/2}^{n} - E_x\big|_{i,j,k-1/2}^{n}}{\Delta z} - \rho'_{i,j,k} H_y\big|_{i,j,k}^{n}\right)$$

$$\frac{H_z\big|_{i,j,k}^{n+1/2} - H_z\big|_{i,j,k}^{n-1/2}}{\Delta t} = \frac{1}{\mu_{i,j,k}}\left(\frac{E_x\big|_{i,j,k+1/2}^{n} - E_x\big|_{i,j,k-1/2}^{n}}{\Delta y} - \frac{E_y\big|_{i+1/2,j,k}^{n} - E_y\big|_{i-1/2,j,k}^{n}}{\Delta x} - \rho'_{i,j,k} H_z\big|_{i,j,k}^{n}\right)$$

$$\frac{E_x\big|_{i,j,k}^{n+1} - E_x\big|_{i,j,k}^{n}}{\Delta t} = \frac{1}{\varepsilon_{i,j,k}}\left(\frac{H_z\big|_{i,j+1/2,k}^{n+1/2} - H_z\big|_{i,j-1/2,k}^{n-1/2}}{\Delta y} - \frac{H_y\big|_{i,j,k+1/2}^{n+1/2} - H_y\big|_{i,j,k-1/2}^{n+1/2}}{\Delta z} - \sigma_{i,j,k} E_x\big|_{i,j,k}^{n+1/2}\right)$$

$$\frac{E_y\big|_{i,j,k}^{n+1} - E_y\big|_{i,j,k}^{n}}{\Delta t} = \frac{1}{\varepsilon_{i,j,k}}\left(\frac{H_x\big|_{i,j,k+1/2}^{n+1/2} - H_x\big|_{i,j,k-1/2}^{n-1/2}}{\Delta z} - \frac{H_z\big|_{i+1/2,j,k}^{n+1/2} - H_z\big|_{i-1/2,j,k}^{n+1/2}}{\Delta x} - \sigma_{i,j,k} E_y\big|_{i,j,k}^{n+1/2}\right)$$

$$\frac{E_z\big|_{i,j,k}^{n+1} - E_z\big|_{i,j,k}^{n}}{\Delta t} = \frac{1}{\varepsilon_{i,j,k}}\left(\frac{H_y\big|_{i+1/2,j,k}^{n+1/2} - H_y\big|_{i-1/2,j,k}^{n-1/2}}{\Delta x} - \frac{H_x\big|_{i,j+1/2,k}^{n+1/2} - H_x\big|_{i,j-1,2,k}^{n+1/2}}{\Delta y} - \sigma_{i,j,k} E_z\big|_{i,j,k}^{n+1/2}\right)$$

Appendix C

Six FDTD equations, see (2-14).

$$H_x\big|_{i,j,k}^{n+1/2}=\left(\frac{1-\frac{\dot{\rho}_{i,j,k}\,\Delta t}{2\mu_{i,j,k}}}{1+\frac{\dot{\rho}_{i,j,k}\,\Delta t}{2\mu_{i,j,k}}}\right)H_x\big|_{i,j,k}^{n-1/2}+\left(\frac{\frac{\Delta t}{\mu_{i,j,k}}}{1+\frac{\dot{\rho}_{i,j,k}\,\Delta t}{2\mu_{i,j,k}}}\right)\left(\frac{E_y\big|_{i,j,k+1/2}^{n}-E_y\big|_{i,j,k-1/2}^{n}}{\Delta z}-\frac{E_z\big|_{i,j+1/2,k}^{n}-E_z\big|_{i,j-1/2,k}^{n}}{\Delta y}\right)$$

$$H_y\big|_{i,j,k}^{n+1/2}=\left(\frac{1-\frac{\dot{\rho}_{i,j,k}\,\Delta t}{2\mu_{i,j,k}}}{1+\frac{\dot{\rho}_{i,j,k}\,\Delta t}{2\mu_{i,j,k}}}\right)H_y\big|_{i,j,k}^{n-1/2}+\left(\frac{\frac{\Delta t}{\mu_{i,j,k}}}{1+\frac{\dot{\rho}_{i,j,k}\,\Delta t}{2\mu_{i,j,k}}}\right)\left(\frac{E_z\big|_{i+1/2,j,k}^{n}-E_z\big|_{i-1/2,j,k}^{n}}{\Delta x}-\frac{E_x\big|_{i,j,k+1/2}^{n}-E_x\big|_{i,j,k-1/2}^{n}}{\Delta z}\right)$$

$$H_z\big|_{i,j,k}^{n+1/2}=\left(\frac{1-\frac{\dot{\rho}_{i,j,k}\,\Delta t}{2\mu_{i,j,k}}}{1+\frac{\dot{\rho}_{i,j,k}\,\Delta t}{2\mu_{i,j,k}}}\right)H_z\big|_{i,j,k}^{n-1/2}+\left(\frac{\frac{\Delta t}{\mu_{i,j,k}}}{1+\frac{\dot{\rho}_{i,j,k}\,\Delta t}{2\mu_{i,j,k}}}\right)\left(\frac{E_x\big|_{i,j+1/2,k}^{n}-E_x\big|_{i,j-1/2,k}^{n}}{\Delta y}-\frac{E_y\big|_{i+1/2,j,k}^{n}-E_y\big|_{i-1/2,j,k}^{n}}{\Delta x}\right)$$

$$E_x\big|_{i,j,k}^{n+1}=\left(\frac{1-\frac{\sigma_{i,j,k}\Delta t}{2\varepsilon_{i,j,k}}}{1+\frac{\sigma_{i,j,k}\Delta t}{2\varepsilon_{i,j,k}}}\right)E_x\big|_{i,j,k}^{n}+\left(\frac{\frac{\Delta t}{\varepsilon_{i,j,k}}}{1+\frac{\sigma_{i,j,k}\Delta t}{2\varepsilon_{i,j,k}}}\right)\left(\frac{H_z\big|_{i,j+1/2,k}^{n+1/2}-H_z\big|_{i,j-1/2,k}^{n+1/2}}{\Delta y}-\frac{H_y\big|_{i,j,k+1/2}^{n+1/2}-H_y\big|_{i,j,k-1/2}^{n+1/2}}{\Delta z}\right)$$

$$E_y\big|_{i,j,k}^{n+1}=\left(\frac{1-\frac{\sigma_{i,j,k}\Delta t}{2\varepsilon_{i,j,k}}}{1+\frac{\sigma_{i,j,k}\Delta t}{2\varepsilon_{i,j,k}}}\right)E_y\big|_{i,j,k}^{n}+\left(\frac{\frac{\Delta t}{\varepsilon_{i,j,k}}}{1+\frac{\sigma_{i,j,k}\Delta t}{2\varepsilon_{i,j,k}}}\right)\left(\frac{H_x\big|_{i,j,k+1/2}^{n+1/2}-H_x\big|_{i,j,k-1/2}^{n+1/2}}{\Delta z}-\frac{H_z\big|_{i+1/2,j,k}^{n+1/2}-H_z\big|_{i-1/2,j,k}^{n+1/2}}{\Delta x}\right)$$

$$E_z\big|_{i,j,k}^{n+1}=\left(\frac{1-\frac{\sigma_{i,j,k}\Delta t}{2\varepsilon_{i,j,k}}}{1+\frac{\sigma_{i,j,k}\Delta t}{2\varepsilon_{i,j,k}}}\right)E_z\big|_{i,j,k}^{n}+\left(\frac{\frac{\Delta t}{\varepsilon_{i,j,k}}}{1+\frac{\sigma_{i,j,k}\Delta t}{2\varepsilon_{i,j,k}}}\right)\left(\frac{H_y\big|_{i+1/2,j,k}^{n+1/2}-H_y\big|_{i-1/2,j,k}^{n+1/2}}{\Delta x}-\frac{H_x\big|_{i,j+1/2,k}^{n+1/2}-H_x\big|_{i,j-1/2,k}^{n+1/2}}{\Delta y}\right)$$

Appendix D

Ten of twelve split field equations for PML boundaries, see also (2-22) and (2-23).

$$\varepsilon \frac{\partial E_{xy}}{\partial t} = \frac{\partial (H_{zx} + H_{zy})}{\partial y} - \sigma_y E_{xy}$$

$$\varepsilon \frac{\partial E_{xz}}{\partial t} = -\frac{\partial (H_{yz} + H_{yx})}{\partial z} - \sigma_z E_{xz}$$

$$\varepsilon \frac{\partial E_{yz}}{\partial t} = \frac{\partial (H_{xy} + H_{xz})}{\partial z} - \sigma_z E_{yz}$$

$$\varepsilon \frac{\partial E_{yx}}{\partial t} = -\frac{\partial (H_{zx} + H_{zy})}{\partial x} - \sigma_x E_{yx}$$

$$\mu \frac{\partial H_{xy}}{\partial t} = -\frac{\partial (E_{zx} + E_{zy})}{\partial y} - \rho_y^{'} H_{xy}$$

$$\mu \frac{\partial H_{xz}}{\partial t} = \frac{\partial (E_{yz} + E_{yx})}{\partial z} - \rho_z^{'} H_{xz}$$

$$\mu \frac{\partial H_{yz}}{\partial t} = -\frac{\partial (E_{xy} + E_{xz})}{\partial z} - \rho_z^{'} H_{yz}$$

$$\mu \frac{\partial H_{yx}}{\partial t} = \frac{\partial (E_{zx} + E_{zy})}{\partial x} - \rho_x^{'} H_{yx}$$

$$\mu \frac{\partial H_{zx}}{\partial t} = -\frac{\partial (E_{yz} + E_{yx})}{\partial x} - \rho_x^{'} H_{zx}$$

$$\mu \frac{\partial H_{zy}}{\partial t} = \frac{\partial (E_{xy} + E_{xz})}{\partial y} - \rho_y^{'} H_{zy}$$

Appendix E

Twelve equations for the split field components in the PML region, see (2-33).

$$H_{xy}\Big|_{i,j,k}^{n+1/2}=\exp(-\dot{\rho}_y(j)\Delta t/\mu)H_{xy}\Big|_{i,j,k}^{n-1/2}-\frac{1-\exp(-\dot{\rho}_y(j)\Delta t/\mu)}{\dot{\rho}_y(j)\Delta y}\begin{pmatrix}E_{zx}\Big|_{i,j+1/2,k}^{n}+E_{zy}\Big|_{i,j+1/2,k}^{n}\\-E_{zx}\Big|_{i,j-1/2,k}^{n}-E_{zy}\Big|_{i,j-1/2,k}^{n}\end{pmatrix}$$

$$H_{xz}\Big|_{i,j,k}^{n+1/2}=\exp(-\dot{\rho}_z(k)\Delta t/\mu)H_{xz}\Big|_{i,j,k}^{n-1/2}+\frac{1-\exp(-\dot{\rho}_z(k)\Delta t/\mu)}{\dot{\rho}_z(k)\Delta z}\begin{pmatrix}E_{yz}\Big|_{i,j,k+1/2}^{n}+E_{yx}\Big|_{i,j,k+1/2}^{n}\\-E_{yz}\Big|_{i,j,k-1/2}^{n}-E_{yx}\Big|_{i,j,k-1/2}^{n}\end{pmatrix}$$

$$H_{yx}\Big|_{i,j,k}^{n+1/2}=\exp(-\dot{\rho}_x(i)\Delta t/\mu)H_{yx}\Big|_{i,j,k}^{n-1/2}+\frac{1-\exp(-\dot{\rho}_x(i)\Delta t/\mu)}{\dot{\rho}_x(i)\Delta x}\begin{pmatrix}E_{zx}\Big|_{i+1./2,j,k}^{n}+E_{zy}\Big|_{i+1/2,j,k}^{n}\\-E_{zx}\Big|_{i-1/2,j,k}^{n}-E_{zy}\Big|_{i-1/2,j,k}^{n}\end{pmatrix}$$

$$H_{yz}\Big|_{i,j,k}^{n+1/2}=\exp(-\dot{\rho}_z(k)\Delta t/\mu)H_{yz}\Big|_{i,j,k}^{n-1/2}-\frac{1-\exp(-\dot{\rho}_z(k)\Delta t/\mu)}{\dot{\rho}_z(k)\Delta z}\begin{pmatrix}E_{xy}\Big|_{i,j,k+1/2}^{n}+E_{xz}\Big|_{i,j,k+1/2}^{n}\\-E_{xy}\Big|_{i,j,k-1/2}^{n}-E_{xz}\Big|_{i,j,k-1/2}^{n}\end{pmatrix}$$

$$H_{zx}\Big|_{i,j,k}^{n+1/2}=\exp(-\dot{\rho}_x(i)\Delta t/\mu)H_{zx}\Big|_{i,j,k}^{n-1/2}-\frac{1-\exp(-\dot{\rho}_x(i)\Delta t/\mu)}{\dot{\rho}_x(i)\Delta x}\begin{pmatrix}E_{yz}\Big|_{i+1./2,j,k}^{n}+E_{yx}\Big|_{i+1/2,j,k}^{n}\\-E_{yz}\Big|_{i-1/2,j,k}^{n}-E_{yx}\Big|_{i-1/2,j,k}^{n}\end{pmatrix}$$

$$H_{zy}\Big|_{i,j,k}^{n+1/2}=\exp(-\dot{\rho}_y(j)\Delta t/\mu)H_{zy}\Big|_{i,j,k}^{n-1/2}+\frac{1-\exp(-\dot{\rho}_y(j)\Delta t/\mu)}{\dot{\rho}_y(j)\Delta y}\begin{pmatrix}E_{xy}\Big|_{i,j+1/2,k}^{n}+E_{xz}\Big|_{i,j+1/2,k}^{n}\\-E_{xy}\Big|_{i,j-1/2,k}^{n}-E_{xz}\Big|_{i,j-1/2,k}^{n}\end{pmatrix}$$

$$E_{xy}\big|_{i,j,k}^{n+1}=\exp(-\sigma_y(j)\Delta t/\varepsilon)E_{xy}\big|_{i,j,k}^{n}+\frac{1-\exp(-\sigma_y(j)\Delta t/\varepsilon)}{\sigma_y(j)\Delta y}\begin{pmatrix}H_{zx}\big|_{i,j+1/2,k}^{n+1/2}+H_{zy}\big|_{i,j+1/2,k}^{n+1/2}\\-H_{zx}\big|_{i,j-1/2,k}^{n+1/2}-H_{zy}\big|_{i,j-1/2,k}^{n+1/2}\end{pmatrix}$$

$$E_{xz}\big|_{i,j,k}^{n+1}=\exp(-\sigma_z(k)\Delta t/\varepsilon)E_{xz}\big|_{i,j,k}^{n}\frac{1-\exp(-\sigma_z(k)\Delta t/\varepsilon)}{\sigma_z(k)\Delta z}\begin{pmatrix}H_{yz}\big|_{i,j,k+1/2}^{n+1/2}+H_{yx}\big|_{i,j,k+1/2}^{n+1/2}\\-H_{yz}\big|_{i,j,k-1/2}^{n+1/2}-H_{yx}\big|_{i,j,k-1/2}^{n+1/2}\end{pmatrix}$$

$$E_{yx}\big|_{i,j,k}^{n+1}=\exp(-\sigma_x(i)\Delta t/\varepsilon)E_{yx}\big|_{i,j,k}^{n}\frac{1-\exp(-\sigma_x(i)\Delta t/\varepsilon)}{\sigma_x(i)\Delta x}\begin{pmatrix}H_{zx}\big|_{i+1/2,j,k}^{n+1/2}+H_{zy}\big|_{i+1/2,j,k}^{n+1/2}\\-H_{zx}\big|_{i-1/2,j,k}^{n+1/2}-H_{zy}\big|_{i-1/2,j,k}^{n+1/2}\end{pmatrix}$$

$$E_{yz}\big|_{i,j,k}^{n+1}=\exp(-\sigma_z(k)\Delta t/\varepsilon)E_{yz}\big|_{i,j,k}^{n}+\frac{1-\exp(-\sigma_z(k)\Delta t/\varepsilon)}{\sigma_z(k)\Delta z}\begin{pmatrix}H_{xy}\big|_{i,j,k+1/2}^{n+1/2}+H_{xz}\big|_{i,j,k+1/2}^{n+1/2}\\-H_{xy}\big|_{i,j,k-1/2}^{n+1/2}-H_{xz}\big|_{i,j,k-1/2}^{n+1/2}\end{pmatrix}$$

$$E_{zx}\big|_{i,j,k}^{n+1}=\exp(-\sigma_x(i)\Delta t/\varepsilon)E_{zx}\big|_{i,j,k}^{n}+\frac{1-\exp(-\sigma_x(i)\Delta t/\varepsilon)}{\sigma_x(i)\Delta x}\begin{pmatrix}H_{yz}\big|_{i+1/2,j,k}^{n+1/2}+H_{yx}\big|_{i+1/2,j,k}^{n+1/2}\\-H_{yz}\big|_{i-1/2,j,k}^{n+1/2}-H_{yx}\big|_{i-1/2,j,k}^{n+1/2}\end{pmatrix}$$

$$E_{zy}\big|_{i,j,k}^{n+1}=\exp(-\sigma_y(j)\Delta t/\varepsilon)E_{xy}\big|_{i,j,k}^{n}\frac{1-\exp(-\sigma_y(j)\Delta t/\varepsilon)}{\sigma_y(j)\Delta y}\begin{pmatrix}H_{xy}\big|_{i,j+1/2,k}^{n+1/2}+H_{xz}\big|_{i,j+1/2,k}^{n+1/2}\\-H_{xy}\big|_{i,j-1/2,k}^{n+1/2}-H_{xz}\big|_{i,j-1/2,k}^{n+1/2}\end{pmatrix}$$

Appendix F

Table F.1. Eight TFSF connecting equations to produce an *Ez,Hy* plane wave, see Section 2.11. Each equation is calculated at one face of the connecting surface, linking the total and scattered field regions, over the following ranges of *i, j* and *k*.

Face	*i*	*j*	*k*	Equation
k=k0	i0+1/2,...i1-1/2	j0,...j1	k0	$E_x\|_{i,j,k_0}^{n+1} = E_x\|_{i,j,k_0}^{n+1} + \frac{\Delta t}{\varepsilon_0 \Delta} H_{y,inc}\|_{i,j,k_0-1/2}^{n+1/2}$
k=k1	i0+1/2,...i1-1/2	j0,...j1	k1	$E_x\|_{i,j,k_1}^{n+1} = E_x\|_{i,j,k_1}^{n+1} - \frac{\Delta t}{\varepsilon_0 \Delta} H_{y,inc}\|_{i,j,k1+1/2}^{n+1/2}$
i=i0	i0	j0,...j1	k0+1/2...k1-1/2	$E_z\|_{i_0,j,k}^{n+1} = E_z\|_{i_0,j,k}^{n+1} - \frac{\Delta t}{\varepsilon_0 \Delta} H_{y,inc}\|_{i_0-1/2,j,k}^{n+1/2}$
i = i1	i1	j0,...j1	k0+1/2...k1-1/2	$E_z\|_{i_1,j,k}^{n+1} = E_z\|_{i_1,j,k}^{n+1} + \frac{\Delta t}{\varepsilon_0 \Delta} H_{y,inc}\|_{i_1+1/2,j,k}^{n+1/2}$
j=j0-1/2	i0,...i1	j0-1/2	k0+1/2...k1-1/2	$H_x\|_{i,j_0-1/2,k}^{n+1/2} = H_x\|_{i,j_0-1/2,k}^{n+1/2} + \frac{\Delta t}{\mu_0 \Delta} E_{z,inc}\|_{i,j_0,k}^{n}$
j=j1+1/2	i0,...i1	j1+1/2	k0+1/2...k1-1/2	$H_x\|_{i,j_1+1/2,k}^{n+1/2} = H_x\|_{i,j_1+1/2,k}^{n+1/2} + \frac{\Delta t}{\mu_0 \Delta} E_{z,inc}\|_{i,j_1,k}^{n}$
i=i0-1/2	i0-1/2	j0...j1	k0+1/2...k1-1/2	$H_y\|_{i_0-1/2,j,k}^{n+1/2} = H_y\|_{i_0-1/2,j,k}^{n+1/2} - \frac{\Delta t}{\mu_0 \Delta} E_{z,inc}\|_{i_0,j,k}^{n}$
i=i1+1/2	i1+1/2	j0...j1	k0+1/2...k1-1/2	$H_y\|_{i_1+1/2,j,k}^{n+1/2} = H_y\|_{i_1+1/2,j,k}^{n+1/2} + \frac{\Delta t}{\mu_0 \Delta} E_{z,inc}\|_{i_1,j,k}^{n}$

Appendix G

This appendix is referenced from Section 3.3. The tissues defined in the Zubal head are listed in the first column of Table G.1. The Zubal classification has been done by tissue name and not tissue type, and is not designed for electromagnetics; hence many of the tissues do not have known electrical properties. Medical experts at Sheffield University have reclassified the original list from tissue types with known conductivity and permittivity values. This process is not exact and approximations have been made. Also included are the percentage volumes of the head for each tissue.

Table G.1. The reclassification of the Zubal head.

Zubal Classification	New Sheffield Classification of Zubal Head	% Volume of Head
white matter	white matter	13.79
Fat	fat	13.59
skull	1/3 cancellous, 2/3 cortical	12.84
skeletal muscle	muscle	10.21
temporal lobes	1/2 grey matter, 1/2 white matter	6.51
skin	skin	6.30
cerebral fluid	Cerebrospinal fluid (CSF)	5.14
sinuses/mouth cavity	internal air	4.73
cerebellum	cerebellum	4.00
parietal lobes	1/2 grey matter, 1/2 white matter	3.43
frontal lobes	1/2 grey matter, 1/2 white matter	3.19
occipital lobes	1/2 grey matter, 1/2 white matter	1.98
cartilage	cartilage	1.58
prefrontal lobes	1/2 grey matter, 1/2 white matter	1.49
fat	fat	1.33
parotid gland	gland	0.87
tongue	tongue	0.65
pons	70% grey matter, 30% white matter	0.62
hard palate	cartilage	0.61
blood pool	40% blood, 60% blood vessel	0.51
spine	spinal cord	0.47
horn of mandible	1/3 bone cancellous, 2/3 bone cortical	0.41

superier sagittal sinus	1/2 blood, 1/2 CSF	0.38
insula cortex	grey matter	0.37
eyeball	sclera	0.37
eye	humor	0.36
thalamus	90% grey matter, 10% white matter	0.34
corpus collosum	white matter	0.31
caudate nucleus	grey matter	0.28
putamen	grey matter	0.27
lateral ventricles	CSF	0.25
zygoma	1/3 bone cancellous, 2/3 bone cortical	0.25
internal capsule	white matter	0.25
spinal canal	spinal cord	0.23
third ventricle	CSF	0.20
hippocampus	grey matter	0.20
turbinates	cartilage	0.17
special region frontal lobes	1/2 grey matter, 1/2 white matter	0.16
jaw bone	1/3 bone cancellous, 2/3 bone cortical	0.15
nasal septum	cartilage	0.15
frontal portion eyes (eyelids)	skin	0.14
pharynx	cartilage	0.13
medulla oblongata	30% grey matter, 70% white matter	0.12
cerebral falx	dura	0.11
amygdala	grey matter	0.11
globus palidus	grey matter	0.11
spinal cord	spinal cord	0.08
lacrimal glands	gland	0.07
fourth ventricle	CSF	0.05
dens of axis	1/3 bone cancellous, 2/3 bone cortical	0.04
optic nerve	nerve	0.04
septum pellucidum	muscle	0.03
bone marrow	bone marrow	0.02
uncus (ear bones)	1/3 bone cancellous, 2/3 bone cortical	0.02
lens	lens	0.01
cerebral aquaduct	CSF	0.01
pituitary gland	gland	0.00

Appendix H

H.1 Introduction to the genetic algorithm used in Chapter 5

A genetic algorithm (GA) mimics nature's survival of the fittest selection approach to find the good solutions to a particular problem. In this case a pair of spectacles is sought that produces the maximum SAR in the eye. Two texts on GAs are [1, 2]. Each pair of spectacles in Chapter 5 can be described by the seven parameters listed in Table 5.1. Each parameter is called a gene and the seven genes that describe a pair of spectacles are called a chromosome.

An initial population is composed of a number of chromosomes, whose genes are chosen at random from the predefined range, so the solution domain is evenly sampled [3]. In this research the population size is chosen to be 80 chromosomes. A fitness value can be assigned to each chromosome; in this case the SAR in the eye is used, by evaluation with the FDTD model. This level of fitness allows the population of chromosomes to be ranked according to their fitness value. A new population of chromosomes is found by breeding the previous population of parent chromosomes. This allows the attributes of the successful chromosomes to be combined with other successful chromosomes so that the new population is largely composed of a mixture of the genes that produced the highest level of fitness. The genes can also be mutated to create new genetic material. In nature this allows a species to survive and adapt to changes in their environment. In a GA, mutation stops the algorithm getting stuck in a local minimum.

The fitness values of this second population of chromosomes are then evaluated and the process continues in a loop until a predefined termination criterion is reached. Prior to the search the maximum SAR in the eye was not known hence the GA was run for twenty generations and then terminated, generally the GA converged after twelve generations. A flowchart of the GA process is shown in Figure H.1.

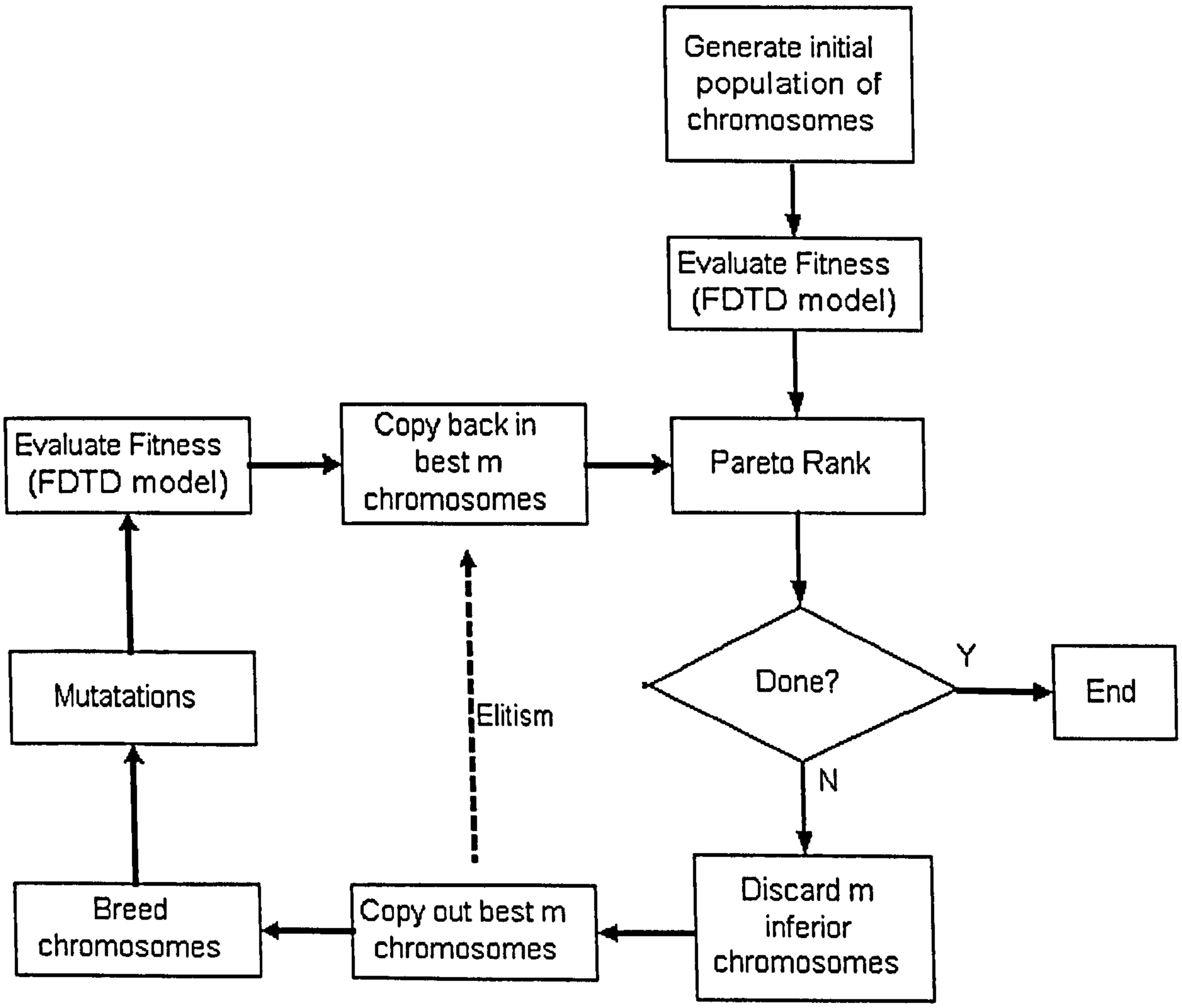

Figure H.1. A genetic algorithm process. N.B. in this thesis Pareto ranking has been used.

H.2 Pareto ranking

Results in chapter 4 have shown that the effects of metallic spectacles at microwave frequencies are larger towards the front of the head and especially in the eye, which may be particularly vulnerable. In this thesis the chromosomes are ranked with two objectives; the average SAR in the eye and the maximum SAR averaged over 1g in the eye. Pareto ranking involves using dominance values to produce a single scalar fitness function from a vector of these two objectives [4, 5]. If no gene can be altered without producing a worse pair of spectacles in terms of either objective, it is not dominated and is said to be a Pareto optimal chromosome. The goal of a Pareto ranked GA is to find a Pareto optimal set of Pareto optimal chromosomes. This is a set of chromosomes that are better than other chromosomes but not better than each other. At the end of the GA process, the most suitable chromosome must be picked manually from the Pareto optimal set. A simplified Pareto ranking algorithm for two arbitrary objectives A and B is shown in Figure H.2.

An advantage of Pareto ranking is no knowledge of the solution range is needed before computation. Most GAs use weighting functions based on the maximum value of the solution, in Pareto ranking chromosomes are ranked according to dominance. Both best least dominated and best most dominated have been used with success [6].

As stated in Chapter 1 the aim of the GA was to find a near optimal solution, the convergence time was less important. It is possible that a slightly higher convergence rate could be achieved with another selection strategy such as population decimation, proportionate selection (roulette wheel), or tournament selection [3].

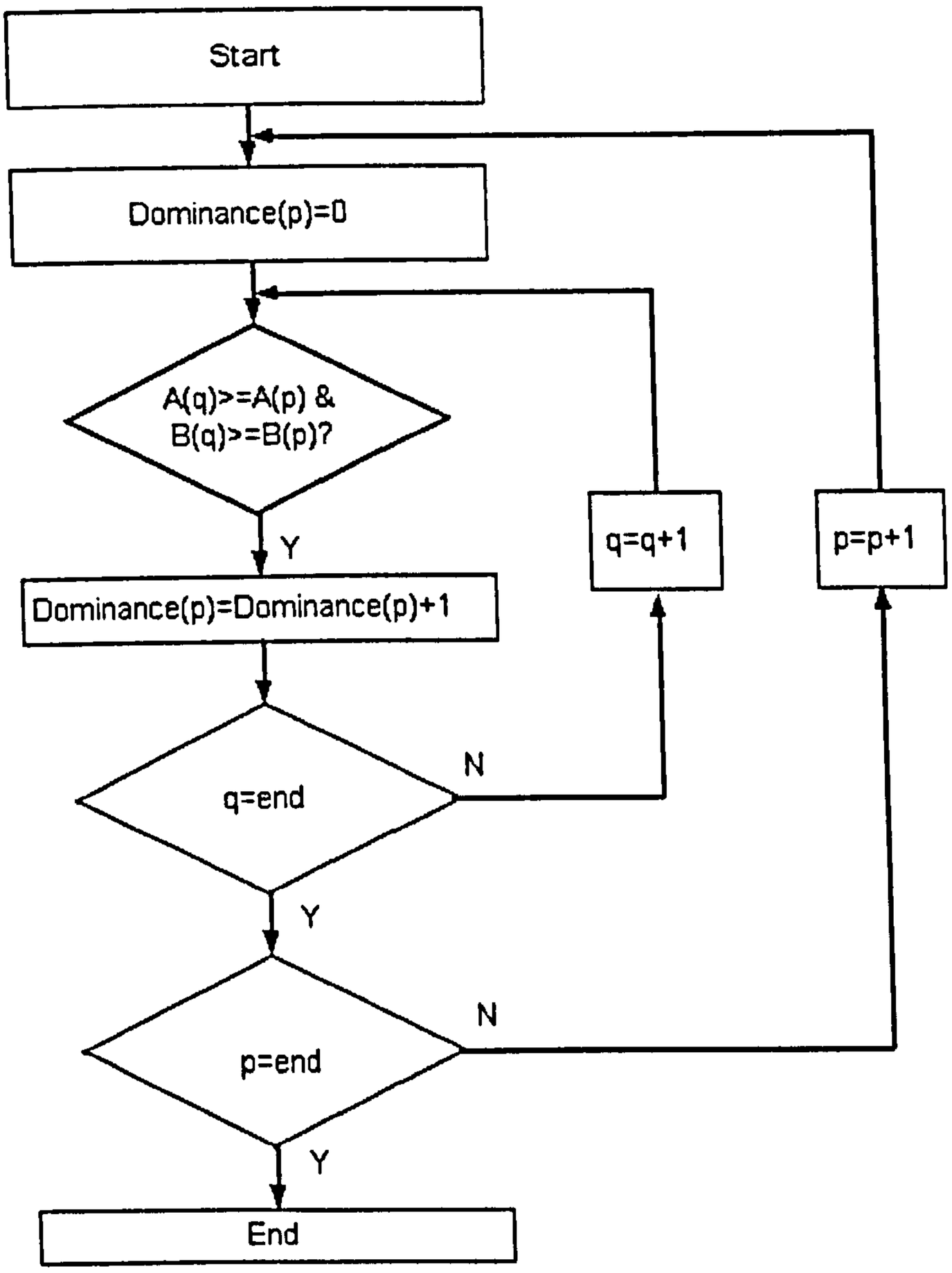

Figure H.2. Simplified Pareto dominance algorithm for two attributes.

H.3 The GA crossover breeding process

Figure H.1 shows that after the chromosomes have been ranked, further improvements to the population are sought by combining good candidates. Parent chromosomes are bred with each other to produce a second generation of children. They can be paired randomly, from the top to the bottom of the list, or best with worst. Haupt [7] found that pairing from the top to the bottom worked best and this is the strategy implemented in this GA. No chromosome is allowed to breed more than once. A crossover point is

chosen at random and indicates how many genes each parent passes onto the child. In this way two parent chromosomes are blended together to produce two offspring chromosomes. In Figure H.3 two arbitrary parent chromosomes each with seven genes are blended, with the crossover point randomly chosen as being between the third and fourth genes. Two new offspring chromosomes replace the two parent chromosomes.

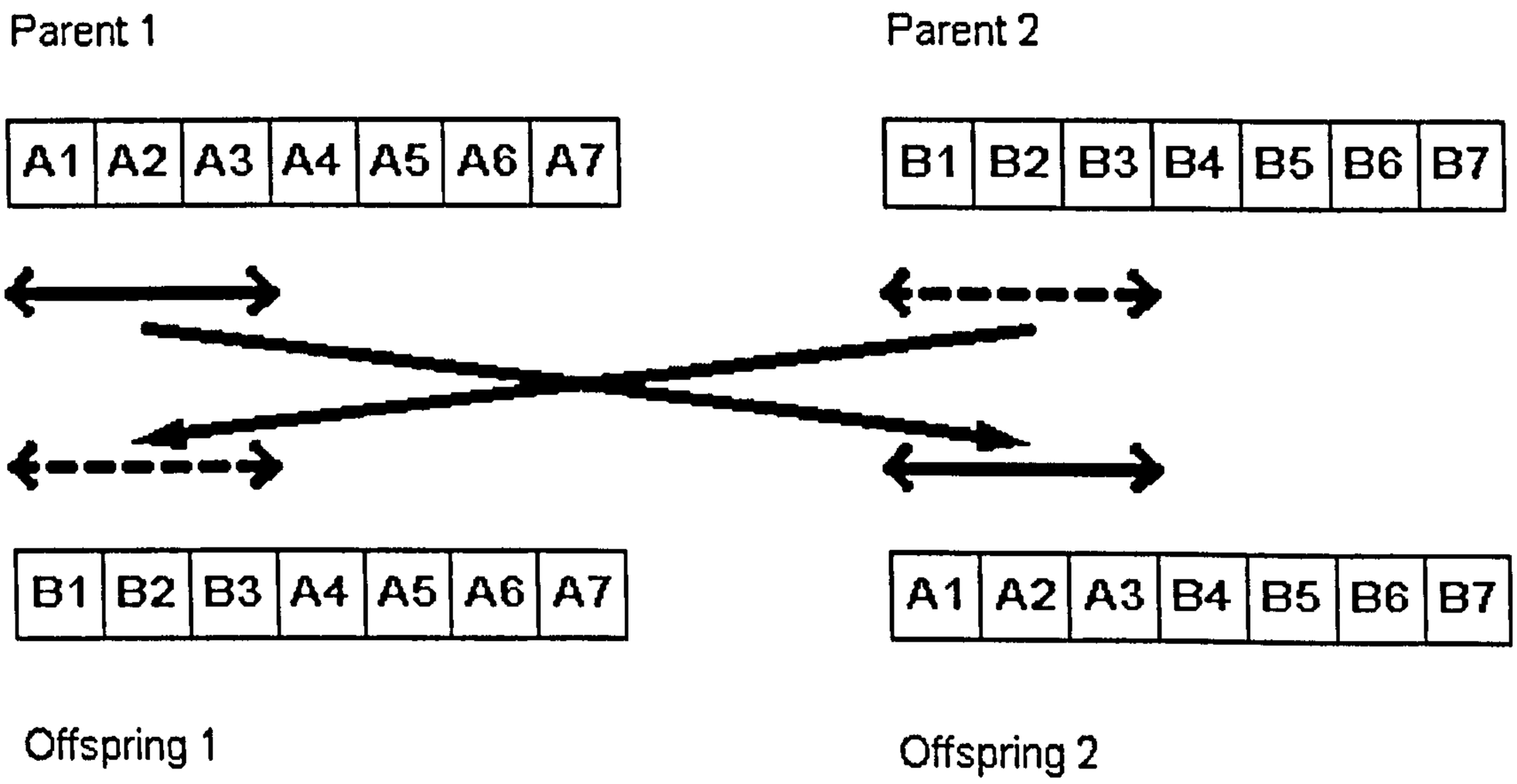

Figure H.3. The crossover technique of breeding two chromosomes in a GA.

H.4 Mutating a gene of a chromosome

As shown in Figure H.1, after the new population of chromosomes has been created, each chromosome is then given a small probability (0.1) that one of its genes will mutate. Mutations introduce new genetic material to the population and can stop the GA getting stuck in a local maximum and not finding the global maximum. 10% is a relatively high probability of mutation compared to other GAs; this value was chosen as the GA used in this research does not produce new genetic material via the breeding process.

H.5 Elitism

The GA process can be improved by using a technique called elitism [3]. This has been included in Figure H.1. The *m* least suitable chromosomes are discarded and the *m* most suitable are copied out to ensure their genetic material is not lost in the breeding or mutation process. In this research *m* has a value of 16. The advantage of elitism is that it means that subsequent generations of populations can not produce worse answers. The best *m* candidates are copied, so that they can both be used as breeding parents and as offspring in the new generation. As the elite chromosomes have already had their fitness functions calculated, the answers can be stored in look-up tables and do not need to be re-calculated. The population remains constant using elitism, however *m* chromosomes are not used for breeding and there are *m* less fitness values that need to be evaluated, hence the active population is reduced. In this research the active population is reduced from 80 to 64.

H.6 Convergence

There are many different variations of GA, all of which work better with a specific problem. Other alternatives include using binary as opposed to continuous genes. Different pairing strategies are possible. The parent chromosomes can be bred in such a way to introduce new genetic material at the breeding stage by using fractions of each gene of each parent. It is likely that a different GA exists that would have been a more efficient optimization routine. It is also possible that a different search technique such as simulated annealing may have found a solution faster. The GA described above is not necessarily the perfect search tool for this problem; however it is a functional tool that

finds a good solution much faster than an exhaustive search. It was considered beyond the scope of this thesis to investigate the merits of different search techniques. The GA used in this research generally converged after twelve generations, but was run for twenty. Also test runs found good solutions with a population size as small as twenty, of which the best four were copied out each generation. Therefore, the GA used in this thesis could have been made to evaluate less pairs of spectacles and therefore have a reduced computational runtime, with minimal reduction in the quality of results found. Running the code for more generations and with a larger population increases the probability of finding a more suitable solution at a cost of longer runtimes, hence a compromise must be found.

H.7 References

1. Deb, K., *Multi-objective optimization using evolutionary algorithms*. 2001: Wiley.
2. Haupt, R., L. and S.E. Haupt, *Practical genetic algorithms*. 1998: Wiley.
3. Johnson, J.M. and Y. Rahmat-Samii, *Genetic algorithms in engineering electromagnetics*. IEEE Antennas and Propagation Magazine, 1997. **39**(4): p. 7-25.
4. Horn, J., N. Nafpliotis, and D. Goldberg. *A niched Pareto genetic algorithm for multiobjective optimization. Proc. first IEEE Conference on Evolutionary Computation. IEEE World Congress on Computational Intelligence.* 1994. IEEE Service Centre. p. 82-87
5. Edwards, R.M., G.G. Cook, S.K. Khamas, R.J. Aidley, and B. Chambers, *Design of a circularly polarised printed spiral antenna using dual objective genetic algorithm.* Electronic Letters, 1998. **34**(7): p. 608-609.
6. Edwards, R.M., *Optimal synthesis of printed wire spiral antennas using an efficient curved segment method with a genetic algorithm (thesis), EEE Department*. 2000, University of Sheffield, UK.
7. Haupt, R.L., *An introduction to genetic algorithms for electromagnetics*. IEEE Antennas and Propagation Magazine, 1995. **37**(2): p. 7-15.

Appendix I

Further technical information of the measurements made in Chapter 6 using the DASY4 measurement system, from the DASY4 System Handbook and www.dasy4.com.

I.1 DASY4 system description

The DASY4 system for performing compliance tests consists of the following items:

- A standard high precision 6-axis robot (Staubli RX family)

- A dosimetric probe, i.e., an isotropic E-field probe optimized and calibrated for usage in tissue simulating liquid. The probe is equipped with an optical surface detector system.

- A data acquisition electronics (DAE) which performs the signal amplification, signal multiplexing, AD-conversion, offset measurements, mechanical surface detection, collision detection, etc.

- The SAM twin phantom enabling testing left-hand and right-hand usage.

- Tissue simulating liquid mixed according to the given recipes.

- Validation dipole kits.

Requirements for the room: Approximately constant room temperature is recommended (because of the sensitivity of the liquid parameters). The floor should be stable, flat and vibration free. For dosimetric measurements, no RF-absorbers are needed. A typical DASY4 system is shown in Figure I.1.

Figure I.1. The DASY4 measurement system.

Multi-standard compatibility: The worldwide effort for the harmonization of standards for the compliance testing of handheld transmitters has made significant progress in recent years. The drafted standards IEEE P1528 - 200X and IEC 62209 are technically harmonized and provide well-defined and scientifically sound procedures. DASY4 is designed and equipped to fully comply with these highly strict requirements.

Spatial peak SAR evaluation: The DASY4 software includes all numerical procedures necessary to evaluate the spatial peak SAR values. Based on the draft: SCC-34, SC-2, WG-2 - Computational dosimetry, IEEE P1529/D0.0 (Draft recommended practice for determining the spatial-peak specific absorption rate (SAR) associated with the use of wireless handsets - computational techniques), a new algorithm has been implemented. The spatial-peak SAR can be computed over any required mass. The base for the evaluation is a cube measurement in a volume of $(30mm)^3$ (7x7x7 points). The

algorithm to find the cube with highest averaged SAR is divided into the following stages: extraction of the measured data, calculation of the SAR value at every measurement point, generation of a high-resolution mesh within the measured volume, interpolation of all measured values from the measurement grid to the high-resolution grid, extrapolation of the entire 3-D field distribution to the phantom surface over the distance from sensor to surface, calculation of the averaged SAR within masses of 1g and 10g. The spatial-peak SAR must be evaluated in cubical volumes containing a mass that is within 5% of the required mass. The cubical volume should not consist of more than 10% of air.

I.2 Specific details of measurements made in Chapter 6

Test laboratory: Loughborough University, Centre for Mobile Communications Research

DUT: Dipole 1800 MHz; Type: D1800V2; Serial: 2d050

Communication system: CW; Frequency: 1800MHz; Duty cycle: 1:1

Medium: HSL1800 (σ = 1.37 S/m, ε_r = 40.48, ρ = 1000 kg/m^3)

Phantom section: Right section

Probe: ET3DV6 - SN1758; ConvF(5.3, 5.3, 5.3); Calibrated: 3/7/2003

Sensor-surface: 4mm (Mechanical and optical surface detection)

Electronics: DAE3 Sn552; Calibrated: 3/3/2003

Phantom: SAM; Type: SAM 4.0; Serial: 1268

Measurement SW: DASY4, V4.1 Build 47; Post processing SW: SEMCAD, V1.6 Build 115

Appendix J

J.1 Exciting a dipole of finite length at different frequencies

The FDTD code was carefully validated and Chapter 3 demonstrated that the results of the SAR levels using different excitations and geometries were in agreement with those in published papers. This appendix includes further analytical results that validate the code. The impedance along a fixed length dipole was investigated over a frequency range. Hockanson [1] excited a dipole of fixed length with frequencies over the range $0.25 \leq L/\lambda \leq 2$, where L is the length of the dipole. This was replicated by exciting a 0.15m dipole with frequencies ranging from 0.5 to 4.0GHz. The dipole is resonant at 1GHz. Changing the ratio of the length of the antenna to the wavelength alters the impedance, this can be seen in figures J.1 and J.2.

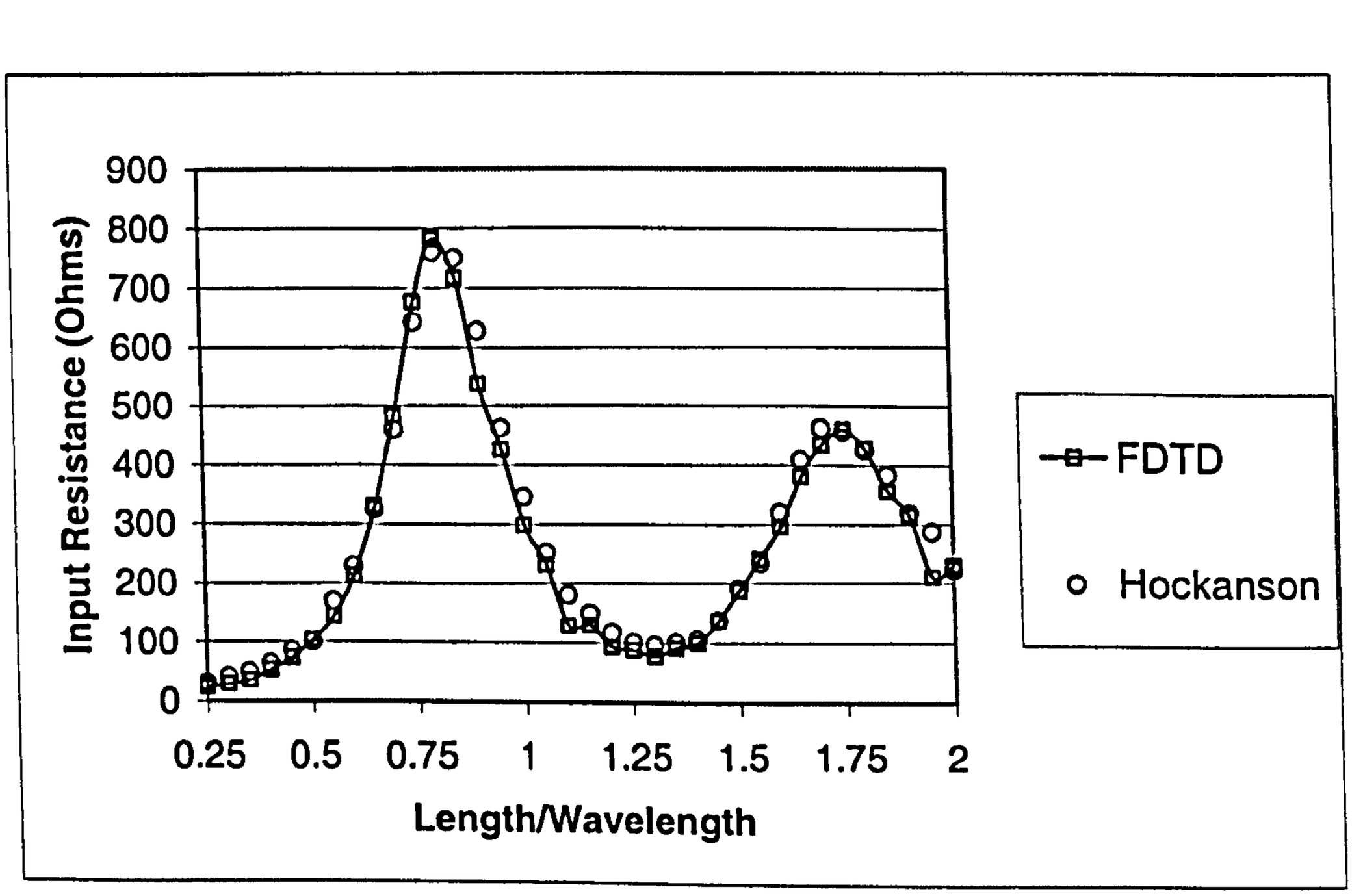

Figure J.1. FDTD input resistance comparison for a fixed length dipole antenna at different frequencies compared with published paper.

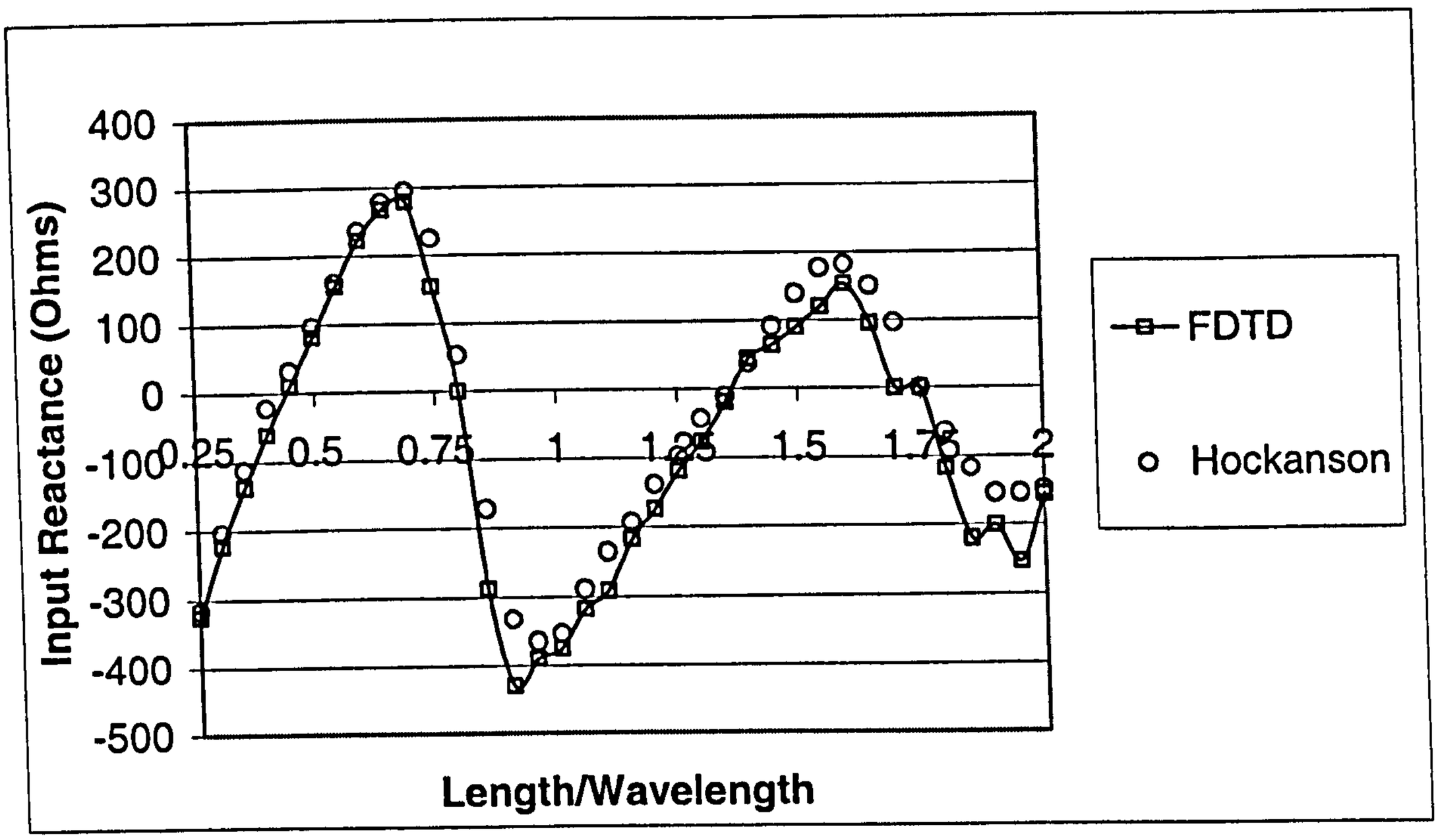

Figure J.2. FDTD input reactance comparison for a fixed length dipole antenna at different frequencies compared with published paper.

The results in figures J.1 and J.2 show the input impedance as a function of the excitation frequency is in agreement with Hockanson [1]. Hockanson used the FDTD method, and his paper showed that the above results were in close agreement with results from the NEC method of moments computer program [2]. Thus the results in figures J.1 and J.2 validate the code against both the FDTD code used by Hockanson and the NEC results. These results and those in Chapter 3 show the independent FDTD code used in this thesis has been implemented correctly.

J.2 References

1. Hockanson, D.M., J.L. Drewniak, T.H. Hubing, and P. Van Doren, *FDTD modeling of common-mode radiation from cables.* IEEE Trans. Electromagnetic Compatibility, 1996. **38**(3): p. 376-387.
2. Burke, G.J. and A.J. Poggio, *Numerical electromagnetics code (NEC) - method of moments.* 1981: Lawrence Livermore Laboratory Report UCID-18834.

Appendix K

K.1 Scattering properties of wire loops

This thesis has examined the effects of metallic spectacles on the SAR in the head. The head is a complicated heterogeneous structure and the spectacles are also complex, however it is believed that the mechanism for these effects is based on the scattering properties of a thin wire loop. The spectacles resemble a loop when the source is vertically polarised and the horizontal sections of the frames become less significant.

Kraus [1] reviewed the radar scattering of thin loops. He divided the subject into three regions: the high frequency (optical) region where the target >> λ, the low frequency (Rayleigh) region where the target << λ and the resonance region where the target ~ λ. A resonance occurs for the radar cross section of a sphere when the λ ≈ circumference of the sphere.

Figure K.1 shows the radar cross section in square wavelengths of thin loops as a function of the circumference of the loop in wavelengths [1]. Two different thicknesses of perfectly conducting wire are used. The loop is assumed to be in the far field of the source. The figure shows that there is a resonance in the radar cross section when the circumference of the loop is roughly equal to one wavelength. The thickness of the loop, affects the radar cross section. In the FDTD model the thickness of the spectacle frames is equal to the Yee cell size. The loop becoming a resonant object when the circumference is roughly equal to the wavelength was also reported by Bhattacharyya [2], who showed that the radar cross section of loops was resonate when the radius of the loop was approximately equal to 0.17λ.

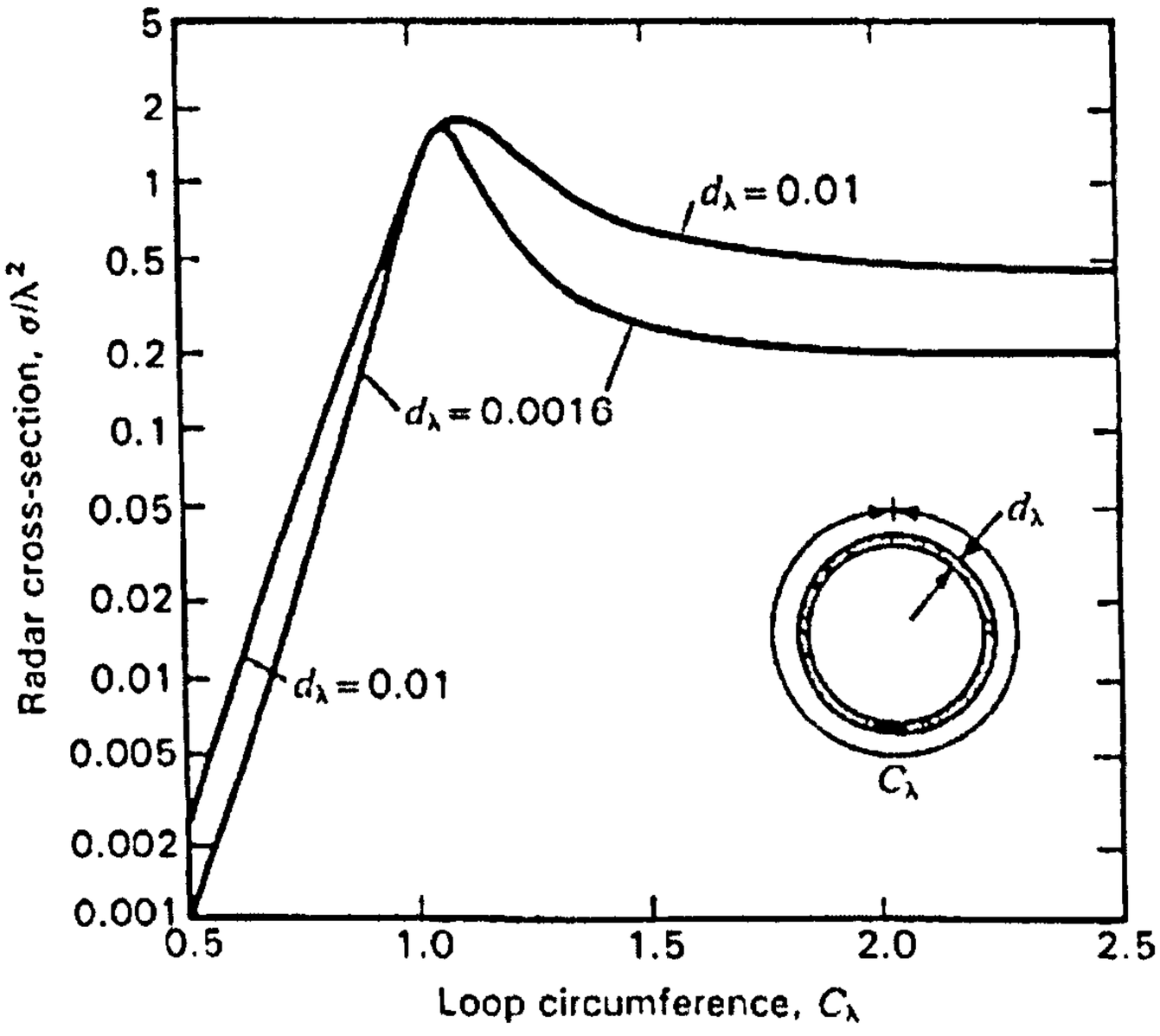

Figure K.1. Broadside radar cross section (in λ^2) of loops as a function of loop circumference (in λ), $C\lambda$, for loop conductor diameters $d\lambda = 0.0016$ and 0.01λ [1].

The spectacles that produced the largest SAR in the eye with a vertically polarised plane wave had dimensions 36x38mm. Therefore the circumference is 148mm. This is in the resonance region at 1.8GHz ($\lambda \approx 167$mm). Note that Figure 4.3 showed that the presence of a dielectric lens reduces the resonant frequency. Although the loop represents a simple model of a pair of spectacles, a real pair on a real head are a more complicated system. For example the spectacles that produced the lowest SAR in the eye (46x38mm), have a circumference of 168mm which is also approximately 1λ.

K.2 References

1. Kraus, J., D., *Antennas*. 2nd ed. 1988: McGraw-Hill Inc.
2. Bhattacharyya, A.K. and D.L. Sengupta, *Radar cross section analysis and control*. 1991: Artech House Inc.